

DEVELOPMENT OF A STRUCTURAL DESIGN METHODOLOGY FOR  
POLYMERIC SPRAY APPLIED PIPE LININGS

By

ZAHRA KOHANKAR KOUCHESFEHANI



Presented to the Faculty of the Graduate School of  
The University of Texas at Arlington in Partial Fulfillment  
of the Requirements  
for the Degree of

DOCTOR OF PHILOSOPHY

THE UNIVERSITY OF TEXAS AT ARLINGTON

August 2020

Copyright © by Zahra Kohankar Kouchesfehani 2020

All Rights Reserved



## **Acknowledgements**

I would like to express my sincere gratitude to my advisor, Professor Mohammad Najafi, for his continuous and precious supports throughout my Doctoral study and related research, for his patience, motivation, and immense knowledge.

I would like to thank my dissertation committee members, Dr. Shih-Ho Chao, Dr. Jay Michael Rosenberger, Dr. Mohsen Shahandashti, and Dr. Xinbao Yu for their insightful comments that helped me to widen my research from various perspectives.

I will forever be thankful to the Civil Engineering Department Chair, Professor Ali Abolmaali, who provided me with the opportunity to join the Civil Engineering team at UTA. I would like to thank him for his continuous supports throughout my Ph.D. study.

The present dissertation includes results of a pool-funded project from National Cooperative Highway Research Program (NCHRP) that was funded by seven departments of transportation (DOTs) of Ohio DOT (leader), DeIDOT, FDOT, MnDOT, NCDOT, NYSDOT and PennDOT. I would like to thank the Principal Investigator of the project, Dr. M. Najafi, the DOTs representatives, Mr. Jeffrey Syar, Mr. Brian Carmody, Ms. Sherry Little, Mr. Matthew S. Lauffer, Mr. Charles Smith, Mr. Paul Rowekamp, Mr. Carlton Spirio, Mr. Nicholas Dean, and Co-PI of this project, Dr. Xinbao Yu, for their technical and financial support.

In addition, I would like to thank, Sprayroq Company, Contech Engineering, Forterra Pipe and Precast, HVJ Associates, MTS Systems Corporation, and Micro-Measurement for providing this research project with various products and services that were most essential. Many thanks to Mr. Chip Johnson, Dr. Firat Sever, Mr. Lynn Osborn, Mr. Ed Kampbell, Mr. Mario Tamez, and Mr. Mark Garrison.

I would like to give my warmest thank to my friends and colleagues, Dr. Amin Darabnough Tehrani and Dr. Amir Tabesh for their motivation and heartwarming supports. I would like to thank other graduate students at CUIRE, Satish Kakkera, Juhil Makwana, and Shobhit Srivastava who helped me with the test setup preparation and Samrat Raut for the Finite Element Modeling (FEM).

Last but not the least, I specially thank my beloved mother for supporting me spiritually throughout writing this dissertation and my life in general. She has sacrificed her life for me and provided me with her unconditional love and care. I love her so much, and I would not have made it this far without her.

August 31, 2020

*I dedicate this thesis to  
my beloved mother  
for her constant support and unconditional love.  
I love you dearly.*

## Abstract

### Development of a Structural Design Methodology for Polymeric Spray Applied Pipe Linings

Zahra Kohankar Kouchesfehiani, PhD

The University of Texas at Arlington, 2020

Supervising Professor: Mohammad Najafi

Buried culverts are important components of the highway infrastructure. Most large culverts are built decades ago from corrugated metal or reinforced concrete materials and now have reached their design lives. Trenchless renewal techniques can be utilized to enhance load carrying capacity of the existing deteriorated culverts and provide them a new design life. Spray applied pipe lining (SAPL) is a trenchless renewal methodology to renew damaged pipes and culverts by applying layers of liner on the interior surface of the deteriorated host culvert. The development of practical spray applied pipe linings could be of enormous benefit to the Departments of Transportation. Such linings could be a key strategy in extending service life and managing the future burden expected from the aging culverts and drainage structures. The SAPLs generally fall into two categories of cementitious and polymeric materials. Currently, there is no available standard for structural design of SAPLs. In absence of a standard design methodology, some vendors and contractors currently utilize the cured-in-place pipe (CIPP), ASTM F1216 methodology and others are using various classical analytical structural design equations developed for other purposes. To provide an understanding for development of a design methodology, the first objective of this dissertation was to investigate structural capacity of fully deteriorated invert large circular and arch corrugated metal pipes (CMPs) renewed with polymeric SAPL.

The second objective of this dissertation was to compare the load carrying capacities of SAPL renewed circular and arch CMPs. The third objective of this dissertation was to check the applicability of ASTM F1216 CIPP design equation for SAPL method. The fourth objective of this dissertation was to develop a design methodology for structural application of polymeric SAPL using for renewal of large

diameter (span larger than 36 in.) circular and arch culverts. To conduct this research, before application of SAPL, the inverts of CMP samples were cut to simulate fully deteriorated culverts in service conditions and to maximize the applied static load on the SAPL. The pipe samples were buried under two feet of soil cover. The performances of SAPL renewed CMPs were compared with a same size invert-cut bare CMP under same testing conditions. The results indicated that dependent on the thickness, application of polymeric SAPL can improve the structural capacity of a fully deteriorated invert CMP culvert. Under conditions of testing performed, a modified CIPP design equation, with an enhancement factor of 2.738, in a fully deteriorated pipe condition is applicable for polymeric SAPLs for structural renewal. An adapted AWWA C950 design equation is applicable for polymeric SAPLs. The moment of inertia in these equations needed to be calculated based on the corrugated profile.

## Table of Contents

<b>CHAPTER 1 INTRODUCTION AND BACKGROUND.....</b>	<b>1</b>
1.1 Culverts and Storm Sewers.....	1
1.1.1 Culvert Shapes.....	3
1.1.2 Culvert Materials.....	3
1.1.3 Culvert Hydraulics and Flow Conditions .....	5
1.1.4 Types of Flow Control .....	6
1.1.5 Culvert Structural Behavior .....	7
1.2 Corrugated Metal Pipe Culverts (CMPs).....	15
1.2.1 CMP Types and Corrugation Profiles.....	15
1.2.2 Corrugated Metal Pipe Design Considerations.....	17
1.2.3 Durability and Structural Performance of CMPs .....	18
1.3 Renewal of Deteriorated Culverts using Trenchless Technology .....	23
1.3.1 Sliplining .....	24
1.3.2 Cured-in-Place Pipe Lining (CIPP).....	25
1.3.3 Close-fit Pipe Lining .....	26
1.3.4 Spiral Wound Lining (SWP).....	26
1.3.5 Thermoformed Pipe (ThP).....	27
1.3.6 Spray Applied Pipe Lining (SAPL).....	28
1.4 Dissertation Objectives .....	31
1.5 Methodology .....	31
1.6 Scope.....	32
1.7 Hypothesis .....	33
1.8 Expected Outcome .....	33
1.9 Overview of the Chapters .....	33
1.10 Chapter Summary.....	34
<b>CHAPTER 2 LITERATURE REVIEW.....</b>	<b>35</b>

2.1	Spray Applied Pipe Linings.....	35
2.1.1	Polymeric Spray Applied Pipe Liners .....	35
2.1.2	Cementitious Spray Applied Pipe Liners.....	41
2.2	SAPL Renewed Pipe Testing .....	43
2.3	Soil-Pipe System Testing .....	48
2.4	Structural Analysis of Sewer Linings .....	51
2.4.1	Structural Classification of Sewer Linings .....	52
2.4.2	Critical Buckling Pressure Theories available for Design of Circular Flexible Linings used for Sewer Pipes.....	52
2.5	Review of Design Methods for Flexible Sewer Pipe Liners.....	53
2.5.1	ASTM F1216-16 (2016).....	54
2.5.2	ASTEE 3R2014 (2014).....	63
2.5.3	DWA-A 143-2 (2015).....	65
2.5.4	WRc SRM (2014) .....	66
2.5.5	Comparison of Available Flexible Sewer Liner Design Methods .....	67
2.6	Chapter Summary.....	70

**CHAPTER 3 SAPL SITE VISIT INSPECTIONS AND FIELD DATA COLLECTION ..... 72**

3.1	Introduction .....	72
3.2	Objectives of Culvert Inspections .....	74
3.3	Selection of Culverts.....	74
3.4	Inspection Tools.....	76
3.5	Inspection Procedure.....	77
3.6	SAPL Issues due to Lack of Standard.....	79
3.7	SAPL Thickness .....	83
3.8	Rating Systems.....	84
3.9	Condition Assessment of SAPLs.....	90



3.10	Comparative Status of Cementitious and Geopolymer SAPLs .....	90
3.11	Discussion of Results .....	91
3.12	Limitations, Findings and Recommendations.....	93
3.13	Chapter Summary.....	95

**CHAPTER 4 FULL SCALE LABORATORY SOIL BOX TESTING..... 97**

4.1	Experimental Test Setup for Soil Box Testing.....	97
4.1.1	Host Pipe Samples .....	103
4.1.2	Burial Configuration .....	106
4.1.3.	CMP Surface Preparation and Polymeric SAPL Installation .....	114
4.2	Polymeric SAPL Installation .....	117
4.2.1	Polymeric SAPL Sampling for Material Property Testing.....	118
4.2.2	SAPL Installation Temperature .....	120
4.3	Instrumentation .....	121
4.3.1	Strain Gauges.....	122
4.3.2	Earth Pressure Cells .....	125
4.3.3	LVDT and CDS.....	125
4.3.4	DIC Measurement and Pipe Monitoring .....	127
4.4	SAPL Thickness Measurement .....	130
4.5	SAPL Material Property Testing, Test Samples and Procedures .....	131
4.6	Soil Box Testing Loading Configuration and Operations.....	131
4.6.1	Live Load Distribution According to the AASHTO LRFD Bridge Design Specifications .....	133
4.7	Chapter Summary.....	135

**CHAPTER 5 SOIL BOX TESTING RESULTS AND DISCUSSIONS ..... 136**

5.1	Control Test Results .....	136
5.1.1	Invert Detachment Effect.....	136
5.1.2	Bare CMPs Behavior under the Static Load .....	138

5.1.3	Bare CMPs Load Carrying Capacity .....	147
5.1.4	Results of Earth Pressure Cells .....	150
5.1.5	Results of Strain Gauges .....	153
5.1.6	Thrust Force and Bending Moment.....	156
5.1.7	Results of DIC Deflection Measurement .....	158
5.2	Soil Box Testing – SAPL Renewed Circular CMPs.....	159
5.2.1	SAPL Material Property Testing Results .....	159
5.2.2	SAPL Thickness Survey Installed Inside Circular CMPs .....	160
5.2.3	Comparison of Bare and SAPL Renewed Circular CMPs Load Bearing Capacities (Responses to Static Load) .....	163
5.2.4	Pressure around the circular CMPs (Earth Pressure Cell Results) .....	170
5.2.5	Strain Gauges Results for SAPL Renewed Circular CMPs .....	172
5.2.6	Pipe Profile Measurement using DIC for SAPL Renewed Circular CMPs .....	174
5.3	Soil Box Testing – SAPL Renewed Arch CMPs.....	178
5.3.1	SAPL Thickness Survey Installed Inside Arch CMPs .....	178
5.3.2	Arch CMP Invert Detachment Response .....	180
5.3.3	Comparison of Bare and SAPL Renewed Arch CMPs Load Bearing Capacities (Responses to Static Load) .....	180
5.3.4	Pressure around the Arch CMPs (Earth Pressure Cell Results).....	187
5.3.5	Strain Gauges Results for SAPL Renewed Arch CMPs .....	192
5.3.6	Pipe Profile Measurement using DIC for SAPL Renewed Arch CMPs .....	194
5.4	<i>Chapter Summary</i> .....	198
5.4.1	Control Test of Bare CMPs .....	198
5.4.2	SAPL Renewed Circular CMPs.....	199
5.4.3	SAPL Renewed Arch CMPs.....	200

**CHAPTER 6 FINITE ELEMENT MODELING (FEM)..... 202**

6.1	Model setup .....	202
6.2	Comparison of the Soil Box Testing Results Presented in Chapter 5 and FEM Results of Fully Deteriorated Invert Circular CMPs Renewed with Polymeric 0.25 SAPL. ...	204
6.2.1	0.25 in. SAPL Renewed CMP Sample.....	204
6.2.2	0.5 in. SAPL Renewed CMP Sample .....	209
6.2.3	1.0 in. SAPL Renewed CMP Sample .....	213

6.2.4	FEM Simulation of 0.75, 1.5, and 2.0 in. SAPLs .....	217
6.2.5	Comparison of Different SAPL Thicknesses Installed Inside the Fully Invert Deteriorated Circular CMPs .....	220
6.3	Comparison of the Soil Box Testing Results Presented in Chapter 5 and FEM Results of Fully Deteriorated Invert Circular CMPs Renewed with Polymeric 0.5 SAPL. ....	220
6.3.1	0.25 in. SAPL Renewed CMP Sample .....	220
6.3.2	0.5 in. SAPL Renewed CMP Sample .....	225
6.3.3	1.0 in. SAPL Renewed CMP Sample .....	229
6.3.4	FEM Simulation of 0.75, 1.5, and 2.0 in. SAPLs .....	233
6.3.5	Comparison of Different SAPL Thicknesses Installed Inside the Fully Invert Deteriorated Circular CMPs .....	237
6.4	Chapter Summary.....	237
6.4.1	Fully Deteriorated Invert Circular CMP Renewed with SAPL .....	238
6.4.2	Fully Deteriorated Invert Arch CMP Renewed with SAPL .....	238
6.4.3	FEM Limitations.....	238
<b>CHAPTER 7 DEVELOPMENT OF A DESIGN METHODOLOGY .....</b>		<b>239</b>
7.1	Existing Rehabilitation/Renewal Lining Design Theory .....	239
7.1.1	Vehicle and Earth Loads for Liner Designs .....	240
7.2	Design of Liner Thickness Using Polymeric SAPL Materials .....	243
7.2.1.	CIPP Design Equations for Fully Deteriorated Pipe Condition .....	244
7.2.2	AWWA C950 Design Equations .....	244
7.2.3	Modified CIPP Design Equations for Fully Deteriorated Pipe Condition.....	245
7.2.4	Adapted AWWA C950 Design Equations .....	248
7.3	Proposed Design Method for Polymeric Materials .....	250
7.4	Chapter Summary.....	252
<b>CHAPTER 8 CONCLUSIONS AND RECOMMENDATIONS FOR FUTURE RESEARCH .....</b>		<b>254</b>
8.1	Summary .....	254
8.2	Conclusions .....	254
8.2.1	Bare CMP Control Tests (First Soil Box Test Setup) .....	255

8.2.2	SAPL Renewed Circular CMPs (Second Soil Box Test Setup) .....	256
8.2.3	SAPL Renewed Arch CMPs (Third Soil Box Test Setup) .....	257
8.3	Limitations and Recommendations for Future Research .....	258
<b>REFERENCES.....</b>		<b>259</b>
<b>APPENDIX A FIELD INSPECTION AND DATA COLLECTION .....</b>		<b>270</b>
<b>APPENDIX B PHOTO GALLERY.....</b>		<b>289</b>
<b>BIOGRAPHICAL INFORMATION .....</b>		<b>293</b>

## List of Illustrations

Figure 1-1 American society of civil engineers' report card for America's infrastructure (2017). .....	1
Figure 1-2 Corrugated metal pipe culverts (CMPs): (a) multi-cell CMPs (Source: Contech), .....	2
Culverts are available in variety of shapes for both, closed conduits, and open-bottom conduits. The most common shapes of closed conduits are circular, box (rectangular), elliptical, and pipe-arch, as illustrated in Figure 1-4 (a). However, the open-bottom culverts are mostly in arch configuration, as illustrated in Figure 1-3 (b). These typical culvert shapes have the same material on the entire perimeter (FHWA 2012).....	3
Figure 1-4 Commonly used culvert shapes: (a) closed conduit culvert shapes, .....	3
Figure 1-5 Culvert materials (ODOT 2018).....	4
Figure 1-6 Typical "inlet control" flow section for a partly full culvert (FHWA 2012). .....	5
Figure 1-7 Typical "outlet control" flow in both full flow (submerged) and partly full flow (unsubmerged) conditions (FHWA 2012). .....	6
Figure 1-8 Deflection of a circular flexible pipe (Najafi 2008). .....	8
Figure 1-9 Failure modes of flexible conduits: (a) wall crushing, (b) seam separation, (c) elastic local buckling, (d) inelastic (snap-through) buckling, and (e) plastic yielding (excessive deflection).....	9
Figure 1-10 Active pressure distribution around circular conduit.....	12
Figure 1-11 Bresse Model for calculating the critical buckling pressure of a thin unconstraint .....	13
Figure 1-12 Rigid Pipes under vertical loading: (a) rigid pipe stress zones (Hydraulics Manual M 23-03.06 2019), and (b) finite element modeling of a rigid reinforced concrete pipe (RCP).....	15
Figure 1-13 Types of corrugated metal pipes (CMPs): (a) helical, (b) annular and (c) spiral rib CMPs.....	16
Figure 1-14 Common Defects of Culverts: (a) invert corrosion, (b) invert abrasion, (c) joint separation, (d) crack, (e) joint infiltration, (f) spalling in concrete culverts, (g) wall damages in plastic culverts, (h) piping beneath a culvert and (i) outlet scour (Piratla et al. 2017). .....	20
Figure 1-15 Culvert failure in Maryland (American Concrete Pipe Association 2008).....	21
Figure 1-16 Culvert failure in Timonium (American Concrete Pipe Association 2008).....	21
Figure 1-17 Culvert failure in British Columbia, Canada (American Concrete Pipe Association 2008). ....	22
Figure 1-18 Culvert failure in Bakersfield, California (American Concrete Pipe Association 2008). .....	22

Figure 1-19 Trenchless renewal solutions. .... 24

Figure 1-20 Segmental sliplining method (Source: Hobas Pipe USA)..... 25

Figure 1-21 CIPP method installation process (Source: Insituform Technologies). .... 26

Figure 1-22 Three main variations of ThP process (Najafi and Gokhale 2005). .... 27

Figure 1-23 Corrugated metal pipe culverts (CMPs) before and after SAPL rehabilitation: (a) cementitious SAPL installation using spin casting machine (Source: CentriPipe) and (b) polymeric SAPL installation with hand spray (Source: Sprayroq). .... 29

Figure 1-24 A sample of SAPL renewed twin culvert, North Carolina ..... 30

Figure 1-25 Research Methodology..... 32

Figure 2-1 Performance comparison of polyurea, polyurea hybrid, polyurethane and epoxy coatings applied on steel substrate (Adapted from Cain 2016). .... 38

Figure 2-2 CMP renewal using SprayWall® Polyurethane SAPL, Norristown, PA: (a) Before Renewal, and (b) CMP Renewal during SAPL Application, 2007 (Sprayroq Inc.)..... 41

Figure 2-3 Comparison of spray-on lining methods using material property testing: (a) long-term flexural testing, (b) long-term creep tensile testing and (c) hydrostatic test setup (Motlagh et al. 2013). .... 43

Figure 2-4 Dead-load testing of reinforced concrete pipes (RCPs) renewed with polymeric SAPLs: (a) tested concrete rings covered by polyurea coating, (b) spraying polyurea coating system ..... 44

Figure 2-5 The structural behavior and performance of a fast-setting polyurea–urethane (PUU) SAPL as a structural lining material for rehabilitating water pipes (Ha et al. 2016). .... 45

Figure 2-6: Significant increase in renewed CRP structural capacity (Entezarmahdi, 2015). .... 47

Figure 2-7 Soil box laboratory testing of corrugated metal pipes: (a) single axle loading configuration, and (b) schematic tandem axle loading configuration (Garcia and Moore 2015). .... 49

Figure 2-8 Field testing of a shallow cover severely deteriorated arch CMP (Sargand et al. 2018). .... 50

Figure 2-9 Global and local imperfections (Thepot et al. 2015). .... 54

Figure 2-10 Partially deteriorated pipe terminology according to the (F1216-16 2016). .... 55

Figure 2-11 Aggarwal's 1984 hydrostatic buckling data compared with contemporary theories..... 57

Figure 2-12 Experimental ovality factors for liner of  $D/t = 45$  compared with ASTM F1216 C-factor (Gumbel 1998). .... 59

Figure 2-13 Liner deformations implicit in the ASTM F1216 design formula based on linear theory of unrestrained buckling with enhancement factor K and ovality factor C: (a) C value for a circular .....	59
Figure 2-14 Steps in non-linear hydrostatic buckling of restrained circular liner pipe .....	60
Figure 2-15 Wrinkle model used for DWA-A 143-2 state III flexible liner design.....	66
Figure 3-1 Geographical distribution of selected SAPL culverts.....	75
Figure 3-2 Issues found with SAPLs.....	79
Figure 3-3 SAPL measured thicknesses versus 2 in. design thickness .....	83
Figure 3-4 SAPL average installed thicknesses versus 1.5 in. design thickness .....	84
Figure 3-5 Condition assessment of SAPLs. It shows (a) SAPL original condition given as percent of liner condition, (b) SAPLs structural condition given as percent of liner structural condition. ....	90
Figure 3-6 Correlation of age, H/R, thickness and AOR of SAPLs. It shows (a) A, H/R and AOR (b) A, T and (AOR), and (C) H/R, T and AOR.....	93
Figure 4-1 CUIRE Laboratory at UTA: (a) UTA Civil Engineering .....	98
Figure 4-2 Overview of soil box testing steps. ....	100
Figure 4-3 Corrugated metal pipe (CMP) samples. ....	101
Figure 4-4 Circular CMP samples for control test: (a) intact 60 in. circular CMP, .....	102
Figure 4-5 CMP sample details: (a) corrugation profile, (b) detachable invert schematic, and (c) the bare CMP sample with the detachable invert (Kohankar Kouchesfehni et al. 2020).....	104
Figure 4-6 End strips of the invert-cut CMP samples. ....	105
Figure 4-7 Detachable invert mechanism (in four stages) for SAPL renewed pipe samples .....	105
Figure 4-8 Pipe installation: (a) longitudinal configuration of arch CMPs in the soil box of.....	106
Figure 4-9 The CMPs' burial configuration (1 <sup>st</sup> set of soil box testing-control test): (a) plan view, (b) profile view of the aligned CMPs in the soil box, and (c) cross-section view of both circular and arch CMPs....	108
Figure 4-10 The CMPs' burial configuration (2 <sup>nd</sup> set of soil box testing): (a) plan view, (b) profile view of the aligned CMPs in the soil-box, and (c) cross sectional view of the circular CMP. ....	109
Figure 4-11 The arch CMPs' burial configuration (3 <sup>rd</sup> set of soil box testing): (a) plan view, (b) profile view of the aligned arch CMPs in the soil-box, and (c) cross sectional view of the arch CMP.....	110
Figure 4-12 Nuclear density measurement (CUIRE). ....	111

Figure 4-13 The contour plot of the averaged values for the soil moisture content and compaction rate in 8 in. lifts measurement: (a) 1 <sup>st</sup> set of soil box testing, (b) 2 <sup>nd</sup> set of soil box testing, .....	113
Figure 4-14 CMP surface preparation for SAPL installation: (a) dirt and dust on the CMP, .....	115
Figure 4-15 SAPL installation of invert-cut circular CMPs: (a) before SAPL installation (stage 2 of Figure 4-7), (b) after SAPL installation (stage 3 of Figure 4-7), and (c) end strips detachment .....	116
Figure 4-16 Arch CMP preparation for SAPL installation: (a) Arch CMP before gap sealing, (b) the invert-cut gap sealing with Styrofoam and plastic sheets, (c) spraying Sprayroq's polyurethane material inside arch CMPs, (d) prepared pipe prior to the SAPL installation, and (e) the SAPL renewed arch CMPs. ...	116
Figure 4-17 Hand spray SAPL installation. ....	117
Figure 4-18 SAPL installation on circular CMP, CUIRE laboratory, UTA, 10/29/2019: (a) outside of the laboratory, and (b) inside of the soil box. ....	118
Figure 4-19 SAPL sampling for circular CMPs test setup: (a) sample plates prior to the cut into required shape for flexural and tensile test, and (b) the sampling site with Sprayroq installation truck. ....	119
Figure 4-20 Plate sampling from the SAPL batch to provide material test samples.....	120
Figure 4-21 Strain gauges configuration and details: (a) schematic profile view at the crown of the bare circular CMP, (b) schematic profile view at the crown of SAPL renewed circular CMP, (c) physical protection of outer surface strain gauges, and (d) installed strain gauges on the .....	124
Figure 4-22 Strain gauges connected to a data acquisition system (DAQ).....	124
Figure 4-23 Earth pressure cell: (a) Geokon 4800 series, (b) 4 in. distance from the CMP at the springline, and (c) connection to a data acquisition system (DAQ).....	125
Figure 4-24 LVDTs and cable displacement sensors. ....	126
Figure 4-25 LVDT and CDS DAQ, and alternating current (AC) .....	126
Figure 4-26 Pipe Monitoring: (a) cameras used for capturing changes,.....	128
Figure 4-27 Instrumentation: LVDTs, CDSs, DIC targets and cameras inside the pipe sample. ....	128
Figure 4-28 Instrumentation: (a) LVDTs, CDSs, DIC targets and cameras inside the pipe sample,.....	129
Figure 4-29 SAPL thickness measurement: (a) thickness gauge and calibration sample, (b) longitudinal measured locations, (c) circular CMP circumferential measured locations, .....	130



Figure 4-30 The 330-kip MTS actuator hydraulic actuator attached to a reaction steel frame located at the CUIRE Laboratory at the University of Texas at Arlington.....	132
Figure 4-31 Steel load pad: (a) 10 × 20 in., and (b) 20 × 40 in. pad size. ....	133
Figure 4-32 AASHTO-approved live loading specifications for standard H20 trucks .....	134
Figure 4-33 Load distribution below the wheel area ( <i>AASHTO LRFD Bridge Design Specifications 2020</i> ). ....	134
Figure 5-1 CMP movement due to the invert detachment (without any end strips) before loading.....	137
Figure 5-2 60 in. invert-cut circular bare CMP, pipe profiling using DIC technique. ....	138
Figure 5-3 Control test - applied load through the steel load pad versus soil settlement. ....	139
Figure 5-4 Control test - pressure on the soil surface under the load pad versus soil settlement.....	139
Figure 5-5 Control test - pressure on top of the CMP samples vs soil settlement.....	140
Figure 5-6 Results of DIC measurement for 60 in. intact circular CMP: (a) before loading, and (b) after loading at the end of the test.....	141
Figure 5-7 Circular CMP movement due to the invert detachment: (a) the movement mechanism, and (b) The gap closure at the cut location due to vertical loading.....	142
Figure 5-8 60 in. Invert-cut circular CMP soil box testing: (a) before loading, and (b) after loading. ....	143
Figure 5-9 Results of DIC measurement at the end of the test – 60 in. invert-cut circular CMP.....	144
Figure 5-10 Arch CMP movement due to the invert detachment: (a) the movement mechanism, and (b) the uplift of the invert-cut arch CMP after loading and soil compaction.....	145
Figure 5-11 47×71 in. invert-cut arch CMP soil box testing: (a) before loading, and (b) the local buckling failure of the pipe sample after loading. ....	146
Figure 5-12 Results of DIC measurement at the end of the test – 47×71 in. invert-cut arch CMP.....	147
Figure 5-13 Load versus displacement of CMPs at different locations for the control test: (a) intact 60 in. circular CMP under a 10×20 in. steel load pad, (b) invert-cut 60 in. circular CMP under a 20×40 in. steel load pad, and (c) invert-cut 47×71 in. arch CMP under a 20×40 in. steel load pad. ....	149
Figure 5-14 Results of earth pressure cells for the CMP control test: (a) intact circular CMP, (b) invert-cut circular CMP, and (c) invert-cut arch CMP. ....	152

Figure 5-15 Results of strain gauges for the CMP control test: (a) intact circular CMP, (b) invert-cut circular CMP, and (c) invert-cut arch CMP. ....	155
Figure 5-16 Internal forces on intact, invert-cut circular and invert-cut arch CMP samples: (a) bending moment, and (b) thrust forces for the invert-cut arch, invert-cut circular and circular intact CMPs. ....	157
Figure 5-17 Pipe profiling using DIC results before loading and after loading at the ultimate load carrying capacity of the samples: (a) intact CMP, (b) invert-cut circular CMP, and (c) invert-cut arch CMP. ....	159
Figure 5-18 Polymeric SAPL material property test results: (a) flexural test (ASTM D790), .....	160
Figure 5-19 Thickness measurement results of polymeric SAPL renewed circular CMPs: (a) 0.25 in. thick SAPL, (b) 0.5 in. thick SAPL, (c) 1 in. thick SAPL, and (d) measured locations in circumferential and longitudinal direction. ....	162
Figure 5-20 Load vs. displacement results for CMP samples and soil: (a) bare invert cut CMP, (b) 0.25 in. SAPL renewed CMP, (c) 0.5 in. SAPL renewed CMP, and (d) 1 in. SAPL renewed CMP. ....	166
Figure 5-21 Formation of the first structural crack. It shows (a) 0.25 in. SAPL renewed .....	167
Figure 5-22 Load improvement by SAPL application: (a) ultimate load comparison of renewed SAPL circular CMPs with bare CMP, and (b) load comparison of renewed SAPL CMPs.....	169
Figure 5-23 Earth pressure cells' results: (a) bare circular CMP, (b) 0.25 in. SAPL renewed circular CMP (c) 0.5 in. SAPL renewed circular CMP, and (d) 1 in. SAPL renewed circular CMP. ....	172
Figure 5-24 Strain gauge results for SAPL renewed circular CMP: (a) at the crown and (b) around the SAPL at the time of first structural crack. ....	174
Figure 5-25 DIC results of SAPL renewed circular CMP: (a) and (b) bare CMP, (c) and (d) 0.25 in. SAPL renewed CMP, (e) and (f) 0.5 in. SAPL renewed CMP, (g) and (h) 1 in. SAPL renewed CMP. ....	176
Figure 5-26 Pipe profiling using DIC technique at the time of failure: (a) 0.25 in. SAPL, (b) 0.5 in. SAPL, and (c) 1.0 in. SAPL renewed circular CMP. ....	177
Figure 5-27 Thickness measurement results of polymeric SAPL renewed CMPAs: (a) quarter, (b) half, (c) one inch SAPL renewed arch CMPs, and (d) measured locations in circumferential direction.....	179
Figure 5-28 Invert-cut arch CMP end-strip detachment to remove the host pipe's ring stiffness: (a) over-sprayed SAPL and cutting process on the end-strip location, and (b) unbolted end-strip.....	180

Figure 5-29 Bare and SAPL renewed arch CMPs Load-Displacement graphs: (a) invert-cut bare arch CMP, (b) 0.25 in. SAPL renewed arch CMP, (c) 0.5 in. SAPL renewed arch CMP, ..... 184

Figure 5-30 Formation of the first structural crack: (a) 0.25 in. SAPL renewed arch CMP at 29.32 kips, (b) 0.5 in. SAPL renewed arch CMP at 26.27 kips, and (c) 1 in. SAPL renewed arch CMP at 41.08 kips.... 186

Figure 5-31 Fully Invert deteriorated arch CMPs ultimate load carrying capacity improvement ..... 187

Figure 5-32 Pressure vs. crown displacement graphs: (a) invert-cut bare arch CMP, (b) 0.25 in. SAPL renewed arch CMP, (c) 0.5 in. SAPL renewed arch CMP, and (d) 1 in. SAPL renewed arch CMP. .... 190

Figure 5-33 Arch CMP behavior due to the vertical load, where the red boxes show the soil support under the pipe on the west haunch area and the blue boxes illustrates the pipe upward movement. .... 190

Figure 5-34 Strain gauge results: (a) invert-cut bare arch CMP, (b) 0.25 in. SAPL renewed arch CMP, (c) 0.5 in. SAPL renewed arch CMP, (d), 1 in. SAPL renewed arch CMP..... 194

Figure 5-35 Pipe profiling using DIC results: (a) and (b) bare arch CMP, (c) and (d) 0.25 in. SAPL renewed arch CMP, (e) and (f) 0.5 in. SAPL renewed arch CMP, and (g)..... 196

Figure 5-36 Pipe profiling using DIC technique at the time of failure: (a) 0.25 in. SAPL, (b) 0.5 in. SAPL, and (c) 1.0 in. SAPL renewed arch CMPs. .... 197

Figure 6-1 FEM of the SAPL soil box testing showing the boundary conditions (Source: CUIRE). .... 203

Figure 6-2 Comparison of the soil box testing results and FEM with respect to the occurrence of the first crack: (a) plastic strain predicted by FEM (Source: CUIRE FEM report), ..... 204

Figure 6-3 Crack propagation and fracture in 0.25 SAPL at the crown of the pipe at the ultimate load: (a) FEM (Source: CUIRE FEM report), and (b) SAPL soil box testing results. .... 205

Figure 6-4 SAPL Deflection at the ultimate load at the crown of the pipe: (a) FEM results (Source: CUIRE FEM report), and (b) DIC results of pipe profiling (0.25 in. SAPL). .... 206

Figure 6-5 Load versus displacement – comparison of soil box testing results and FEM (Source: CUIRE FEM report) results (0.25 in. SAPL)..... 206

Figure 6-6 The comparison of soil box testing results and FEM (Source: CUIRE FEM report) results for distributed pressure on top of the pipe versus displacement at the crown location (0.25 in. SAPL)..... 208

Figure 6-7 The comparison of soil box testing results and FEM (Source: CUIRE FEM report) results for the applied load on the soil surface versus distributed pressure on top of the pipe ..... 208

Figure 6-8 Crack propagation and fracture in 0.5 SAPL at the crown of the pipe at ultimate load condition: (a) FEM (Source: CUIRE FEM report), and (b) SAPL soil box testing results..... 209

Figure 6-9 SAPL Deflection at the ultimate load at the crown of the pipe: (a) FEM results (Source: CUIRE FEM report), and (b) DIC results (0.5 in. SAPL). ..... 210

Figure 6-10 Load versus displacement – comparison of soil box testing and FEM results (0.5 in. SAPL). ..... 210

Figure 6-11 The comparison of soil box testing results and FEM (Source: CUIRE FEM report) results for distributed pressure on top of the pipe versus displacement at the crown location (0.5 in. SAPL). ..... 212

Figure 6-12 The comparison of soil box testing results and FEM (Source: CUIRE FEM report) results for the applied load on the soil surface versus distributed pressure on top of the pipe ..... 212

Figure 6-13 Occurrence of first plastic strain in 1.0 in. SAPL at the crown of the pipe: (a) FEM (Source: CUIRE FEM report), and (b) SAPL soil box testing results. .... 213

Figure 6-14 SAPL Ultimate load condition: (a) Von Mises stress around the SAPL (Source: CUIRE FEM report), and (b) crack propagation and fracture at the crown of the pipe (1.0 in. SAPL). ..... 213

Figure 6-15 SAPL Deflection at the ultimate load at the crown of the pipe: ..... 214

Figure 6-16 Load versus displacement – comparison of soil box testing results and FEM (Source: CUIRE FEM report) results (0.1 in. SAPL). ..... 215

Figure 6-17 The comparison of soil box testing results and FEM (Source: CUIRE FEM report) results for distributed pressure on top of the pipe versus displacement at the crown location (1.0 in. SAPL). ..... 216

Figure 6-18 The comparison of soil box testing results and FEM (Source: CUIRE FEM report) results for the applied load on the soil surface versus distributed pressure on top of the pipe ..... 216

Figure 6-19 the fully deteriorated invert circular CMP renewed with SAPL: (a), (c) and (e) formation of the plastic strain at the crown of the pipe, and (b), (d) and (f) SAPL. Deflection ..... 217

Figure 6-20 Load versus displacement – FEM results for 0.75, 1.5, and 2.0 in. SAPLs ..... 219

Figure 6-21 Load versus displacement plots – comparison of different SAPL thicknesses installed inside the fully deteriorated invert circular CMPs (Source of FEM: CUIRE FEM report). ..... 220

Figure 6-22 The deflection comparison soil box testing results and FEM (Source: CUIRE FEM report) for 0.25 in. SAPL, installed inside the fully deteriorated invert arch CMP, ..... 221

Figure 6-23 FEM results – stress distribution at the ultimate load for 0.25 in. SAPL: ..... 222

Figure 6-24 Load versus displacement – comparison of SAPL soil box testing and the FEM (Source: CUIRE FEM report) results for 0.25 in. SAPL installed inside the ..... 223

Figure 6-25 The comparison of soil box testing results and FEM (Source: CUIRE FEM report) results for distributed pressure on top of the pipe versus displacement at the crown location (0.25 in. SAPL). ..... 224

Figure 6-26 The comparison of soil box testing results and FEM (Source: CUIRE FEM report) results for the applied load on the soil surface versus distributed pressure on top of the pipe ..... 225

Figure 6-27 The deflection comparison of FEM simulation (Source: CUIRE FEM report) and soil box testing results for 0.25 in. SAPL, installed inside the fully deteriorated invert arch CMP, ..... 226

Figure 6-28 Load versus displacement – comparison of SAPL soil box testing and the FEM (Source: CUIRE FEM report) results for 0.5 in. SAPL installed inside the fully ..... 227

Figure 6-29 The comparison of soil box testing results and FEM (Source: CUIRE FEM report) results for distributed pressure on top of the pipe versus displacement at the crown location (0.5 in. SAPL). ..... 228

Figure 6-30 The comparison of soil box testing results and FEM (Source: CUIRE FEM report) results for the applied load on the soil surface versus distributed pressure on top of the pipe ..... 229

Figure 6-31 The deflection comparison of FEM simulation (Source: CUIRE FEM report) and soil box testing results for 0.25 in. SAPL, installed inside the fully deteriorated invert arch CMP, ..... 230

Figure 6-32 Load versus displacement – comparison of SAPL soil box testing and the FEM (Source: CUIRE FEM report) results for 1.0 in. SAPL installed inside the ..... 232

Figure 6-33 The comparison of soil box testing results and FEM (Source: CUIRE FEM report) results for distributed pressure on top of the pipe versus displacement at the crown location (1.0 in. SAPL). ..... 232

Figure 6-34 The comparison of soil box testing results and FEM (Source: CUIRE FEM report) results for the applied load on the soil surface versus distributed pressure on top of the pipe ..... 233

Figure 6-35 the fully deteriorated invert arch CMP samples renewed with SAPL: (a), (c) and (e) formation of the plastic strain at the crown of the pipe, and (b), (d) and (f) SAPL deflection at the crown of the pipe (Source: CUIRE FEM report). ..... 234

Figure 6-36 Load versus displacement – FEM results for 0.75, 1.5, and 2.0 in. SAPLs ..... 236

Figure 6-37 Load versus displacement plots – comparison of different SAPL thicknesses installed inside the fully deteriorated invert arch CMP samples (Source: CUIRE FEM report).....	237
Figure 7-1 Details of corrugated metal pipe for calculation of the moment of inertia ( $I$ ). .....	245
Figure 7-2 Normal probability plot of the linear regression predictive model.....	247
Figure 7-3 The $Y$ (values obtained from the adapted CIPP design equation using ( $I$ ) for the corrugated geometry) and the predicted $Y$ (test results) using the predictive model.....	247
Figure 7-4 Residual analysis using a linear regression compared to the test data. ....	247
Figure 7-5 Normal probability plot of the linear regression predictive model.....	248
Figure 7-6 The $Y$ (values obtained from the adapted AWWA C950 design equation using ( $I$ ) for the corrugated geometry) and the predicted $Y$ (test results) using the predictive model. ....	249
Figure 7-7 Residual analysis using a linear regression compared to the test data. ....	249
Figure 7-8 Comparison of the potential design equations, modified design equations .....	250

## List of Tables

Table 1-1 Resistance factor. ....	18
Table 2-1 Structural classification of flexible liners used for sewer pipes according to four national and international standards. ....	69
Table 3-1 List of selected SAPL culverts for field inspection. ....	76
Table 3-2 SAPL and existing culvert defects. ....	78
Table 3-3 SAPL field inspection findings. ....	80
Table 3-4 SAPLs' issues found for each culvert. ....	82
Table 3-5 Rating modifier values. ....	85
Table 3-6 Rating scale to evaluate general conditions of SAPLs. ....	86
Table 3-7 SAPLs overall average rating score (OAR) and adjusted overall structural rating score (AOR). ....	89
Table 3-8 Comparative status of cementitious and geopolymer SAPLs (according to OAR). ....	91
Table 3-9 Summary of findings and recommendations. ....	94
Table 3-10 Inspection plan. ....	95
Table 4-1 List of experimental soil box testing and pipe samples. ....	102
Table 4-2 Burial configuration details. ....	107
Table 4-3 Instrumentation. ....	122
Table 4-4 Details of specimens used for flexural and tensile properties testing. ....	131
Table 4-5 LRFD wheel contact area dimensional increase factor ( <i>AASHTO LRFD Bridge Design Specifications 2020</i> ). ....	135
Table 4-6 Live load distribution of $1.15 \times H$ for select granular fill. ....	135
Table 5-1 Control test of bare CMPs - the ultimate load and pressure and the maximum displacement at the time of failure. ....	153
Table 5-2 The circular CMPs' load bearing capacity, crown deflection and the soil displacement at initial crack and failure. ....	168
Table 5-3 Soil pressure results around the circular CMPs at the time of failure. ....	170

Table 5-4 The circular CMPs' load bearing capacity, crown deflection and the soil displacement at initial crack and failure. ....	191
Table 5-5 Soil pressure results around the arch CMPs at the time of failure. ....	191
Table 6-1 Soil properties used in ABAQUS (Source: CUIRE FEM report). ....	203
Table 6-2 Load-displacement results – comparison of SAPL soil box testing and FEM (Source: CUIRE FEM report) at the time of first crack and ultimate load (0.25 in. SAPL). ....	207
Table 6-3 The comparison of soil box testing results and the FEM predicted pressure value at the time of first crack on top of the pipe (0.25 in. SAPL). ....	207
Table 6-4 Load-displacement results – comparison of SAPL soil box testing and FEM (Source: CUIRE FEM report) at the time of first crack and ultimate load (0.5 in. SAPL). ....	211
Table 6-5 Load-displacement results – comparison of SAPL soil box testing and FEM (Source: CUIRE FEM report) at the time of the first crack and the ultimate load (1.0 in. SAPL). ....	215
Table 6-6 FEM results for the simulated 0.75, 1.5, and 2.0 in. thicknesses of SAPL (Source: CUIRE FEM report).....	218
Table 6-7 Load-displacement results – comparison of SAPL soil box testing and FEM (Source: CUIRE FEM report) at the time of the first crack and the ultimate load (0.25 in. SAPL). ....	223
Table 6-8 Load-displacement results – comparison of SAPL soil box testing results and FEM (Source: CUIRE FEM report) results at the time of the first crack and the ultimate load (0.5 in. SAPL). ....	228
Table 6-9 Load-displacement results – comparison of SAPL soil box testing results and FEM (Source: CUIRE FEM report) results at the time of the first crack and the ultimate load (1.0 in. SAPL). ....	231
Table 6-10 FEM results for the simulated 0.75, 1.5, and 2.0 in. thicknesses of SAPL (Source: CUIRE FEM report).....	235
Table 7-1 Existing design equations and theories to calculate the critical buckling pressure on flexible pipes. ....	239
Table 7-2 Live load distribution factor for buried structures ( <i>AASHTO LRFD Bridge Design Specifications</i> 2020). ....	240
Table 7-3 SAPL moment of inertia for the tested SAPL thicknesses. ....	246



Table A- 1 Ohio DOT, site 1, SAPL inspection information and photos. ....	270
Table A- 2 Ohio DOT, site 2, SAPL inspection information and photos. ....	271
Table A- 3 Ohio DOT, site 3, SAPL inspection information and photos. ....	272
Table A- 4 Ohio DOT, site 4, SAPL inspection information and photos. ....	272
Table A- 5 Ohio DOT, site 5, SAPL inspection information and photos. ....	273
Table A- 6 PennDOT, site 6, SAPL inspection information and photos. ....	274
Table A- 7 NYSDOT, site 7, SAPL inspection information and photos. ....	275
Table A- 8 DeIDOT, site 8, SAPL inspection information and photos. ....	276
Table A- 9 DeIDOT, site 9, SAPL inspection information and photos. ....	277
Table A- 10 NCDOT, site 10, SAPL inspection information and photos. ....	278
Table A- 11 NCDOT, site 11, SAPL inspection information and photos. ....	279
Table A- 12 NCDOT, site 12, SAPL inspection information and photos. ....	280
Table A- 13 NCDOT, site 13, SAPL inspection information and photos. ....	281
Table A- 14 NCDOT, site 14, SAPL inspection information and photos. ....	282
Table A- 15 NCDOT, site 15, SAPL inspection information and photos. ....	283
Table A- 16 MnDOT, site 16, SAPL inspection information and photos. ....	284
Table A- 17 MnDOT, Site 17, SAPL inspection information and photos. ....	285
Table A- 18 MnDOT, site 18, SAPL inspection information and photos. ....	286
Table A- 19 FLDOT, site 19, SAPL inspection information and photos. ....	287
Table A- 20 FLDOT, site 20, SAPL inspection information and photos. ....	288

# Chapter 1

## Introduction and Background

Drainage infrastructure systems including culverts, storm sewers, outfall and related drainage elements represent an integral portion of Department of Transportations' assets that routinely require inspection, maintenance, repair, and renewal. According to ASCE Infrastructure Report Card (2017), illustrated in Figure 1-1, America's cumulative infrastructure grade is D+, which means the condition and performance is in a poor quality and needs investments and improvements. Failure of these systems is costly for DOTs both directly due to the replacement of the failed system and indirectly due to the time and money and even in some cases lives lost for commuters. Therefore, drainage infrastructure systems need special attention in terms of proactive/preventive asset management strategy.

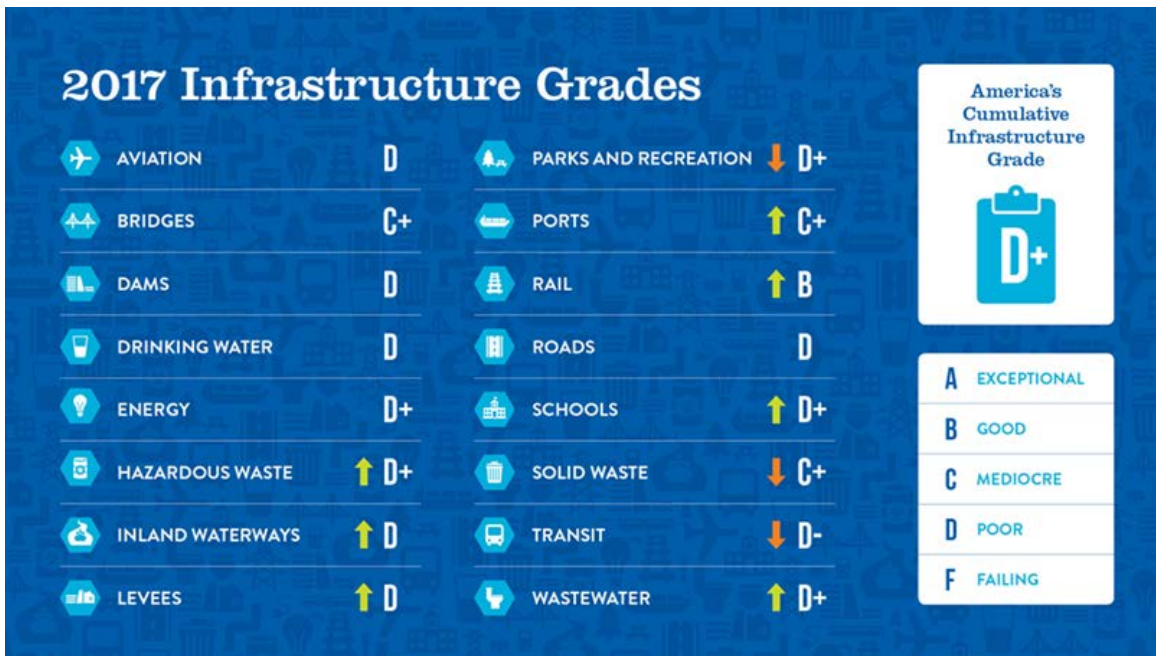


Figure 1-1 American society of civil engineers' report card for America's infrastructure (2017).

### 1.1 Culverts and Storm Sewers

Culverts and storm sewers are important components of highway infrastructures. Corrugated metal pipes (CMPs) and reinforced concrete pipes (RCPs) are commonly used as culverts in the United States (Darabnough Tehrani et al. 2019). Assessment and Rehabilitation of Existing Culverts by the National

Cooperative Highway Research Program (NCHRP), Synthesis 303, defines storm sewers as any “structure used to convey storm runoff where storm sewers and storm drains are connected, that sometimes called a pipe or culvert”. Culvert is a structure that conveys water or forms a passageway through an embankment (Najafi and Gokhale 2005). According to the federal highway administration (FHWA), the United States has approximately 4.12 million miles (6.63 million kilometers) of roadways, making it the largest in the world with millions of culverts hidden underneath. Culvert Management Manual by Ohio Department of Transportation (ODOT) defines culverts as “any structure that conveys water or forms a passageway through an embankment and is designed to support a super-imposed earth load or other fill material plus live loads (even though they may support traffic loads directly) with a span, diameter, or multi-cell (with a total span) less than 10 ft (3.1 m) when measured parallel to the centerline of the roadway,” as shown in Figure 1-2 (ODOT 2018). Culverts are designed to withstand soil overburden, pavement and traffic loadings. Among different types of culverts, Corrugated Metal Pipes (CMPs) are most common in the United States, however, they are exposed to abrasion and corrosion damage (Arnoult 1986). Many culverts in the United States have reached their service life and they need to be repaired, renewed, or replaced (Wyant 2002).



Figure 1-2 Corrugated metal pipe culverts (CMPs): (a) multi-cell CMPs (Source: Contech), and (b) invert deteriorated CMP (Source: Metal Culverts Inc.).

**1.1.1 Culvert Shapes**

Culverts are available in variety of shapes for both, closed conduits, and open-bottom conduits. The most common shapes of closed conduits are circular, box (rectangular), elliptical, and pipe-arch, as illustrated in Figure 1-4 (a). However, the open-bottom culverts are mostly in arch configuration, as illustrated in Figure 1-3 (b). These typical culvert shapes have the same material on the entire perimeter (FHWA 2012).

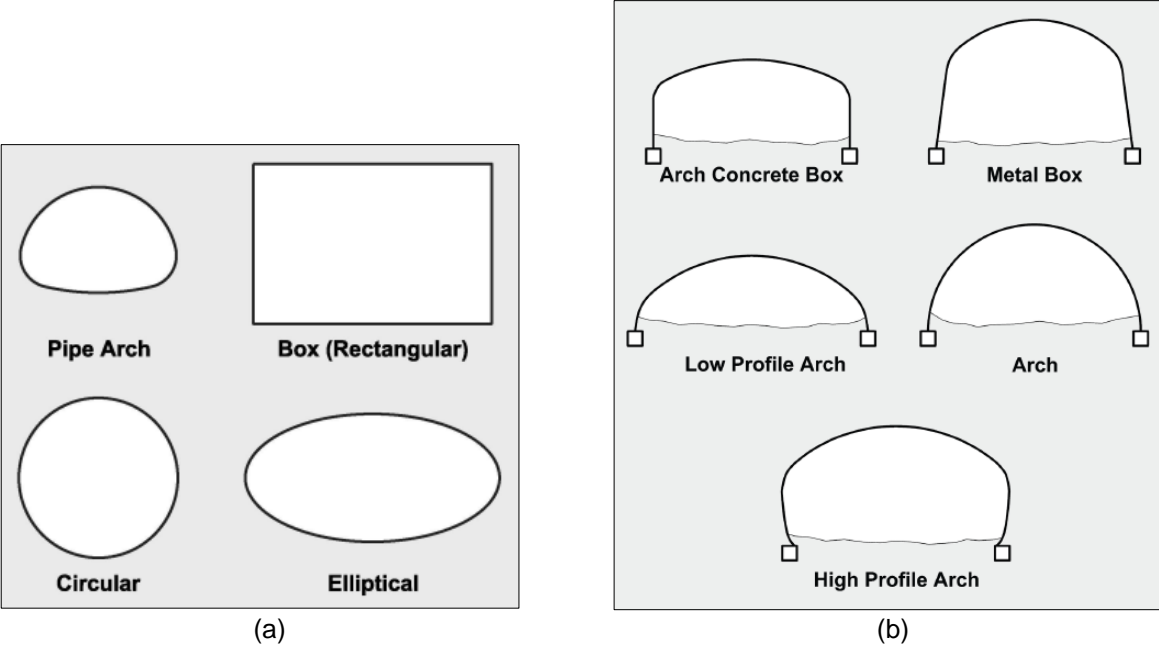


Figure 1-4 Commonly used culvert shapes: (a) closed conduit culvert shapes, and (b) open-bottom culvert shapes (FHWA 2012).

**1.1.2 Culvert Materials**

According to the culvert management manual by Ohio Department of Transportation (ODOT 2018), the most commonly used culvert materials are plain or reinforced concrete, corrugated metal (aluminum or steel), verified clay, cast or ductile iron, aluminum alloy, brick, field tile (clay), corrugated plastic, steel casing, stone, timber, polyvinyl chloride (PVC) and high-density polyethylene (HDPE), as illustrated in Figure 1-5. The selection of a culvert material may depend upon structural strength, hydraulic roughness, durability (corrosion and abrasion resistance) and constructability (FHWA 2012).



Figure 1-5 Culvert materials (ODOT 2018).

**1.1.3 Culvert Hydraulics and Flow Conditions**

Culvert may flow partly full (free surface flow or open channel flow), or full over the entire length (full flow or pressure flow) which rarely happens. Water surface profile calculation determines the flow level in the culvert barrel (FHWA 2012). Froude number,  $F_r$  (dimensionless), determines the appropriate flow regime, as presented in Eq. 1-1.

$$F_r = \frac{v}{\sqrt{gy}} \tag{Eq. 1-1}$$

where,

$v$  = the average velocity of flow, ft/s,

$g$  = the gravitational acceleration, ft/s<sup>2</sup>, and

$y$  = a representative depth, ft, (typically the equivalent depth in circular sections or the hydraulic depth for other shapes).

In circular section the equivalent depth is the square root of one-half of the cross-sectional flow area  $(A/2)^{0.5}$  and for other shapes the hydraulic depth is cross-sectional flow area divided by the width of the free water surface  $(A/T)$ . By evaluating the Froude number, three flow regimes are defined as subcritical, critical, and supercritical. The flow is considered subcritical and is characterized as tranquil if the Froude number,  $F_r$  is less than 1, and is called critical if Froude number,  $F_r$  is equal to 1. The flow is called supercritical and is characterized as rapid if the Froude number,  $F_r$  is greater than 1. For a culvert in a partly full flow condition, as illustrated in Figure 1-6, the subcritical flow exists in the upstream channel, the critical depth occurs at the inlet location and the supercritical flow in the culvert barrel (FHWA 2012).

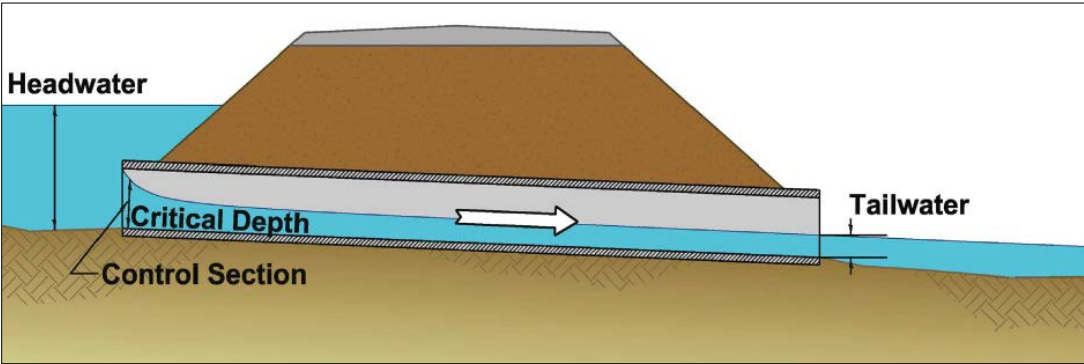


Figure 1-6 Typical “inlet control” flow section for a partly full culvert (FHWA 2012).

**1.1.4 Types of Flow Control**

A culvert capacity is affected by its shape, geometry, skew angle of inlet, and most importantly the inlet edge configuration. Two types of flow control in a culvert are called inlet control and outlet control.

**1.1.4.1 Inlet Control**

The culvert is called “inlet control” flow condition if its barrel can convey more flow than the inlet will accept. The critical depth for an inlet control culvert occurs at entrance, as illustrated in Figure 1-6. In the inlet control condition, the culvert capacity is not impacted by downstream hydraulic characteristics.

**1.1.4.2 Outlet Control**

The culvert is called “outlet control” flow condition if its barrel capacity is not enough to convey as much flow as the inlet will receive. In an outlet control flow condition, the culvert capacity is determined by its geometry, hydraulic characteristics, and the elevation of water surface at the outlet. In an “outlet control” flow condition, the control section is located at the culvert downstream, as illustrated in Figure 1-7. Full flow culverts (pressure flow) or subcritical flow culverts are considered as outlet control conditions (FHWA 2012; Wisconsin DOT 1997).

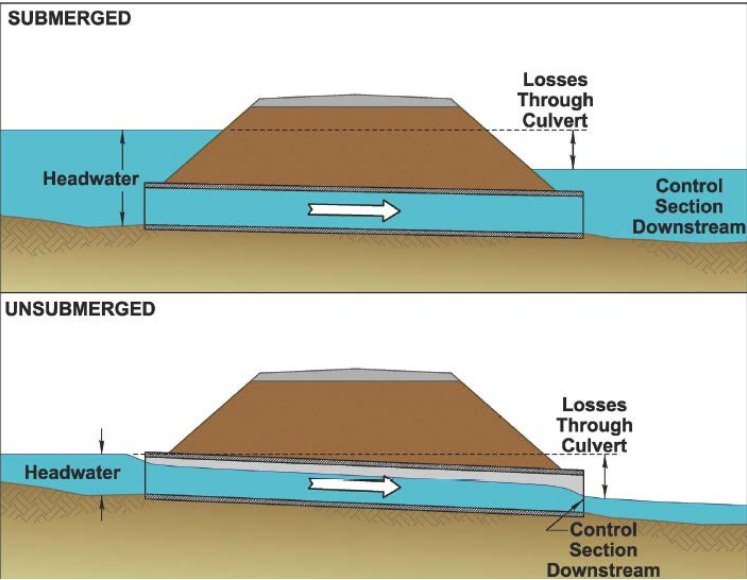


Figure 1-7 Typical “outlet control” flow in both full flow (submerged) and partly full flow (unsubmerged) conditions (FHWA 2012).

### **1.1.5 Culvert Structural Behavior**

Buried conduits obtain their structural capacity to withstand the imposed loads from two sources (Spangler 1960):

- (a) The inherent strength of the pipe to bear the external pressures.
- (b) The lateral pressure of the soil at the pipe sides.

Pipe culverts structurally can be classified as flexible and rigid, based on material type and how they perform when installed (Hydraulics Manual M 23-03.06 2019). A proper backfill is required for both flexible and rigid pipes to allow the load transfer from the pipe to the soil. Flexible pipes under loading deflect against the backfill, and the load is transferred to and carried by the backfill. In case of rigid pipes under loading, the load is transferred through the pipe wall into the bedding material (Omara 1997).

#### **1.1.5.1 Flexible Pipe**

Flexible pipes are made of materials such as corrugated metal or thermoplastic. Flexible pipes can be flexed or distorted significantly without cracking (Hydraulics Manual M 23-03.06 2019). A flexible culvert is a composite structure of culvert barrel and the surrounding soil (Najafi 2008). Proper soil support is an important element to the flexible culvert structural performance. Soil support degradation and embankment settlement can occur due to soil erosion and scour through the culvert voids, poor backfill material, inadequate compaction, lack of headwall or cutoff walls in granular soil types and insufficient surface drainage design (FHWA 2012). Flexible pipes under loading attempt to deflect. In case of a circular flexible pipe under loading, the vertical diameter decreases and the horizontal diameter increases, as shown in Figure 1-8. Soil pressure resists the increase in horizontal diameter of a flexible pipe due to loading. The thrust force can be calculated, based on the diameter of the pipe and the load placed on the top of the pipe.



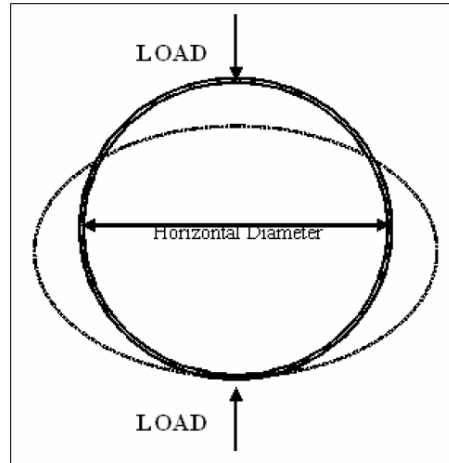
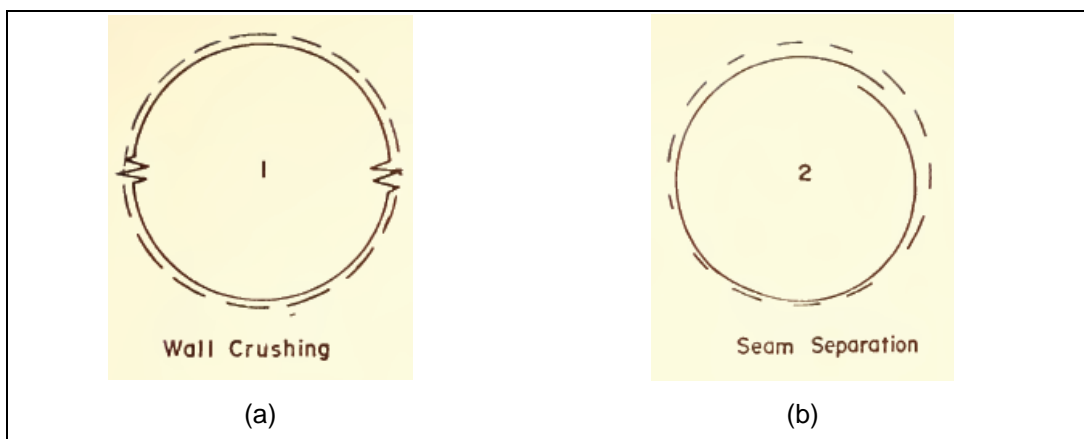


Figure 1-8 Deflection of a circular flexible pipe (Najafi 2008).

#### 1.1.5.1.1 Flexible Pipe Modes of Failure

Flexible conduits, as illustrated in Figure 1-9 are designed to withstand five primary modes of failure including:

- 1) Wall crushing (compressive stress due to circumferential thrust exceeds the yield stress),
- 2) Separation of seams (thrust exceed the seam strength),
- 3) Initial buckling (elastic state of stress),
- 4) Inelastic buckling, and
- 5) Excessive deflection or flattening (plastic yielding under combined compressive and bending stresses) (Leonards and Stetkar 1978).



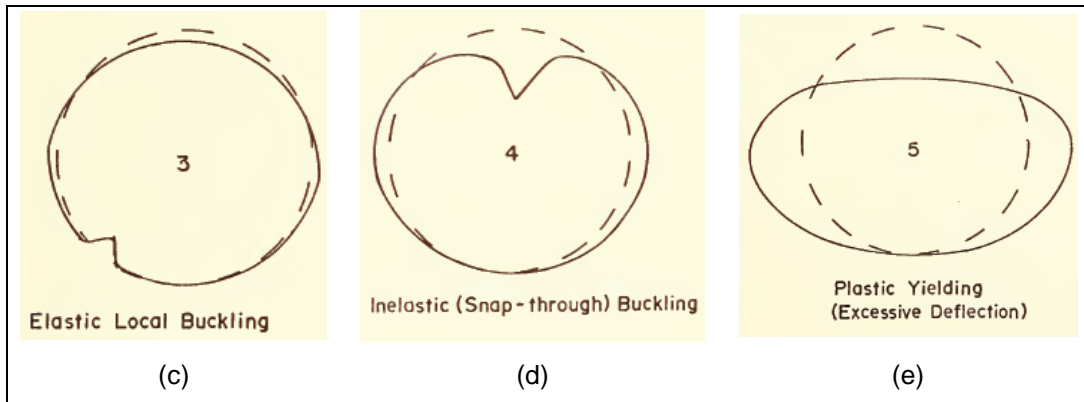


Figure 1-9 Failure modes of flexible conduits: (a) wall crushing, (b) seam separation, (c) elastic local buckling, (d) inelastic (snap-through) buckling, and (e) plastic yielding (excessive deflection) (Leonards and Stetkar 1978).

For the first two modes of failures, the magnitude of circumferential thrust can be less impacted by the soil properties or pipe stiffness. For initial buckling, inelastic buckling and excessive modes of failures, the pipe bending stress is impacted by soil properties and pipe stiffness.

**Elastic Buckling**

Elastic buckling of flexible conduits can occur in a high mode with many waves around the pipe circumference, or in a low mode with a small number of waves around the entire circumference. Elastic local buckling can occur with a crimp or crease in a small portion of the pipe circumference. A flexible conduit due to the residual stresses and geometric imperfection can exhibit different types of elastic buckling which cannot be easily distinguished by visual inspection (Leonards and Stetkar 1978).

**Inelastic Buckling**

Inelastic buckling of a flexible conduit wall occurs in a low mode after passing the plastic yielding point. Snap-through buckling of a flexible conduit can manifest itself as a sudden inversion or curvature reversal in the pipe wall that can results in instability. Local buckling of a flexible conduit wall may not immediately results in instability (Leonards and Stetkar 1978).

### 1.1.5.1.2 *Buckling Theories of Cylindrical Shells or Rings*

Shell elements are used to model structures in which one dimension, the thickness, is significantly smaller than the other dimensions. The thickness of a cylindrical shell element is very small compared with the radii of curvature. The following have presented different theories regarding buckling of cylindrical shells or rings:

#### a) **Timoshenko and Gere 1961** (Elastic Buckling in High Modes)

Buckling of buried flexible conduits was modeled by a circular ring subjected to a uniform hydrostatic external pressure and the critical external normal pressure,  $p$ , was derived by Timoshenko and Gere (1961) and given as Eq. 1-2 .

$$P_c = \frac{EI(n^2-1)}{R^3} \quad \text{Eq. 1-2}$$

where,

$E$  = Young's modulus, psi,

$I$  = moment of inertia of ring wall, in.<sup>4</sup>/in.

$R$  = radius, in.

$n$  = buckling mode =  $\frac{\pi R}{l}$ , where  $l$  = half wavelength of the buckled shape.

The Eq. 1-2 is resulted from the equilibrium of a deformed ring element in which only circumferential stresses were considered by Timoshenko and Gere. In this equation nonlinear deflection terms were neglected (Leonards and Stetkar 1978).

#### b) **Klöppel and Glock 1970** (Elastic Local Buckling)

For flexible steel pipes, vertical deflection to a magnitude of 20% of the pipe diameter results in conduit instability (Spangler 1941). Spangler stated that using a safety factor of 4, limits the permissible vertical deflection to 5 percent of the pipe diameter that is a criterion in culvert design.

The instability of initially deflected buried flexible conduits was developed by Kloppel and Glock (1970). Two interaction zones at the crown (upper portion of the conduit wall) and springline (lower portion of the conduit wall) of the flexible buried conduits are introduced by them. At the upper portion interaction zone, the pipe wall is subjected to active earth pressure and deflects away from the surrounding soil. At the lower portion interaction zone, the pipe wall is subjected to the passive pressure and deflects or presses

into the surrounding soil. An instability is most probable to occur at the crown or upper portion interaction zone due to a reduction in the soil support (Klöppel and Glock 1970; Leonards and Stetkar 1978). Klöppel and Glock (1987) modeled the upper portion interaction zone of a buried flexible conduit wall by a hinged arch with circumferential radial elastic soil support  $\left[\frac{E_s}{R(1+\nu_s)}\right]$  as well as tangential ( $K_T$ ) and rotational ( $K_R$ ) elastic soil support at hinges that are restrained by the lower section of conduit (Leonards and Stetkar 1978). The developed model by Klöppel and Glock considered:

- i. Elliptical flexible conduits as well as circular flexible conduits,
- ii. Friction at the conduit-soil interface,
- iii. Nonuniform radial pressures having a maximum value at the crown (hence, buckling was always initiated at the crown),
- iv. Modulus of soil restraint either constant or stress-level dependent,
- v. Symmetric displacements prior to buckling,
- vi. The influence of a plastic hinge at the crown.

The horizontal active pressure at the springline was given by Eq. 1-3.

$$P_{springline} = P_S \lambda \quad \text{Eq. 1-3}$$

where,

$P_S$  = the vertical crown pressure (overburden pressure + live load pressure), psi, and

$\lambda$  = coefficient of active earth pressure (commonly  $\lambda=0.5$ ).

The active radial pressure distribution around the conduit circumference, as illustrated in Figure 1-10 (a), was expressed by Eq. 1-4.

$$P = P_S \cos \left[ \frac{\pi}{2} \cdot \frac{\psi}{\psi_B} \right] \quad \text{Eq. 1-4}$$

$$\psi_B = \frac{\pi^2}{4 \cos^{-1} \lambda} \quad \text{Eq. 1-5}$$

Assuming the common value of  $\lambda = 0.5$ , the  $\psi_B$  will be equal to  $\frac{3\pi}{4}$  radians.

In order to solve the instability issue, an arch section of the conduit (defined by  $2 \phi_o$ ), as illustrated in Figure 1-10 (b), was analyzed by Klöppel and Glock. The provided restraint by the bottom portion of the conduit was introduced by rotational ( $K_R$ ) and tangential ( $K_T$ ) elastic moduli at the arch supports. The

boundary pressure distribution around the conduit circumference on the arch section was divided into a uniform pressure of  $P_0$ , and a nonuniform pressure of  $P_1$ , as described in Figure 1-7.

$$P = P_0 + P_1 \sin \left[ \frac{\pi}{2} \cdot \frac{\phi}{\phi_0} \right] \quad \text{Eq. 1-6}$$

where,

$$P_0 = P_s \cos \frac{\pi \phi_0}{2 \psi_B}, \text{ and}$$

$$P_s = P_0 + P_1 = \text{vertical overburden plus live load pressures at crown, psi.}$$

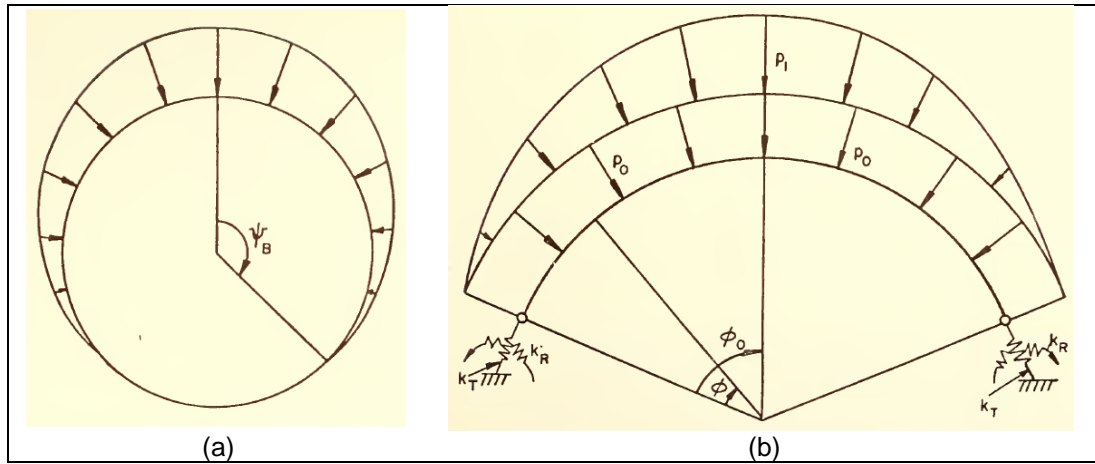


Figure 1-10 Active pressure distribution around circular conduit  
(Klöppel and Glock 1970; Leonards and Stetkar 1978).

**c) Cheney (1971)**

Cheney (1963) studied the hydrostatic buckling pressure of a thin ring encased in rigid cavity using the small-deflection linear theory. He analyzed the stability of a circular ring under plane stress conditions, subject to circumferential support by elastic springs, under a uniform external pressure distribution on the ring wall. Cheney's model is presented by Eq. 1-7.

$$P_{cr} = \frac{(K_{cr}^2)EI}{R^3} \quad \text{Eq. 1-7}$$

where,

$P_{cr}$  = critical buckling pressure (psi),

$$K_{cr} = 1.57(R/i)^{2/5},$$

$i$  = radius of gyration, in.,

$R$  = radius of the ring, in.,

$E$  = Young's modulus, psi,

$I$  = Modulus of Elasticity, in.<sup>4</sup>/in.

For relatively thin infinitely long pipes (e.g., SDR > 30), the critical pressure can be expressed as Eq. 1-8.

$$P_{cr} = \frac{2.55E}{1-\nu^2} \left(\frac{t}{D}\right)^{11/5} \quad \text{Eq. 1-8}$$

where,

$P_{cr}$  = critical buckling pressure, psi,

$t$  = thickness of the ring, in.,

$D$  = diameter of the ring, in.,

$E$  = Young's modulus, psi,

$I$  = Modulus of Elasticity, in.<sup>4</sup>/in.

$\nu$  = Poisson's ratio.

**d) Bresse (1866)**

Bresse (1866), using the small deflection theory, studied the stability of a thin unconstrained circular ring under external hydrostatic pressure, as it is given by Eq. 1-9. Bresse's model is illustrated in Figure 1-11.

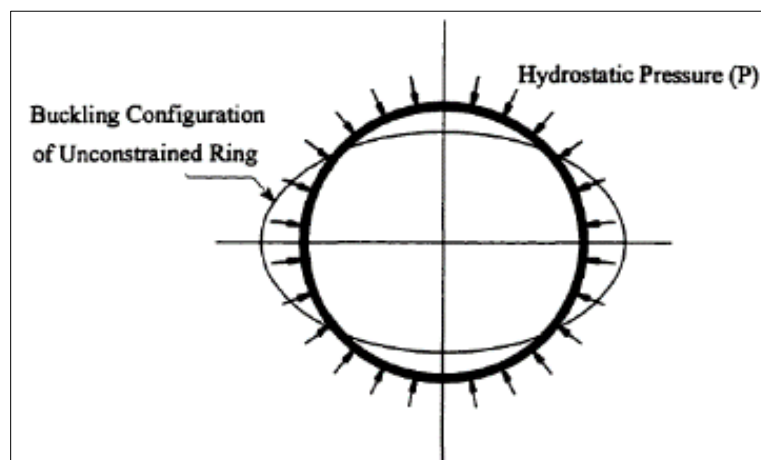


Figure 1-11 Bresse Model for calculating the critical buckling pressure of a thin unconstrained circular ring under external hydrostatic pressure.

$$P_{cr} = \frac{3EI}{R^3} \quad \text{Eq. 1-9}$$

where,

$P_{cr}$  = critical buckling pressure, psi,

$E$  = Young's modulus, psi,

$I$  = Modulus of Elasticity, in.<sup>4</sup>/in.

**e) G.H. Bryan (1888)**

G. H. Bryan (1888), using the minimum potential energy criterion of stability, studied the critical buckling pressure for an infinitely long free-standing pipe under hydrostatic external pressure, as it is given by Eq. 1-10. In this equation the term of  $\frac{E}{(1-\nu^2)}$  accounts for the plain strain condition of the infinitely long pipe.

$$P_{cr} = \frac{2E}{(1-\nu^2)} \left(\frac{t}{D}\right)^3 \quad \text{Eq. 1-10}$$

where,

$P_{cr}$  = critical buckling pressure, psi,

$t$  = thickness of the ring, in.,

$D$  = diameter of the ring, in.,

$E$  = Young's modulus, psi,

$I$  = Modulus of Elasticity, in.<sup>4</sup>/in.

$\nu$  = Poisson's ratio.

**1.1.5.2 Rigid Pipe**

Rigid pipes are stiff and do not deflect appreciably. Rigid pipes are unable to deflect more than 2% without significant structural distress such as cracking (Omara 1997).

Rigid pipes are made of materials such as concrete that provides the primary resistance to bending. The load carrying capacity of a rigid pipe is provided by the structural strength of the pipe itself, with some additional support from the surrounding bedding and backfill. A rigid pipe under vertical loads, that is prone to tension and compression in different zones, is illustrated in Figure 1-12. Steel reinforcement can be added to the tension zones to enhance the tensile strength of a concrete pipe. A rigid pipe is stiffer than the surrounding soil and it carries a substantial portion of the applied load. Shear stress in the haunch area can be critical for heavily loaded rigid pipe on hard foundations, especially if the haunch support is inadequate

(Hydraulics Manual M 23-03.06 2019). The performance of rigid pipes is dependent on foundation and bedding stability (AASHTO LRFD Bridge Design Specifications 2020).

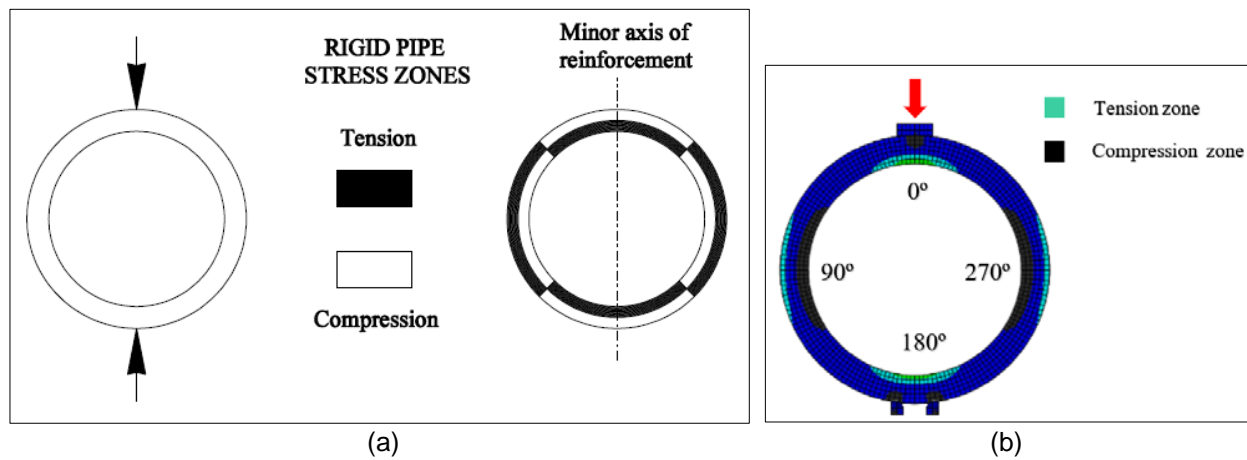


Figure 1-12 Rigid Pipes under vertical loading: (a) rigid pipe stress zones (Hydraulics Manual M 23-03.06 2019), and (b) finite element modeling of a rigid reinforced concrete pipe (RCP) (Darabnoush Tehrani 2016).

## 1.2 Corrugated Metal Pipe Culverts (CMPs)

Corrugated metal pipe (CMPs) and concrete culverts have been in service in the U.S. pipeline system for more than 70 years. Availability of CMPs in variety of shapes and sizes, and modification capability to increase their durability has made this material preferable in many sites. CMPs are ideal for shipping due to their light weight and are easy for assembly and installation. However, CMPs are sensitive to high or low soil pH or water pH which may result in CMP corrosion. Due to presence of sand and/or rock in a high velocity stream, abrasion may cause loss of CMP metal (Najafi 2008). The following sections will focus on CMP, as it is topic of this dissertation.

### 1.2.1 CMP Types and Corrugation Profiles

There are generally three types of CMPs: helical, spiral rib, and annular CMP (Darabnoush Tehrani et al. 2019). Helical CMP is a corrugated tube, fabricated with a tube-shaped shell in a spiral arrangement, as illustrated in Figure 1-13 (a). Spiral rib CMP is similar to helical CMP, where the pipe is manufactured from a continuous metallic strip passed through a roll forming line that forms the external ribs, edges and



joined by lock seaming, as illustrated in Figure 1-13 (b) (NCSPA 2017). The annular CMP is usually fabricated from bent hot-dip galvanized steel<sup>1</sup> sheets along their edges using bolts or rivets, as illustrated in Figure 1-13 (c). CMP, due to its corrugation profile, has higher hoop and bending strengths compared with a same thickness plane steel pipe. Several CMP profiles have been used across the North America since its introduction in 1896, which are the 1½×¼ in., 2⅔×½ in., 3×1 in., and 5×1 in. The CMP industry later added the 6×2 in. metal sheets for erecting pipe arch structures of sizes 61 in. by 55 in., and larger. From these available sizes, the most common encountered corrugation profiles are the 2⅔×½ in., 3×1 in., and 6×2 in. Common CMP corrugation profiles in the North America are presented in Table 1- 1. The 2⅔×½ in. and 3×1 in. corrugation profiles may have a riveted construction (annular corrugations) or lock seam construction (helically wound corrugations), while the 6×2-in. corrugation profile is made up by bolting standard panels together.

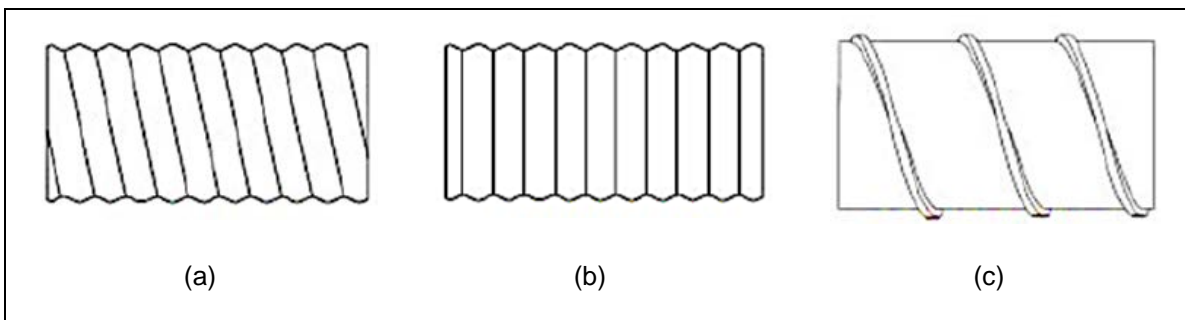
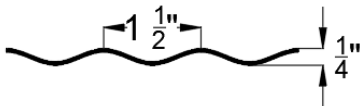
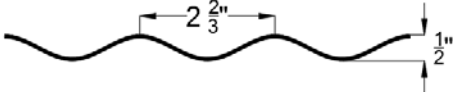
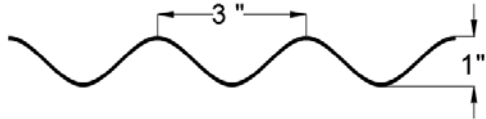
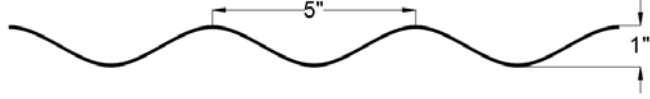
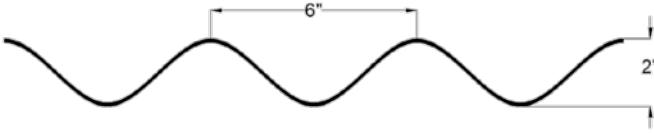


Figure 1-13 Types of corrugated metal pipes (CMPs): (a) helical, (b) annular and (c) spiral rib CMPs.

Table 1- 1 Common CMP corrugation profile in North America (PCPIPE 2016).

CMP Type	Corrugation Profile	Thickness (in.)
Helical and Annular		0.052" & 0.064"
		0.064" - 0.168"

<sup>1</sup> The process of dipping fabricated steel into a kettle or vat containing molten zinc.

CMP Type	Corrugation Profile	Thickness (in.)
		0.064" - 0.168"
		0.064" - 0.168"
Annular		0.1" - 0.168"

**1.2.2 Corrugated Metal Pipe Design Considerations**

**1.2.2.1 Materials**

Aluminum for corrugated metal pipe and pipe-arches shall comply with the requirements of AASHTO M 196 (ASTM B745 2015). Steel for corrugated metal pipe and pipe-arches shall comply with the requirements of AASHTO M 36 (ASTM A760 2020). Steel for structural plate pipe, pipe-arch, arch, and box structures shall meet the requirements of AASHTO M 167M/M 167 (AASHTO LRFD Bridge Design Specifications 2020).

**1.2.2.2 Soil Classification System**

The performance of a flexible corrugated steel pipe is dependent on soil-structure interaction and soil stiffness. Soil Parameters to be Considered (ASTM A796 2017):

- The type and anticipated behavior of the foundation soil under the design load must be considered.
- The type compacted density and strength properties of the soil envelope immediately adjacent to the pipe shall be established.
- Good side-fill material is considered to be a granular material with little or no plasticity and free of organic material.
- Soils meeting the requirements of Groups GW, GP, GM, GC, SW, and SP are acceptable, when compacted to 90 % of maximum density. Soil types SM and SC are acceptable but require closer

control to obtain the specified density; the recommendation of a qualified geotechnical or soils engineer is advisable, particularly on large structures.

**1.2.2.2 Limit State and Resistance Factors**

Limit state design or Load and Resistance Factor Design (LRFD) is a structural design method for a condition that beyond which the structure is unable to fulfil the required design criteria. Buried structures and their foundations shall be designed by the appropriate methods specified in Articles 12.7 through 12.15 to resist the load combinations as specified in AASHTO Standard Articles 12.5.2 and 12.5.3. The factored resistance,  $R_r$ , shall be calculated for each applicable limit state as presented in Eq. 1-11 (*AASHTO LRFD Bridge Design Specifications 2020*):

$$R_r = \phi R_n \tag{Eq. 1-11}$$

where,

$R_n$  = the nominal resistance, and

$\phi$  = the resistance factor specified in Table 1-1.

Table 1-1 Resistance factor.

Metal Circular Pipe, Arch, and Pipe Arch Structures		Resistance Factor
Annular pipe with spot-welded, riveted, or bolted seam:	Minimum wall area and buckling	1.00
	Minimum longitudinal seam strength	0.67
	Bearing resistance to pipe arch foundations	0.45

**1.2.3 Durability and Structural Performance of CMPs**

Many culverts in the United States that were installed four to five decades ago, now have reached their design life and need to be repaired, renewed, or replaced (Najafi 2008). In the pipeline industry, problems with corroded metallic and fiber reinforced concrete pipes are of the major concerns. The pipeline deterioration has a direct impact on economics and public services.

The durability of a CMP is mainly impacted by duration of water contact, pH, dissolved salts, alkalinity, hardness, and abrasiveness. Due to the abrasion, the CMP corrosion rate (for both inner and

outer surfaces) increases. The occurrence of waterside (inner surface) corrosion is faster compared to the soil side (outer surface) corrosion. Hence, the CMP waterside corrosion is considered as the controlling factor (Bednar n.d.).

Culvert deterioration can be classified as serviceability-related and strength-related issues, as follows (Najafi 2008):

**Serviceability-related deterioration:**

- Scour and erosion of streambed and embankments,
- Inadequate flow capacity,
- Corrosion and abrasion of metal culverts,
- Abrasion and deterioration of concrete and masonry culverts,
- Sedimentation and blockage by debris,
- Separation and/or drop-off of sections of modular culverts, and
- Inadequate length.

**Strength-related deterioration:**

- Cracking of rigid culverts,
- Undermining and loss of structural support,
- Loss of the invert of culverts due to corrosion or abrasion,
- Over-deflection and shape deformation of flexible culverts, and
- Stress cracking of plastic culverts.

Common defects in culverts can include crack, corrosion, loss of pipe wall thickness, joint infiltration, joint exfiltration, invert deterioration, joint misalignment, shape distortion, debris, loss of wall thickness, and bedding voids, as illustrated in Figure 1-14 (Piratla et al. 2017).

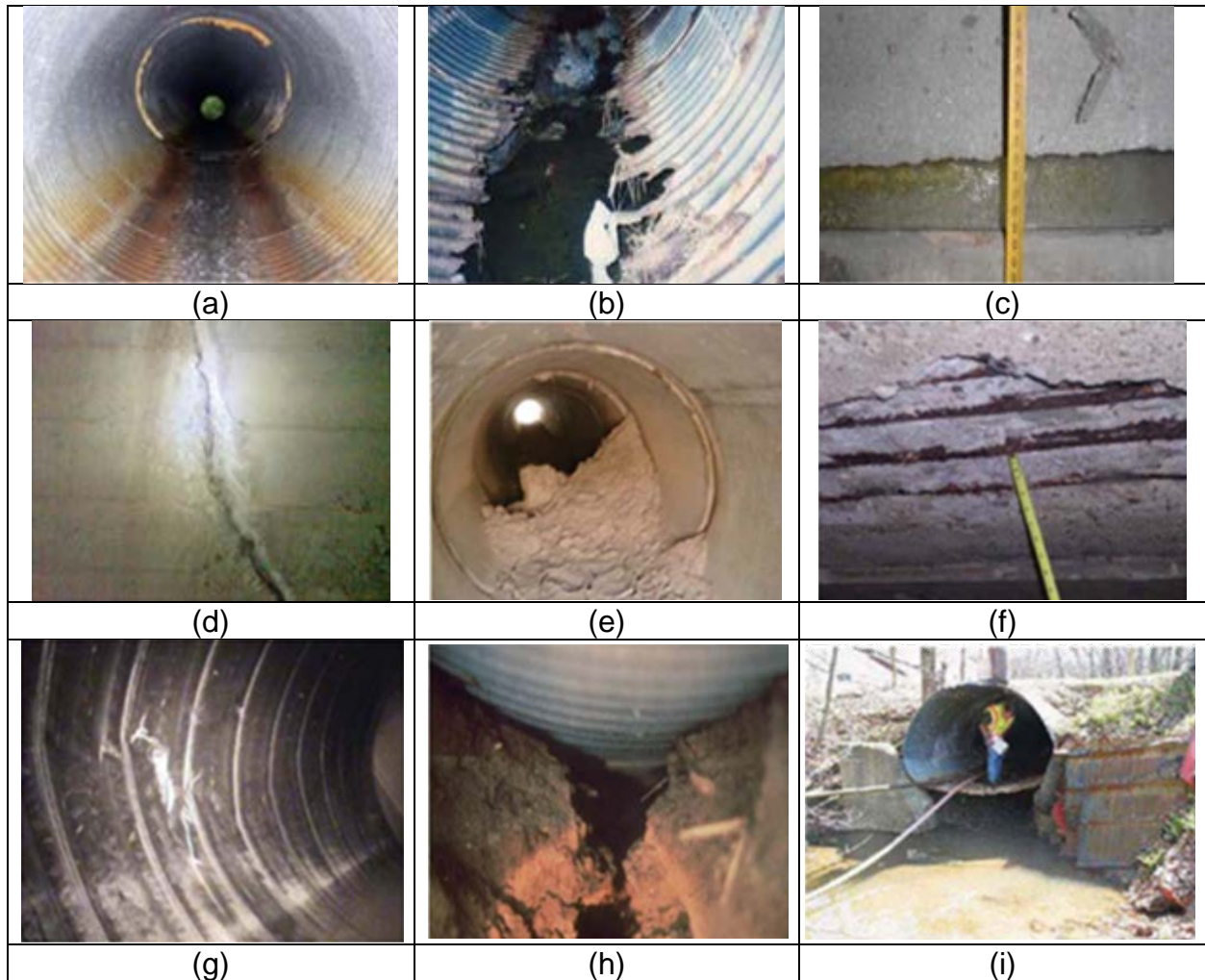


Figure 1-14 Common Defects of Culverts: (a) invert corrosion, (b) invert abrasion, (c) joint separation, (d) crack, (e) joint infiltration, (f) spalling in concrete culverts, (g) wall damages in plastic culverts, (h) piping beneath a culvert and (i) outlet scour (Piratla et al. 2017).

The structural performance of a CMP is impacted by the improper backfill material, the level of backfill soil compact and the presence of groundwater or hydrostatic pressure (Sehn and Duncan 1994). Culvert failures are sudden and may cause flooding potholes or total failure of the roadway. Four examples of culvert failures follow:

- a) The failure of a 17-year-old 84 in. diameter CMP culvert in Maryland caused a car fell into a 20 in. wide by 20 in. deep sinkhole, as shown in Figure 1-15. The passengers were a mother and daughter that injured. More than 13,000 volts of electricity coursed through feeder lines just below the car.



Figure 1-15 Culvert failure in Maryland (American Concrete Pipe Association 2008).

- b) A 4-year old, 48-in. diameter HDPE culvert collapsed in the parking lot at the Low's Home Improvement Warehouse, Timonium Caused at a cost of \$500,000, the contractor replaced the failed pipe with precast concrete pipe, as shown in Figure 1-16.



Figure 1-16 Culvert failure in Timonium (American Concrete Pipe Association 2008).

- c) Approximately three years after installation, the "World's Largest Corrugated Steel Arch" Collapsed on the Alaska Highway in British Columbia, Canada, as shown in Figure 1-17.



Figure 1-17 Culvert failure in British Columbia, Canada (American Concrete Pipe Association 2008).

- d) A 30-year old CMP collapsed in the downtown area of Bakersfield and caused revoking of CMP use, as shown in Figure 1-18.



Figure 1-18 Culvert failure in Bakersfield, California (American Concrete Pipe Association 2008).

### 1.3 Renewal of Deteriorated Culverts using Trenchless Technology

Trenchless renewal and replacement methods can be used to line, rehabilitate, upgrade, or renovate existing pipelines (Najafi 2010). It is seen that utilities spend a great amount of money on replacement of old pipes. Although, one of the solutions is open-cut replacement of the deteriorated pipe and reconstruction; it is however, very expensive and disruptive to traffic. To reduce social cost to commuting public, trenchless technology can offer innovative and nondestructive approaches, which make pipe renewal easier (Kohankar Kouchesfehni et al. 2017). A pipe renewal technique takes the advantage of employing the remaining usable pipe and extending its design life by the application of lining methods (Najafi 2010). If a pipe exceeds the preventative maintenance stage but still maintains its structural integrity, then using trenchless renewal methods is the proper corrective action. If a pipe deteriorates to a point where its structural integrity or soil support is lost, then pipe replacement would be the appropriate corrective action (Wyant 2002).

The most important step in designing a trenchless renewal technique is selection of the most appropriate, cost-effective and reliable method. Decision making process for selection of a pipeline renewal solution should consider many factors such as existing pipeline conditions, constructability and site limitations, strengths and limitations of potential renewal methods, pipe geometry, costs and availability of contractor and technology providers (Najafi 2016). The design of a pipeline renewal system involves 1) identification of pipe conditions, problem recognition and classification, 2) prioritization of problem considering strategies and long-term plans, 3) selection of an appropriate pipeline renewal method and 4) designing renewal methods based on project specific conditions (Kouchesfehni et al. 2018; Najafi and Gokhale 2005).

Trenchless renewal methods include several techniques. Sliplining (SL), cured-in-place pipe (CIPP), close-fit pipe (CFP), spiral wound lining, fold-and-form PVC lining, spray-in-place pipe (SIPP) and spray applied pipe lining (SAPL) are some of the trenchless rehabilitation techniques, as shown in Figure 1-19 (Syar et al. 2019). SIPP and SAPL are conceptually the same, however, SIPP applies to potable water pipelines constructed of metallic or asbestos cement piping in the diameter ranges of 4 in. to 36 in., (F3182-16 2016). SAPL is a pipeline renewal solution to support severely damaged large diameter (larger than 36 in. span) gravity storm pipes such as culverts and drainage structures to protect these pipes from further



deterioration (Najafi 2016). These trenchless renewal methods have many social and environmental benefits over traditional open-cut or cut-and-cover methods. These methods should be used when the project surface and subsurface conditions allow utilizing the trenchless technology. Compared with other trenchless methods, SAPL methodology has the benefit of fast installation, is cost effective, environmentally friendly, corrosion and erosion resistant without hydraulic capacity loss and minimum laydown area (Darabnoush Tehrani et al. 2019; Kohankar Kouchesfehane et al. 2019).

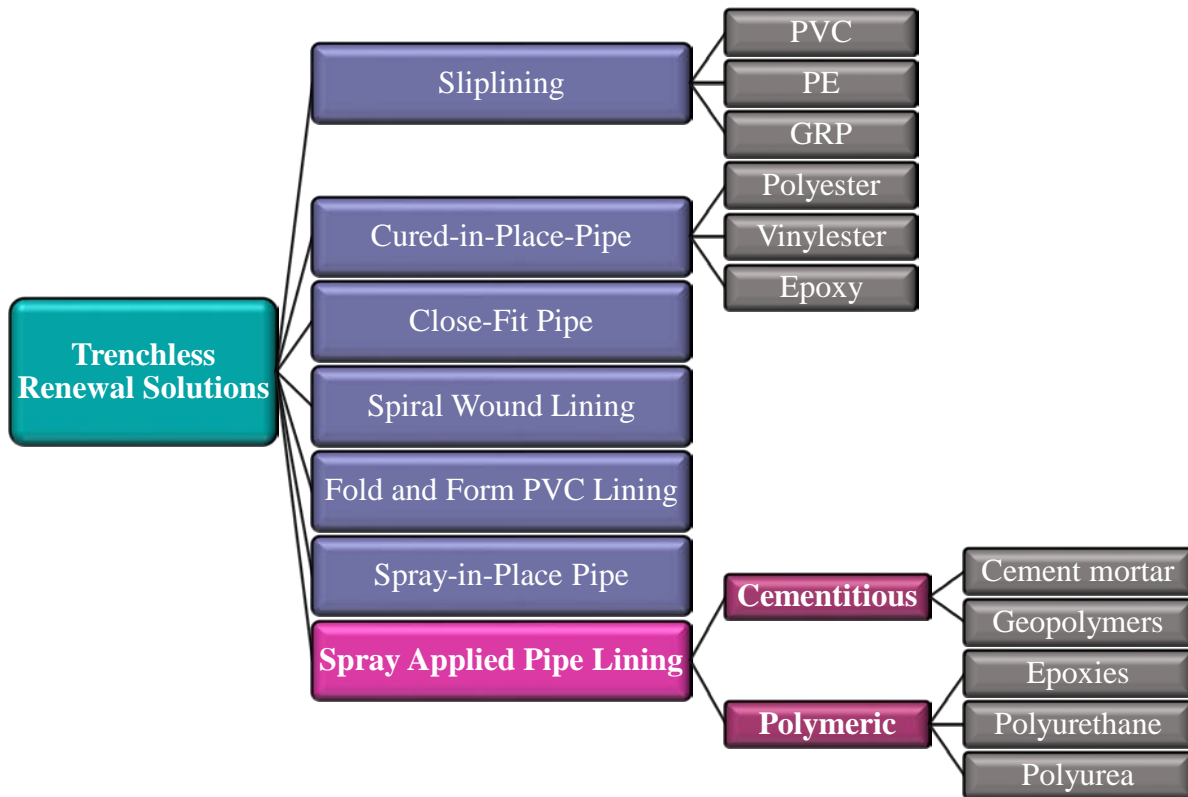


Figure 1-19 Trenchless renewal solutions.

### 1.3.1 Sliplining

Sliplining trenchless renewal technique is mainly used for structural applications when the old pipe does not have joint settlements or misalignments. In this method, a new pipeline of smaller diameter is inserted into the old pipe and usually the annulus space between the old pipe and new pipe is grouted. This installation method has the merit of simplicity and is relatively inexpensive. However, there can be a

significant loss of hydraulic capacity. This method is applicable for diameters greater than 24 in. Figure 1-20 illustrates a segmental sliplining method (Najafi and Gokhale 2005).



Figure 1-20 Segmental sliplining method (Source: Hobas Pipe USA).

### **1.3.2 Cured-in-Place Pipe Lining (CIPP)**

The cured-in-place pipe lining (CIPP) process involves the insertion of a resin-impregnated fabric tube into an old pipe by use of water inversion or winching. The resin impregnation is referred to “wetout.” Usually the fabric is a polyester material, fiberglass reinforced or similar. Usually hot water or steam is used for inversion process. The pliable nature of the resin-saturated fabric prior to curing allows installation around curves, filling of cracks, bridging of gaps, and maneuvering through pipe defects. CIPP can be applied for structural or non-structural purposes. Figure 1-21 illustrates CIPP installation process (Najafi and Gokhale 2005).



Figure 1-21 CIPP method installation process (Source: Insituform Technologies).

### **1.3.3 Close-fit Pipe Lining**

Not commonly used for culvert renewal, close-fit pipe trenchless renewal temporarily reduces the cross-sectional area of the new pipe before it is installed, then expands it to its original size and shape after placement to provide a close fit with the existing pipe. This method can be used for both structural and non-structural purposes. Lining pipe can be reduced on-site or in the manufacturing plant and reformed by heat and/or pressure or naturally. There are three versions of this approach: Fold and Formed (F&F), Drawdown (DD) and Rollover (RD) (Najafi and Gokhale 2005).

### **1.3.4 Spiral Wound Lining (SWP)**

Spiral wound trenchless renewal method is used for gravity sewers only. In this process, a new pipe is installed inside the existing pipe from a continuous strip of PVC 20 to 30 cm width. The strip has tongue-and-groove castings on its edges. It is fed to a special winding machine placed in a manhole, which creates a continuous helically wound liner that proceeds through the host pipe. The continuous spiral joint, which runs the length of the pipe, is watertight. Upon completion of the lining process, grouting of the annulus space between the lining and the host pipe wall is usually required, although there is a technique in which the lining is close-fit to the existing wall, thereby removing the need for grouting (Najafi and Gokhale 2005).

This process can be used for circular and non-circular pipe. Further, as the new pipe is formed directly against the wall of the host pipe, this method can be used to renew an existing pipe with a minimal loss of diameter as compared to conventional sliplining processes that rely on prefabricated pipes of fixed diameters. Hydraulic capacity of pipes lined in this manner may minimally increase because of reduction in flow area (Najafi and Gokhale 2005).

### 1.3.5 **Thermoformed Pipe (ThP)**

Not commonly used for culvert renewal, thermoformed pipe trenchless renewal technique can be used for sewers systems, potable water and gas supply lines, and industrial applications. ThP can be used for structural (including renewal of severely distressed pipeline) or nonstructural purposes and for pipelines from 4 in. to greater than 30 in. diameter and for lengths up to 1,500 ft. This technology can negotiate bends in the existing pipeline and generally provides a small footprint, minimal community disruption, and very brief service disruption. There are three methods of ThP as illustrated Figure 1-22 (Najafi and Gokhale 2005).

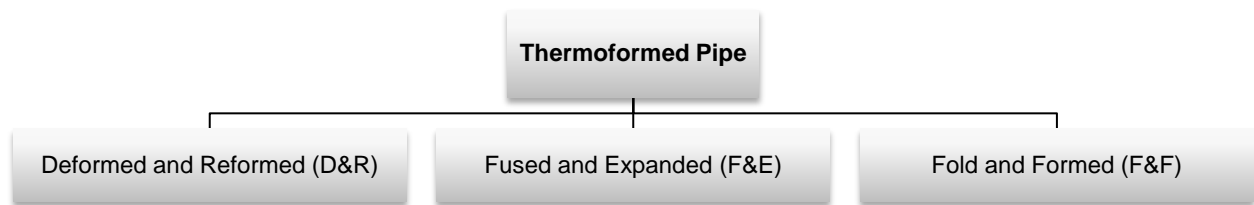


Figure 1-22 Three main variations of ThP process (Najafi and Gokhale 2005).

#### 1.3.5.1 **Fold & Formed (F&F)**

In the first method of ThP, called fold and formed (F&F), PVC pipes are flattened in the factory during production, then wound onto large reels, and folded during insertion. F&F methods can be used for gravity and/or pressure pipelines, including sanitary sewer, storm sewer and culvert, and potable water pipes and can be designed to provide full, independent structural integrity. Following the delivery to the renewal site, the new PVC pipe is heated with steam until it becomes flexible. Once in place, the new pipe is forced against the inside surface of the existing pipe using steam and air pressure to form a new PVC

pipeline tightly inside the old pipe. Maximum diameter varies across vendors with sizes available up to 24 in. (Najafi and Gokhale 2005).

#### **1.3.5.2 Deformed and Reformed (D&R)**

The second ThP method is deformed and reformed (D&R), where high-density polyethylene (HDPE) pipe is deformed into a U shape in the factory and wound into large coils. This method is used for gravity and/or pressure pipelines and for structural purposes. The new HDPE pipe is pulled at ambient temperature from manhole-to-manhole with a winch cable through the existing pipe. After the new pipe is inserted into position, it is heated with steam to revert it to its round memory and pressurized to push it out against the host pipe. Maximum diameter is 24 in. with sizes above 18 in. butt-fused and deformed in the field immediately prior to installation (Najafi and Gokhale 2005).

#### **1.3.5.3 Fused and Expanded (F&E)**

With the third method, called fused and expanded (F&E), PVC pipes are fused in the field prior to insertion. F&E pipes can be used for high-pressure pipelines exceeding 150 psi, including potable water pipes. Following delivery to the renewal site, the new PVC pipe is butt-fused and inserted through access pits as would be typical of sliplining. Once in place, the new pipe is heated with a hot liquid and highly pressurized to thermoform the new pipe tightly against the inside surface of the existing pipe. The maximum available diameter continues to expand with sizes exceeding 30 in. having been installed (Najafi and Gokhale 2005).

#### **1.3.6 Spray Applied Pipe Lining (SAPL)**

Spray applied pipe lining (SAPL) is a trenchless renewal methodology and an application that inhibits further deterioration and can structurally support severely damaged pipes, culverts and drainage structures. SAPL can potentially be used for structural renewal and load carrying capacity enhancement of culverts by applying a monolithic layer, ranging from 1.0 in. to 3.0 in., to the culvert inner surface (Darabnoush Tehrani 2016; Syar et al. 2020). SAPL can be installed either manually with hand spray or with a rotatory spin casting machine using a sled, as illustrated in Figure 1-23. The primary materials used

for SAPLs can be categorized into (1) cementitious such as geopolymers and (2) polymeric materials such as polyurethanes (Johnson and Hammon 2017). SAPLs can be a key strategy in extending service life and managing the future burden expected from the aging network of culverts, as shown in Figure 1-24. SAPL is environmentally friendly, compatible with complex geometry, durable, corrosion and erosion resistant and fast for installation without hydraulic capacity loss of the culvert (Syar et al. 2019).

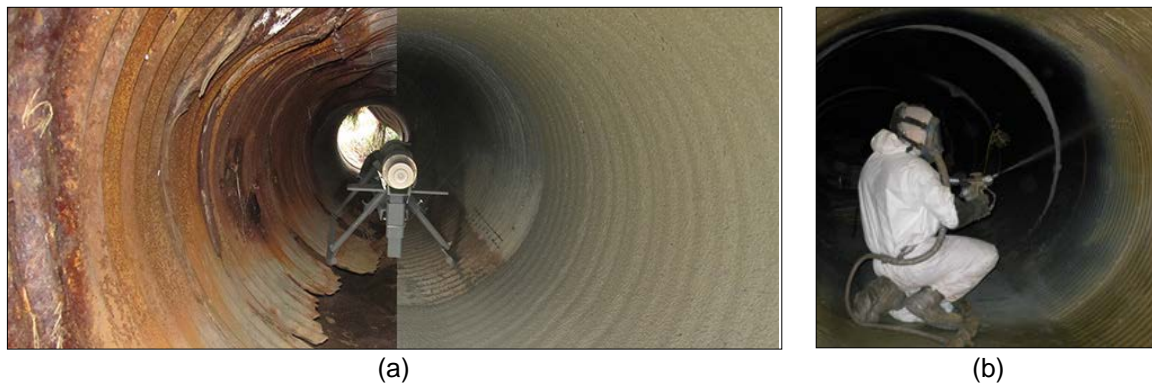


Figure 1-23 Corrugated metal pipe culverts (CMPs) before and after SAPL rehabilitation: (a) cementitious SAPL installation using spin casting machine (Source: CentriPipe) and (b) polymeric SAPL installation with hand spray (Source: Sprayroq).

To reduce emergency projects and impacts to the travelling public, departments of transportation (DOTs) can use spray applied pipe linings (SAPLs) to renew deteriorated gravity storm water conveyance conduits and culverts provided they discovered prior to loss of soil-structure interaction. However, currently no standardized structural design methodology exists for this technology (neither cementitious nor polymeric SAPLs). Most lining vendors utilize cured-in-place pipe (CIPP), ASTM F1216 design methodology. Others use various classical analytical structural design equations, such as beam element or shell element. The development of a practical spray-applied culvert/pipe lining methodology could be of enormous benefit to the DOTs. Such linings could be a key strategy in extending service life and managing the future burden expected from the aging network of culverts and storm sewers.



Figure 1-24 A sample of SAPL renewed twin culvert, North Carolina  
(Photo by Zahra Kohankar Kouchesfehni, CUIRE).

The key factor in a design guideline for SAPL is whether the existing pipe is structurally sound enough to support the earth, live, and hydrostatic loads imposed on it. It is well known that existing flexible pipes gain structural strength through the soil-structural interaction, thus making them a composite system (Syar et al. 2019). There are many documented instances of existing corrugated metal pipes with significant invert loss that continue to hold their shape due to the load carrying capacity of the surrounding soil. If the existing pipe is structurally sound enough to continue to maintain shape and carry the earth and live loads imposed on it then several internal lining techniques might be applicable, including sliplining (SL), cured-in-place pipe (CIPP), spray applied pipe lining (SAPL), and close-fit pipe (CFP) (Najafi 2016).

ASTM F1216-16 divides deterioration of existing pipe conditions into two classes: “partially deteriorated” and “fully deteriorated” (F1216-16 2016). The assignment of a partially or a fully deteriorated design procedure depends upon condition of existing pipe or its expected structural contribution over the liner design period. The main objective of a structural renewal is to inhibit further deterioration and be able to structurally renew the severely damaged culverts and drainage structures (Najafi 2016).

## 1.4 Dissertation Objectives

The objectives of this dissertation are:

- To evaluate structural capacity of a fully deteriorated invert CMP renewed with polymeric spray applied pipe lining (SAPL) for both circular and arch shapes.
- To examine whether polymeric spray applied linings can be “fully structural” or not.
- To investigate the CIPP design equations and their applicability for polymeric SAPLs.
- To develop a structural design methodology for polymeric spray applied pipe linings.

## 1.5 Methodology

To evaluate the structural capacity of renewed CMPs, full scale soil box testing was conducted at the Center for Underground Infrastructure Research and Education (CUIRE) at the University of Texas at Arlington (UTA). The magnitude of forces, pressures and displacements of the crown, invert and springline of the pipe samples were obtained. The potential base equations for the design of polymeric SAPLs were recognized through a comprehensive literature search. The obtained values from the soil box testing were compared with the back calculated values of base equations. The based applicable equations were modified through statistical curve fitting and are presented in Chapter 7 of this dissertation. The research methodology is illustrated in Figure 1-25.



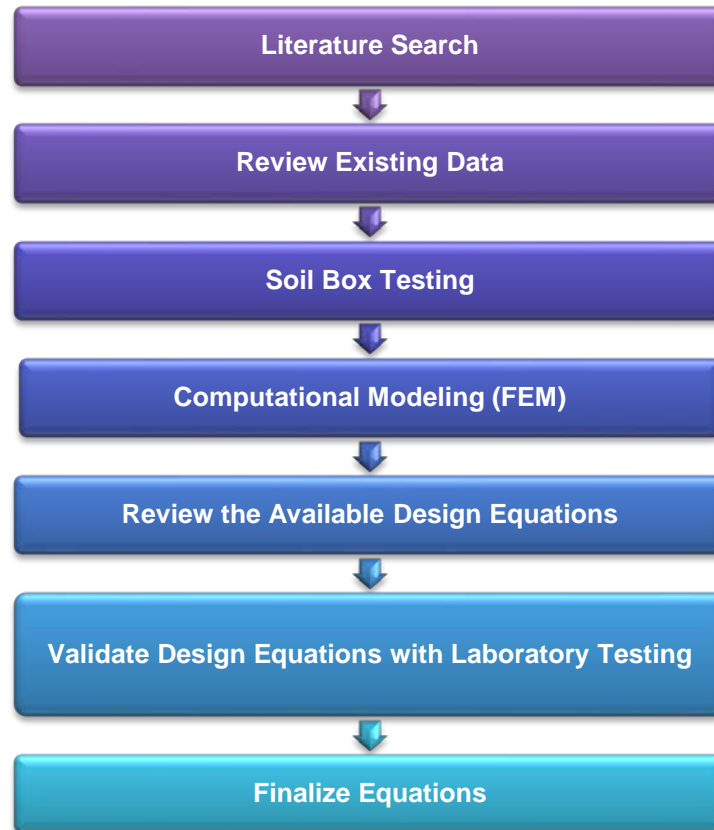


Figure 1-25 Research Methodology.

## 1.6 Scope

The scope of the dissertation includes:

- Literature review on SAPLs.
- Field inspection and data collection of the SAPL renewed projects and study on results.
- Experimental testing on fully deteriorated invert circular and arch CMPs renewed with polymeric SAPL application.
- Investigation on CIPP design equations applicability.
- Numerical model development for a SAPL design base equation.
- Design equations methodology development.

## **1.7 Hypothesis**

The hypothesis of this dissertation is summarized as following:

- Polymeric SAPL is fully structural and is able to increase the load carrying capacity of a fully deteriorated invert culvert.
- Polymeric SAPL Renewed circular CMP has a higher load bearing capacity than a polymeric SAPL renewed arch CMP.
- CIPP or modified CIPP design equations developed with this dissertation are applicable for polymeric SAPLs.

## **1.8 Expected Outcome**

The expected outcome of this dissertation is listed below:

- To evaluate whether polymeric SAPL can restore structural integrity of the CMP that has been lost due to corrosion, age and/or environmental factors through large-scale soil box testing.
- To develop a design methodology for polymeric SAPL trenchless renewal application.

## **1.9 Overview of the Chapters**

This dissertation includes eight chapters. Chapter 1 presents an introduction and background of spray applied pipe lining (SAPL) trenchless rehabilitation methodology used in renewal of storm sewer culverts. Chapter 2 summarizes a literature review of conducted studies on SAPL materials and the SAPL renewed pipes' testing. Chapter 3 presents site visit inspection and field data collection of twenty-four culverts renewed with SAPL application. Chapter 4 discusses in details a full-scale laboratory soil box testing of buried CMPs renewed with polymeric SAPL. Chapter 5 provides the results and discussions of the soil box testing. Chapter 6 presents finite element modeling (FEM) of polymeric SAPL renewed CMPs for different thickness of liner. Chapter 7 outlines development of a design methodology for polymeric SAPL and at the end conclusions and recommendations for future research are presented in Chapter 8 of this dissertation.

## 1.10 Chapter Summary

This chapter presented an introduction and background of the culverts and storm sewers including culvert shapes, culvert materials, culvert hydraulics and flow conditions, culvert types of flow control and culvert structural behavior.

Corrugated metal pipes (CMPs) are of the most common material types used for culverts. CMPs along with CMP types and corrugation profiles, and CMP design considerations were discussed in this chapter according to the AASHTO LRFD Bridge Design Specifications (AASHTO 2017).

In addition, a summary of trenchless technology applications for renewal of corroded and damaged culverts were presented. Sliplining, cured-in-place pipe (CIPP), spiral wound (SWP), and spray applied pipe lining (SAPL) are main trenchless renewal applications.

The rest of this chapter presented the dissertation objectives, methodology, scope, hypothesis, and expected outcomes, respectively.

## Chapter 2

### Literature Review

#### 2.1 Spray Applied Pipe Linings

Spray applied pipe lining (SAPL) application dates to 1930s, which is the pioneer technique for pipe renewal (Najafi 2010). SAPL applies layers of liner on the interior surface of the host pipe to provide corrosion protection and structural capacity enhancement. SAPL substances can be cementitious such as cement mortar and geopolymers, or polymeric material including epoxy, polyurethane, and polyurea. Uncertainty about the structural capacity of some SAPL materials have categorized their application in the past as a non-structural renewal method (Ellison et al. 2010; Najafi et al. 2019).

##### 2.1.1 Polymeric Spray Applied Pipe Liners

Accelerated corrosion problems in today's infrastructure have led to development and use of coatings and linings to enhance infrastructure life expectancies. Due to inherent safety, performance, and quick return to service attributes, solvent-free 100% solids polymers have advantages for successful structural renewal and corrosion protection of infrastructures. Polymers can be formulated for structural or nonstructural pipeline renewal/rehabilitation applications. (ASCE Manual of Trenchless Renewal of Culverts and Storm Sewers, 2010). There are two major categories of protective polymeric coating technologies: epoxies and polyurethane-type systems, which include polyurethanes, polyureas and hybrids of these two chemistries (Cain 2016).

##### 2.1.1.1 Epoxy

Epoxies coatings are used as corrosion protection for factory-applied metals and as primers (sometimes zinc-rich) in multi-coat systems . Epoxies can provide a good adhesion to metals and high moisture resistant. High-solids or 100%-solids are the most common used epoxies. However, epoxies do not exhibit a good performance and become brittle at low temperatures. Epoxies are not very flexible and can crack in applications with any substrate movement. Hence, polyurethane and its derivative coatings,

due to their higher flexibility compared with epoxies, are widely used as metal corrosion protection with a high level of adhesion and moisture resistant (Cain 2016).

#### **2.1.1.2 Polyurethane**

Polymeric SAPL is developed in 1970s. Initially, it was based on 100% solid elastomeric polyurethane. In mid-1990s 100% solids rigid polyurethane coating was developed, which was able to form a three-dimensional cross-linked structure, resulted in a superior resistance to chemicals, water penetration, and high temperatures (Matthews and Simicevic, 2012). Polymeric SAPLs can be applied through a spin caster machine or hand sprayed. Polyurea, provides high degree of chemical resistance and is able to cure rapidly (about 5 to 15 seconds). Many Departments of Transportation (DOTs) have already approved polymeric coatings for rehabilitation of culverts in the United States, such as Ohio DOT, Virginia DOT, Florida DOT, etc. (Ellison et al. 2010).

Polyurethane coatings can range from very flexible (elastomeric) to very rigid. Polyurethane coatings can exhibit a good combination of flexibility/elongation and harness compared with epoxy coatings. Polyurethane coatings have excellent adhesions to different substrates. Polyurethane coatings cure rapidly, even at lower temperatures, but most require a catalyst. Compared to epoxies, and polyureas, most 100%-solids polyurethane coatings are sensitive to moisture and susceptible to blistering. Solvent-based polyurethane coatings are typically applied as a thin layer of less than 5 mil using airless sprayers. Compared to solvent-based polyurethanes, 100% solid polyurethanes can be applied at a thicker layer of greater than 20 mil. Installation of 100% solid polyurethanes need the use of a plural component spray technique that can mix the resin and catalyst components together prior to spraying (Cain 2016).

#### **2.1.1.3 Polyurea**

Polyurea coatings are 100% solids, zero-Volatile Organic Compound (zero-VOC) formulations. Polyurea coating cures rapidly in around 30 seconds without use of a catalyst or heat at low temperatures. Polyurea coatings are not sensitive to moisture due to the existence of the urea linkage. Polyurea coatings are water resistant and no blistering occurs when they are applied on substrates in the presence of liquid

water. Polyurea coatings exhibit excellent mechanical properties (stiffness, tear and abrasion resistance, thermal shock and impact resistance) (Cain 2016).

Polyureas can be applied at very high thickness, compared with polyurethane, and enhance the structural integrity of the substrate. Installation of polyurea coatings need the application of high-pressure, plural component sprayers, and a trained applicator. Polyurea elastomers are unsuitable for applications requiring less than 5 mil thickness coatings. Polyureas are used a replacement for epoxies in applications that mechanical properties such as elongation and impact resistance are important.

A performance comparison using the mechanical properties of polyurea, polyurea hybrid, polyurethane and epoxy coatings applied on steel substrate is illustrated in Figure 2-1.

Walker and Guan (Walker and Guan 1997) conducted a set of material property tests in accordance with ASTM standards and reviewed the performance of five primary materials of sprayed liners used in North America. Their tests included 100% solids rigid polyurethane, 100% solids epoxy, solvent amine-based epoxy, 100% solids elastomeric polyurethane and cement mortar lining for the internal renewal of potable water steel pipelines. Their study stated the 100% solids polyurethane had a better performance to be used in potable water steel pipelines. Ha et al. (Ha et al. 2016) conducted a series of laboratory testing to investigate the applicability of the fast-setting polyurea-urethane (PUU) lining as a structural lining material, applied inside of small diameter (5.91 in.) water pipes. Their study included pull off bond test, hole or gap spanning test, angular displacement test, transverse shear test and fatigue cyclic tests. It was concluded the fast-setting PUU lining can be used as a structural lining material for water pipelines. Szafran and Matusiak (Szafran and Matusiak 2017) studied the structural behavior of reinforced concrete rings renewed from inside and outside surfaces with polyurea SAPL through the three-edge bearing test (Al-Lami 2020). They concluded the used polyurea SAPL membrane for standard application in two layers on both surfaces increased the compressive capacity of concrete rings by 21.9%. Authors stated further research is needed to explore the performance of polyurea SAPL in the existence of soil-pipe interaction system.

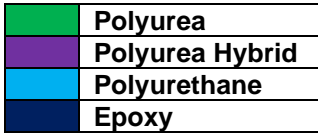
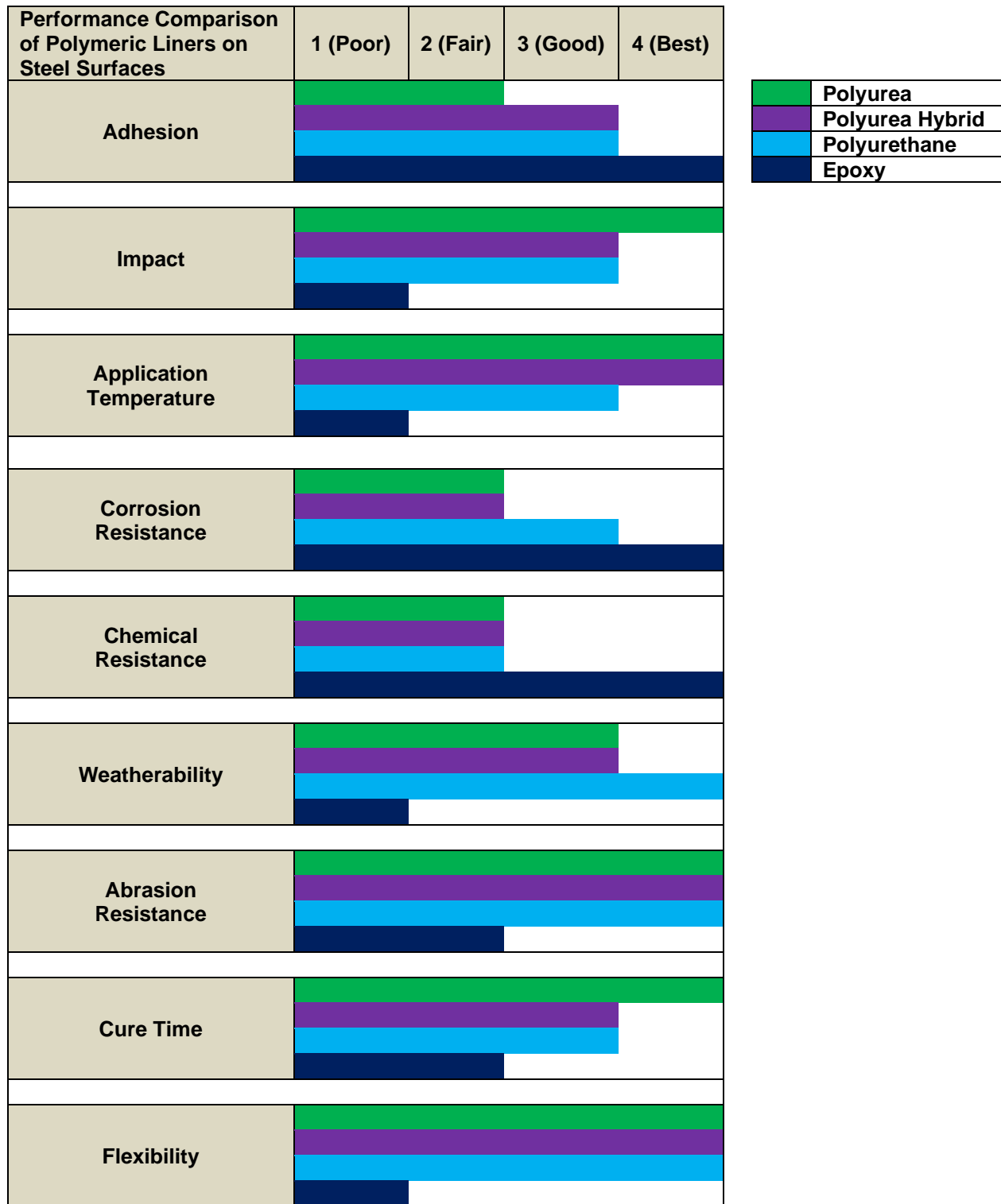


Figure 2-1 Performance comparison of polyurea, polyurea hybrid, polyurethane and epoxy coatings applied on steel substrate (Adapted from Cain 2016).

Primeaux II (Primeaux 1989) introduced the concept of 100% solids spray elastomer polyurea coatings that differentiated polyurea coatings (products based on isocyanates/amines) from polyurethane coatings (products based on isocyanates/polyols). Since then, 100% solids polyurea spray elastomers have been promoted as a new coating technology with polyurea advantage (Broekaen 2002). The author concluded that spray polyurea elastomers is capable and versatile for different variety of applications due to its several advantages as: fast reactivity and cure, relative water insensitivity, two-component, 100% solids (1:1 volume ratio) , excellent physical properties, high thermal stability (up to 350 °F), wide formulation flexibility, easily pigmented, and ease of application (spray or pour techniques).

In 2000, the industry formed the Polyurea Development Association (<https://www.pda-online.org/>) to promote market awareness, and the understanding and acceptance of polyurea technology through the development of educational programs, product standards, safety, environmental, and usage recommendations.

Guan (2003) studied the chemistry, history, and the developments of 100% elastomeric polyurethane, 100% elastomeric polyurea, and 100% solids rigid (structural) polyurethane. He discussed a newly developed ceramic-modified 100% solids rigid polyurethane coatings that meet the challenge of highly abrasive or high-flow applications and offer ultimate durability and impact resistance. Another improvement of 100% solids polyurethane/polyurea involves incorporating a non-leachable antimicrobial additive, that enables these coatings to provide long-term corrosion protection. The development of a 100% solids rigid aliphatic polyurethane coating is another improvement, which has a better adhesion on non-primed steel or galvanized surfaces, faster initial film development, and superior corrosion and chemical resistance. The author concluded the developed ceramic-modified 100% solids rigid polyurethane coatings meet the challenge of highly abrasive or high-flow applications and offer ultimate durability and impact resistance.

Guan (Guan et al. 2004) studied an advanced 100% solids rigid (or structural) polyurethane coating used for rehabilitating of welded joints, (steel) oil/gas and water/wastewater pipelines. Traditionally, most pipe rehabilitation field applications have been based on 100% solids elastomeric polyurethane; however, since the mid-1990s, the movement in North America has been toward the development and use of 100% solids rigid polyurethane coatings. The 100% solids rigid polyurethane forms a 3-dimensional cross-linked



structure resulting in a coating with superior resistance to chemicals, water penetration, and extreme temperatures. The sprayable resin has a 1:1 mixing ratio with balanced viscosities between two reactive components, which enables easier metering of the components in the field. The author concluded the 100% solids rigid polyurethane field-applied coating technology outperforms the 100% solids elastomeric polyurethanes.

According to Guan (Guan et al. 2004), a good field applied corrosion protection system with high performance properties shall be environmentally friendly, worker-safe, durable and economic. Performance of pipeline lining systems depends on several factors. Guan (Guan et al. 2004) listed twelve most essential performance properties of a coating system for pipeline rehabilitation: adhesion to pipe substrate, abrasion, impact and penetration resistance (hardness), chemical and corrosion resistance, dielectric strength and resistance to cathodic disbondment, flexibility, stability at low or elevated temperatures and service conditions, water absorption or water vapor permeability.

For example, SprayWall® is a self-priming polyurethane lining from Sprayroq Protecting Lining System Company for pipeline rehabilitation that reinstates structural integrity, provides infiltration control and chemical resistance. It may be applied up to 0.25" thick in a single application or lift. It begins to gel in about 8 seconds, with a tack-free condition after 2 minutes. Within 60 minutes, the initial cure is complete, and the structure is capable of accepting flow, while complete curing continues over the next 72 hours. SprayWall®'s quick curing time allows the newly protected structure to be returned to service shortly after the application is completed, making it ideal for use on water, wastewater and stormwater rehabilitation, and on DOT projects, when keeping flow and traffic disruption to a minimum is critical (<https://www.sprayroq.com/spraywall>). A galvanized corrugated steel pipe culvert, 60 in. diameter and 1,800 ft in length, was renewed with SprayWall® polyurethane, using the SAPL technique in Norristown, PA, 2007, as illustrated in Figure 2-2 (a) and (b).



Figure 2-2 CMP renewal using SprayWall® Polyurethane SAPL, Norristown, PA: (a) Before Renewal, and (b) CMP Renewal during SAPL Application, 2007 (Sprayroq Inc.).

Entezarmahdi (Entezarmahdi 2015) conducted laboratory testing according to the ASTM standards C39, C76 and C497 to examine the structural capabilities of renewed RCP samples with different SAPL materials including epoxy, multi structural liners with modified pleurae and foam, polyurethane, and cement mortar. It was concluded that all of the tested lining materials enhanced the structural capacity of the pipe samples. Royer and Iseley (Royer and Iseley 2017) conducted a series of laboratory D-Load testing on rehabilitated pipe samples, including CMP, Reinforced Concrete Pipe (RCP) and cardboard tubes, using a geopolymer SAPL in different thicknesses to investigate the externally applied load that yields a D-Load crack. Moore and García (García and Moore 2015; Moore and García 2015) conducted a series of large-scale laboratory testing to examine the performance of deteriorated steel culverts rehabilitated with cementitious SAPL buried under 2 ft of soil cover. The result showed that the cementitious SAPL enhances the culvert response to the applied load.

### **2.1.2 Cementitious Spray Applied Pipe Liners**

Cementitious SAPL is the oldest method to line culverts. Cement mortar SAPL, has been in existence since the 1900s and is one of the most common lining methods used today. The first successful trial of cementitious SAPL took place in early 1930s (AWWA-C602, 2000). Cementitious SAPL can be classified as ordinary Portland cement mortar and geopolymer.

### **2.1.2.1 Ordinary Portland Cement**

Conventional cement mortar has brittle behavior and is easy to crack due to the shrinkage of the materials, concentration of stress and low tensile stress (Banthia et al. 2014). Under an applied load, the existing micro-cracks in concrete propagate and results in formation of macro-cracks. The macro-cracks allow moisture and chloride penetration into the cement mortar. By increasing the load, the condition of macro-cracks can be critical which causes a reduction in the load-bearing capacity of the structure, and a failure is expected (Kohankar Kouchesfehane et al. 2019). Therefore, cracks act as a detrimental agent resulting in steel corrosion, freeze-thaw damage, scaling, discoloration and early saturation (Banthia et al. 2014). To enhance the mechanical properties of conventional mortar, adding fibers of different materials in different sizes such as steel, carbon, polypropylene, polyester, nylon, glass and cellulose can limit the formation, growth of cracks and chemical intrusion (Banthia et al. 1994, 2014; Chiaia et al. 2009; Hsie et al. 2008).

Fiber reinforced mortar is a composite material of fibers as reinforcing and cement mortar as the binding matrix (Luk 2001). Addition of fibers to cement mortar adds resistance to it by bridging the cracks and limiting the crack propagation which will delay the perfusion of shrinkage cracks (El Debs and Naaman 1995). The cohesive and adhesive characteristics of binding matrix help to transfer stress from matrix to fibers through the interface(Luk 2001). Additional fibers improve the durability of composite reinforced cement mortar like abrasion resistance and freeze thaw resistance by its impermeability and cracking control capability (Izaguirre et al. 2011; Luk 2001; Spadea et al. 2015). Moreover, presence of fiber reinforcement can enhance the bond strength between the old substrate (host pipe) and the repair material (SAPL) (Dawood and Ramli 2011; Iucolano et al. 2013; Luo et al. 2013; Zanotti et al. 2014).

### **2.1.2.2 Geopolymer**

Geopolymer Spray Applied Pipe Lining (SAPL) material compared with the ordinary Portland cement mortar or reinforced cementitious material provides less shrinkage cracks, high chemical resistance, low creep, and less CO<sub>2</sub> emissions, as well as better physical properties. Geopolymer SAPL is

achieved by a mixture of aluminosilicate materials such as fly ash, metakaolin, silica fume, slag, rice-husk ash, or red mud with highly alkaline solutions such as hydroxides or silicates (Darabnoush Tehrani 2020).

## 2.2 SAPL Renewed Pipe Testing

Motlagh et al. (2013) studied and compared spray-on linings applications used in renewal of water pipeline. The objectives of their study were to provide a comparison of spray-on lining methods, including cement mortar, epoxy, polyurethane, and polyurea linings, and to provide an overview of their advantages and limitations. Their methodology involved short-term material property testing (according to different ASTM standards) and long-term tensile creep testing plans of polymer spray-on linings, which were commercially available. Experimental procedure followed for carrying out the long-term tensile creep testing (10,000 hours) was being conducted at the Center for Underground Infrastructure Research and Education (CUIRE) Laboratory, as illustrated in Figure 2-3. The authors discussed the advantages and limitations of spray-on lining methods including cement mortar linings, epoxy linings, polyurea linings and polyurethane linings. Their paper concluded rapid reaction and curing time characteristics of polymers may provide an effective solution to other pipeline renewal technologies (Motlagh et al. 2013).

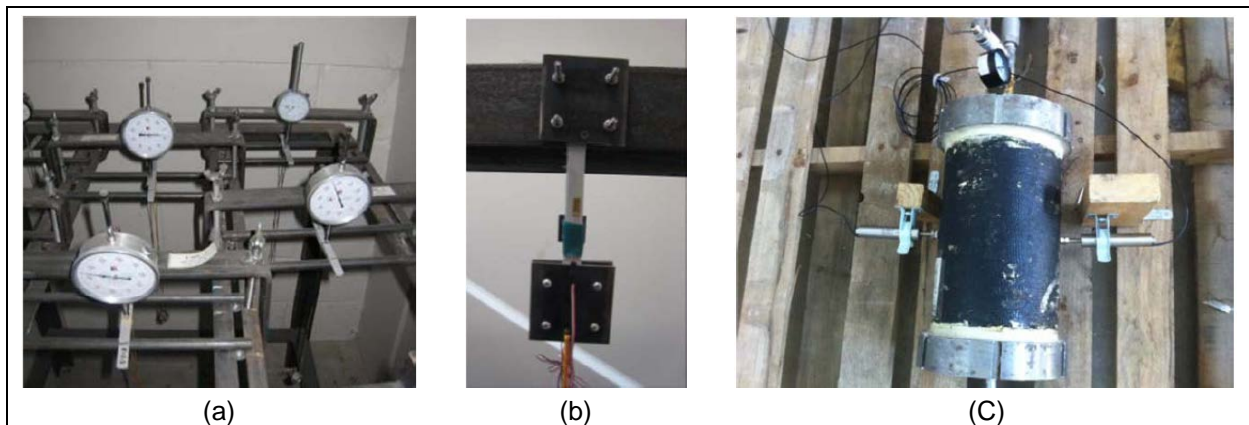


Figure 2-3 Comparison of spray-on lining methods using material property testing: (a) long-term flexural testing, (b) long-term creep tensile testing and (c) hydrostatic test setup (Motlagh et al. 2013).

Szafran and Matusiak (2017) studied the structural behavior and compressive strength of reinforced concrete pipes (RCPs) renewed with polyurea SAPL through D-Load testing, which ignored the

impact of soil-pipe-structure interactions. The objective of their study was to evaluate and determine structural behavior and increased compressive strength of RCPs lined with polyurea SAPL. Their methodology was involved static compressive testing on RCP with and without internal and external polyurea SAPL application. Results of these tests indicated that using polyurea SAPL on both internal and external surfaces of RCP increased the peak load of failure by about 21.9%. These results concluded that polyurea SAPL increases the compressive strength of RCP. The authors used external coating and internal spraying, as illustrated in Figure 2-4, which are not usable for the application of renewal of existing culverts (Szafran and Matusiak 2017).



Figure 2-4 Dead-load testing of reinforced concrete pipes (RCPs) renewed with polymeric SAPLs: (a) tested concrete rings covered by polyurea coating, (b) spraying polyurea coating system on concrete ring, and (c) D-load testing frame (Szafran and Matusiak 2017).

Ha et al. (2016) studied the structural behavior and performance of a fast-setting polyurea–urethane (PUU) SAPL as a structural lining material for rehabilitating water pipes, as showed in Figure 2-5. The objectives of their study were to investigate the bonding between a fast-setting PUU SAPL and steel specimens, the spanning capability of the lining on the water pipes, the bending and shear behavior of PUU lining, and the fatigue behavior of a renewed water pipe with PUU. Their methodology involved a series of experimental tests to assess the bond strength, hole and gap spanning capabilities, angular displacement ability, transverse shear resistance, and fatigue cyclic loading resistance. From these tests, the hole spanning capability of water pipe with 0.2 in. hole was observed to be 1,595 psi. Peel off failure of PUU occurred at an angular displacement capacity of 6.74° and no failure of PUU was observed at a transverse shear capacity of 25% of the diameter. The fatigue resistance of PUU in the range of  $10^5$  cyclic loadings was achieved. As the result, the authors found that the fast-setting PUU lining can be used in renewal of water pipes. Their paper ignored the impact of soil-pipe-structure interactions (Ha et al. 2016).

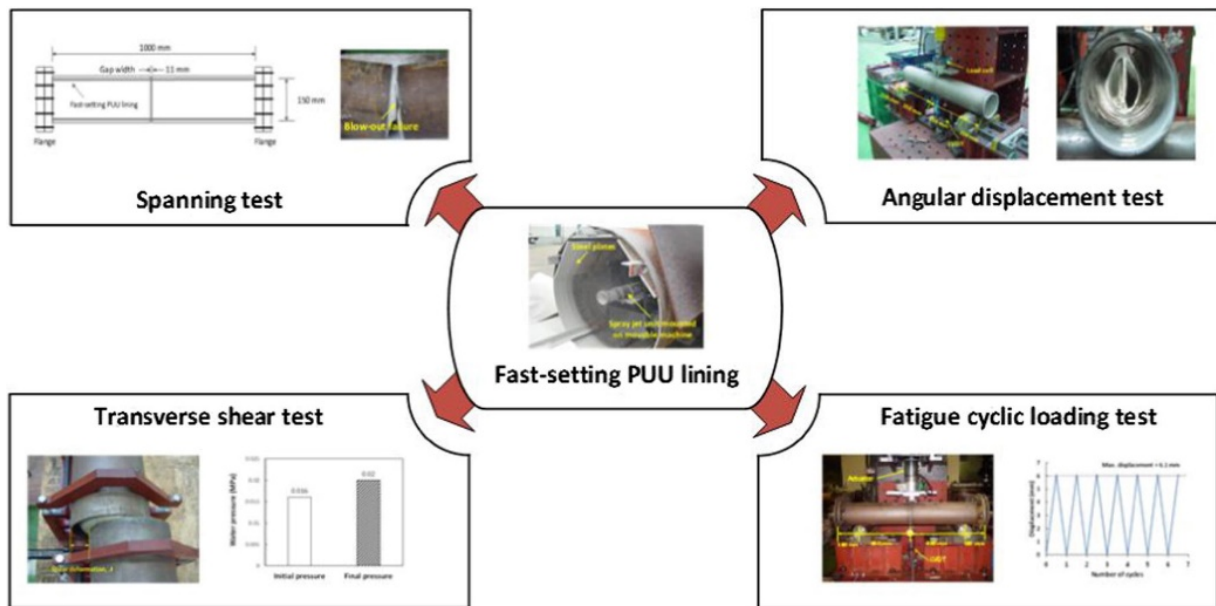


Figure 2-5 The structural behavior and performance of a fast-setting polyurea–urethane (PUU) SAPL as a structural lining material for rehabilitating water pipes (Ha et al. 2016).

The U.S. Army Corps of Engineers released the results of their field study on the performance of concrete-lined corrugated metal pipe (CLCMP) for use as an alternative to reinforced concrete pipe in November of 1986. Approximately 12,000 linear feet of concrete-lined pipe were inspected during their 15-month long study. Essentially, all were relatively new installations (less than two years old) with the concrete lining installed at the manufacturing plant. The only exception to this was a 26-year old installation that had the concrete lining installed in the field. The pipe manufacturer was ARMCO. The objective of this evaluation was to verify the manufacturer's claims, that this product offered the hydraulic efficiency of concrete pipe and the structural efficiency of corrugated metal pipe. All these pipes had the valleys of the corrugations filled and a specified minimum lining of 0.375-in. over the crests of the corrugations; but the actual minimum thickness was found to usually be 0.750 in. The result of this study led to development of the ASTM A979 - Concrete Pavements and Linings Installed in Corrugated Steel Structures in the Field standard. It was recommended in this standard to fill the corrugation valleys with concrete lining (ASTM A979, 2003). The result of the Army Corps study showed that the concrete liner increased the load bearing capacity of the pipes.

Garcia and Moore (2015) conducted laboratory testing to evaluate the performance of deteriorated helical corrugated metal pipes renewed with cementitious spray applied liners under different burial depths and truck axles. The CMP diameters were 47 in. and were corroded at the invert location with some perforations at hunch area. The pipe samples were buried at the 47.2 in. and 82.6 in (4 ft and 8 ft) cover depths using poorly graded sandy gravel (GP-SP) backfill material. The culverts samples were renewed with geopolymer (i.e., cementitious) non-ceramic liner at 3 and 2 in. thickness respectively. The installation was done using a spin caster spray machine that applies the liner by the cementitious liner by an air powered rotating nozzle. The results showed that no sign of failure was observed in the rehabilitated pipelines. The pipe, with thicker liner showed stiffer response to the live load. Load reduction effect of the cover depth was evident on the deeper cover.

Moore and Garcia (2015) studied the ultimate strength of two deteriorated metal culverts renewed with cementitious SAPL. The specimen size and burial configuration is same as their previous study (Garcia and Moore, 2015). However, the load was applied until the failure of the system was achieved. The load-control loading regime was applied and consequently, the post failure behavior of the system was not

obtained. The results showed that the liner increased the ultimate bearing capacity of the deteriorated culverts. The sample 1 with 2 in. of SAPL failed at 200 kips and the sample 2 with 3 in. of SAPL failed at 260 kips in tandem axle configuration. It was noted that the thickness of the SAPL was not the same everywhere, and its variation at some location was almost two times greater than the designed thickness.

Entezarmahdi (2015) conducted structural evaluation on 17 reinforced concrete pipes (CRPs), renewed with epoxy lining and tested through three-edge bearing test. The pipe samples had 24 in. inside diameter and were selected from class II category of the ASTM C76 (2015). Different types of liners including epoxy, Polyurethane, Multi structural liners with modified pleurae and foam, cementitious, and resin impregnated cured-in-place lining (CIPP) were applied on different layers and thicknesses. The author summarized the results in one graph as the significant increase in renewed CRP structural capacity by using different liners, showed in Figure 2-6.

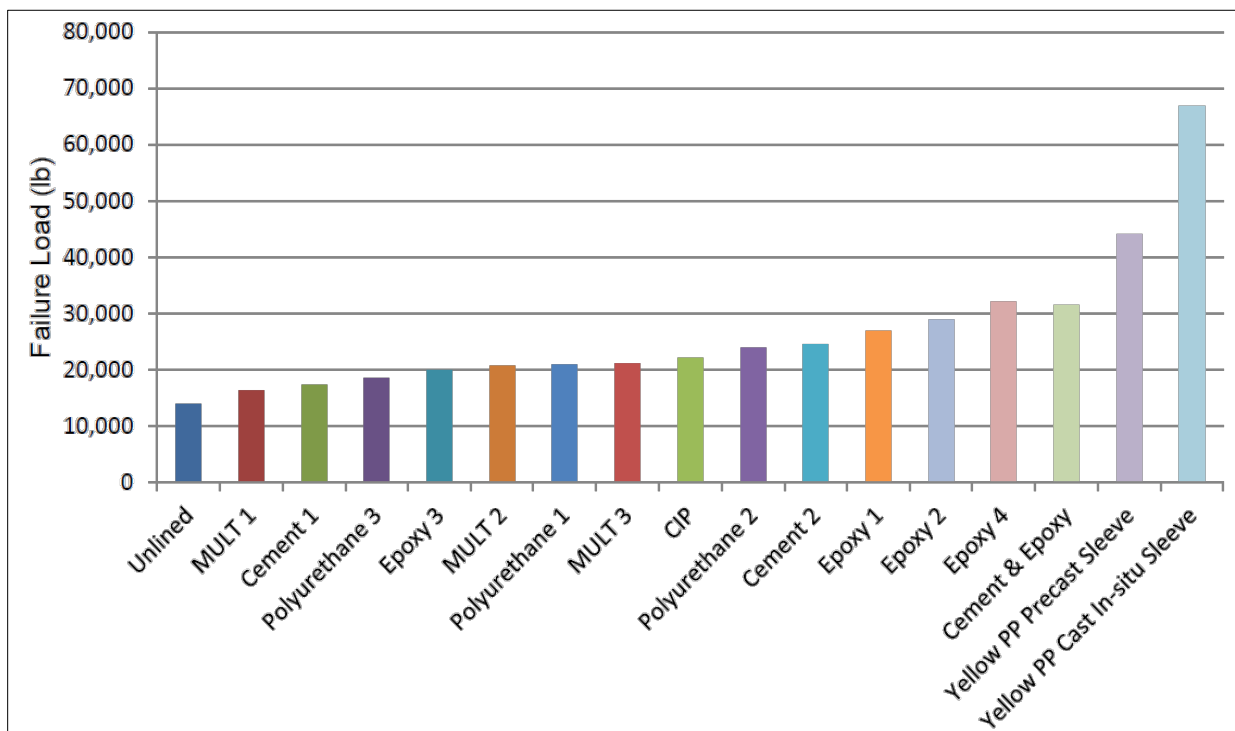


Figure 2-6: Significant increase in renewed CRP structural capacity (Entezarmahdi, 2015).



### 2.3 Soil-Pipe System Testing

Mai et al. (2013) conducted experimental study on two deteriorated 71-in. CMPs (Mai et al. 2013). The pipe samples had different level of deterioration. They were corroded and perforated along both side of the invert. Both CMPs had bitumen asbestos protective coating, which was removed prior to the testing. The pipe samples were embedded with well-graded sandy gravel soil with 95% of the maximum dry unit weight achieved in a standard Proctor test (Standard Proctor Dry Density or SPDD). The CMPs were backfilled and tested with two different cover of 2 and 3 ft using single axle and tandem load configuration. The result showed that higher deflection occurs at lower cover with single axle loading configuration. In addition, despite the pipes were loaded several times under different conditions, which caused irrecoverable deformations, they were able to take the full-service load 38.22 kips in tandem configuration.

Garcia and Moore (2015) conducted laboratory testing to evaluate the performance of deteriorated helical corrugated metal pipes renewed with cementitious spray applied liners under different burial depths and truck axles, as illustrated in Figure 2-7 (García and Moore 2015). The CMP diameters were 47 in. and were corroded at the invert location with some perforations at hunch area. The pipe samples were buried at the 47.2 in. and 82.6 in. (4 ft and 8 ft) cover depths using poorly graded sandy gravel (GP-SP) backfill material. The compaction rate of backfill under the hunch area was 84.8% of the SPDD and from hunch to top cover was 92% of SPDD. The testing was conducted for axial and tandem configuration using hydraulic jack to simulate the Canadian design truck before and after pipe sample rehabilitation. For bare CMP (i.e., without liner), the loads were applied in two cycles for full-service load of 45.6-kips. The first cycle applied in one increment and immediately removed to settle the system and to eliminate the effect of irrecoverable ground deformations. Then, the second cycle was applied in 20% increments to represent the incremental response of the system under repeated surface loads, similar to the pipeline in service. The test result showed that the higher force applies under the load pad. The pipes responses were higher at the first cycle (before consolidation). The tandem axle showed lower diameter change than single axle. At the end, no sign of structural failure observed at any stage of testing (García and Moore 2015).

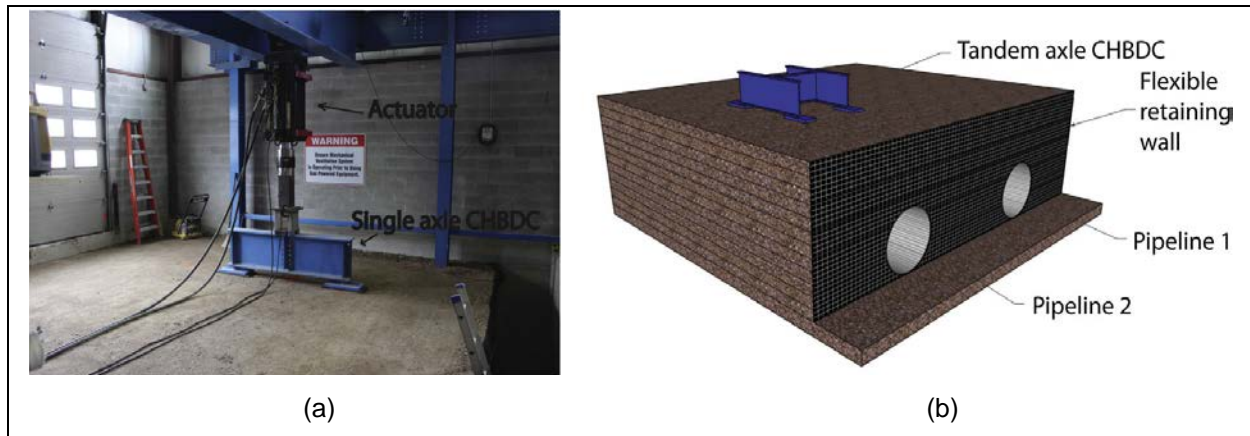


Figure 2-7 Soil box laboratory testing of corrugated metal pipes: (a) single axle loading configuration, and (b) schematic tandem axle loading configuration (Garcia and Moore 2015).

Masada (2017) carried out field and laboratory testing on an intact, a deteriorated invert, and an invert paved 60-in. CMP. The field test was conducted using H20 truck placed on the top of the culvert (Masada 2017a; b). The laboratory testing was carried out using a hydraulic jack at the outdoor load frame facility, which provided a controlled-testing condition including load rate and loading method. The first laboratory test was conducted on an intact helical CMP using 68 in. by 108 in. load pad over the crown of the buried pipe sample. The load was applied incrementally until the pipe sample wall at one of the shoulders buckled at 923-kips. The second test was carried out on another CMP, backfilled in the same procedure similar to the first test. The invert of the installed CMP was cut partially to simulate perforations in the invert of a deteriorated culvert in field. The result showed the partially invert deteriorated culvert had 26.6% capacity reduction under relatively large distributed load (with a load pad size of 68×108 in.) applied over the pipe's crown. During the test, a separation of pipe sample's helical interlocking seems separation was observed at 81% of the ultimate load carrying capacity of 667-kips. The third set of tests was carried out similar to the second test, except the whole invert was paved with mesh reinforced cementitious material. The pipe sample failed at 13.3% lower load carrying capacity of the intact CMP at the load of 800-kips. However, it should be considered that none of the tested pipe samples had a fully deteriorated invert. The remaining invert sections partially maintained the resistance to ring compression and played an

important role in the CMP's stability and load carrying capacity. While, there are still many culverts in service with fully invert section gone and their structural behavior and load carrying capacity are yet unknown.

Sargand et al. (2018) conducted field testing of a shallow cover severely deteriorated arch CMP at Coopermill Road in Muskingum County, Ohio. Asphalt concrete pavement was applied on the half of the pipe sample's invert as a repair method and the other half was left unpaved. Static loading was applied at the top of the paved and unpaved pipe sample sections respectively. The test results showed that the unpaved section was subjected to higher transverse strain at the crown compared to the paved section, while transverse strain difference at the springline was inconsequential. Moreover, despite the advanced level of deterioration, both sections of the culvert carried significant load capacity. For untreated section the plastic limit of the steel was exceeded at the crown with the load of 60-kip. It should be noted that, due to different levels of water exfiltration, soil strength around different locations of the pipe sample may not have been the same and level of CMP's deterioration might not have been the same along the culvert (Sargand et al. 2018).



Figure 2-8 Field testing of a shallow cover severely deteriorated arch CMP (Sargand et al. 2018).

The synopsis of similar studies, presented above, discusses laboratory testing condition. However, there are generally two methods of soil-pipe testing; placing the pipe sample in field and backfilling to a required cover height and passing or placing a truck with a specified weight and wheel size on the top of

the pipe sample (Chaallal et al. 2014; Darabnoush Tehrani et al. 2020c; Rakitin and Xu 2014). In this method, the load is applied continuously and fast. Basically, to prevent damage to the truck and instrumentations, these tests are not designed to monitor soil-pipe structure failure. The other method is to carry out the tests in the laboratory condition using a hydraulic actuator that provides more control on the applied loading rate and condition (García and Moore 2015; Khatri et al. 2015; Kunecki and Kubica 2004). However, in many similar studies, particularly when it is in displacement control, the load rate is not reported.

Lougheed (2008) used 0.039 in./min for testing a buried deep corrugated large-span arch culvert in an incremental regime where the displacement is applied at a predefined increment and held for a known period of time before exerting the next increment (Lougheed 2008). ASTM D2412 suggests 0.5 in./min for testing flexible pipes, such as CMPs, under the parallel-plate testing configuration (ASTM-D2412 2018). However, Schluter and Shade (1999) studied the effect of load rate on the parallel-plate testing and suggested 0.05 in./min instead of 0.5 in./min and stated that the 0.5 in./min does not ASTM D2414 deflection rate does not relate to the real world behavior of pipes (Darabnoush Tehrani et al. 2020c; Schluter and Shade 1999). Similar study has been done by Sargand and Hazen (1998) for plastic pipes and a rate between 0.01 to 0.06 in./min is suggested. In addition to the suggested load rates for flexible pipes, ASTM D1633 suggests 0.05 in./min loading rate for testing compressive strength of soil-cement cylinders (ASTM D1633 2013). Therefore, a reasonable load rate value should be within the range of the numbers in agreement with soil and pipe testing values.

## **2.4 Structural Analysis of Sewer Linings**

Trenchless renewal applications are being widely used to restore hydraulic integrity of sewer pipes and to provide them with a new design life. Spray applied pipe linings (SAPL) and cured-in-place pipe linings (CIPP) can benefit from their compatibility with different geometries and taking the shape of host pipe. The imposed deformations of the host pipe and the existing hydrostatic pressure impacts a liner installed inside the old pipe. The originated stresses in the liners due to the deformations of buried structure (that are generally small) are almost negligible. Conversely, the existing groundwater pressure can cause lining failure or material breakdown. Hence, a liner must be designed to resist the external hydrostatic

pressure that is the only loading case with a high probability of occurrence. If the host pipe material is damaged or degraded after the liner installation or if the sewer is in an unstable condition, the surrounding static soil load transfers partially from the host pipe to the liner that causes deformation. But, in most cases, the existing pipe-soil structure continues to carry soil load and traffic loads (Thepot 2000).

#### **2.4.1 Structural Classification of Sewer Linings**

Falter (1996) classified sewer linings into two categories of Type 1 and Type 2:

- Type 1: Liner is bonded to the existing pipe. The liner and existing pipe both behave as a rigid structure.
- Type 2: Liner is not bonded to the existing pipe and behaves as a flexible pipe. Liner receives support from the existing pipe and soil.

According to the Falter (1996) classification, the discussed and tested polymeric material in this dissertation is under Type 2 category which the liner was not bonded to the host pipe. Many of polymeric materials are brittle and fail in fracture and hence the limiting tensile strain is the suitable failure criteria. Therefore, an appropriate polymeric material used for sewer pipe lining fails in tension not compression. Any failure of polymeric sewer lining materials will happen due to either elastic buckling itself or a sharp increase in displacement, stress and strain that may result in instability and the occurrence of buckling failure and material failure simultaneously (Boot and Gumbel 1997).

#### **2.4.2 Critical Buckling Pressure Theories available for Design of Circular Flexible Linings used for Sewer Pipes**

An appropriate liner used in sewer pipes to restore the hydraulic integrity of the host pipe needs to be designed to resist groundwater buckling pressure. Withstanding the hydrostatic pressure is always the critical criteria for calculation of the liner thickness. It should be noted that even after renewal of an old pipe, there are always the possibility of further deterioration of the host pipe over the time. Hence, the potential of carrying the soil and traffic loads does not depend on the pipe condition at the time of renewal. If the host pipe condition at the time of lining shows that it is vulnerable to further deterioration after lining, then the surrounding soil settles to a new equilibrium over the time. Therefore, the flexible liner afterward may be

subject to maximum 2% ring deflection. However, the applied compressive stress from the soil will be small and noncritical (Heavens and Gumbel 2004).

#### **2.4.2.1 Timoshenko Critical Buckling Pressure**

According to Timoshenko's formula, the critical buckling pressure of an unconstrained pipe subjected to uniform hydrostatic pressure in terms of the transverse flexural stiffness and the radius of the middle axis of the pipe wall is given by Eq. 2-1 (Timoshenko and Gere 1961).

$$P_{cr} = \frac{3EI}{R^3} \quad \text{Eq. 2-1}$$

where,

$P_{cr}$  = critical buckling pressure, psi,

EI = the transverse flexural stiffness, lb.in.<sup>2</sup>, and

R = the radius of the middle axis of the pipe wall, in.

#### **2.4.2.2 Glock Critical Buckling Pressure**

According to the Glock's formula, the critical buckling pressure of a liner subjected to external uniform pressure (the liner – pipe interface is perfectly frictionless) in terms of the liner thickness and, the average pipe diameter and the Young's modulus of the liner material is given by Eq. 2-2.

$$P_{cr} = E \left( \frac{t}{D} \right)^{2.2} \quad \text{Eq. 2-2}$$

where,

$P_{cr}$  = critical buckling pressure, psi,

t = the liner thickness, in., and

D = the pipe average diameter, in.

## **2.5 Review of Design Methods for Flexible Sewer Pipe Liners**

There are four main national sewer pipe renewal design methods available for calculating a flexible liner thickness, including:

- 1) ASTM F1216-16 (2016) for circular linings in the United States,

- 2) ASTEE 3R-2014 (2014) in France,
- 3) DWA-A 143-2 (2015) in Germany, and
- 4) WRc-SRM (2014) in the United Kingdom.

The four available standards studied with this dissertation have different categorization for the state of the host pipe and utilize different theoretical approaches from Timoshenko's or Glock's formula in the calculation of a design thickness for flexible liners. Sections 2.5.1 to 2.5.4 describe each standard in details. According to all the four mentioned standards, the liner needs to be designed to withstand the hydrostatic pressure. In these design approaches, the buckling and deflection are the limit states. The host pipe shape and any imperfection (global and local) in the geometry can impact the strength of the liner to resist the hydrostatic pressure. Annular gap, for instance, which is uniformly distributed around the pipe circumference is considered as a global imperfection. Local intrusion, for example, which is limited to a portion of the pipe circumference is considered as a local imperfection as illustrated in Figure 2-9 (Thepot et al. 2015).

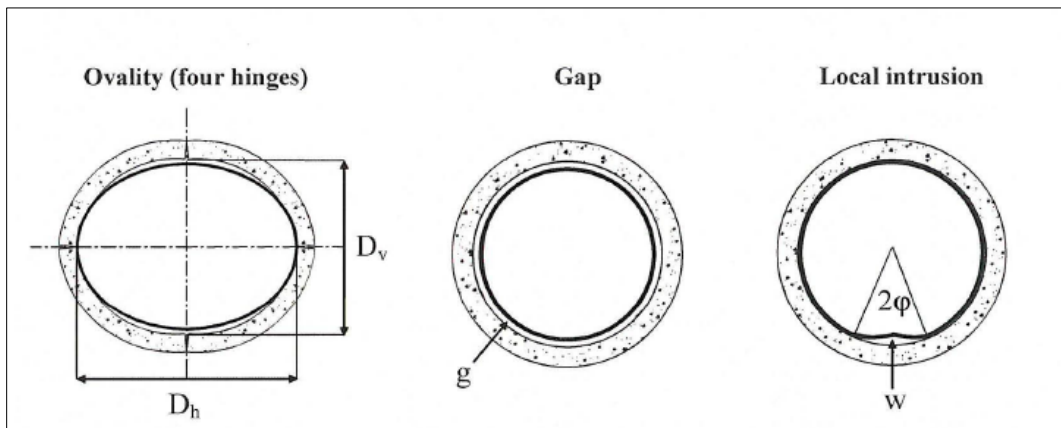


Figure 2-9 Global and local imperfections (Thepot et al. 2015).

### 2.5.1 *ASTM F1216-16 (2016)*

ASTM Standard F1216 was first published in 1989 with a focus on small diameter sanitary sewer pipes, ranging from 8 in. to 12 in. diameters. However, a non-mandatory appendix on the design thickness of CIPP liners was included in the ASTM F1216 (X1. Design Considerations). The ASTM F1216 standard considers two external load cases for calculating the finished wall thickness of the proposed liner pipe.

According to ASTM F1216 (2016), pipeline renewal encompasses two general existing pipe conditions of partially deteriorated and fully deteriorated.

### **2.5.1.1 Partially Deteriorated Pipe Condition**

#### **2.5.1.1.1 Partially Deteriorated Terminology**

Partially deteriorated terminology includes those in which the existing pipe continues to bear the loads, but has corrosion, inflow and infiltration problems. In this condition, the host pipe is stable, and the liner is designed to resist the groundwater pressure acting in the annular space between the liner pipe and the host pipe (Gumbel 1998). This is the so-called partially deteriorated pipe condition (PD). Even where the permanent groundwater table is below the pipe invert level, according to the F1216 ASTM standard, the liner must generally be designed to resist a long-term external hydrostatic head which can be possible under storm conditions. The partially deteriorated terminology according to the Appendix X1.1.1 of the ASTM F1216 is presented in Figure 2-10 (F1216-16 2016).

**ASTM F1216 - X1.1.1 partially deteriorated pipe** – the original pipe can support the soil and surcharge loads throughout the design life of the rehabilitated pipe. The soil adjacent to the existing pipe must provide adequate side support. The pipe may have longitudinal cracks and up to 10% distortion of the diameter. If the distortion of the diameter is greater than 10%, alternative design methods are required.

Figure 2-10 Partially deteriorated pipe terminology according to the (F1216-16 2016).

#### **2.5.1.1.2 CIPP Liner Design Thickness**

According to ASTM F1216 for the partially deteriorated pipe condition, the CIPP liner is designed to support the hydraulic loads due to groundwater, since the soil and surcharge loads can be supported by the original pipe. The groundwater level should be determined by the purchaser and the thickness of the CIPP should be sufficient to withstand this hydrostatic pressure without collapsing. For calculating the external hydrostatic pressure, ASTM F1216 uses the Timoshenko formula modified by an experimentally derived enhancement factor of 7.0. The Eq. 2-3 and Eq. 2-6 may be used to determine the external groundwater pressure and the required CIPP liner thickness (F1216-16 2016):



$$P_w = \frac{2KE_L}{(1-\nu^2)} \times \frac{1}{(DR-1)^3} \times \frac{C}{N} \quad \text{Eq. 2-3}$$

where,

$P_w$  = the external groundwater pressure, psi, measured above the pipe invert,

$K$  = the enhancement factor of the soil and existing pipe adjacent to the new pipe (a minimum value of 7.0 is recommended where there is full support of the existing pipe). The enhancement factor is the ratio between the restrained buckling pressure and the unrestrained buckling pressure.

$E_L$  = the long-term modulus of elasticity, psi,

$\nu$  = the Poisson's ratio (0.3 average),

DR = the dimension ratio of CIPP ( $DR = \frac{D_O \text{ (mean outside Diameter)}}{t \text{ (thickness)}}$ ),

$C$  = ovality reduction factor ( $C = \left[ \left( \frac{D_O \text{ min}}{D_O \text{ max}} \right)^2 \right]^3 \left( \frac{\left[ 1 - \frac{\Delta}{100} \right]}{\left[ 1 - \frac{\Delta}{100} \right]^2} \right)^3$ ),

$\Delta$  = percentage ovality of original pipe =  $100 \times \frac{\text{Mean Inside Diameter} - \text{Minimum Inside Diameter}}{\text{Minimum Inside Diameter}}$ , or

$100 \times \frac{\text{Maximum Inside Diameter} - \text{Mean Inside Diameter}}{\text{Mean Inside Diameter}}$ ,

$N$  = safety factor (typically  $N = 1.5 - 2$ ).

### 2.5.1.1.3 *Origins of the ASTM F1216 Formula for Hydrostatic Buckling for Partially Deteriorated Host Pipe Condition*

The formula for hydrostatic buckling of the liner, used in ASTM F1216, is based on the theoretical hydrostatic buckling pressure of a long, perfectly circular, unrestrained pipe given by Eq. 2-4 (modified Timoshenko formula)(Gumbel 1998) .

$$(P_{cr})_0 = \frac{24E^*I}{D^3} \quad \text{Eq. 2-4}$$

where,

$(P_{cr})_0$  = the unrestrained hydrostatic buckling pressure, psi, measured above the pipe invert,

$E^* = \frac{E}{(1-\nu^2)}$  = the plane strain modulus, psi,

$E$  = flexural modulus, psi,

$\nu$  = the Poisson's ration (0.3 average),

$I$  = the moment of inertia =  $\frac{t^3}{12}$ , in.<sup>4</sup>/in.

$D$  = median diameter of the pipe ring = outside pipe diameter minus pipe thickness, in.

An empirical factor of  $K=7$  for design purposes is applied to the above unrestrained hydrostatic buckling pressure formula Eq. 2-4 by Aggarwal and Cooper (1984) to justify the observed enhancement of hydrostatic pressure in the first experiments on CIPP liners installed inside steel casings subjected to external water pressure, as illustrated in Figure 2-11. Hence, this was the figure subsequently adapted for CIPP in the ASTM F1216 (Gumbel 1998).

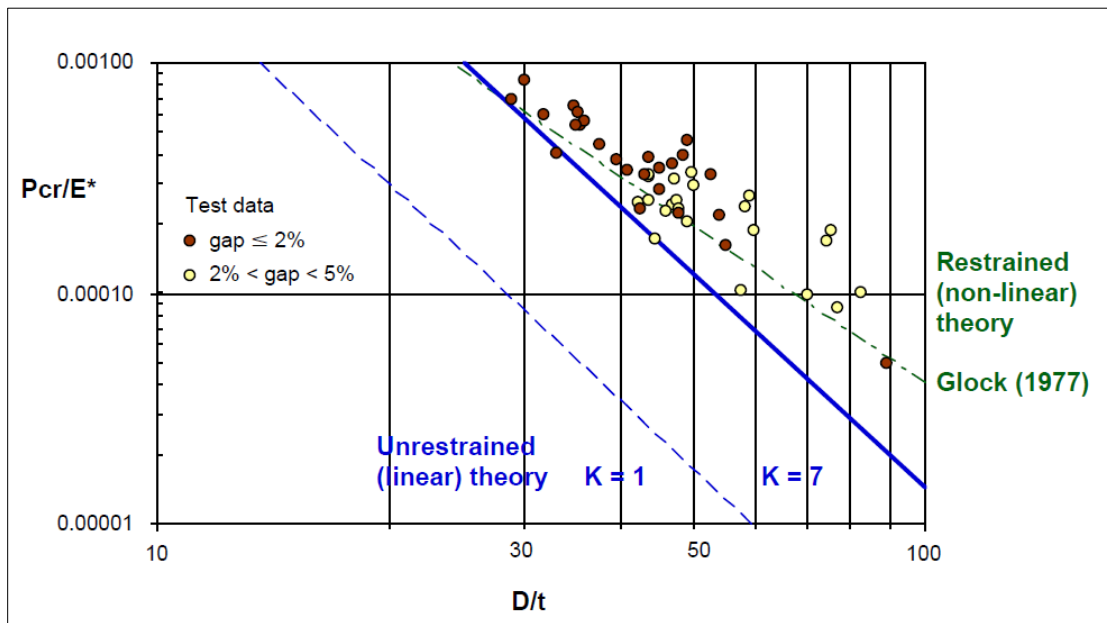


Figure 2-11 Aggarwal's 1984 hydrostatic buckling data compared with contemporary theories (Gumbel 1998).

The design procedure as illustrated in Figure 2-11 is empirical and limited in validity to the particular CIPP product and range of dimension ratio  $D/t$  tested. In another study (Straughan et al. 1995), the authors developed a test procedure and evaluated CIPP products to simulate the sustained hydrostatic pressure experienced by liners constrained in partially deteriorated condition. Their study showed that the estimated

long-term buckling pressure was greater than the predicted design considerations in ASTM F 1216. Hence, their study resulted in different experimental K-factors (Gumbel 1998; Straughan et al. 1995).

Gumbel (1998) stated that the assumed linear buckling mode presented in Eq. 2-4, takes into account liner deformations breaching the boundary conditions imposed by the restraining host pipe, as illustrated in Figure 2-13 (Gumbel 1998). However, there exists a restrained non-linear theory consistent with the boundary conditions (Glock 1977), as depicted in Figure 2-11, which suggests the mean K-factor increases with increasing the ratio of D/t. Hence, the ASTM F1216 formulae considered the initial ovality induced by vertical deformation of the pipe prior to the lining. Then ASTM F1216 buckling pressure formula in partially deteriorated condition is modified to:

$$P_{cr} = 2KCE^* \left(\frac{t}{D}\right)^3 \quad \text{Eq. 2-5}$$

where,

C is a semi-intuitive ovality factor derived by substituting for radius  $R = D/2$  in the buckling formula for unrestrained circular liner pipe (Eq. 2-4), and  $R'$  is the local maximum radius of curvature of an elliptically deformed host, as illustrated in Figure 2-13 (b). The validity of the ovality factor was tested by Boot & Welch (1996) and suggested the C factor in the ASTM F1216 formula (Eq. 2-3) is conservative, as illustrated in Eq. 2-4 (Gumbel 1998).

Some researches evaluated the C factor and studied theoretical considerations to examine the validity of attempting to isolate the impact of ovality as an independent factor on hydrostatic buckling pressure (Boot and Gumbel 1997; Seemann et al. 2001). The need for an integrated approach to predict the combined effect of ovality, gap and other imperfections provides a further imperative for updating the current theoretical model (Gumbel 1998).

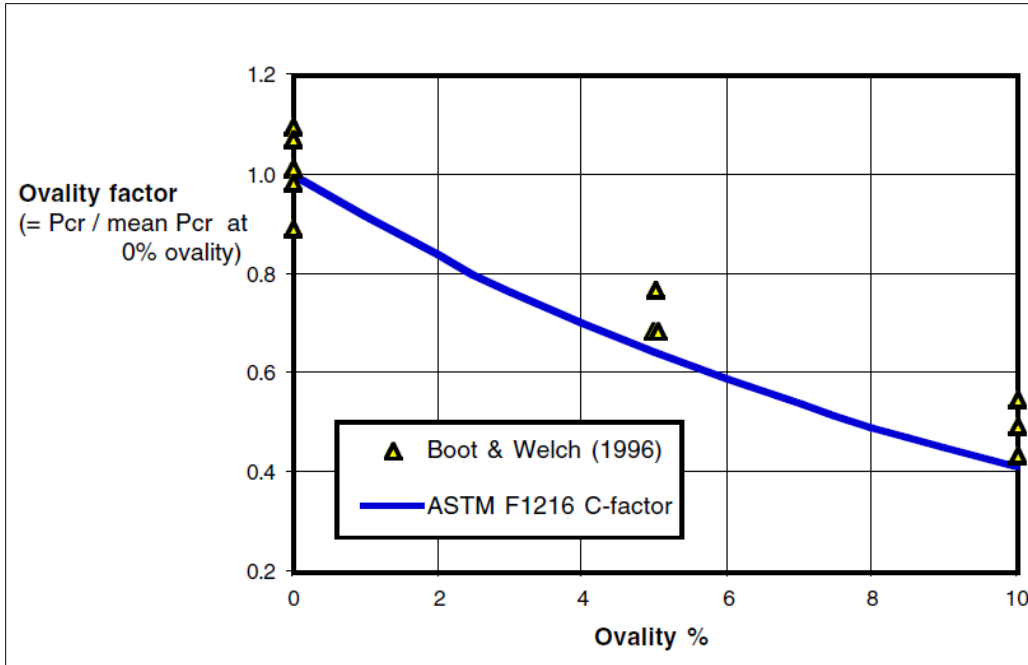


Figure 2-12 Experimental ovality factors for liner of  $D/t = 45$  compared with ASTM F1216 C-factor (Gumbel 1998).

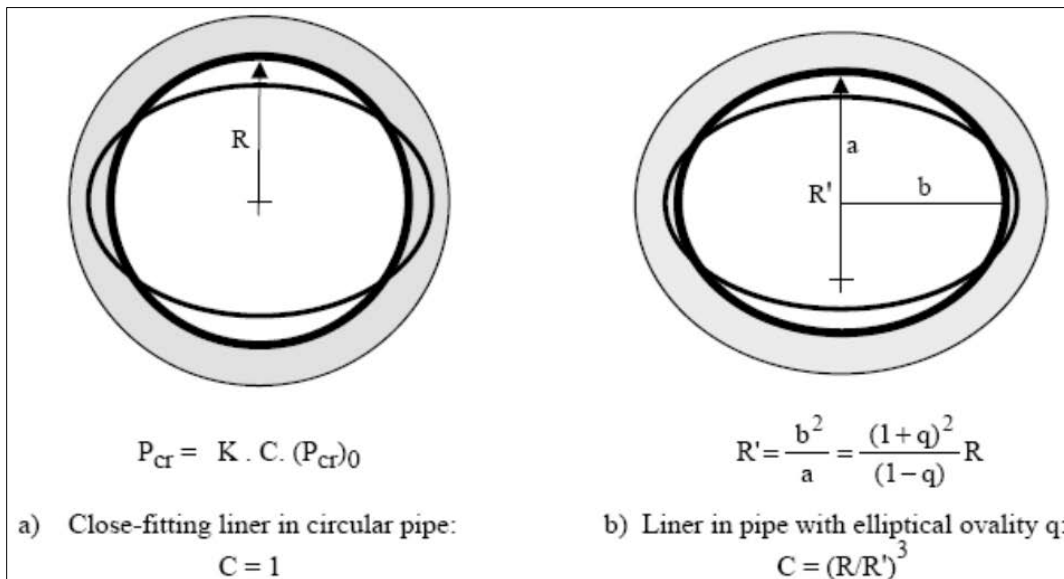


Figure 2-13 Liner deformations implicit in the ASTM F1216 design formula based on linear theory of unrestrained buckling with enhancement factor  $K$  and ovality factor  $C$ : (a)  $C$  value for a circular flexible liner, and (b)  $C$  value for an elliptical flexible liner (Gumbel 1998).

Figure 2-14 illustrates the buckling failure steps of a restrained circular liner under the hydrostatic pressure that were examined and observed in numerous laboratory experiments in the US and UK (Boot and Javadi 1998; Boot and Welch 1996; Gumbel 1998; Straughan et al. 1995). Step 1 of Figure 2-14 illustrates the unloaded liner which is a tight fit to the host pipe and can deform by uniform hoop compression. Step 2 of Figure 2-14 illustrates that the liner can lift away from the host pipe in two modes of asymmetric (one-lobe) or symmetric (two-lobe) due to slack in the system. As pressure is further increased, the inward deformation of the lifted lobe/lobes is accompanied by a decrease in lobe length and increase in ring compressive strain. Step 3 of Figure 2-14 illustrates the eventual snap-through phenomenon at critical buckling pressure with a critical lobe length at failure (geometric instability). The critical lobe length increases as a result of initial annular gap and both elastic and creep compressive strains contributing to further reduction in liner perimeter under pressure. This controlling influence of hoop compressive strains distinguishes the buckling mode as essentially non-linear (Gumbel 1998).

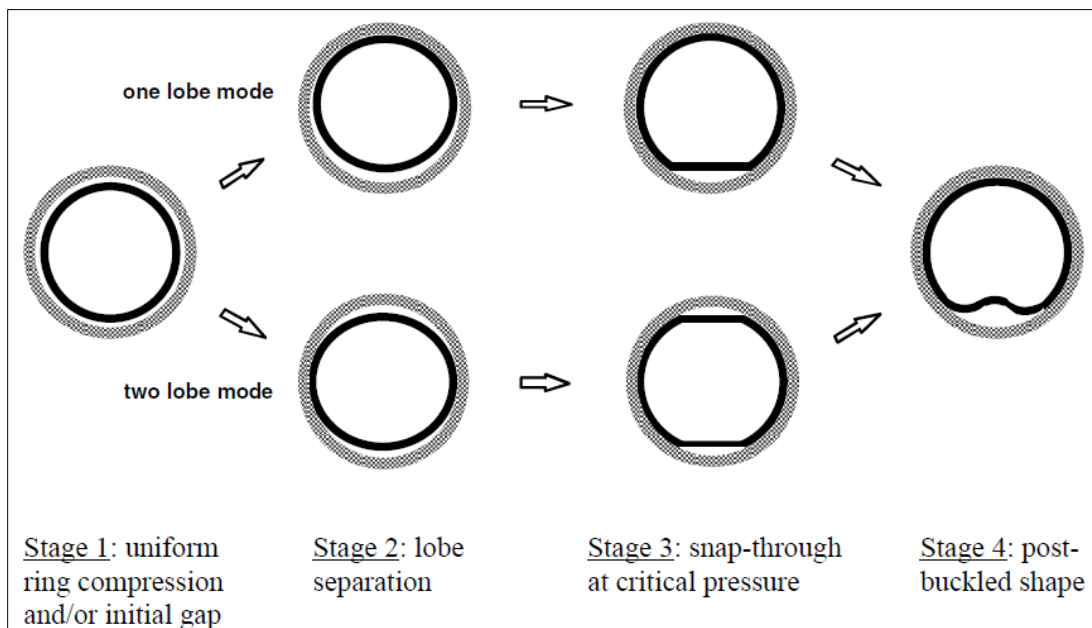


Figure 2-14 Steps in non-linear hydrostatic buckling of restrained circular liner pipe (liner deformations fully consistent with boundary conditions) (Gumbel 1998).

Given the above discussion, to calculate the required minimum wall thickness to resist external hydrostatic buckling pressure acting on the liner, the ASTM F1216 equation for the partially deteriorated

pipe condition takes the actual groundwater pressure as the critical buckling pressure and solves the Eq. 2-6 (Eq X1.1 of ASTM F1216) for using the ovality reduction factor of C and safety factor of N:

$$t = \frac{D_o}{\left(\frac{2KE_L C}{P_w N(1 - \nu^2)}\right)^{1/3} + 1} \quad \text{Eq. 2-6}$$

### 2.5.1.2 Fully Deteriorated Pipe Condition

Fully deteriorated terminology includes those in which new pipe, liner or other reinforcement is added to help bear the loads. In this condition, the soil and traffic loads will in due course be transferred from the existing pipe-soil structure to the liner pipe. This is the so-called fully deteriorated pipe condition (FD). In fully deteriorated condition, the host pipe has lost its ring and bending stiffness and is likely to collapse. In this condition, the liner is designed to resist groundwater pressure, soil pressure and traffic loads. The likelihood of this condition is assumed to be a function of the condition of the sewer at the time of lining (Najafi and Gokhale 2005). However, some researchers studied that in the majority of practical situations a very negligible load transfers to the liner because the lining process effectively locks in the existing equilibrium of even severe deteriorated sewer structures (Falter 1996; Gumbel 1998; Thepot 2000).

According to the Gumbel (1998) for fully deteriorated host pipe condition, the ASTM F1216 overestimates the transferred soil load to the liner and considers the liner as a direct buried pipe, which is conservative. While, if the host pipe may continue deteriorating even after the application of the liner, the more accurate methodology to be considered is more similar to the tunnel lining (Schrock and Gumbel 1997).

The ASTM F1216 and ASTM F1743 specify use of a modified AWWA C950 design equation for a fully deteriorated gravity flow pipe. This equation adds an ovality reduction factor for consideration of long-term creep effects and a design safety factor of 1.5, instead of the AWWA safety factor of 1.8. AWWA C950 equation was originated and modified from the critical buckling pressure of buried flexible pipes derived by Luscher (Luscher 1966; Omara 1997; Watkins and Anderson 1999). Eq. 2-8 presents the modified AWWA C950 equation, to calculate the CIPP design thickness:

$$P = \left(0.593 \frac{R_w E_s E I}{0.149 r^3}\right)^{1/2} \quad (\text{AWWA C950}) \quad \text{Eq. 2-7}$$

where,

$P$  = collapse pressure of unconstrained pipe, psi,

$R_w$  = the buoyancy factor (0.67 minimum) =  $1 - 0.33(H_w/H)$ , dimensionless,

$E_s$  = the modulus of elasticity of adjacent soils or soil reaction, psi,

$E$  = modulus of elasticity at operating temperature of the pipe, psi,

$I$  = moment of inertia, in.<sup>4</sup>/in.

$r$  = radius with no ovality, in.

$$q_t = \frac{1}{N} [32R_w B' E'_s C (E_L I / D^3)]^{1/2} \quad \text{Eq. 2-8}$$

where,

$q_t$  = the total pressure due to water, soil, and live load acting on pipe =  $0.433H_w + wHR_w/144 + W_{s'}$ , psi,

$w$  = soil density, lb/ft<sup>3</sup>,

$W_{s'}$  = live load, psi,

$R_w$  = the buoyancy factor (0.67 minimum) =  $1 - 0.33(H_w/H)$ , dimensionless,

$H_w$  = height of water on top of the pipe, ft,

$H$  = height of soil above top of pipe, ft,

$B'$  = the empirical coefficient of elastic support =  $1/(1 + 4e^{-0.065H})$  (inch-pound units, dimensionless),

$I$  = moment of inertia of CIPP liner, in.<sup>4</sup>/in. ( $I = t^3/12$ ),

$t$  = thickness of CIPP liner, in.,

$E'_s$  = the modulus of elasticity of adjacent soils or soil reaction, psi,

$E_L$  = long-term modulus of elasticity for liner, psi,

$C$  = ovality reduction factor,

$D_o$  = mean inside diameter of original pipe, in.,

$N$  = factor of safety.

Modified AWWA C950 formula specifies CIPP to have a minimum 50% of required stiffness ( $EI/D_o^3$ ), which is 0.093 (inch-pound units). As Eq. 2-9 presents, to obtain a thickness of 0.093 in. or more, a pipe designed with a flexural modulus of elasticity (E) of 350,000 psi would have a dimension ratio of 67.

Therefore, if the CIPP stiffness is too low, the wall thickness must be increased accordingly to ensure the design condition in Eq. 2-9 is met.

$$\frac{EI}{D_o^3} = \frac{E}{12(DR)^3} \geq 0.093 \quad \text{Eq. 2-9}$$

where,

E = the flexural modulus of elasticity of the CIPP, psi, and

I = the moment of inertia, in.<sup>4</sup>/in.,  $I = t^3/12$ .

According to the ASTM F1216, Eq. 2-10 should be used to calculate the CIPP thickness required to withstand the groundwater level, soil type, dead and live loads.

$$t = 0.721D_o \left( \frac{(Nq_t)^2}{CE_L R_w B' E'} \right)^{1/3} \quad \text{Eq. 2-10}$$

It should be noted that a flexible liner design for partially deteriorated condition to withstand the hydrostatic pressure sets the minimum thickness for the liner. However, a flexible liner design for fully deteriorated host pipe condition, neglects the presence of the host pipe and assumes all the soil, traffic and hydrostatic pressures will be carried out by the liner. Although, this assumption qualitatively and quantitatively is wrong, it is considered as the worst-case scenario by ASTM F1216, and sets a maximum flexible liner design thickness. All aspects of a liner response depend on the existing pipe-soil structure. The assumption of a safe liner design by neglecting the presence of the existing structure is not correct; since the development of annular gap and the buckling under hydrostatic pressure can be more critical than the same pipe buried directly in the soil (Heavens and Gumbel 2004).

### **2.5.2 ASTEE 3R2014 (2014)**

A design method for non-circular sewer lining was developed by Olivier Thepot that examines the effect of external long-term hydrostatic pressure. Thepot design methodology categorizes lining into critical linings and subcritical linings. Using a modified-Glock solution for the buckling of flexible liners installed in existing pipes (an encased condition) developed by Olivier Thepot (Thepot 2000), it can be used for both circular and non-circular geometries making it fit the wide variety of in situ cross-sectional geometries that



the engineer will encounter in sanitary sewer, storm sewer, and especially culvert pipes. The pot's design methodology was codified in France in 2014 as 3R2014 Structural Design for Non-Circular Linings Under Groundwater Pressure. It is an analytical design method applicable to the challenging pipe shapes normally found in sewer and culvert pipes. The ASTEE 3R2014 (2014) considers existing pipe conditions as State I (the host pipe is stable and hydraulically compromised with superficial corrosion), State II (the host pipe is cracked with deformation less than 10% but it is stable and further deformations are likely) and State III (the host pipe lost its ring and bending stiffness, it is unstable and likely to collapse). According to ASTEE 3R2014, a circular flexible liner to withstand the hydrostatic pressure is designed based on Eq. 2-11.

$$P_{cr,we,d} = 0.97k_p K^{0.4} \frac{EI_{L,d}^{0.6} \times EA_{L,d}^{0.4}}{r^{2.2}} \quad \text{Eq. 2-11}$$

where,

$EI_{L,d}$  = design flexural stiffness, kips,

$EA_{L,d}$  = design axial stiffness, kips,

$k_p$  = reduction factor for imperfections,

$K$  = the number of buckling lobe (1 or 2).

According to ASTEE 3R2014 (using a modified version of Glock's equation), a noncircular critical shape flexible liner (such as egg-shape and horseshoe shape) to withstand the hydrostatic pressure is designed based on Eq. 2-12.

$$P_{cr,we} = 2.02K^{0.4} K_{p,g} \frac{EI^{0.6} EA^{0.4}}{P^{0.4} r^{1.8}} \quad \text{Eq. 2-12}$$

where,

$K$  = the number of lobe (1 or 2),

$P$  = the mean perimeter of the lining, in.,

$r$  = the radius of the arc where the lobe develops, in.,

$EI$  = the flexural stiffness of the wall, psi.in.<sup>4</sup>/in.,

$EA$  = the compressive stiffness of the wall, psi.in.<sup>2</sup>,

$K_{p,g}$  = the reduction factor of the critical pressure due to the initial gap.

### 2.5.3 DWA-A 143-2 (2015)

DWA-A 143-2 (2015) considers host pipe conditions as State I (the host pipe structurally sounds and stable), State II (the host pipe is cracked with deformations less than 3% and it is stable but further deformations are unlikely) and State III (the host pipe is cracked with deformation less than 10% but it is unstable and likely to collapse). According to DWA-A 143-2 (using an adapted version of Glock's equation), a circular flexible liner to withstand the hydrostatic pressure is designed based on Eq. 2-13.

$$K_{rit} P_{a,d} = k_{v,s} \times 2.62 \times \left(\frac{r_L}{t_L}\right)^{0.8} \times S_{L,d} \quad \text{Eq. 2-13}$$

Where,

$S_{L,d}$  = design ring stiffness, psi,

$k_{v,s}$  = reduction factor for imperfections

#### 2.5.3.1 State I Host Pipe Condition

In state I condition, the host pipe takes soil and traffic loads. The liner's wall thickness is designed based on the applied groundwater pressure (measured from the invert of the host pipe).

#### 2.5.3.2 State II Host Pipe Condition

In state II condition, the existing pipe-soil system can resist the soil and traffic loads. In this state the host pipe can have longitudinal fractures and small pipe deformation which activates the support of the pipe's bedding vertically and horizontally. This support is confirmed through long-term observation and/or penetrometry measurement that is one method for quantifying the yield stress of semisolid materials. The liner's thickness is calculated based on the groundwater pressure.

#### 2.5.3.3 State III Host Pipe Condition

In state III condition compared with the state II condition, the existing pipe-soil system is no longer capable to resist significant deformation. In this state, the liner is designed to carry soil and traffic loads. In State III, even after installation of the liner, the host pipe can get further deformations under load (Thepot et al. 2015).

The design load for both state I and state II host pipe conditions are given as external water pressure only. If no groundwater pressure exists, a virtual water column equal to the pipe's diameter plus 4 inches or 5 feet above the invert, whichever is greater, is used in the calculation of the liner design load. The design load for state III host pipe condition requires consideration of the external water pressure, soil load, and traffic load. For the soil load the DWA-A 143-2 limits it to 0.75 times the weight of the soil prism directly above the pipe.

It should be noted that the DWA-A 143-2 calculation model for state III uses a complicated second-order analysis of the Wrinkle model, as illustrated in Figure 2-15, consisting of a spring system (for modeling surrounding soil) that necessitates the design engineer using Finite Element Analysis. In this model all the loads are applied all together at once to the renewed soil-pipe system.

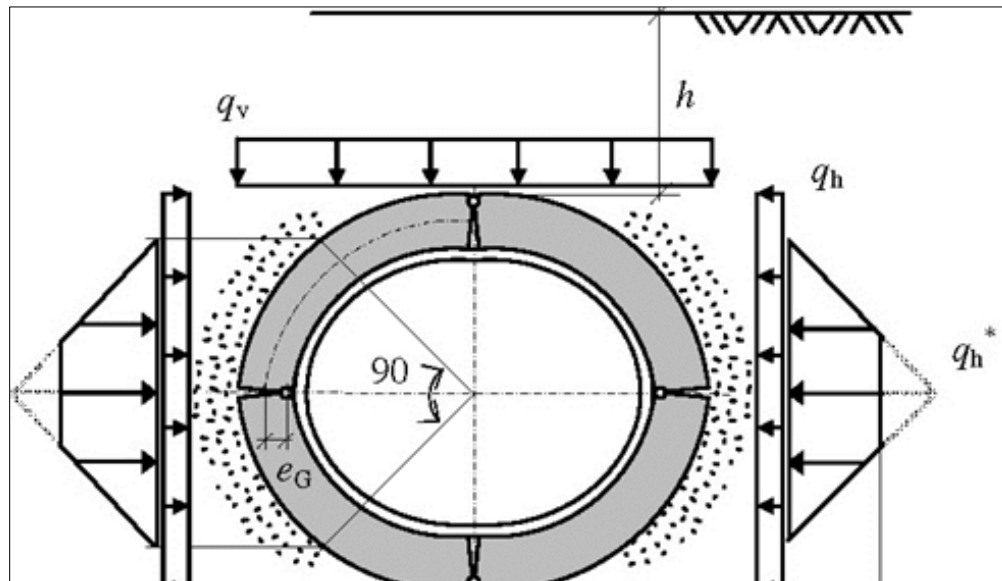


Figure 2-15 Wrinkle model used for DWA-A 143-2 state III flexible liner design.

#### 2.5.4 WRc SRM (2014)

WRc SRM Volume III design procedures are generally suitable for sewer pipes with a diameter less than 72in. The WRc SRM (2014) has different categorization for the existing pipe conditions, which are Type I (lining integral with host pipe) and Type II (no soil load applied from host pipe to the liner). According to WRc SRM (2014), the design equation for calculating a circular flexible liner used for renewal of sewer

pipes to withstand the hydrostatic pressure is similar to ASTM F1216, as described in Eq. 2-1 and Eq. 2-14. All the parameters in Eq. 2-14 are defined with Eq. 2-1.

$$P_w = \frac{2KE_L}{(1 - \nu^2)} \times \frac{1}{(DR - 1)^3} \times \frac{C}{N} \quad \text{Eq. 2-14}$$

#### **2.5.4.1 Type I Liner Design**

The lining, grout (where present), and existing sewer act as a rigid composite section. A bond is required between the lining and existing sewer (and grout where present).

#### **2.5.4.2 Type II Liner Design**

In Type II, the host pipe is in equilibrium at the time of lining and the equilibrium continues to be preserved by the liner. In this type, the host pipe support to the traffic and surrounding soil and the liner only be designed to resist groundwater pressure. The lining is designed as a flexible pipe and it does not require a bond between the lining, and grout (where present) or the existing sewer. The existing structure is assessed to be fundamentally sound without fractures and deformations as described in the Manual of Sewer Condition Classification (which follows the NASSCO PACP).

Worker-entry size linings may be designed as Type I or Type II structures. For non-man entry size flexible sewer linings, the WRc SRM states that they should be designed as Type II structures, as adequate bond to the existing sewer cannot confidently be achieved. Therefore, with respect to CIPP, Type II lining is the common practice in the UK. The Type II lining thickness is typically calculated based on hydrostatic buckling of the liner due to groundwater pressure.

### **2.5.5 Comparison of Available Flexible Sewer Liner Design Methods**

According to the all four mentioned national standards, in all conditions, the liner is designed to resist the groundwater pressure. The cracks in the host pipe may result in percolating the water through them. The cross section and imperfections in geometry, especially in non-circular pipes, affect the liner design to resist the hydrostatic pressure. The mentioned national standards, offer formulas for general buckling in circular lining. This general buckling formulae, in ASTM F1216-16 (2016) and WRc-SRM (2014)

are based on Timoshenko's concept (Timoshenko, 1961), which is modified by use of an enhancement (K) factor of, commonly set as 7.0. These standards consider a safety factor of 2 and a reduction factor for ovality of the host pipe. The standard guidelines recommend use of long-term modulus for creep behavior of the liner to prevent buckling. The ASTEE 3R2014 (2014) considers an ovality reduction factor for imperfections with a minimum value of 1%. Conversely, the other three mentioned standards offer a formula for buckling pressure in non-circular liners. ASTEE 3R2014 (2014) uses Finite Element Modeling (FEM) analysis and an analytical solution (Thepot 2000) to calculate the buckling pressure for convex shapes (they presented a close result for buckling pressure), which extends Glock's analysis (Glock 1977) to non-circular lining. WRc-SRM (2014) considers failure by a bending formula for egg-shaped and oval linings for Type II host pipe. According to this standard, two conditions which are bending stress and maximum deflection must be verified. DWA A143-2 (2015) offers an equivalent circular lining for 3 by 2 egg shapes and FEM analysis for other non-circular shapes.

The liner design for fully deteriorated host pipe, according to the ASTM F1216-16 (2016), among other factors is based on the soil conditions around the host pipe. The buckling is the limit state for this category and the most effective parameter is soil modulus. The ASTEE 3R2014 (2014) presents a design model based on Law and More numerical modeling of tight fitting flexible liner in damaged sewer under earth loads (Law and More, 2007) without consideration of the liner stiffness. In this model, the soil stiffness controls the pipe deflection and the developed local strains in the liner are affected by the magnitude of those deflections. The interaction between the damaged host pipe and the liner results in concentrated loads at crown and invert of the pipe. In this situation, the liner acts as a ring under parallel plate loads. The DWA A143-2 (2015) recommends a Winkler model, which models the surrounding soil structure interaction directly by soil springs for State III of the host pipe. According to this standard, all the loads are applied to the liner-pipe-soil composite and the most effective parameter is soil modulus.

Table 2-1 Structural classification of flexible liners used for sewer pipes according to four national and international standards.

Standard	Classification	Host Pipe Condition	Design Loads
ASTM F1216 (2016)	Partially Deteriorated	<ul style="list-style-type: none"> <li>The existing pipe continues to bear the loads but has corrosion and I/I problems.</li> <li>The host pipe is stable.</li> </ul>	<ul style="list-style-type: none"> <li>The liner is designed to resist groundwater pressure.</li> <li>The liner design is based on the soil conditions around the host pipe.</li> <li>The buckling is the limit state for this category.</li> <li>The most effective parameter is soil modulus.</li> </ul>
	Fully Deteriorated	<ul style="list-style-type: none"> <li>New pipe or other reinforcement is added to help bear the loads.</li> <li>The pipe, even in its fully deteriorated state, is holding the soil load and in reality, is not fully collapsed.</li> <li>The host pipe has lost its ring and bending stiffness and is likely to collapse.</li> </ul>	<ul style="list-style-type: none"> <li>The liner is designed to resist groundwater pressure, soil pressure and live loads.</li> </ul>
ASTE E 3R2014 (2014)	State I	<ul style="list-style-type: none"> <li>The host pipe is stable and hydraulically compromised with superficial corrosion.</li> </ul>	<ul style="list-style-type: none"> <li>The liner is designed to resist the groundwater pressure.</li> <li>The soil stiffness controls the pipe deflection.</li> <li>The developed local strains in the liner are affected by the magnitude of those deflections.</li> <li>The interaction between the damaged host pipe and the liner results in concentrated loads at crown and invert of the pipe. In this situation, the liner</li> </ul>
	State II	<ul style="list-style-type: none"> <li>The host pipe is cracked with deformation less than 10% but it is stable and further deformations are likely.</li> </ul>	
	State III	<ul style="list-style-type: none"> <li>The host pipe lost its ring and bending stiffness, it is unstable and likely to collapse.</li> </ul>	

Standard	Classification	Host Pipe Condition	Design Loads
			acts as a ring under parallel plate loads.
DWA-A 143-2 (2015)	State I	<ul style="list-style-type: none"> <li>The host pipe structurally sounds and stable.</li> </ul>	<ul style="list-style-type: none"> <li>The liner is designed to resist the groundwater pressure.</li> <li>All the loads are applied to the liner-pipe-soil composite.</li> <li>The most effective parameter is soil modulus.</li> </ul>
	State II	<ul style="list-style-type: none"> <li>The host pipe is cracked with deformations less than 3% and it is stable but further deformations are unlikely.</li> </ul>	
	State III	<ul style="list-style-type: none"> <li>The host pipe is cracked with deformation less than 10% but it is unstable and likely to collapse.</li> </ul>	
WRc SRM (2014)	Type I	<ul style="list-style-type: none"> <li>Lining integral with host pipe.</li> </ul>	<ul style="list-style-type: none"> <li>The liner is designed to resist the groundwater pressure.</li> </ul>
	Type II	<ul style="list-style-type: none"> <li>No soil load applied from host pipe to the liner.</li> <li>The host pipe is in equilibrium at the time of lining and the equilibrium continues to be preserved by the liner.</li> <li>The host pipe support to the traffic and surrounding soil</li> </ul>	<ul style="list-style-type: none"> <li>The liner is designed to resist the groundwater pressure.</li> </ul>

## 2.6 Chapter Summary

This chapter presented a literature review on the following topics:

- Spray applied pipe lining (SAPL) materials:
  - Polymeric SAPL,
  - Cementitious SAPL,
- Previous studies on SAPL renewed pipe testing:
- Previous studies on buried pipes testing,
- Structural analysis of sewer lining:
  - Structural classification of sewer linings,

- Critical buckling pressure theories available for design of circular flexible linings used for sewer pipes,
- Review of design methods for flexible sewer pipe liners:
  - ASTM F1216,
  - ASTEE 3R2014,
  - DWA-A 143-2,
  - WRc SRM.



## Chapter 3

### SAPL Site Visit Inspections and Field Data Collection

#### 3.1 Introduction

One aspect of this dissertation included site visits and field inspection of existing culverts in the seven states participating in this project. The field data collection assisted in determination of culvert pipe defects that could be incorporated in structural analysis and design methodology to reduce maintenance and operation costs after construction.

United States' pipelines and drainage infrastructure are in poor quality and have reached their design life. Culverts are drainage infrastructure under highways to pass excess water from rainfall, melting snow and river overflowing. Durability and viability of culverts are of the importance to the U.S. departments of transportation. Culverts are engineered of different shapes such as box, circular and arch shapes. They are made of different materials such as reinforced concrete, steel and aluminum. Problems with corroded metallic and fiber reinforced concrete pipe culverts are of the major concerns (Darabnoush Tehrani et al. 2020a). The culvert deterioration has a direct impact on economy and public services (Najafi and Gokhale 2005). Hence, it is essential for culverts to be inspected regularly and assess their condition, functionality, stability, hydraulic efficiency and performance prior to any sudden failures.

The culvert inspection outcome can reveal needs to repair, replace or renewal of existing barrel. Governmental agencies such as departments of transportation (DOTs) and municipalities annually spend a great amount of money on repair, replacement or renewal of old pipes (Najafi 2016). Open-cut replacement of old pipes compared to trenchless pipe renewal methods are very expensive and disruptive to traffic. To reduce social cost to commuting public, trenchless technology can offer innovative and nondestructive approaches, which make pipe renewal easier (Najafi 2010). Trenchless pipe renewal methods significantly reduce the negative environmental and social impacts, damage to pavements, and surrounding infrastructure (Jozaghi et al. 2019; Kohankar Kouchesfehane et al. 2017).

Trenchless renewal methods are used to extend the design life of the existing pipe or culvert (Najafi and Gokhale 2005). The design and installation of a trenchless renewal project need to be executed following a standard design and installation guideline to restore the culvert capacity to an acceptable level

of structural adequacy and integrity. Once this has been accomplished, appropriate inspection and maintenance plans can be undertaken to retain the renewed culvert's performance and extended useful service life.

Trenchless renewal methods include sliplining (SL), cured-in-place pipe (CIPP), spiral wound lining, spray-in-place pipe (SIPP) or spray applied pipe lining (SAPL) are some of the trenchless rehabilitation techniques (Syar et al. 2019). These methods should be used when the project surface and subsurface conditions allow utilizing the trenchless technology.

SIPP and SAPL are conceptually the same, however, SIPP applies to potable water pipelines constructed of metallic or asbestos cement piping in the diameter ranges of 4 in. to 36 in., according to (F3182-16 2016). While SAPL, that is the main focus of this dissertation, is a pipeline renewal solution to protect severely damaged storm sewer pipes from further deterioration (Kohankar Kouchesfehiani et al. 2019; Najafi 2016).

SAPL can potentially be used for structural renewal and load carrying capacity enhancement of culverts by applying a monolithic layer, ranging from 1.0 in. to 3.0 in. (Darabnoush Tehrani 2016; Syar et al. 2020). As there is no design methodology available for SAPLs, most lining vendors utilize cured-in-place pipe (CIPP) design methodology as specified in the ASTM F1216 (F1216-16 2016). Others use various classical analytical structural design approaches, such as beam element design or shell element design.

Inadequate inspection programs, poor maintenance practices and neglecting any risk analysis may cause failure of underground infrastructures sooner than expected (Najafi and Bhattachar 2011). Effective functioning of culverts is of the high importance to the municipalities and departments of transportations. A field inspection and as a result a maintenance strategy can help municipalities for planning a budget allocation based on the vulnerability of the drainage culverts and the severity of the culvert degradation. The Ohio Research Institute for Transportation and the Environment at Ohio University conducted a study on risk assessment and updated inspection procedures for culverts (Mitchell et al. 2005). They inspected 60 culverts and introduced a rating and culvert inspection system. Researchers presented a statistical analysis on the results of their inspection and found that culvert age, material type and flow characteristics were the important factors affecting the performance of those culverts. CUIRE at the University of Texas at Arlington made an important contribution to this topic and developed a culvert inventory and inspection

framework for asset management of culverts and road structures (Najafi and Bhattachar 2011). This study developed a condition rating system for culvert inventory and inspection. The performance of culverts was calculated using an Analytical Hierarchy Process (AHP). They developed their final model for an effective culvert asset management system.

### **3.2 Objectives of Culvert Inspections**

The performance of trenchless renewal methods and SAPLs for any project are dependent on quality of the installations. Appropriately designed and properly installed liner systems will generally perform well throughout their design life. Field data collection of SAPL installations helps with the development of design methodologies and equations for structural application of cementitious and resin-based SAPLs. In addition, proactive maintenance strategies can be scheduled based on the structural condition and performance assessments of the existing structure through the field inspection and collected data. The objective of this chapter is to present the conducted field data collections and in-situ inspections of past SAPL projects to raise renewal defects and installation issues as well as making suggestions for development of proper performance construction specifications. The data collected through the field inspection of SAPL projects is used to assess the structural condition and performance of those projects.

### **3.3 Selection of Culverts**

Twenty-four culverts renewed by SAPL application were selected for field evaluation. Culverts were selected from lists of projects provided by seven DOTs across the U.S. including, DelDOT, FDOT, MnDOT, NCDOT, NYSDOT, Ohio DOT and PennDOT. The selection was based on variations in host culvert material (i.e., corrugated metal pipe and reinforced concrete pipe), corrugation profile, pipe diameter, pipe shape, soil cover depth, age and geographical location. Figure 3-1 illustrates the geographical locations of the selected SAPL culverts from different states (numbered in the order of inspection). A listing of these selected culverts along with their construction and identification details are summarized in Table 3-1.

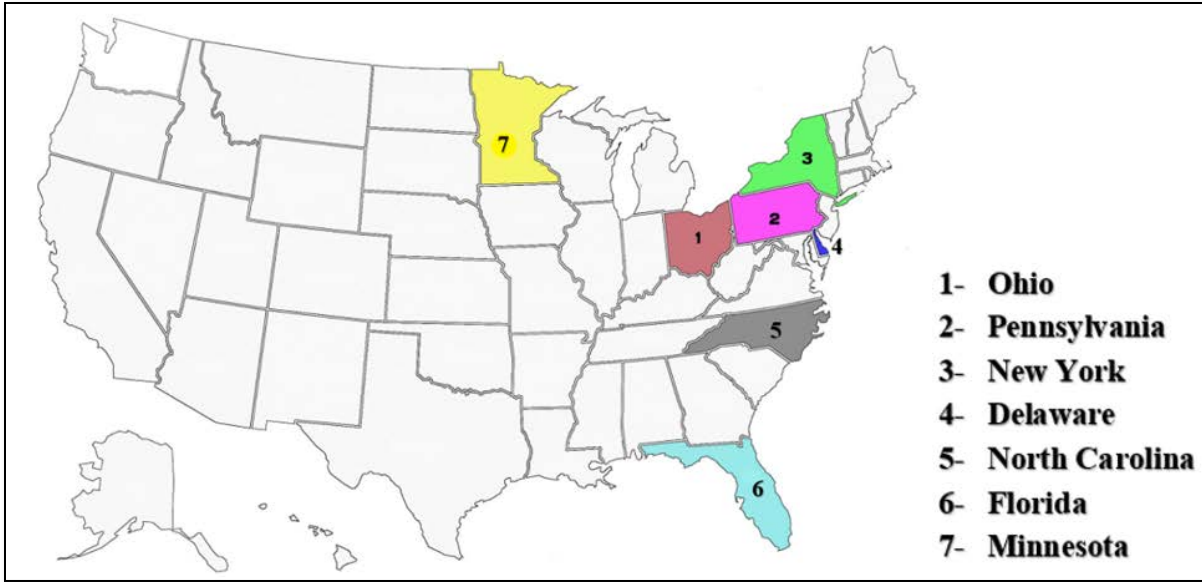


Figure 3-1 Geographical distribution of selected SAPL culverts.

There were five culverts in Ohio, one in Pennsylvania, one in New York, two twin culverts (overall four) in Delaware, 8 in North Carolina (including two twin culverts), three in Minnesota and two in Florida (twin culverts are constructed at a very close spacing from each other). The number of inspected culverts in each state was based on the respective DOT decision and approval. A total of 65% of the selected culverts were circular shapes and 35% were arch shapes. Twenty-one culverts or 87.5% of total were CMPs and three or 12.5% of total were RCPs. All culverts were large diameter and worker-entry sizes, ranging from 54 in. to 156 in. A total of 54% of culverts were lined with reinforced cementitious SAPL material and 46% were lined with geopolymer material. SAPL materials of the inspected culverts were provided by three cementitious SAPL vendors (A, D and E) and two geopolymer SAPL vendors (B and C). Overall, 6 culverts were lined by Vendor A, 2 lined by Vendor B, 9 lined by Vendor C, four lined by Vendor D and three lined by Vendor E. The age range of SAPLs varied from one week to approximately four years. Depth of soil cover on the culvert varied from one ft to 25 ft and SAPL structural design thicknesses varied from 0.65 in. to 2.5 in.

Table 3-1 List of selected SAPL culverts for field inspection.

No.	State	Existing Culvert						SAPL		
		Shape	Material	Diameter (in.)	Length (ft)	Soil Cover (ft)	Vendor	Material	Designed Thickness (in.)	Age (Month)
1	Ohio	Cr*	CMP	78	60	4	C	Geopolymer	1.3	26.9
2	Ohio	Cr	CMP	60	314	15	B	Geopolymer	1	22.2
3	Ohio	Cr	CMP	60	228	12	E	Cementitious	1.5	2.0
4	Ohio	Cr	CMP	54	160	29.15	E	Cementitious	0.65	26.6
5	Ohio	Cr	CMP	84	194	15	C	Geopolymer	1.5	26.1
6	Pennsylvania	Cr	CMP	68	50	2	A	Cementitious	1	36.0
7	New York	Cr	RCP & CMP	60	167	10	A	Cementitious	1	48.0
8	North Carolina	Cr	CMP	72	43	1	C	Geopolymer	1.5	1.0
9	North Carolina	Cr	CMP	84	71	1	C	Geopolymer	1.5	1.0
10	(Twin Culverts)									
11	North Carolina	Ar*	CMP	72x108	48	1	C	Geopolymer	1.5	1.0
12	North Carolina	Ar	CMP	72x96	31	1	C	Geopolymer	1.5	1.0
13	North Carolina	Ar	CMP	72x96	40	1	C	Geopolymer	1.5	1.0
14	(Twin Culverts)									
15	North Carolina	Ar	CMP	72x90	45	2	C	Geopolymer	1.5	1.0
16	Delaware	Ar	CMP	81x59	110	3.27	D	Cementitious	2	3.0
17	(Twin Culverts)									
18	Delaware	Ar	CMP	98x69	125	5.33	D	Cementitious	2	3.0
19	(Twin Culverts)									
20	Minnesota	Cr	RCP	84	550	23-24	A	Cementitious	1	36.0
21	Minnesota	Cr	RCP	60 & 54	790	2-12	A	Cementitious	1	48.0
22	Minnesota	Cr	RCP	54	652	2-10	A	Cementitious	1	48.0
23	Florida	Cr	CMP	156	100	1-2	A	Cementitious	1	101.3
24	Florida	Ar	CMP	71x103	74	6	E	Cementitious	2	63.4

\*Cr: Circular, Ar: Arch.

### 3.4 Inspection Tools

To measure the SAPL thickness, a nondestructive Olympus ultrasonic thickness measurement device (Model 38DL) was initially used. Ultrasonic thickness gages work by very precisely measuring how long it takes for a sound pulse that has been generated by a small probe called an ultrasonic transducer to

travel through a test piece and reflect back from the inside surface or far wall. Because sound waves reflect from boundaries between dissimilar materials, this measurement is normally made from one side in a "pulse/echo" mode (Olympus 2020). A grinder was used for preparing a smooth surface of liner to be perfectly attached to the ultrasonic transducer and enabled it for wave propagation. However, unlike the preliminary calibration and testing in the laboratory with a cementitious SAPL sample, the device was unable to measure the thickness in the field. One possible reason for this issue could be the difference between the density and void ratio of the liner sample material in the laboratory and the applied liner in the field. SAPLs with lower density material and larger voids probably resulted in increasing the wave attenuation rate in the material and disabling the device to measure the thickness. In addition, in case of concrete host pipes, the small amount of impedance mismatch between the cementitious/geopolymer SAPL and the host pipe could cause wave transmission rather than wave reflection. Therefore, an alternative mechanical measurement of the SAPL thickness was carried out by drilling into the liner and measuring the depth of the hole by a digital caliper with 0.001 in. accuracy. The drilling was done in a very low pace and the number of drilling points was limited to prevent any probable perforation in the host pipe. All drilling holes were patched with a high strength cement mortar. During the inspection, due to storm water flow, SAPL thickness measurement at the invert was not possible.

Regular tape and laser-distance meter were used for pipe length and inside diameter measurements. The research team were equipped with safety boots, hard hats, gloves and safety glasses. A high-resolution DSLR Canon Rebel T5i camera was used for video recording and photo capturing of all lined culverts. The liners conditions were documented systematically in a data collection form specially prepared for this purpose.

### **3.5 Inspection Procedure**

The first step in inspection procedure was to obtain design submittal documents, such as SAPL previously test results, wall thickness design and installation details for each specific culvert. The research team evaluated construction inspection and any quality control notes to be able to interpret the visual characteristics of SAPL. The selected inspection methodology was to measure thickness of SAPLs and compare with design requirements suggested by vendors and installers. In addition, the research team

identified, visualized and measured all SAPL fractures, deflections, de-bonding, spalling, holes, corrosion, and cracks.

The National Association of Sewer Service Companies' (NASSCO's) Pipeline Assessment & Certification Program (NASSCO 2019) codes were used for recording some of the SAPL defects during field data collection. Some types of defects were observed in the SAPLs that there was no defined code for them in the NASSCO PACP. Hence, new codes were defined by author to record them. The observed defects along with their identifying codes are listed in Table 3-2. Any SAPL installation irregularities were documented in proper context. The data obtained in this research can be utilized as a baseline for comparison with future inspections.

Table 3-2 SAPL and existing culvert defects.

<b>Cementitious and Geopolymer SAPL Defects Observed in Field Inspection</b>					
<b>Defect</b>		<b>Code</b>		<b>Defect</b>	<b>Code</b>
<b>Defined by NASSCO PACP</b>	Circumferential Crack	CC	<b>Defined by Author</b>	Bolt Heads Visible	BHV
	Longitudinal Crack	CL		Troweling the Liner	LT
	Multiple Cracks	CM		Concrete Patched on the Liner	LCP
	Circumferential Fracture	FC		Nonuniform Liner Thickness	LNT
	Longitudinal Fracture	FL		Low Bond between Liner and Pipe	LB
	Multiple Fracture	FM		Bare Host Pipe	BHP
	Infiltration Weeper	IW		Iron Oxidation on the Liner Surface	LIO
	Infiltration Runner	IR		Efflorescence on the Liner Surface	SLE
	Infiltration Dropper	ID		Irregular Liner Installation	ILI
	Infiltration Gusher	IG		Heavy and Thick Liner Sagging off	LHS
	Lining Failure	LF		Liner Disturbed before Hardening	LHD
	Detached Liner	LFD		Delamination of the Liner	SLD
	Buckled Liner	LFBK		Liner Collapse	XL
	Surface Spalling	SSS		Frog	VF
	Aggregate Visible (dry)	SAV		Centipedes and Worm	VW
	Hole	H			
	Cockroach (V: Vermin)	VC			
	Rat (V: Vermin)	VR			
<b>Existing Culvert Defect Defined by NASSCO PACP</b>					
<b>Defect</b>		<b>Code</b>	<b>Defect</b>		<b>Code</b>
Corrosion of Metal Pipe		SCP	Settled Fine Deposits		DSF
Deformed		D	Settled Hard/Compacted Deposits		DSC
Joint Offset		JO	Settled Gravel Deposits		DSGV
Joint Separated		JS	Root		R

### 3.6 SAPL Issues due to Lack of Standard

As stated earlier, currently there are no standard design methodology and construction specifications for proper performance of SAPLs. Lack of standard can be the main cause for SAPL defects, as it is presented in Appendix A. Technical performance construction specifications determine the quality of the product and the required performance. Technical specifications help to install the liner in a feasible and economical manner. Identification and classification of probable SAPL issues help with preparation of performance construction specifications in a manner to avoid and limit those issues. According to the results of field inspection, the photographs of twelve most common SAPL issues are shown in Figure 3-2 Issues found with SAPLs.



Figure 3-2 Issues found with SAPLs

A summary of field inspection findings of most common issues along with descriptions are listed in Table 3-3. The existing culverts in the order of field inspection trips, their lengths, liners' vendors, age of



SAPLs and observed issues after inspection of each culvert are provided in Table 3-4 and illustrated in Appendix A.

Table 3-3 SAPL field inspection findings.

Findings		Description
<b>Cracks and Fractures</b>	<ul style="list-style-type: none"> <li>Hairline, circumferential, longitudinal, and multiple cracks.</li> <li>A few circumferential fractures.</li> <li>Less circumferential cracks in geopolymer SAPLs in comparison with cementitious SAPLs.</li> <li>Most of circumferential and longitudinal cracks in cementitious SAPLs (including geopolymers) are due to shrinkage of materials.</li> </ul>	<ul style="list-style-type: none"> <li>Hairline cracks are inherent in concrete SAPL linings because of the rigid lining in a flexible CMP.</li> <li>Hairline cracks typically will heal by efflorescence formation when kept wet.</li> <li>Insufficient water cement ratio could result in multiple cracks in SAPLs.</li> <li>Most of circumferential cracks were early age shrinkage cracks.</li> </ul>
<b>Efflorescence</b>	<ul style="list-style-type: none"> <li>Efflorescence on SAPL surface mostly along with weepers.</li> </ul>	<ul style="list-style-type: none"> <li>It was created due to chemical process between cementitious SAPL materials and water (mostly the water coming through the pinholes and weepers).</li> <li>In some cases, as a remedy, efflorescence blocked the pinholes and stopped it from further leakage.</li> </ul>
<b>Rust Staining</b>	<ul style="list-style-type: none"> <li>SAPL surface rust staining mostly appeared as a circumferential pattern.</li> <li>Less effect of rust staining on SAPL surface in corrugated aluminum pipes.</li> </ul>	<ul style="list-style-type: none"> <li>Rust staining on SAPL surface can be due to corrosion of the existing CMP or corroded rebars of RCP.</li> </ul>
<b>Infiltration</b>	<ul style="list-style-type: none"> <li>Infiltration weepers and sometimes drippers on SAPL surface.</li> </ul>	<ul style="list-style-type: none"> <li>Most of them were along with rust staining.</li> </ul>

Findings		Description
<b>SAPL Thickness</b>	<ul style="list-style-type: none"> <li>• Inconsistent SAPL thickness.</li> <li>• Most of thick and heavy SAPL materials (Figure 2) tended to sag off from both sides of the crown and move towards the springlines. So, the maximum nominal thickness of them were at the crown and around the springlines.</li> <li>• As inspected, hand spray and shotcrete did not provide a consistent thickness of SAPL.</li> </ul>	<ul style="list-style-type: none"> <li>• Installation variabilities and lack of quality control was the most common reasons for inconsistent SAPL thicknesses.</li> <li>• Proper structural design thickness of SAPL and the quality of installation are of the important parameters affecting the SAPL construction performance.</li> </ul>
<b>Installation Issues</b>	<ul style="list-style-type: none"> <li>• Installation variabilities.</li> <li>• SAPL was disturbed (lack of proper finish) before hardening.</li> <li>• Rough surface SAPL.</li> <li>• Shadowing (non-uniformity of spray nozzle movement, Figure 2) of cementitious SAPL materials caused deeper SAPL valleys at the crown of the culvert and thicker SAPL valleys above the springlines.</li> <li>• Original coating and lining on the CMP at the time of host culvert installation caused detaching SAPL from host pipe.</li> </ul>	<ul style="list-style-type: none"> <li>• Considering the concept of SAPL, it is a centrifugally cast in place rehabilitation methodology for structural reinforcement, improving hydraulic characteristics, abrasion and corrosion protection and sealing of existing culvers.</li> <li>• Shadowing is due to tendency of materials to sag from crown towards the springlines.</li> </ul>
<b>Vermin</b>	<ul style="list-style-type: none"> <li>• Cockroach.</li> <li>• Worm.</li> <li>• Frog.</li> </ul>	<ul style="list-style-type: none"> <li>• Several cockroach and worms with their nests were found on the SAPL surface.</li> <li>• No SAPL defect was observed by vermin.</li> </ul>
<b>Deposits</b>	<ul style="list-style-type: none"> <li>• Settled gravel and fine aggregates were found in a few locations.</li> </ul>	

Table 3-4 SAPLs' issues found for each culvert.

Existing Culvert		SAPL			
No.	Length (ft)	Vendor	Age (mo.)	Defects	
1	60	C	26.9	9 CC, BHV, CM, 3 IW, 3 LIO, CL, SLE, LNT, FC	
2	314	B	22.2	5 CC, LIO, SLE (every 3 ft), 5 IW, SSS, DSGV, LT, VW (along the pipe)	
3	228	E	2.0	CC, VF	
4	160	C	26.6	LFD, CC (along the pipe), CM, CL	
5	194	B	26.1	CC and LIO (every 3 ft.), VW (along the pipe)	
6	50	A	36.0	3 CC, 2 LIO, CL, 2 CM, SLE, LHD, 2 IW, LNT	
7	20	A	48.0	Aluminum CMP	ILI
	103			RCP	CC and SLE (every 3 ft), 2 ID, 12 LIO, 13 IW, CM
	44			Aluminum CMP	2 LIO, 4 IW, ID, 2 CC, 3 SLE
8	43	C	1.0	SLD, DSC, DSF	
9 10	45	C	1.0	Left from Inlet*	DSGV, JS, LIO, CC
				Right from Inlet*	3 FC, 4 CC, LCP, LIO
11	48	C	1.0	ILI, 2 LB, 2 LHS, BHP	
12	71	C	1.0	2 CC, 4 SLE, 2 ILI, LIO, LNT, LB	
13 14	40	C	1.0	Left from Inlet	2 CC, 2 ILI, SAV
				Right from Inlet	ILI, LB, 4 CC, 2 IW, LNT, BHP, LHS, SLE
15	31	C	1.0	LHS, SLD	
16 17	110	D	3.0	Left from Inlet	3 CM, FM, SAV, 4 CC, FC, 3 IW, SLE, 2 SSS, 3 LIO, LNT
				Right from Inlet	3 CC, 2 FC, 6 IW, 6 LIO, CL, LCP, ID, LNT
18 19	125	D	3.0	Left from Inlet	LNT, 3 CL
				Right from Inlet	LNT, DSC, ILI, 3 CL
20	550	A	36.0	LNT, 12 SLE, 13 LIO, 8 CC, 3 LCP, 7 IW, CM, 2 LT, 3 LHS, 3 ILI	
21	790	A	48.0	FC, ILI, LHS, IW	
22	652	A	48.0	VW, LIO, 3 ILI, 2 CC, IW, 3 SLE	
23	100	A	101.3	20 CC, 7 CM, 2 SLE, 3 LCP, CL, 4 IW, LHS, 2 LIO, 3 FC, LNT	
24	74	E	63.4	12 CC, 12 SLE, LHS, LB, 2 IW, 7 LIO, 2 CL, 3 CM, VZ, VW	

\*Twin culverts are constructed in a very close distance from each other. The inspection team entered the culverts from the inlet and distinguished them by left and right culverts from inlet.

### 3.7 SAPL Thickness

A statistical analysis was performed to compare the SAPL design thickness with the installation. Number of thickness measuring points and drillings was limited by DOTs and the research team was not allowed to drill SAPLs in many locations. Therefore, SAPL thickness for each culvert was measured at springlines and crown in a few locations, mostly at 10-ft intervals and sometimes at 20-ft and 50-ft from upstream locations to avoid any irregularities of inlet and outlet installations. In many cases, aside from the installation issues as illustrated in Figure 3-2, it was observed that the SAPL installation thickness was less than the required design value. Due to the limited numbers of drilling points, it was not possible for all the pipes to measure the SAPL thickness at the same locations with a similar pattern. Variation of all arch culverts renewed with cementitious SAPL with 2 in. design thickness at 3 o'clock or springline, 12 o'clock or crown, and 9 o'clock or springline, for instance, are illustrated in Figure 3-3. The green and black lines are representative of 2 in. required design thickness and the average measurement of installed thickness, respectively. For example, as it is shown, the average of installed SAPL thicknesses at 0° (3 o'clock, springline) is 1.5 in. which is 0.5 in. less than the 2 in. design thickness.

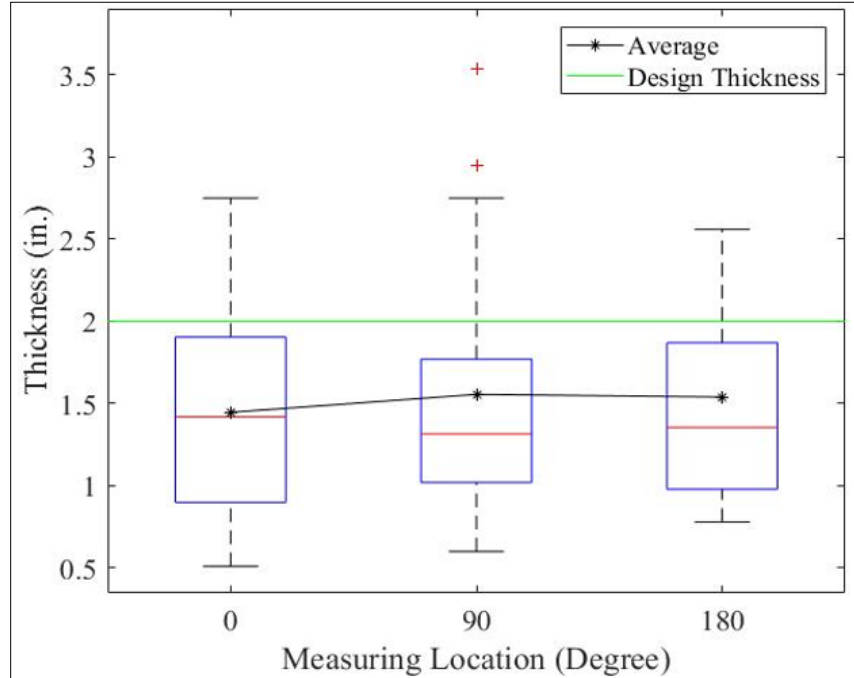


Figure 3-3 SAPL measured thicknesses versus 2 in. design thickness  
(Arch pipes renewed with cementitious SAPL).

The difference of SAPL design and installed thicknesses for an 84-in. circular CMP, as another example, is illustrated in Figure 3-4. The radius of this polar graph shows the SAPL design thickness and the average of installed thickness along the culvert with blue and red lines respectively. The average installed thickness at 0°, 30°, 60°, 80°, 120°, 150° and 180° are shown circumferentially in this graph. As it is shown, the installed SAPL thickness (red line) is less than the required 1.5 in. design thickness (blue line) in all circumferential locations along the culvert.

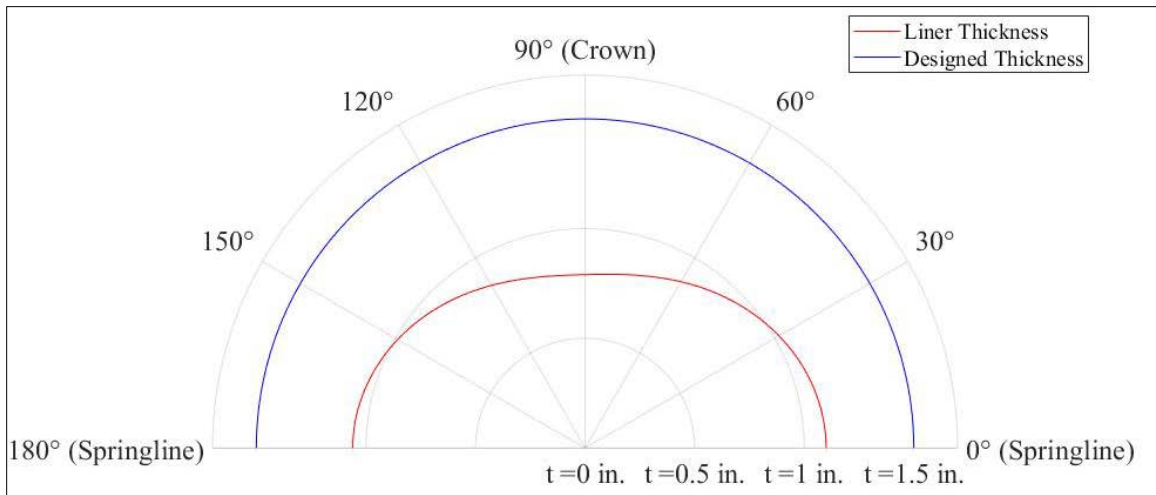


Figure 3-4 SAPL average installed thicknesses versus 1.5 in. design thickness inside an 84-in. diameter circular CMP.

### 3.8 Rating Systems

To summarize and evaluate the condition of SAPLs, a numerical scale rating system from 0 to 9 was established by author to allocate rating to each liner. Also, eight common issues of the structure were monitored and measured for each site. The numerical rating system (0 to 9) and eight common defects of the structure are summarized in Table 3-6. Rating of “9” (Excellent) indicates a structurally sound and functionally adequate (like-new) with no SAPL defects. Rating numbers decrease with worsening condition up to a rating of “0” (Failed), indicating SAPL failure that directly affects the structural or the functional capacity. SAPLs were given a rate for each issue type and finally an average rating was calculated from Eq. 3-1 for each SAPL.

$$OAR = \frac{\sum Rating}{N} \quad \text{Eq. 3-1}$$

where,

OAR = original average rating of the SAPLs, dimensionless,

$\sum Rating$  = summation of general material and installation rating for each observed category of defects, dimensionless, and

N = number of different categories of defects, dimensionless.

The original average rating (OAR) of the SAPLs are summarized in Table 3-7. In case of a shallow cover culvert in a poor condition of SAPL, the condition of the whole structure is more critical. Therefore, a dimensionless rating modifier (M) based on ratio of soil cover thickness and culvert rise was also used for considering potential risks to public motorists in the case of culvert failure. For example, if a culvert with 4 ft rise and 1 ft of soil cover fails, the impacts of failure on the public will be more compared with failure of a culvert with 4-ft diameter and 12 ft of soil cover. Thus, the original average rating needs to be modified and adjusted to have a rating value for the health of whole structure. The adjusted overall structural health rating (AOR) is given by Eq. 3-2.

$$AOR = M \times OAR \quad \text{Eq. 3-2}$$

Where,

AOR = the adjusted overall structural health rating, dimensionless,

M = modifier based on the ratio of soil cover thickness H in ft and culvert rise R in ft, dimensionless.

Masada et al. (2007) provided the rating modifier values. These values are summarized in Table 3-5.

Table 3-5 Rating modifier values.

<b>Ratio Soil Cover (H) to Rise (R)</b>	<b>Modifier Value (M)</b>
$H/R < 2.5$	0.85
$2.5 < H/R < 5$	0.9
$H/R > 5$	1

Table 3-6 Rating scale to evaluate general conditions of SAPLs.

Rate	Category	Description							
		Crack	Fracture	Efflorescence	Corrosion	Infiltration	Deposits	SAPL Surface	SAPL Thickness
9	Excellent	No	No	No efflorescence	Without rust staining	No leakage	No debris, the flow is not obstructed	New condition; No holes; No discoloration of liner surface; No visible joints or head bolts; No surface damage; No roots	As design thickness
8	Very Good	Hairline crack	No	Circumferential cracks without efflorescence	Without circumferential rust staining	No leakage with circumferential cracks	Very minor deposits; No waterway blockages	Surface in a good condition; Discoloration of concrete; No Spalling or delamination, scaling or softening; surface in good condition	0 - 5% different from design thickness
7	Good	Hairline cracks less than 1/16 in.	Circumferential cracks open less than 1/16 in.	5% of cracks with efflorescence	0%-50% of cracks with minor rust staining	10% of cracks with pinholes	Minor deposits; No waterway blockages	Light scaling on less than 10% of exposed area less than 1/8 in. deep; Delaminated/Spalled area less than 1% of surface area.	5 - 10% different from design thickness
6	Satisfactory	Hairline multiple circumferential cracks less than 1/8 in.	Circumferential cracks open greater than 1/16 in.	10% of cracks with efflorescence	50%-100% of cracks with minor staining	Pinholes	Minor waterway blockages are caused between 0%-5% of the total cross-sectional area of culvert. Sediment built up in	Scaling on less than 20% of exposed area less than 1/4 in. deep. Minor delamination or spalling areas less than 5% of surface area. Concrete patched on the liner surface. Heavy and thick liner sagging off	10 - 15% different from design thickness

Rate	Category	Description							
		Crack	Fracture	Efflorescence	Corrosion	Infiltration	Deposits	SAPL Surface	SAPL Thickness
5	Fair	Multiple cracks; Circumferential cracks less than 1/8 in., longitudinal cracks less than 1/16 in.	Circumferential cracks open greater than 1/8 in.	25% of cracks with efflorescence	0%-50% of cracks with moderate rust staining	Infiltration weeper	Minor waterway blockages are caused between 5%-10% of the total cross-sectional area of culvert. Sediment built up in channel, tress or bushes growing in the channel.	Scaling on less than 30% of exposed area less than 3/16 in. deep. Total delaminated/ spalled areas less than 15% of surface area. Liner aggregates are visible.	15 - 20% different from design thickness
4	Poor	Extensive cracking with cracks opens more than 1/8 in.	Longitudinal cracks open greater than 1/8 in.	50% of cracks with efflorescence	50%-100% of cracks with moderate rust staining	Infiltration dripper	Moderate obstruction is caused due to debris between 10%-45% of the total cross-sectional area of culvert, rock settlement causing rock dams, trees or bushes growing into the channel	Spalling at numerous locations; Heavy invert surface scaling greater than 1/2 in.	20 - 25% different from design thickness



Rate	Category	Description							
		Crack	Fracture	Efflorescence	Corrosion	Infiltration	Deposits	SAPL Surface	SAPL Thickness
3	Serious	Extensive cracking greater than 1/8 in.	Extensive fracture	75% of cracks with efflorescence	0%-50% of cracks with large rust staining	Infiltration runner	Heavy obstructions are caused due to settlement of debris 45%-80% of the total cross-sectional area of culvert is lost	Extensive spalling; minor slabbing; Heavy invert surface scaling; 50% loss of wall thickness at invert	25 - 50% different from design thickness
2	Critical	Full depth holes;	Extensive cracking greater than 1/2 in.	100% of cracks with efflorescence	50%-100% of cracks with large rust staining	Infiltration gusher	Culvert is completely blocked; total loss of hydraulic capacity;	Severe liner slabbing; Heavy invert surface scaling; Total delaminated, spalled, and punky cementitious liner areas are greater than 50% of surface area; Very soft cementitious liner	50 - 75% different from design thickness
1	Imminent Failure	Liner partially collapsed, or collapse is imminent. Holes through cementitious liner; 75% loss of wall thickness at invert; Liner partially collapsed							
0	Failed	Liner is collapsed. Liner completely deteriorated at the invert							

Table 3-7 SAPLs overall average rating score (OAR) and adjusted overall structural rating score (AOR).

Culvert	SAPL				Rating								OAR	M	AOR
	Vendor	Age (m)	H/R	Ave. Thickness	Crack	Fracture	SLE	LIO	Infiltration	Settled Deposit	SAPL Surface	Performed Thickness			
Ohio 1	C	26.9	0.62	1.33	7	7	6	7	5	9	8	5	6.75	0.85	5.74
Ohio 2	B	22.2	3.00	1.48	8	9	2	2	5	8	7	5	5.75	0.9	5.18
Ohio 3	E	2.0	2.40	1.50	8	9	9	9	9	9	9	5	8.38	0.85	7.12
Ohio 4	C	26.6	6.48	1.22	7	9	9	9	9	9	8	4	8.00	1	8.00
Ohio 5	B	26.1	2.14	0.95	8	9	9	7	9	8	8	2	7.50	0.85	6.38
Pen	A	36.0	0.35	1.18	6	9	7	7	5	9	7	6	7.00	0.85	5.95
NY	A	48.0	2.00	1.27	8	9	4.5	5	4.5	9	7	4	6.38	0.85	5.42
NC 1	C	1.0	0.17	0.97	9	9	9	9	9	8	7	2	7.75	0.85	6.59
NC 2-L	C	1.0	0.17	0.98	8	9	9	7	9	8	8	3	7.63	0.85	6.48
NC 2-R	C	1.0	0.17	0.89	8	6	7	6	9	9	7	5	7.13	0.85	6.06
NC 3	C	1.0	0.17	2.01	9	9	9	9	9	9	2	2	7.25	0.85	6.16
NC 4	C	1.0	0.14	0.89	8	9	8	9	9	9	2	3	7.13	0.85	6.06
NC 5-L	C	1.0	0.17	1.63	8	9	9	9	9	9	5	2	7.50	0.85	6.38
NC 5-R	C	1.0	0.17	1.51	8	9	9	9	5	9	2	5	7.00	0.85	5.95
NC 6	C	1.0	0.33	1.29	9	9	9	9	9	9	7	2	7.88	0.85	6.69
Del 1-L	D	3.0	0.67	0.99	5	6	5	7	6	8	5	2	5.50	0.85	4.68
Del 1-R	D	3.0	0.67	1.17	5	6	5	7	4	8	5	2	5.25	0.85	4.46
Del 2-L	D	3.0	0.93	1.39	5	9	8	8	8	8	5	2	6.63	0.85	5.63
Del 2-R	D	3.0	0.93	1.20	5	9	8	8	8	7	5	2	6.50	0.85	5.53
Mn 1	A	36.0	3.57	1.00	6	9	6	5	6	9	7	5	6.63	0.9	5.96
Mn 2	A	48.0	1.56	1.00	8	9	9	9	7	9	8	7	8.25	0.85	7.01
Mn 3	A	48.0	1.33	0.50	7	9	7	8	7	9	8	7	7.75	0.85	6.59
FL 1	A	101.3	0.08	1.62	6	6	7	7	5	9	6	2	6.00	0.85	5.10
FL 2	E	63.4	1.16	2.33	6	9	2	6	7	9	6	4	6.13	0.85	5.21

### 3.9 Condition Assessment of SAPLs

The original average rating score (OAR) and the adjusted overall average score (AOR) were used for condition assessment of SAPLs. The condition of SAPL based on OAR are shown in Table 3-5 (a). According to the rating system definition in this chapter, the results indicate that 13% of 24 SAPLs were in a very good condition, 58% in good condition, 17% in satisfactory condition and 13% in fair condition. The adjusted overall average score was used to quantify the structural SAPLs rates according to available data. Similarly, SAPLs structural conditions were evaluated from the AOR. The structural condition of SAPLs from AOR are shown in Table 3-5 (b). The results indicate 4% of SAPLs were in very good condition, 8% in good condition, 38% in satisfactory condition, 42% in fair condition and 8% in poor condition.

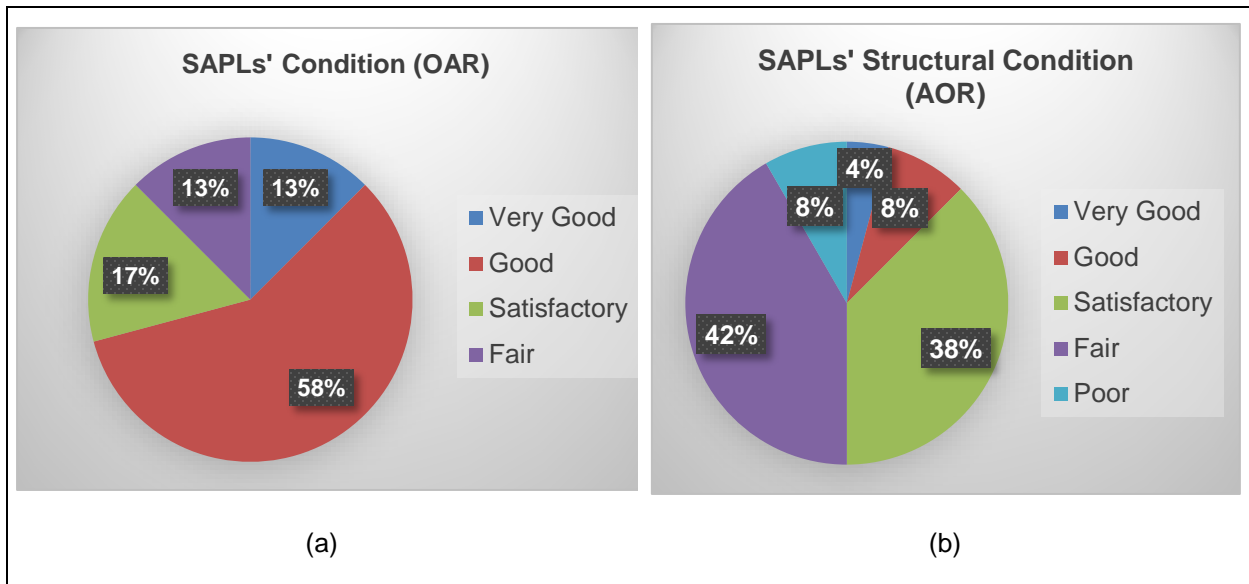


Figure 3-5 Condition assessment of SAPLs. It shows (a) SAPL original condition given as percent of liner condition, (b) SAPLs structural condition given as percent of liner structural condition.

### 3.10 Comparative Status of Cementitious and Geopolymer SAPLs

As Table 3-8 presents, a comparative analysis using the Excel software was conducted on the cementitious and geopolymer SAPLs' conditions. The relative proportions of cementitious and geopolymer SAPLs were 50% and 50% respectively. It is observed that 37% of geopolymer SAPLs are ranked as good condition, which is 29% more than cementitious SAPLs in good conditions.

Table 3-8 Comparative status of cementitious and geopolymer SAPLs (according to OAR).

Vendor	SAPLs Conditions (OAR)			
	Very Good (12.6%)	Good (45.8%)	Satisfactory (29.2%)	Fair (12.5%)
A (Cementitious) 25% (6/24)	4.2%	8.3%	12.5%	-
B (Geopolymer) 8% (2/24)	-	4.2%	-	4.2%
C (Geopolymer) 42% (10/24)	4.2%	33.3%	4.2%	-
D (Cementitious) 17% (4/24)	-	-	8.3%	8.3%
E (Cementitious) 8% (2/24)	4.2%	-	4.2%	-

### 3.11 Discussion of Results

A multi-variable regression analysis using MATLAB software was performed between the H/R ratio, the condition, age, and thickness of SAPLs. There is an expected correlation between these parameters. The multi-linear regression analysis on the H/R ratio, age, the average thickness, and structural condition based on AOR of SAPLs results are expressed by Eq. 3-3.

$$\begin{aligned}
 AOR = & -0.3485 + 1.453\left(\frac{H}{R}\right) + 7.6381(T) - 0.0121(A) - 2.1818\left(\frac{H}{R}\right)(T) + \\
 & 0.0261\left(\frac{H}{R}\right)(A) - 0.0831(T)(A) + 0.1336\left(\frac{H}{R}\right)^2 - 0.1823(T)^2 + 0.0008(A)^2, \\
 r^2 = & 77.8\%,
 \end{aligned}
 \tag{Eq. 3-3}$$

where,

A=SAPL age, month,

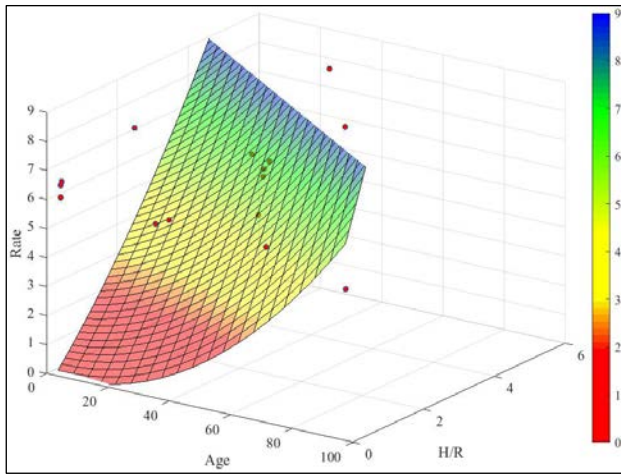
T=SAPL thickness, in.,

variables H, R and H/R are defined in Eq. 3-2,

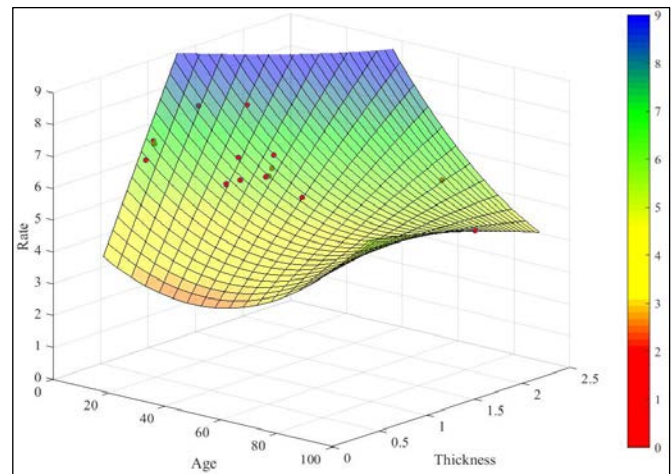
r=regression coefficient.

$R^2$  equals to 77.8% indicates that the correlation is good. The relationship of age (A), thickness (T), H/R ratio and structural condition of SAPLs (AOR) is plotted in Figure 6. A three-dimensional graph is able to illustrate the relationship of three parameters at once. Therefore, three different sets of graphs are used to depict the correlation of A, T, H/R and AOR. The color counter depicts the SAPL structural condition (AOR), dark blue is SAPL in an excellent structural condition and dark red is a failed SAPL sample. The regression analysis and the graphs show the structural condition of SAPLs are more sensitive to the H/R ratio. As it is shown in graph (a), the early age SAPLs with a lower number of H/R show a lower AOR. As it is shown in graph (c), a thicker SAPL not necessarily behaves better than a thinner sample. There are other parameters such as H/R, age, quality of material and installation procedure which plays an important role in the final product of the SAPL.

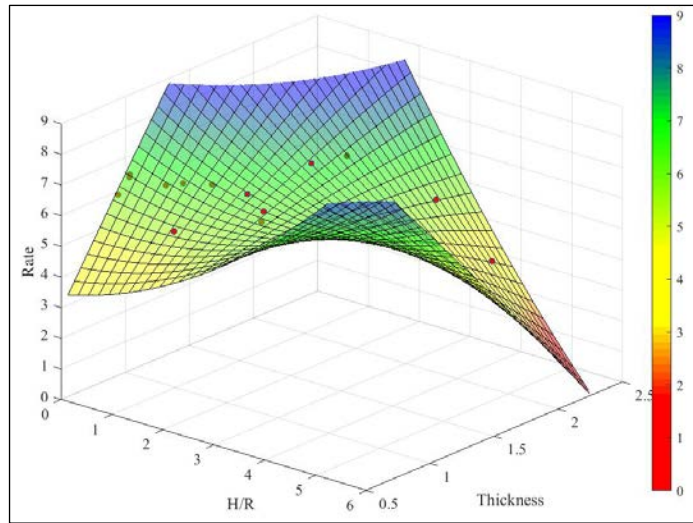
Moreover, variability of SAPL installations were found during the site visit inspection which is mainly due to different design procedures and varied installation practices among DOTs. While SAPL renewal application is favorable practice among some DOTs and it is anticipated to have at least a 50-years design life, it is not probable according to the field inspection data. Thus, there is a strong need of specific design and installation guidelines for these new technologies.



(a)



(b)



(c)

Figure 3-6 Correlation of age, H/R, thickness and AOR of SAPLs. It shows (a) A, H/R and AOR (b) A, T and (AOR), and (C) H/R, T and AOR.

### 3.12 Limitations, Findings and Recommendations

This chapter presented a formula (Eq. 3-3) for relationship of A, T, H/R and AOR of SAPLs for all states in different geographical locations due to lack of enough information in each state. Therefore, it is recommended to have a specific equation for each geographical area.

Due to lack of any polymeric SAPL site at the time of inspection, the SAPL material for all 24 culverts in this chapter fell into cementitious category. Therefore, it is recommended to have a specific rating system and sets of equations for polymeric SAPLs as well. A summary of findings and recommendations to improve SAPL performance are presented in Table 3-9.

Table 3-9 Summary of findings and recommendations.

Summary of Findings	Recommendations
Cracks	<ul style="list-style-type: none"> <li>Hairline cracks are not a reason for concern unless they produce spalls or cause loosening of the lining material.</li> <li>ASTM standard C1090 is recommended for measuring changes in height of cylindrical specimens of hydraulic-cement grout during a stipulated testing period of 28 days.</li> <li>According to the ASTM A979, the water cement ratio shall not exceed 0.5 by weight.</li> <li>According to the ASTM A849, only potable water shall be used.</li> </ul>
Efflorescence	<ul style="list-style-type: none"> <li>Pressure washing along with brushing and rinsing the surface with water may help eliminate it in early age of formation or ameliorate it.</li> </ul>
Rust Staining	<ul style="list-style-type: none"> <li>Corroded areas, areas with any leakage or water seepage, any holes and voids shall be sealed off (with polyurethane or similar grout) before the SAPL application.</li> </ul>
Infiltration	<ul style="list-style-type: none"> <li>Point repair and invert repair (paving the invert as per ASTM A849) shall be done prior to the SAPL application.</li> <li>An installation inspection is recommended to do visual inspection and verify the SAPL is leak free with low probability of rust staining formation.</li> </ul>
Issues with SAPL Thickness	<ul style="list-style-type: none"> <li>The SAPL design thickness recommends being calculated based upon the compressive strength of the SAPL material, the flexural bending strength of the SAPL material and the AASHTO truck loading for culvert pipes based upon the type of the soil used <sup>(1)</sup>.</li> <li>It is recommended the SAPL thickness shall follow the design thickness and be applied uniformly by spin caster along the pipe according to the ASTM A979.</li> </ul>
Installation	<ul style="list-style-type: none"> <li>According to ASTM A979, the SAPL must be placed in one or more passes/coats/lifts to reach the design thickness. Applied SAPL material over the pipe surface should provide a uniform thickness. The SAPL must exhibit an even application both longitudinally and circumferentially with no signs of uncured product.</li> <li>According to ASTM A849, troweled surface finishes that do not have an acceptable level of smoothness are not acceptable.</li> <li>According to the ASTM A849, a clean inside surface of the culvert can provide a good adherence between the pipe and the liner and directly impact the performance of the final product of SAPL.</li> <li>According to ASTM A849, curing operations must begin immediately after SAPL installation and continue for at least 72 hrs. The pipe ends shall be closed with airtight covers and the cementitious SAPL kept wet via an intermediate water source or a liquid membrane-forming compound conforming to ASTM C309.</li> <li>Cleaning and surface preparation shall be done before SAPL application.</li> <li>Before the SAPL application, all the debris must be removed from the culvert and its interior surface should be cleaned with high pressurized water-blast to remove all the remaining dirt.</li> <li>SAPL waste material: As the SAPL application is environmentally friendly, by the end of SAPL installation, having a waste management plan by installer according to the ASTM E3073-17 is recommended.</li> </ul>

<sup>(1)</sup> The compressive and flexural strength of the SAPL material can be achieved according to the ASTM C109 (standard test method for compressive strength of hydraulic cement mortars) and ASTM C1609 (standard test method for flexural performance of fiber-reinforced concrete using beam with third-point loading) respectively.

It is also recommended to have an inspection plan for three different stages: pre-installation inspection, installation inspection and post-installation inspection, as it is presented in Table 3-10.

Table 3-10 Inspection plan.

Inspection	
Pre-Installation Inspection	<ul style="list-style-type: none"> <li>• Proper cleaning and surface preparation must be done before SAPL application.</li> </ul>
Installation Inspection	<ul style="list-style-type: none"> <li>• A minimum of three test specimens of the SAPL material randomly must be taken to verify the required compressive and flexural strengths.</li> <li>• At least 6 random samples (3 in the valleys of the corrugations and 3 over the crest) must be taken for thickness verification in accordance with ASTM D1005 or ASTM D7091.</li> </ul>
Post-installation Inspection	<ul style="list-style-type: none"> <li>• Routine inspections are suggested to be conducted on a defined (5 years) frequency.</li> <li>• Visual and nondestructive condition assessment.</li> </ul>

### 3.13 Chapter Summary

Spray applied pipe linings (SAPLs) have potentials to inhibit further deterioration of culverts and drainage structures and structurally renew the existing host culverts. Field data collection, as part of the SAPL research project to develop design equations for SAPL thickness, highlighted the needs for comprehensive performance construction specifications and dedicated design equations. This chapter showed that installation process is the main key to reach the uniform thickness of SAPL and to achieve structural application. SAPL visual inspection and thickness measurements at each site indicated design requirements for different types of loading on SAPLs. As the corrugated aluminum pipe showed less effect of corrosion on the surface of SAPL compared to corrugated metal pipe, it seems that corrugated aluminum performs better in locations with high levels of corrosive environments. Finally, due to different crack patterns in cementitious and geopolymers, it is recommended to select the type of SAPL materials in accordance with geographical and weather conditions (freeze/thaw), cover depth and skew angle of culvert



with the road for each location. This chapter highlighted SAPL issues and provided recommendations to address them.

This chapter presented the results of SAPL site visit inspection and field data collection of twenty-four culverts renewed with SAPL application to raise renewal defects and installation issues as well as making suggestions for development of proper performance construction specifications. Culverts were selected from lists of projects provided by seven DOTs across the U.S. including, DeIDOT, FDOT, MnDOT, NCDOT, NYSDOT, Ohio DOT and PennDOT.

## Chapter 4

### Full Scale Laboratory Soil Box Testing

#### 4.1 Experimental Test Setup for Soil Box Testing

To evaluate the structural capacity of renewed CMPs, full scale laboratory soil box testing was conducted at the Center for Underground Infrastructure Research and Education (CUIRE) at the University of Texas at Arlington (UTA), illustrated in Figure 4-1 (a). Through the soil box testing, a total number of nine buried CMP culverts were tested with and without polymeric SAPL, by applying a static load on the soil surface. The CUIRE soil box has dimensions of 25 x 12 x 10 ft, as shown in Figure 4-1 (b).



(a)



(b)

Figure 4-1 CUIRE Laboratory at UTA: (a) UTA Civil Engineering Laboratory Building (CELB), and (b) CUIRE soil box.

The laboratory soil box testing of nine CMPs, as illustrated in Figure 4-3, was performed in three separate sets of testing, as listed in Table 4-1. The first set was control testing of three bare CMPs including one intact circular CMP, one fully invert deteriorated circular CMP, and one fully deteriorated invert arch CMP, as illustrated in Figure 4-4 (a), (b) and (c). The control test of bare CMPs examined the load carrying

capacity of intact and invert deteriorated unlined CMP samples (Syar et al. 2020). The second set of testing was included three fully invert deteriorated circular CMPs renewed with different thicknesses of a polymeric SAPL material. The third set of testing included three fully invert deteriorated arch CMPs renewed with different thicknesses of the same polymeric SAPL material. The SAPLs were applied in three different thicknesses of 0.25 in. 0.5 in. and 1 in. and were tested to obtain the ultimate load carrying capacity of renewed CMPs. In the actual field condition, the storm sewer corrugated metal pipes in service mostly are corroded and degraded in the invert section. Hence, in the laboratory soil box testing, the invert section of CMPs were cut and separated to simulate a fully invert deteriorated CMP in the actual field condition and to investigate the structural capacity of SAPLs in the absence of the host pipe ring stiffness. To eliminate the existed ring compression of CMP samples and to apply the load just on the SAPL, the invert-cut section was detached after backfilling. The three sets of soil box testing along with the details of CMP samples and SAPLs for each set are listed in Table 4-1. The whole overview of the laboratory soil box testing steps is illustrated in Figure 4-2. The cross-section and plan views of the soil box tests, as well as the averaged water content and compaction rate distribution at different layers of soil in each test cell are illustrated in Figure 17.



Figure 4-2 Overview of soil box testing steps.



Figure 4-3 Corrugated metal pipe (CMP) samples.



(a)

(b)



Figure 4-4 Circular CMP samples for control test: (a) intact 60 in. circular CMP, (b) invert-cut 60 in. circular CMP, 47 × 71 in. and (c) invert-cut CMP arch.

Table 4-1 List of experimental soil box testing and pipe samples.

Test Name	Test Number	CMP				Polyurethane SAPL
		Dimeter (in.)	Length (ft)	Shape	Condition	Thickness (in.)
<b>1<sup>st</sup> Set</b> Control Test (Bare Circular and Arch CMPs)	1	60	6	Circular	Intact	N/A
	2	60	6	Circular	Invert-cut	N/A
	3	47×71	6	Arch	Invert-cut	N/A
<b>2<sup>nd</sup> Set</b> Polymeric SAPL Circular CMPs	4	60	6	Circular	Invert-cut	0.25
	5	60	6	Circular	Invert-cut	0.5
	6	60	6	Circular	Invert-cut	1.0
<b>3<sup>rd</sup> Set</b> Polymeric SAPL Arch CMPs	7	47×71	6	Arch	Invert-cut	0.25
	8	47×71	6	Arch	Invert-cut	0.5
	9	47×71	6	Arch	Invert-cut	1.0

#### 4.1.1 Host Pipe Samples

A total number of nine annular corrugated metal pipes (CMPs) were tested in the soil box, including three unlined (bare) CMPs, three SAPL renewed circular CMPs and three SAPL renewed arch CMPs, as listed in Table 4-1. The circular CMP samples had the internal diameter of 60 in. and the length of 6 ft. The arch CMP samples had the internal rise of 47 in. and the span of 71 in. The CMP samples had the corrugation profile of  $2 \times \frac{2}{3}$  in. and were gauge 12 thickness. The CMP samples were fabricated from bent hot-dip galvanized sheets along their edges fastened by rivets, as illustrated in Figure 4-5 (a). The steel material of the CMP samples was in compliance with the ASTM A796 (ASTM A796/A796M 2017, CONTECH 2019), with the minimum yield strength ( $f_y$ ) of 33 ksi, the minimum tensile strength ( $f_u$ ) of 45 ksi, and the Young's modulus of 29,000 ksi. The yield strain of  $1,138 \mu\epsilon$  was calculated using the elastic stress-strain relationship.

Observations showed that usually one-third of wetted perimeter of the pipe is more vulnerable to severe corrosion (Masada 2017a). Hence, an 18 in. wide strip of CMPs at the invert location was entirely cut to simulate a culvert in service in fully deteriorated invert condition, except one intact bare circular CMP used as the control test. This 18 in. value as the width of invert-cut section is in conformity with the middle bedding section as specified in AASHTO LRFD bridge design specifications (*AASHTO LRFD Bridge Design Specifications* 2020). The degrading process and corrosion of metal culverts in the actual field condition have a low pace and occurs within several years which usually enables the soil-pipe system to be stabilized. Therefore, the invert-cut sections were kept bolted to the main body of the CMPs to maintain the pipe samples' original geometry during the backfilling process. After the completion of the soil backfilling process and stabilizing the soil-pipe system, the invert-cut sections were unbolted and detached from the main body of CMPs. The detachable invert mechanism and detachable invert section of a bare CMP sample are illustrated in Figure 4-5 (b) and (c).



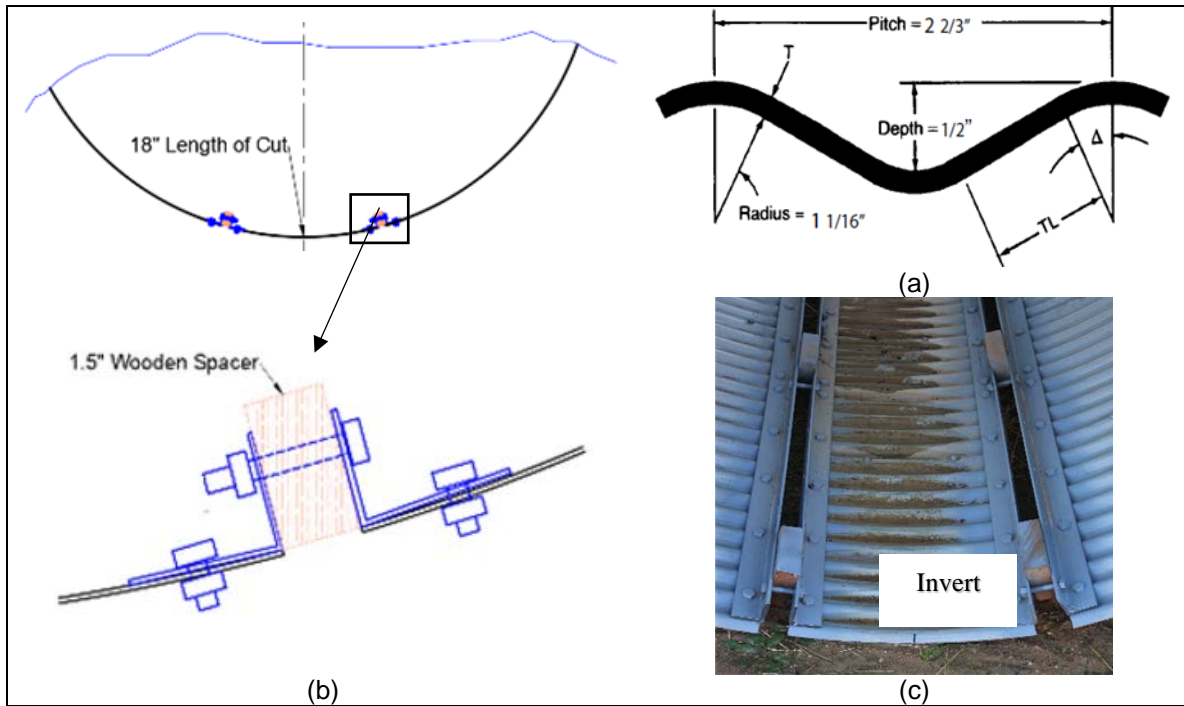


Figure 4-5 CMP sample details: (a) corrugation profile, (b) detachable invert schematic, and (c) the bare CMP sample with the detachable invert (Kohankar Kouchesfehni et al. 2020).

However, after detachment of the invert-cut section, the movement of CMPs due to the soil load was unfavorable and any changes in the original geometry of the CMP sample before the liner installation was a major concern. Hence, to maintain the original geometry of CMP samples before the SAPL installation, two narrow strips of 3 in. wide at both ends of the invert section were kept bolted to the main body of CMP, as illustrated in Figure 4-6. After the SAPL installation and curing process, the 3 in. wide end strips were unbolted and removed to eliminate the ring stiffness of the host pipe (CMP sample). The removal of end strips was essentially required and helped to maximize the magnitude of applied load on the liner itself, as one of the objectives of the presented dissertation was to investigate whether the polymeric SAPL is fully structural or not. The detachable invert mechanism for SAPL renewed CMP samples is illustrated in Figure 4-7. Stage (1) of this figure depicts the invert is bolted to the body of CMP during soil backfilling. Stage (2) illustrates that the middle detachable invert section was removed after completion of soil backfilling and prior to SAPL installation. Stage (3) illustrates the invert section with two end strips after

installation of polymeric SAPL on the inner surface of the pipe samples. Stage (4) shows that the end strips were unbolted to eliminate the host pipe ring stiffness.



Figure 4-6 End strips of the invert-cut CMP samples.

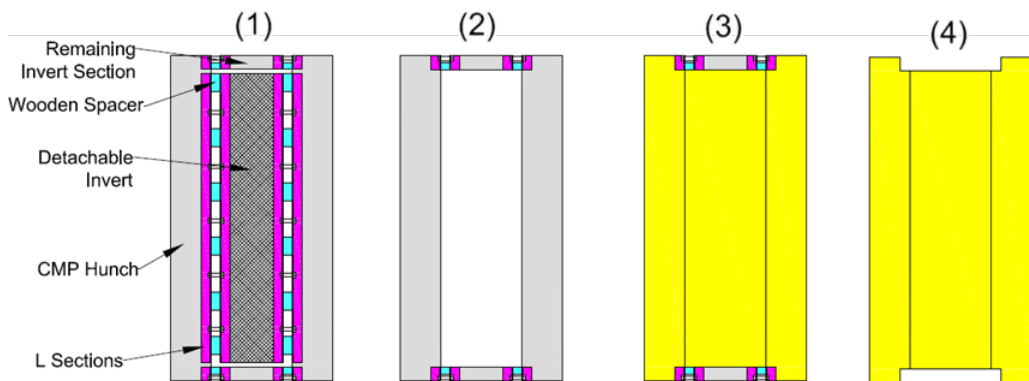


Figure 4-7 Detachable invert mechanism (in four stages) for SAPL renewed pipe samples before and during the SAPL installation (Kohankar Kouchesfehni et al. 2020).

#### 4.1.2 Burial Configuration

Each soil box test setup included three CMPs that were placed longitudinally next to each other in a soil box of 25 ft long, 12 ft wide, and 10 ft deep at the Center for Underground Infrastructure Research and Education (CUIRE) laboratory facility at the University of Texas at Arlington (UTA). The CMP samples were separated by wooden partition walls, as illustrated in Figure 4-8. The CMPs were buried under 2 ft of soil cover including 1 ft layer of granular soil on top and 1 ft layer of poorly graded sand on the bottom. The burial configuration details are presented in Table 4-2. To prevent the effect of soil-wall friction, lubrication was applied on wooden partition walls and a layer of plastic sheet was placed in between the soil and all the partition walls and soil box surrounding walls (Khatri et al. 2015). Any gaps between both ends of CMPs and partition walls were tightly sealed with Styrofoam, as shown in Figure 4-8 (a) and (b).

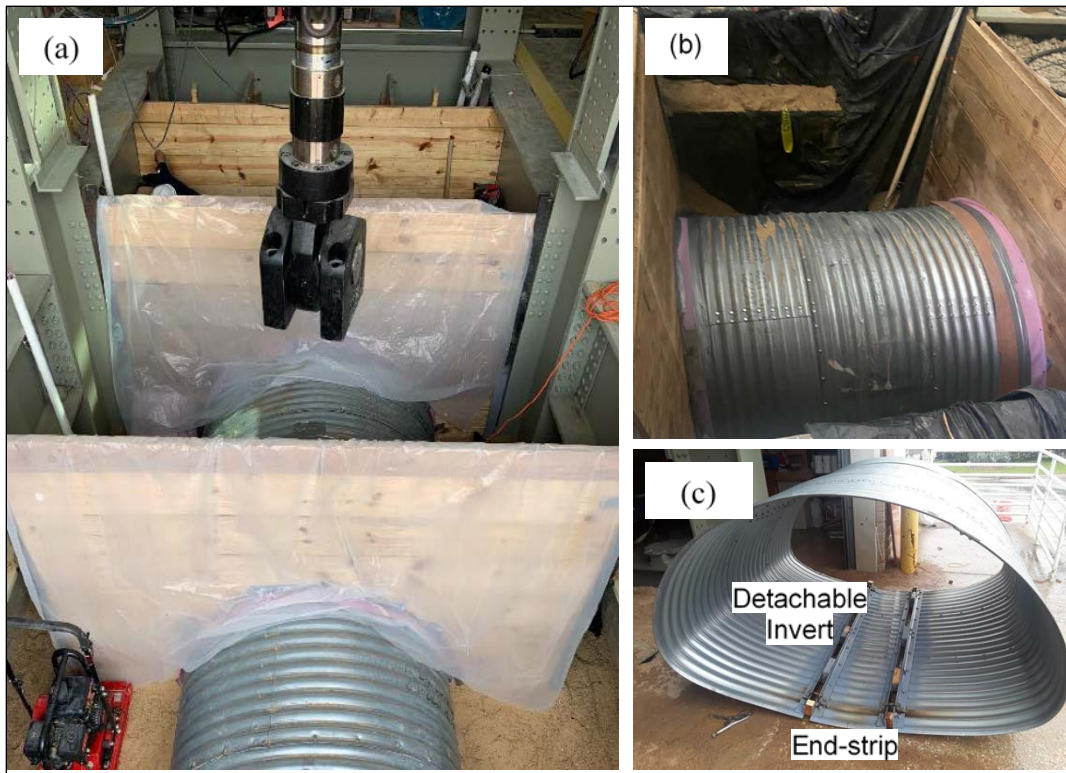


Figure 4-8 Pipe installation: (a) longitudinal configuration of arch CMPs in the soil box of 25 ft × 12 ft × 10 ft at CUIRE, (b) an arch CMP with end sealing, and (c) an arch CMP sample with detachable invert and end-strip section.

For all test setups the burial configuration included foundation, loose bedding, backfill and cover layers. The test setup and burial configuration details are illustrated in Figure 4-9, Figure 4-10 and Figure 4-11. Poorly graded sand (SP), known as concrete sand, with a negligible amount of silt and clay was used for the layers of foundation, bedding and backfill according to the unified soil classification system (USCS). A sieve analysis was conducted according to the ASTM D6913 (ASTM D6913 2004). The standard proctor compaction test was conducted to obtain the maximum Standard Proctor Dry Density (SPDD) of the soil. The proctor test showed the maximum soil unit weight of approximately 115 pcf. It is noteworthy that the density of poorly graded sandy soil was not significantly impacted with the alteration of moisture content (Berney and Smith 2008). Two passes of a plate vibratory compactor with a 4,496 lbs compaction force were utilized at every 8 in. lift of foundation to achieve approximately 96% of the SPDD, which was measured using a nuclear density gauge meter, as illustrated in Figure 4-12.

Table 4-2 Burial configuration details.

Soil Layer	Soil Type	Condition	Layer Height	
Foundation	Poorly Graded Sand (SP)	Compacted	Circular Cell	20 in.
			Arch Cell	33 in.
Loose Bedding	SP	Loosened	4 in.	
Embedment	SP	Uncompacted	Circular Cell	60 in.
			Arch Cell	47 in.
Backfill	SP	Uncompacted	12 in.	
Base Coarse	Crushed Aggregate	Uncompacted	12 in.	

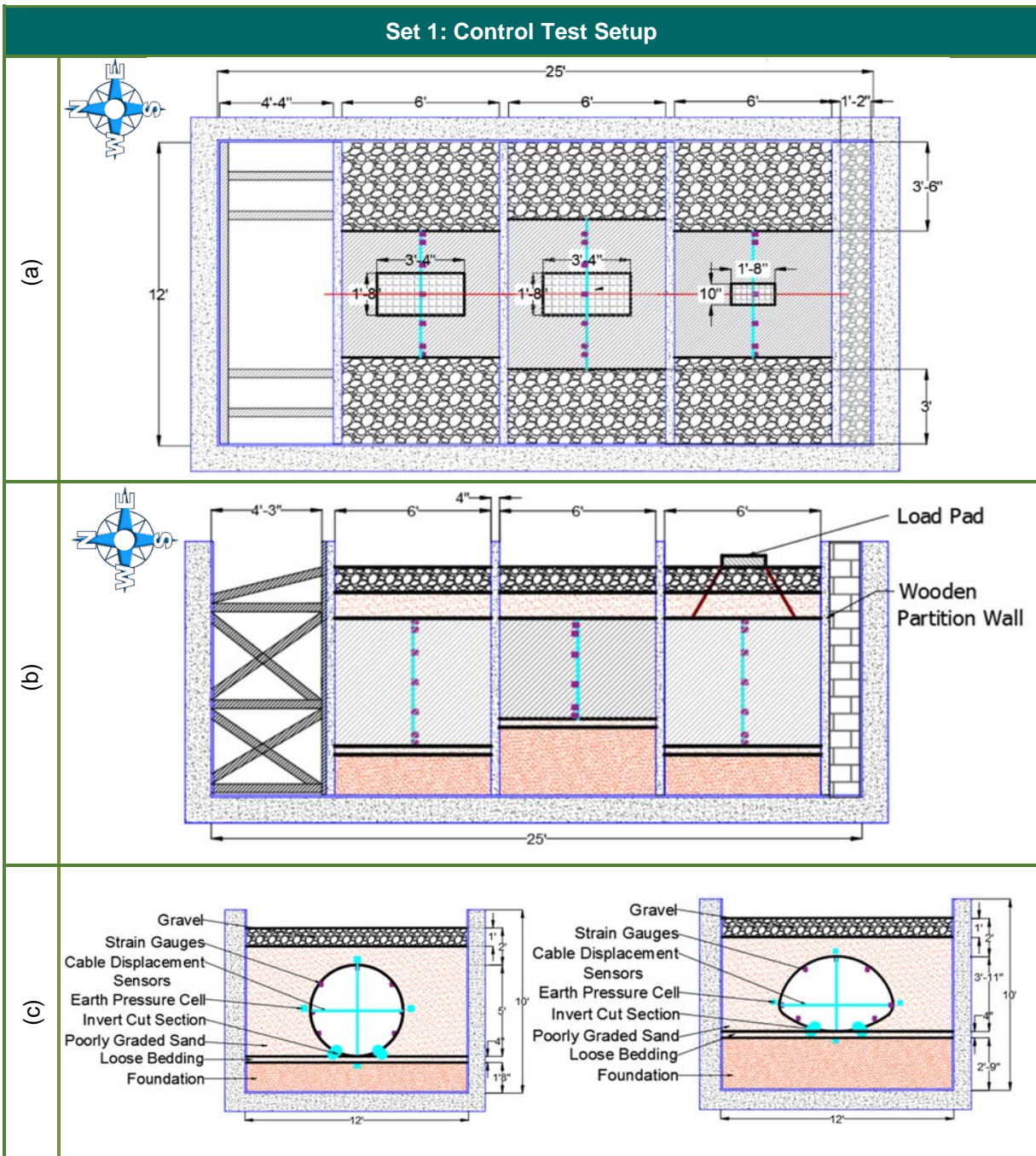


Figure 4-9 The CMPs' burial configuration (1<sup>st</sup> set of soil box testing-control test): (a) plan view, (b) profile view of the aligned CMPs in the soil box, and (c) cross-section view of both circular and arch CMPs.

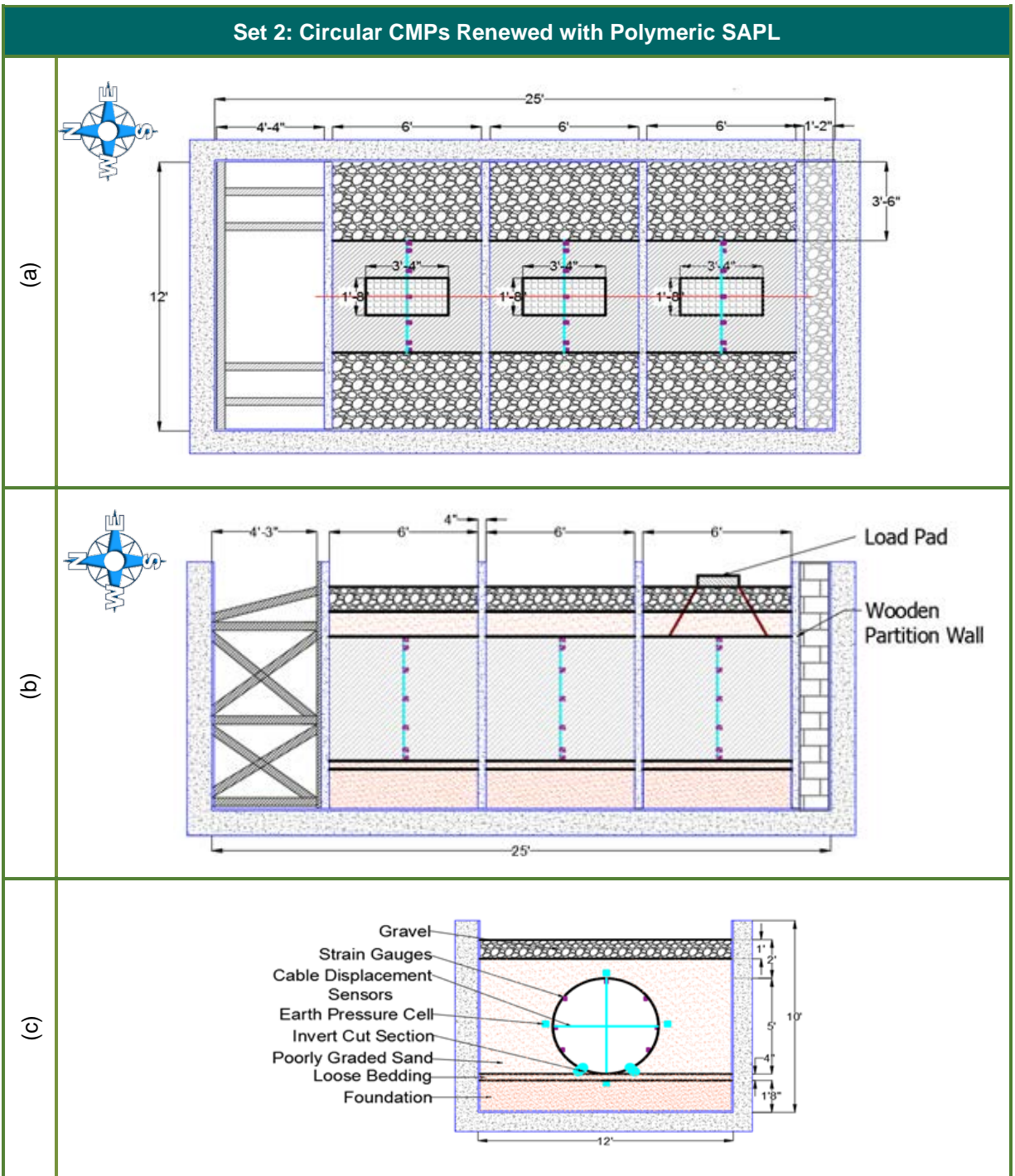


Figure 4-10 The CMPs' burial configuration (2<sup>nd</sup> set of soil box testing): (a) plan view, (b) profile view of the aligned CMPs in the soil-box, and (c) cross sectional view of the circular CMP.

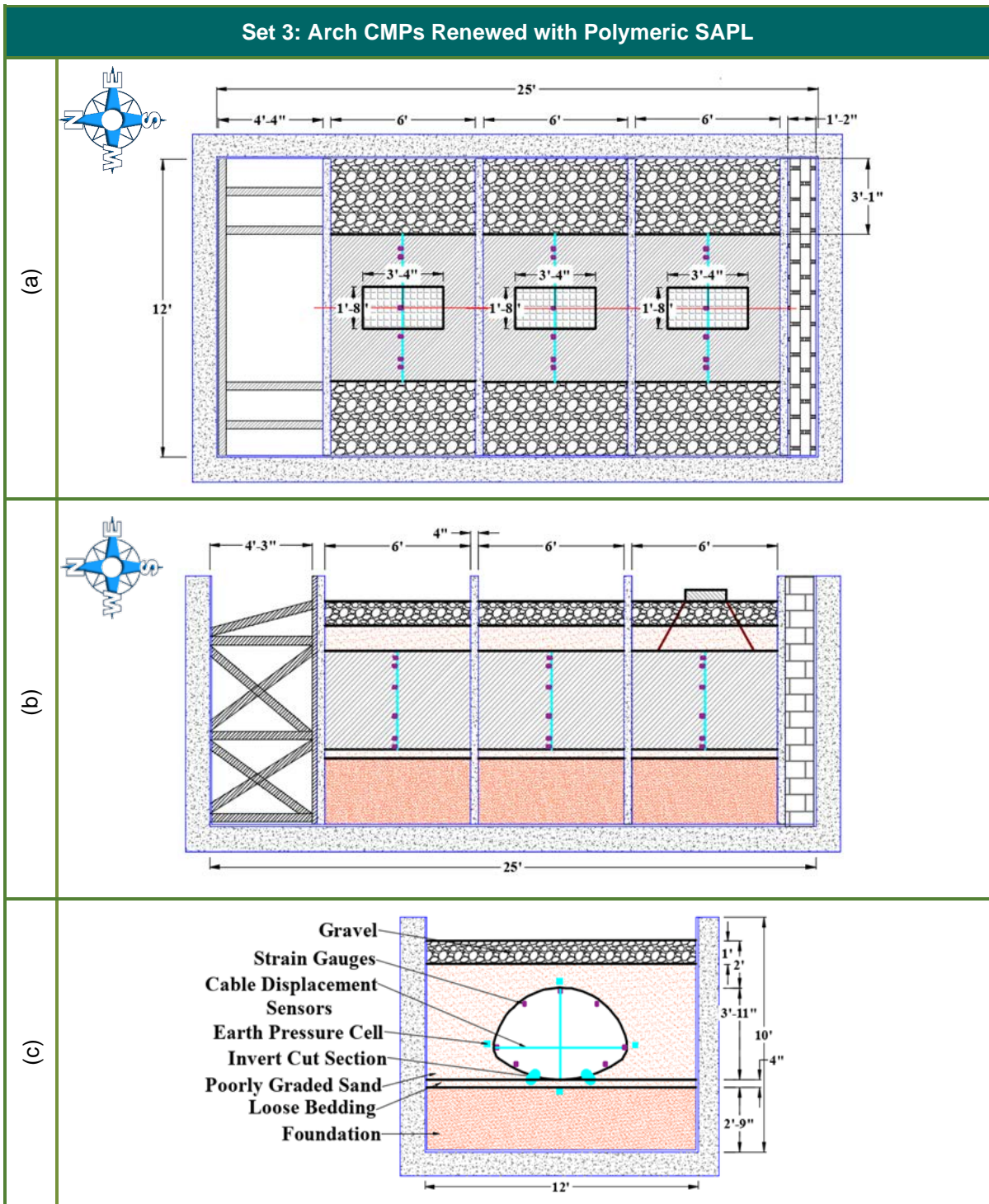


Figure 4-11 The arch CMPs' burial configuration (3<sup>rd</sup> set of soil box testing): (a) plan view, (b) profile view of the aligned arch CMPs in the soil-box, and (c) cross sectional view of the arch CMP.



Figure 4-12 Nuclear density measurement (CUIRE).

#### 4.1.2.1 Foundation

The foundation layer beneath all the circular CMP samples had a height of 20 in. For the foundation layer to achieve approximately 93% of the SPDD, that was measured using a nuclear density gauge meter, two passes of a plate vibratory compactor with a 4,496 lbs compaction force were utilized at every 8-in. lift. The first soil box testing as the control test included both circular and arch CMP geometries. Since the arch CMP sample had a lower rise compared with the other two circular CMPs, to prevent different soil levels on the top of the pipe samples, the foundation height of the CMP arch sample was increased to 33 in. and its crown reached the same level of the crown of the circular CMPs.

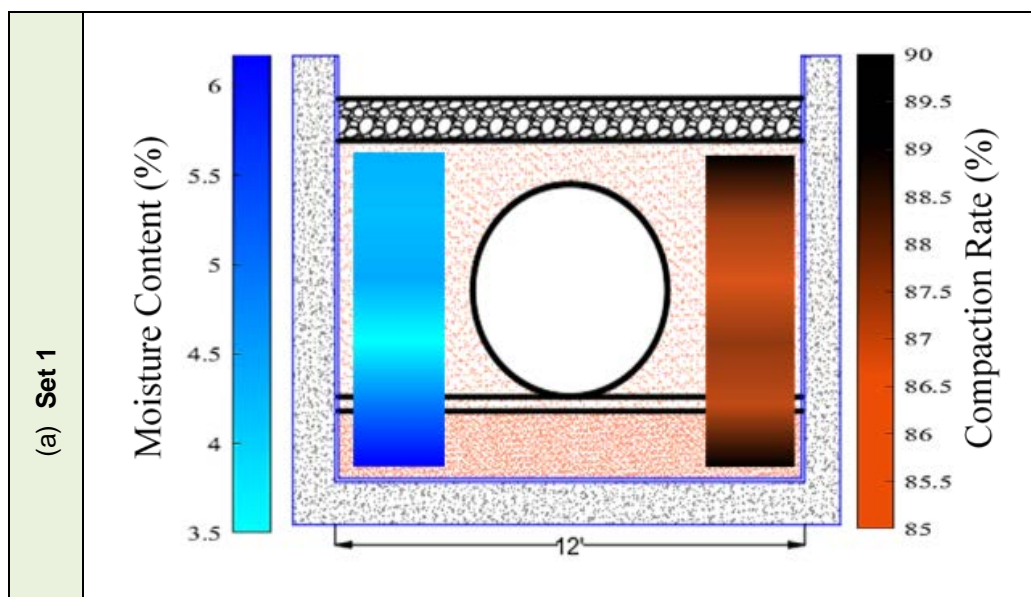


#### 4.1.2.2 Bedding

A 4-in. bedding layer of loose poorly graded sandy (SP) soil was placed on top of the foundation layer at each cell as specified by AASHTO LRFD Bridge Construction Specification (American Association of State Highway and Transportation Officials (AASHTO) 2017). The loose bedding layer enabled the CMP samples to settle properly and to provide even bedding conditions (Moser and Folkman 2008). The loose bedding layer in the laboratory soil box testing could simulate the loosened soil beneath a pipe's invert in the actual field in a fully deteriorated invert condition due to stream passage.

#### 4.1.2.3 Backfilling

The CMPs were placed on the bedding layer and were backfilled with poorly graded sandy (SP) soil up to 1 ft above top of the pipe sample. To simulate poor conditions of soil compaction during the pipe installation in the field, no attempt was made to compact the embedment and backfill. The soil was placed and spread out in 8 in. lifts. The soil water content and the soil compaction rate were measured for each lift using a nuclear density meter at two locations in both sides of the CMPs. The averaged water content and compaction rate of soil for all three cells of each test setup, at the same lifts from foundation to the top level of the backfill, are illustrated in Figure 4-13.



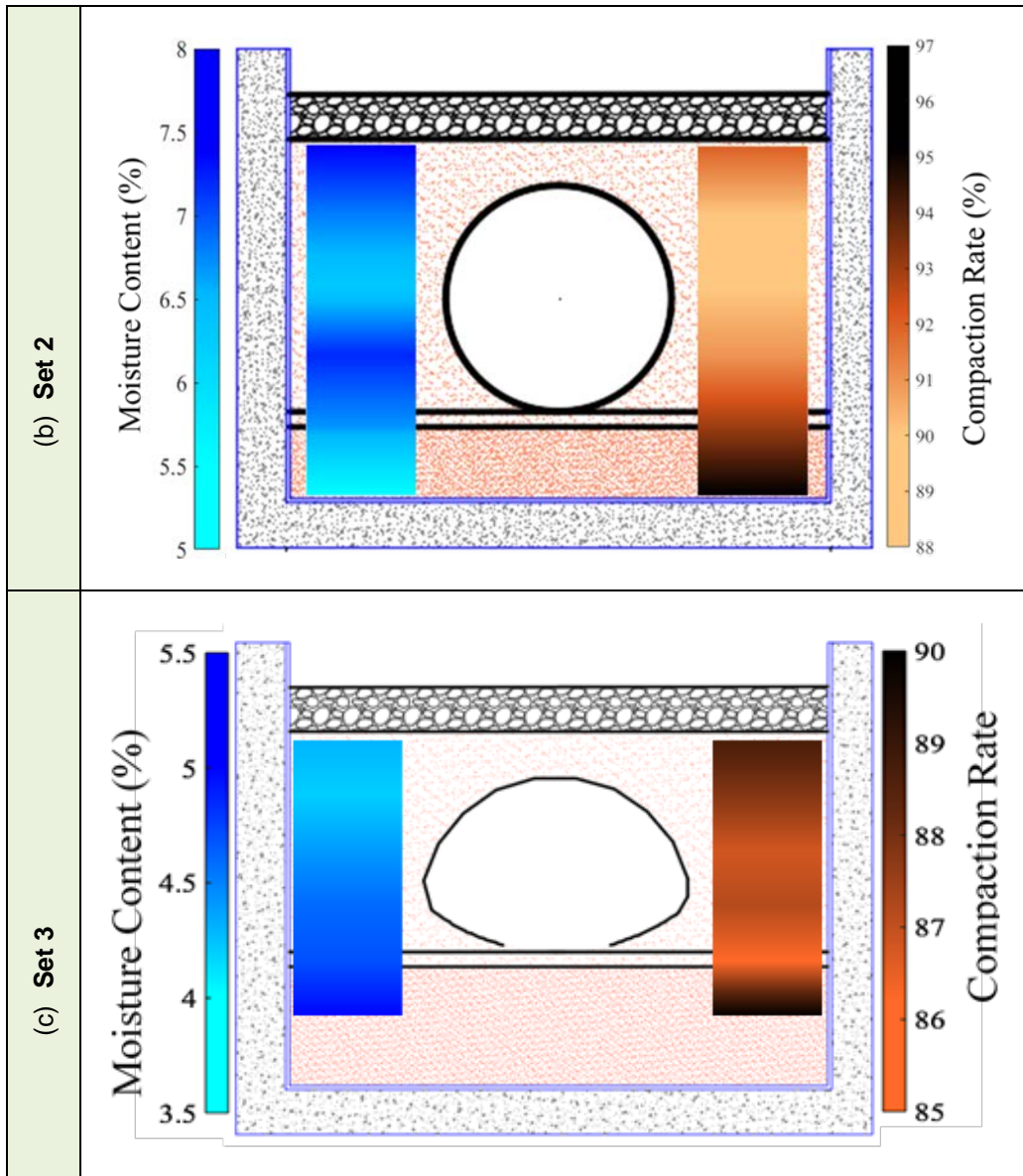


Figure 4-13 The contour plot of the averaged values for the soil moisture content and compaction rate in 8 in. lifts measurement: (a) 1<sup>st</sup> set of soil box testing, (b) 2<sup>nd</sup> set of soil box testing, and (c) 3<sup>rd</sup> set of soil box testing (Kohankar Kouchesfehni et al. 2020).

#### 4.1.2.4 Soil Cover

A one-foot layer of aggregates with maximum particle size of 1.75 in., known as TxDOT 247 grade 1 type D aggregates, was placed on top of the backfill layer to prevent immature soil failure prior to the pipe

sample failure. This layer is representative of the base course as a part of culvert's cover in the field (Khatri et al. 2015). The burial configuration of the control test on the bare fully deteriorated invert CMP was in a similar manner as the SAPL renewed CMP test setup.

#### **4.1.3. CMP Surface Preparation and Polymeric SAPL Installation**

SprayWall (Johnson and Hammon 2017) polymeric SAPL, as a commercially available SAPL material, was selected to renew the CMPs. SprayWall® is a self-priming polyurethane lining by Sprayroq Protecting Lining System Company for pipe and manhole renewal that reinstates structural integrity, provides infiltration control and corrosion resistance. Its quick curing time enables the renewed structure to be returned to service shortly after the completion of the application, which makes it ideal for utilization in water, wastewater, and stormwater pipe renewal. Sprayroq recommends cleaning the host pipe from oil, and other contaminants, which may cause formation of blisters, pinholes, foamed material, debonding, cracking, or delamination of the SAPL from the host pipe.

For the second and third sets of soil box testing, after completion of CMPs' backfilling and instrumentation as described in section 4.3, they were renewed with different thicknesses of SprayWall liner. CMP surface preparation was conducted prior to the pipe installation in the soil box as recommended by the Sprayroq. Hence, the CMPs were power washed using pressurized water jet to remove the dust and dirt attached to their inside surface, similar to the pipe preparation procedure for SAPL installation in field, as illustrated in Figure 4-14.

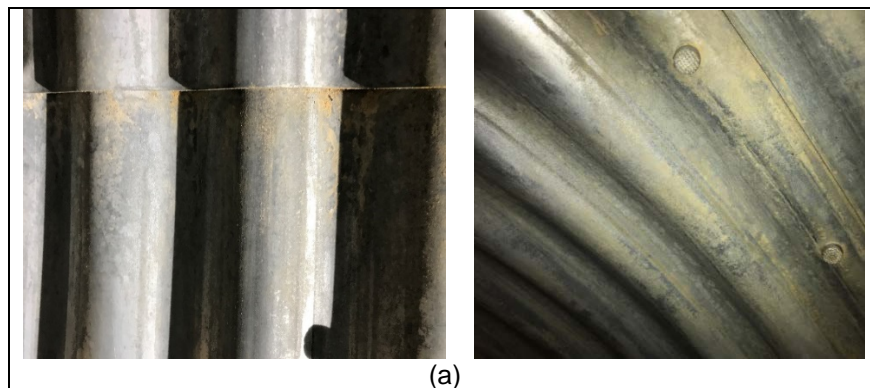




Figure 4-14 CMP surface preparation for SAPL installation: (a) dirt and dust on the CMP, and (b) CMP after power wash without any dirt and dust.

The SAPL was applied up to 0.25 in. thick in each single application or lift. The SprayWall SAPL began solidifying in about 8 seconds and its initial cure was completed within 60 minutes. In the invert section, it was not possible to spray the SprayWall directly on the soil. Therefore, the detached invert section (middle section) was kept in place to receive the liner. There was a 2 in. gap between each side of the invert section and the main body of the CMP which both gaps were filled with Styrofoam and covered with plastic sheets and duct tape. The invert-cut section of circular CMPs before and after SAPL installation is illustrated in Figure 4-15. The arch CMPs invert-cut section, end strips, invert preparation for SAPL installation, and the invert-cut section after the SAPL installation are illustrated in and Figure 4-16.

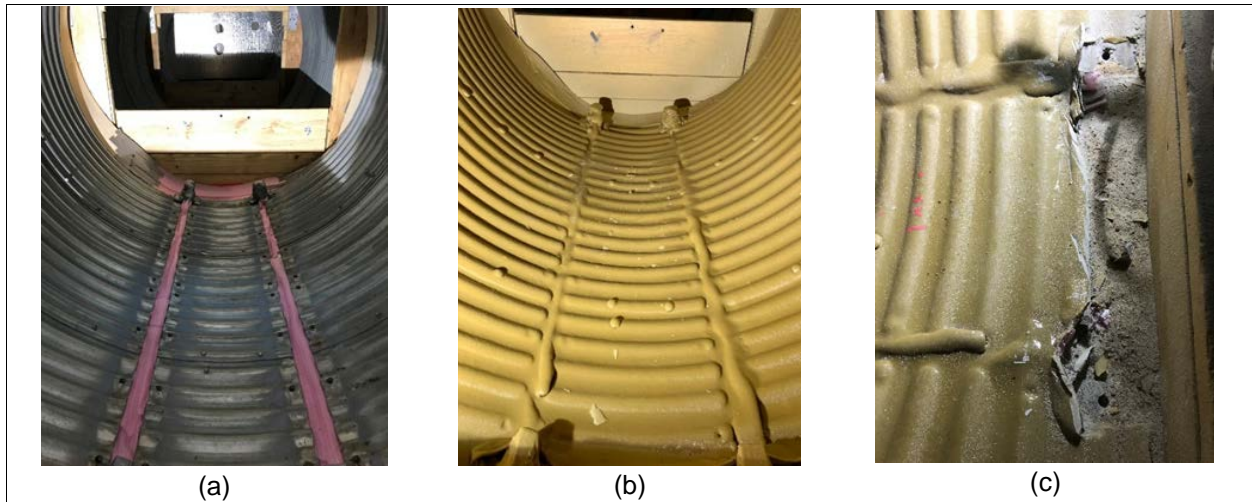


Figure 4-15 SAPL installation of invert-cut circular CMPs: (a) before SAPL installation (stage 2 of Figure 4-7), (b) after SAPL installation (stage 3 of Figure 4-7), and (c) end strips detachment (stage 4 of Figure 4-7) (Kohankar Kouchesfehni et al. 2020).

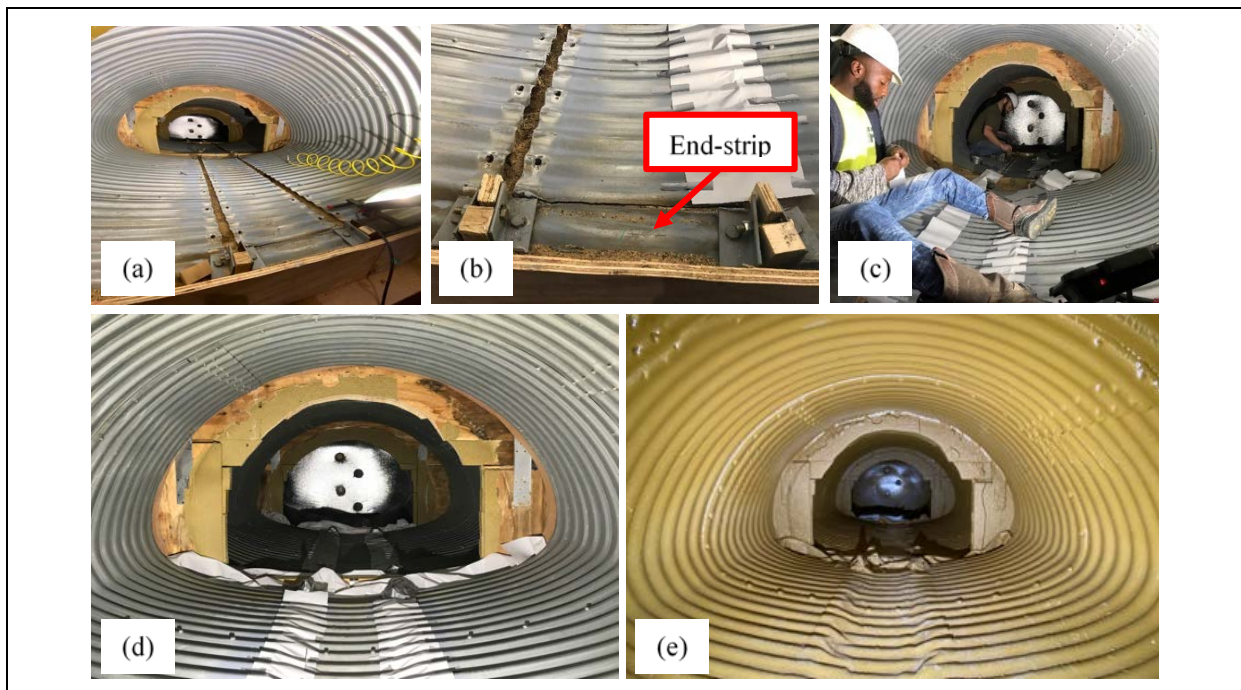


Figure 4-16 Arch CMP preparation for SAPL installation: (a) Arch CMP before gap sealing, (b) the invert-cut gap sealing with Styrofoam and plastic sheets, (c) spraying Sprayroq's polyurethane material inside arch CMPs, (d) prepared pipe prior to the SAPL installation, and (e) the SAPL renewed arch CMPs.

## 4.2 Polymeric SAPL Installation

The SprayWall SAPL was installed by hand spray, as illustrated in Figure 4-17. In order to control the thickness during the installation, with respect to the volume of the sprayed material coming out of the nozzle per unit of time (i.e., second), the vendor's engineer could estimate the amount of material that was sprayed on the arch CMP's inside surface in every second. In addition, by knowing the total volume of the required SAPL, the number of passes required to reach the designed thickness was estimated. However, this type of installation requires the high proficiency and experience of the SAPL installer. The Sprayroq vendor calculated an approximate amount of 179.08 lb, 358.16 lb, and 716.33 lb of SprayWall material that was required to apply 0.25 in., 0.5 in., and 1 in. thicknesses, respectively, on 60-in. CMPs. The Sprayroq vendor calculated an approximate amounts of 230 lb, 460 lb, and 925 lb of SprayWall material that were required to apply 0.25 in., 0.5 in., and 1 in. thicknesses, respectively, on 47×71 in. arch CMPs. These values include a factor of safety to cover material testing sample and installation errors such as over spraying. Figure 4-18 illustrates the Sprayroq truck on October 29, 2019 at CUIRE laboratory for the purpose of SAPL installation for the second set of testing (circular CMP).



Figure 4-17 Hand spray SAPL installation.



Figure 4-18 SAPL installation on circular CMP, CUIRE laboratory, UTA, 10/29/2019: (a) outside of the laboratory, and (b) inside of the soil box.

#### **4.2.1 Polymeric SAPL Sampling for Material Property Testing**

Prior to the SAPL installation, for each test setup of circular CMPs and arch CMPs, four plate samples of about 0.125 in. thick SAPL were sprayed from the same batch. The SAPL plate samples were collected to examine the flexural and tensile properties of the installed SAPL used for the renewal of CMPs,

as illustrated in Figure 4-19 and Figure 4-20. Once the plate samples were fully cured, they were cut into the required plaques for flexural and tensile tests as specified by ASTM standards D790-17 and D638-14. The plaques were precision machined to exact dimensions to minimize edge effects, as shown in Table 4-4.

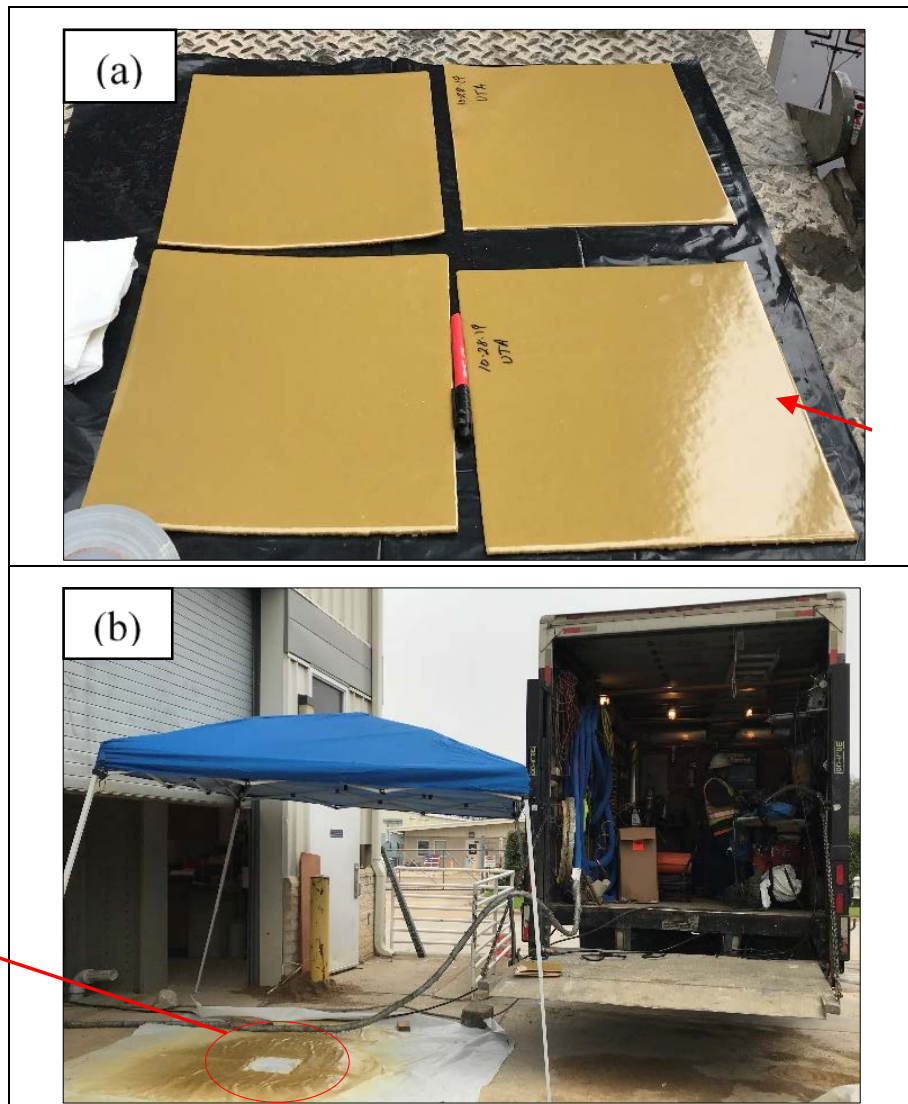


Figure 4-19 SAPL sampling for circular CMPs test setup: (a) sample plates prior to the cut into required shape for flexural and tensile test, and (b) the sampling site with Sprayroq installation truck.





Figure 4-20 Plate sampling from the SAPL batch to provide material test samples for arch CMPs test setup.

#### 4.2.2 SAPL Installation Temperature

According to the SprayWall installation and performance construction specifications guideline, the host pipe surface temperature requires to be at least 70 °F. Otherwise, there is a possibility of crack formation in the installed SAPL. Cracks can also form from a thermal shock, in cases if the material is cooled down quickly or due to uneven SAPL application as it cools down at different rates. In case of a crack formation, Sprayroq suggests to remove of the cracked area and prepare the substrate surface using 40-60 grit sandpaper. After completion of surface preparation, the patch kit SR6100 and a trowel-able high strength epoxy will be used to repair the defect. Taping around the defect area is required to help reduce any subsequent debonding.

The outside and inside CUIRE laboratory temperatures, on the day of renewal circular CMPs by SAPL installation, were registered 72 °F and 70 °F, respectively. The outside and inside CUIRE laboratory temperatures, on the day of renewal arch CMPs by SAPL installation, were registered 32 °F and 57 °F, respectively. The temperature of host pipes was registered a value of 62 °F three hours before the SAPL

installation. However, it was not possible to measure the host pipe temperature during the SAPL installation due to the severely toxic nature of the SAPL material during installation and before solidification (i.e., about 2 minutes).

For both the second (circular CMPs) and third (arch CMPs) sets of soil box testing, the SAPL was installed in three different thicknesses of 0.25 in., 0.5 in., and 1 in. After the SAPL installation in the third set of soil box testing (arch CMPs) within a few hours initial cracks were observed in the applied SAPLs prior to the soil-pipe system loading. A circumferential crack with a length of 5.0 in. was observed in the 0.25 in. thick SAPL at the invert location along the arch CMP's interlocking seams. A circumferential crack was observed in the 0.5 in. thick SAPL, starting from the arch CMP haunch towards the shoulder area at the West side. This crack was formed at a distance of 4 in. away from the partition wall (or end of the pipe). A longitudinal crack with a length of 6-in. was observed in the 1 in. SAPL. The crack was formed along the arch CMP's plate connection on the west shoulder location. The crack formation in the third set of soil box testing could be due to the ambient low temperature at the time of SAPL's curing. No other cracks or defects, such as blisters, pinhole or foamed product were observed, except the mentioned three cracks in the third set of soil box testing (arch CMPs).

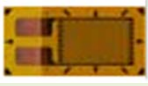




In the third set of testing (arch CMP samples), the crack on the invert location of the 0.25 in. thick SAPL was formed only along the seams. In this thin thickness of the SAPL, the seams could not be perfectly lined and repairing of such a small crack could not be effective. Furthermore, due to the adjacency of the partition wall to the formed circumferential crack in the 0.5-in. thick SAPL, the tasks of cutting the defect area, grinding the surface and applying the SR6100 were challenging in such a confined area. Eventually, it was recommended by the vendor to repair only the 1-in. thick SAPL using SR 6100 epoxy. The SAPL repair procedure was performed five days after the SAPL installation and two days before the detachment of the invert's end-strips.

### **4.3 Instrumentation**

The CMP samples were instrumented with uniaxial strain gauges, linear variable differential transformers (LVDTs), cable displacement sensors (CDSs), earth pressure cells, digital image correlation

(DIC) targets, and digital cameras. All the sensors used in this study were calibrated and certified by their own manufacturers. The instrumentations used in soil box testing is listed in Table 4-3.

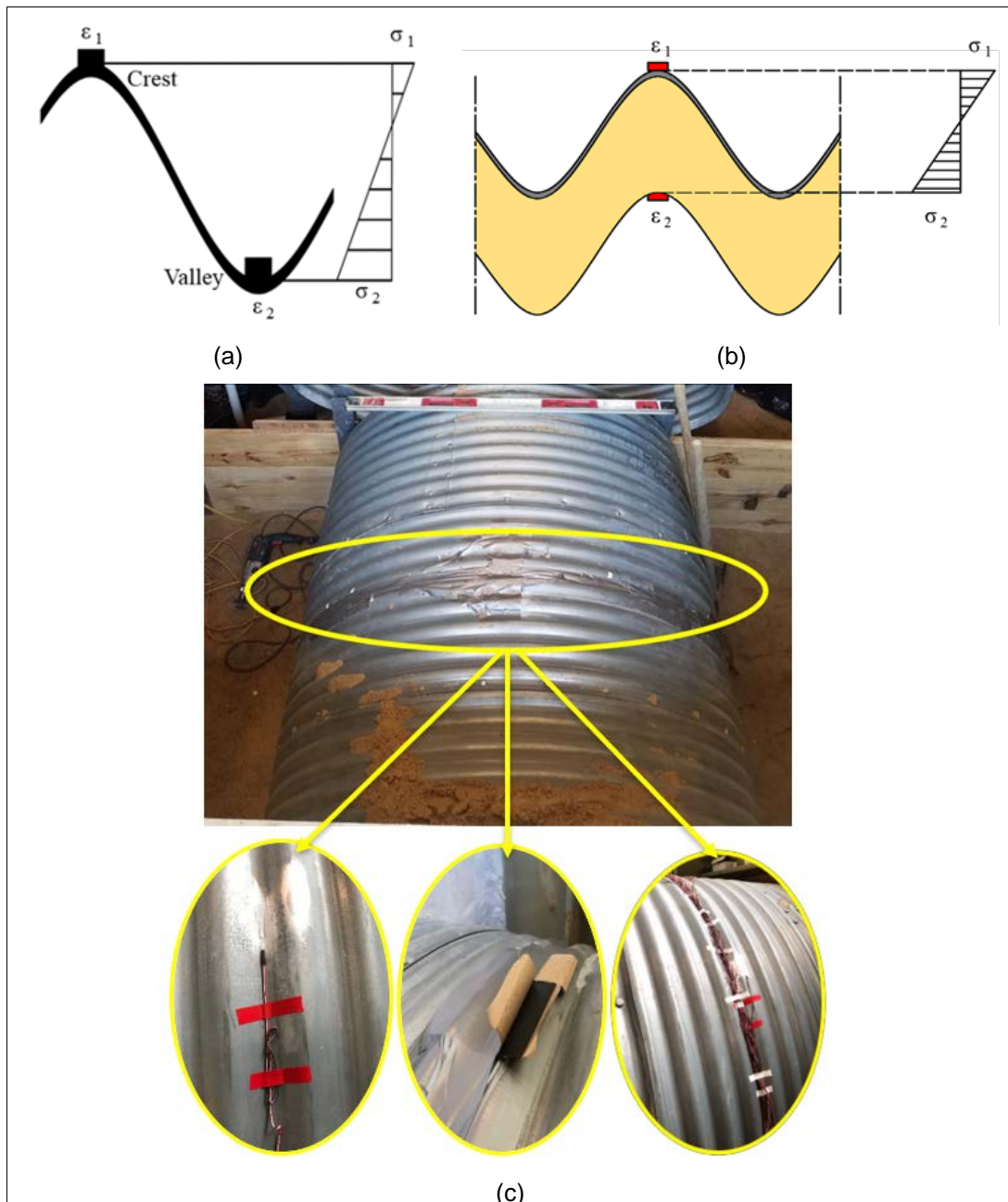
Table 4-3 Instrumentation.

Instrumentation		Number		Location
	Uniaxial Stain Gauges (Micro Measurement C2A-06-250LW-120)	Control Test	16	<ul style="list-style-type: none"> <li>• Circumferentially at 45° intervals at the middle section of the pipe in two layers</li> </ul>
		SAPL Renewed	16	<ul style="list-style-type: none"> <li>• Circumferentially at 45° intervals at the middle section of the pipe</li> <li>• 8 Outer Surface of CMP</li> <li>• 8 Inner Surface of the SAPL</li> </ul>
	Cable Displacement Sensors (CDSs) (Micro-Epsilon WPS-500-MK30-P10)	2		<ul style="list-style-type: none"> <li>• Attached on the inside surface of each CMP at the middle section</li> </ul>
	Linear Variable Differential Transformers (LVDTs) (Omega LD650)	3		<ul style="list-style-type: none"> <li>• All three (crown, shoulder, springline) were installed on a wooden frame, cantilevered to the middle section of each CMP</li> </ul>
	Earth pressure cells (Geokon 4800 series)	4		<ul style="list-style-type: none"> <li>• Around each CMP on top, bottom, and springline within a 4 in. (10.16 cm) distance away from its outer surface</li> </ul>
Digital image correlation (DIC) targets		40-50		<ul style="list-style-type: none"> <li>• Circumferentially in the middle section of each CMP</li> </ul>
	Digital cameras (DSLR Canon Rebel T5i)	3		<ul style="list-style-type: none"> <li>• One at the entrance of each pipe, showing whole view of the CMP</li> <li>• Two were installed on a wooden frame, cantilevered to the middle section of each CMP, targeting the crown and springline</li> </ul>

#### 4.3.1 Strain Gauges

For the first set of testing (control test of bare CMPs), after placing the CMPs on the bedding layer and before backfilling, the pipe samples from both inside and outside surfaces were instrumented with a total of sixteen uniaxial strain gauges (Micro Measurement C2A-06-250LW-120). The strain gauges were installed circumferentially at 45° intervals at the middle section of the CMP sample in two layers of the valley and the crest, as illustrated in Figure 4-21 (a). For the SAPL renewed CMP samples, 8 strain gauges were installed on the outer surface of the CMP and 8 strain gauges on the inner surface of the SAPL, as illustrated in Figure 4-21 (b). After attaching the strain gauges to the samples, the Micro Measurement air drying M-

Coat D was applied to protect gauges from moisture and electrical leakage. Two layers of physical protection were provided by attaching M-Coat FA Aluminum foil tape and M-Coat FN Neoprene rubber sheets to protect gauges from abrasive soil particles movement, as illustrated in Figure 4-21 (c) and (d). The strain gauges were connected to a data acquisition system that digitalized the transmitted analog signals, as illustrated in Figure 4-22.



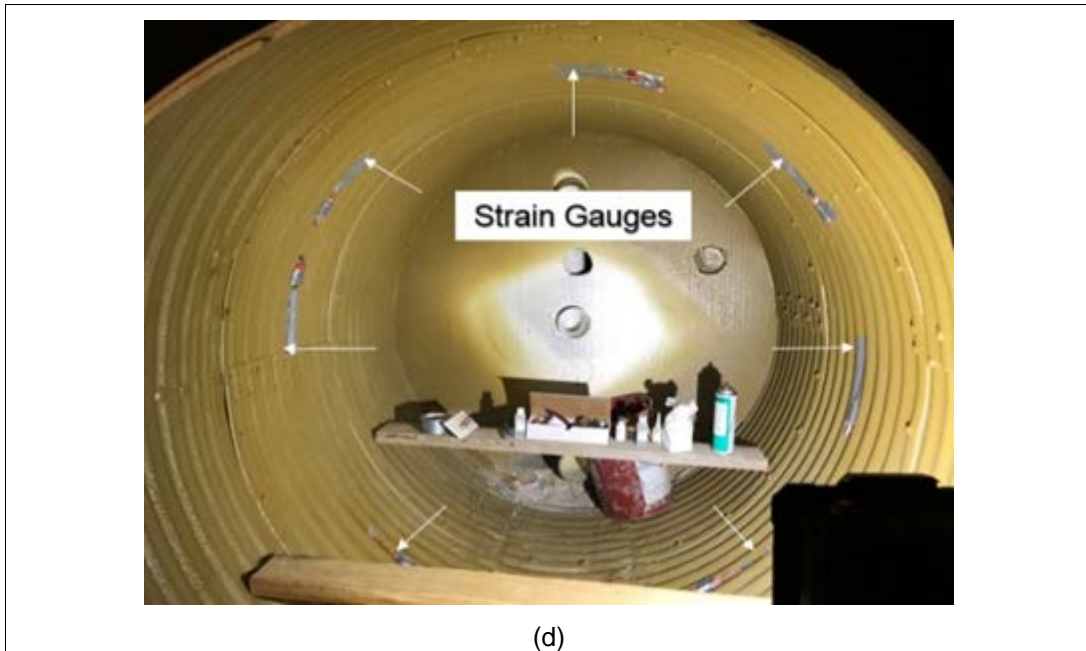


Figure 4-21 Strain gauges configuration and details: (a) schematic profile view at the crown of the bare circular CMP, (b) schematic profile view at the crown of SAPL renewed circular CMP, (c) physical protection of outer surface strain gauges, and (d) installed strain gauges on the inner surface of the SAPL renewed circular CMP.



Figure 4-22 Strain gauges connected to a data acquisition system (DAQ).

### 4.3.2 Earth Pressure Cells

To monitor the applied pressure at different layers of soil, four Geokon 4800 series earth pressure cells, as illustrated in Figure 4-23 (a), were embedded around each CMP on 4 locations of top, bottom, and springlines, as shown in Figure 4-10 (c) and Figure 4-11 (c). The earth pressure cells were located within a 4 in. distance away from the outer surface of the CMP, as it is illustrated in Figure 4-23 (b). The earth pressure cells were connected through wires to a Geokon data acquisition system (DAQ), as illustrated in Figure 4-23 (c). DAQ digitalized the transmitted analog signals from the earth pressure cells during the tests (GEOKON 2019).

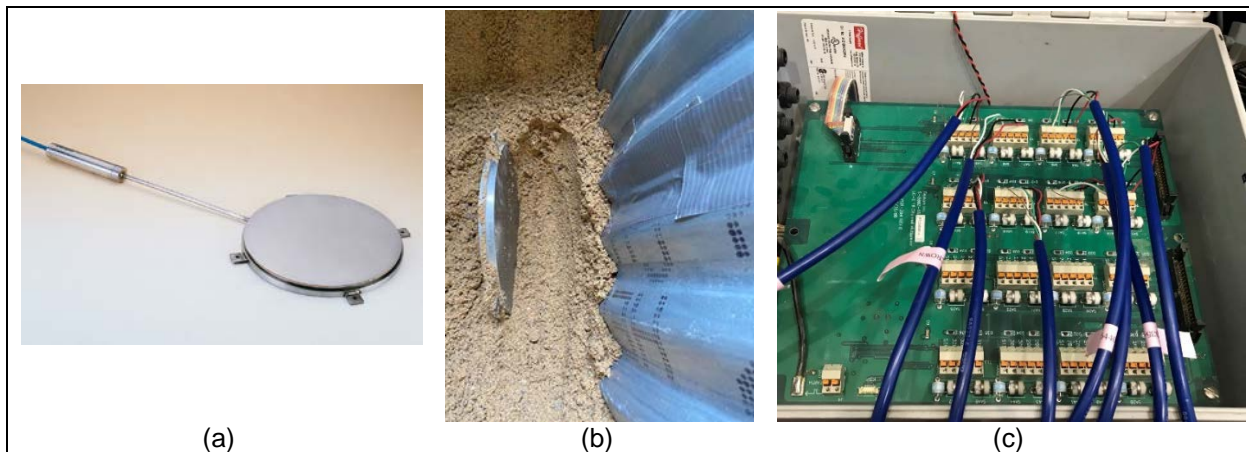


Figure 4-23 Earth pressure cell: (a) Geokon 4800 series, (b) 4 in. distance from the CMP at the springline, and (c) connection to a data acquisition system (DAQ).

### 4.3.3 LVDT and CDS

Cable displacement sensors (CDS) and linear variable differential transformers (LVDT) were utilized to measure the CMP sample deflection in the laboratory condition experimental soil box testing (Darabnoush Tehrani 2016). Two Micro-Epsilon WPS-500-MK30-P10 CDSs were attached on the inside surface of each pipe sample to measure crown and springline deflections at the mid-length of the CMPs (Micro-Epsilon 2019). Three Omega LD650 LVDTs were utilized to measure the crown, springline, and shoulder deflections of the CMP samples during the loading application (OMEGA 2019). The LVDTs were installed on a wooden frame which was cantilevered to the middle of the CMP sample, as illustrated in

Figure 4-24. LVDTs and CDSs were connected to a data acquisition system that digitalized the transmitted analog signals from the sensors during the tests, as illustrated in Figure 4-25.

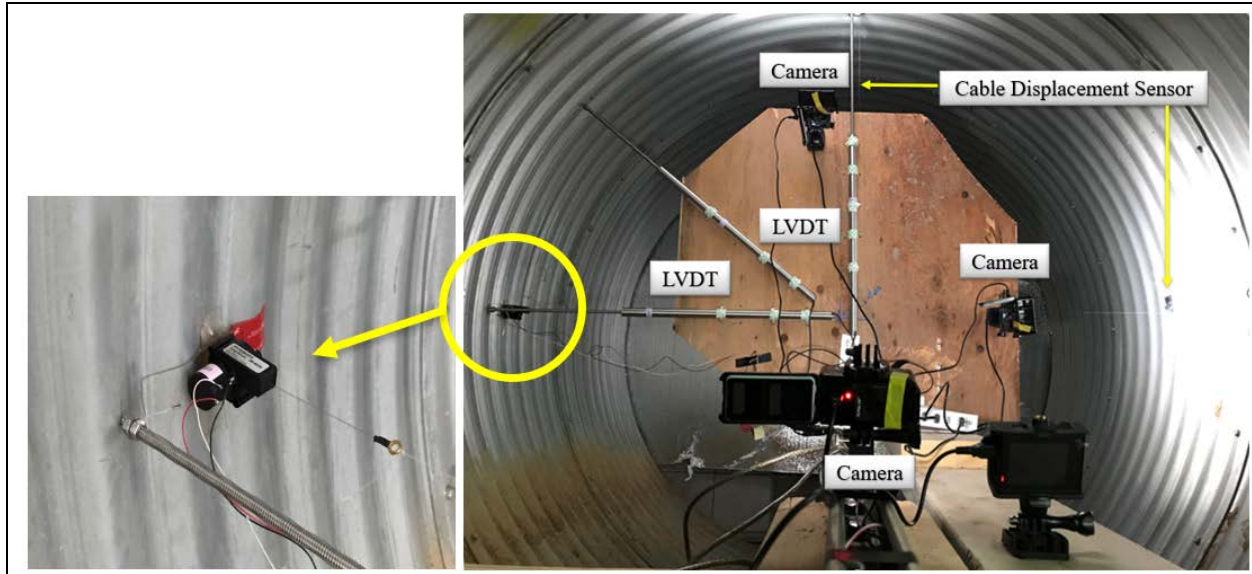


Figure 4-24 LVDTs and cable displacement sensors.

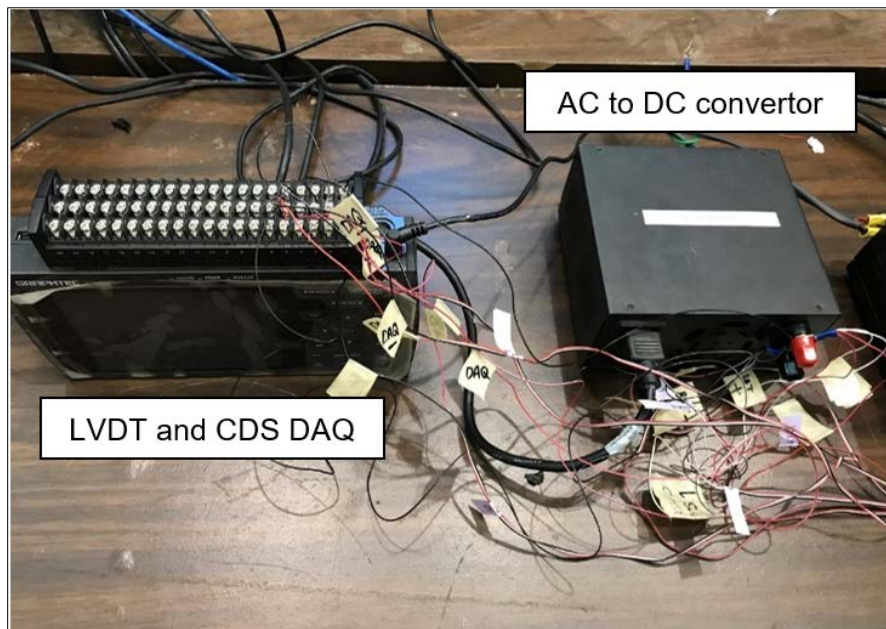
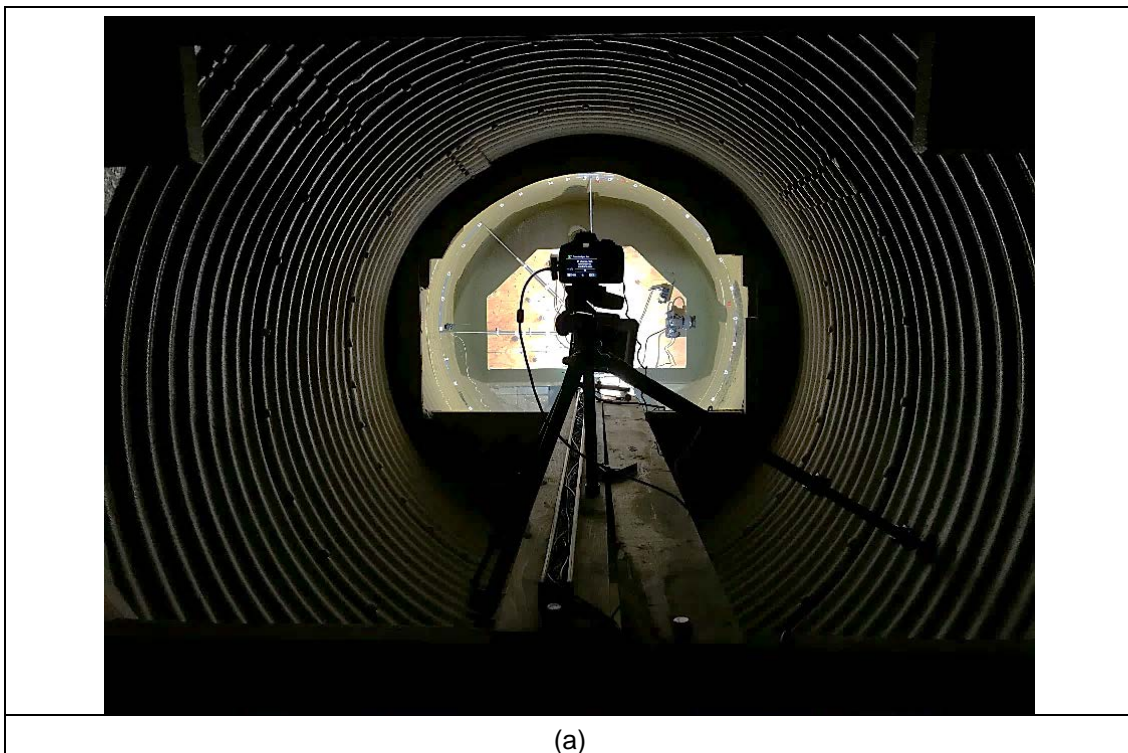


Figure 4-25 LVDT and CDS DAQ, and alternating current (AC) to direct current (DC) convertor (from left to right).

#### 4.3.4 DIC Measurement and Pipe Monitoring

Three DSLR Canon Rebel T5i cameras were used to capture the CMP samples crown and springline changes and monitor crack initiations at the SAPLs at the middle section as well as the CMP profile changing during the tests, as illustrated in Figure 4-26. A total number of around forty to fifty targets circumferentially were attached to the middle section of each CMP sample for the purpose of pipe monitoring and profiling using two-dimensional digital image correlation (DIC) technique (Ham and Darabnough Tehrani 2019). The DIC targets designed and fabricated using high contrast colors of black and white. The DIC targets were attached to the inside surface of the crests of the CMP samples. DIC technique was implemented with the use of the commercially available software of GOM Correlate and a developed MATLAB code. 2D DIC is a powerful technique that enables a multi-point deflection measurement in a 2D plane at any stage of loading (Ham and Darabnough Tehrani 2019). The setup of DIC targets and cameras along with CDSs and LVDTs installed inside one of the circular CMP samples are illustrated in Figure 4-27.





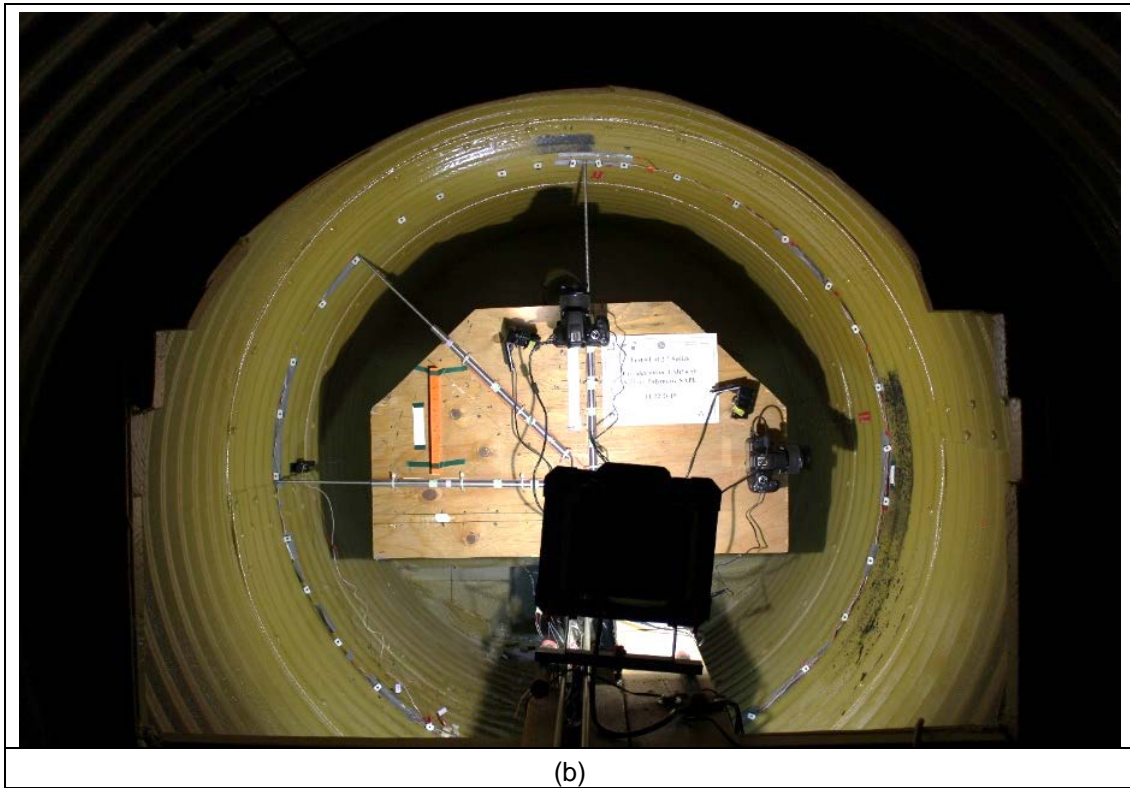


Figure 4-26 Pipe Monitoring: (a) cameras used for capturing changes, and (b) DIC targets for pipe profiling.

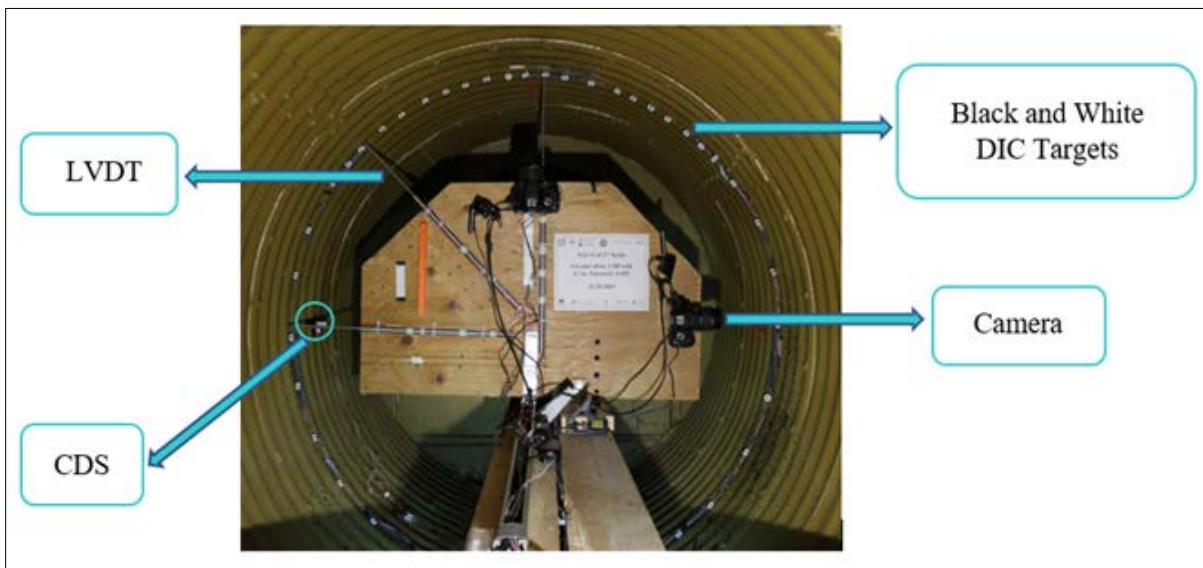


Figure 4-27 Instrumentation: LVDTs, CDSs, DIC targets and cameras inside the pipe sample.

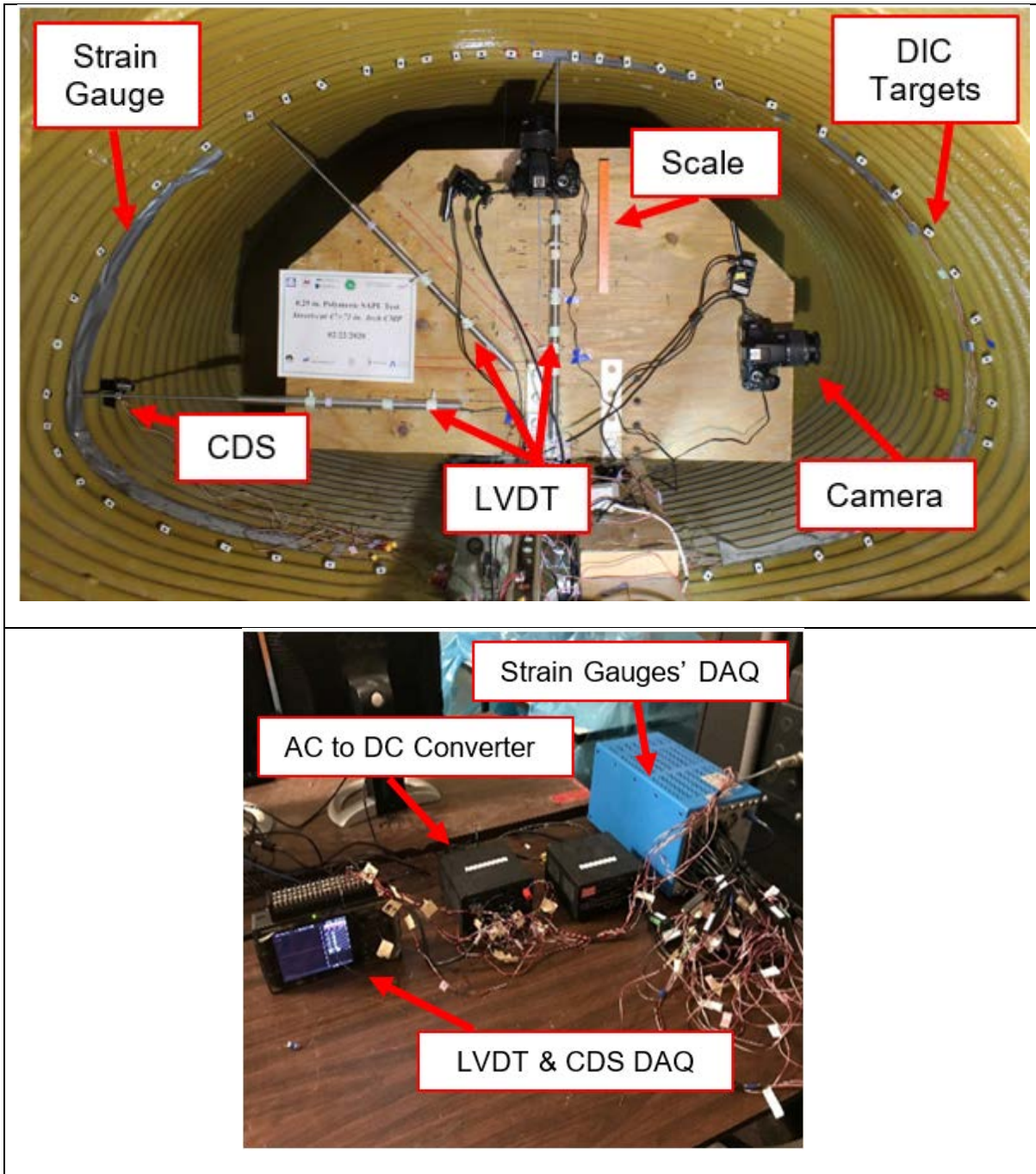


Figure 4-28 Instrumentation: (a) LVDTs, CDSs, DIC targets and cameras inside the pipe sample, and (b) data acquisition systems.

#### 4.4 SAPL Thickness Measurement

For the second and third sets of testing, the thickness measurement of the installed SAPLs were conducted using an OLYMPUS 38DL PLUS® Ultrasonic Thickness Gauge with measuring thickness range of 0.003 in. to 25 in. The SAPL thickness installed inside each CMP samples was measured at three locations longitudinally along the pipe length and circumferentially in 45° intervals. The ultrasonic thickness measurement gauge was calibrated using two samples of 0.25 in. and 1 in thick from the same SAPL material. Since the device probe was too large to be perfectly fitted in the valleys of CMP samples, the thickness measurements were conducted on top of the crest of corrugations at the target locations. Three measurements and readings were conducted at each point, and finally the averaged thickness value for that location was recorded. The thickness measuring locations along with the calibration SAPL samples are illustrated in Figure 4-29 for both circular and arch CMPs.

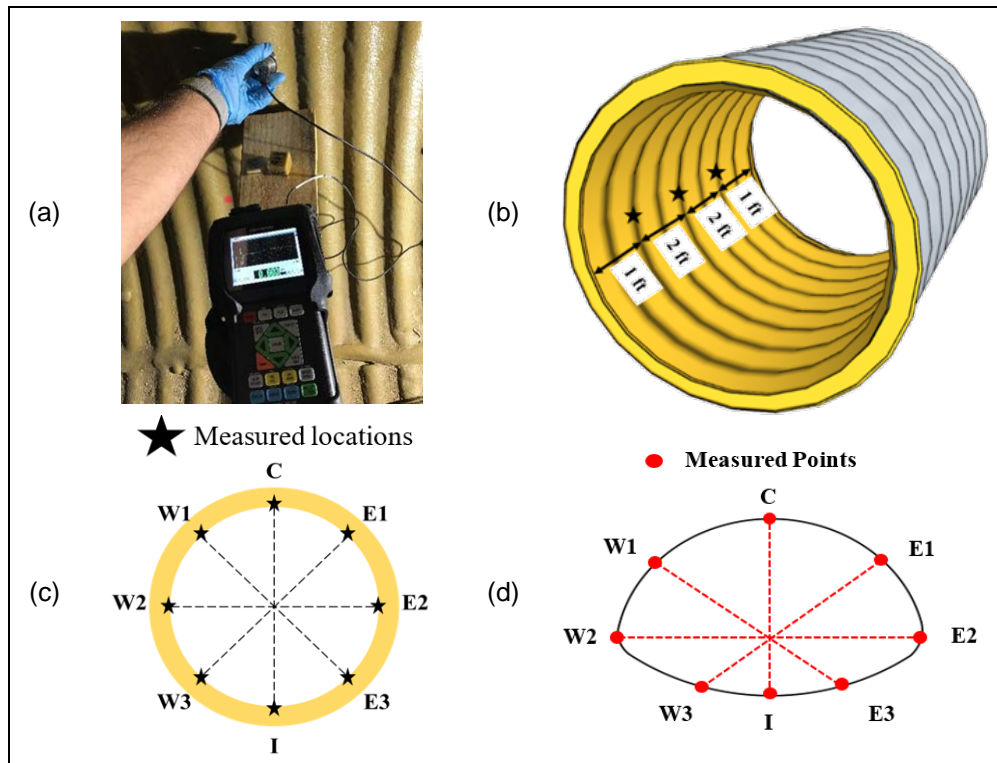



Figure 4-29 SAPL thickness measurement: (a) thickness gauge and calibration sample, (b) longitudinal measured locations, (c) circular CMP circumferential measured locations, and (d) CMP arch circumferential measured locations.

#### 4.5 SAPL Material Property Testing, Test Samples and Procedures

Eight SAPL sample plaques were prepared for the tensile and flexural material property testing (four beam and four dog-bone samples) for each test setup of circular and arch CMPs. ASTM D638 (Test Method for Tensile Properties of Plastics, type I) was followed for conducting the tensile property testing of the dog-bone sample plaques (ASTM D638, 2014). According to the ASTM D638, the gage length of 2 in., grip distance of 4.5 in, and the load rate of 0.2 in/min were selected.

ASTM D790 (Test Method for Flexural Properties of Unreinforced and Reinforced Plastics and Electrical Insulating Materials, Method I procedure A) was followed for conducting the flexural property testing of the beam samples (ASTM D790, 2017). According to ASTM D790, the 3-point bending configuration was used with the load rate of 0.053 in/min and a support span-to-depth ratio of 16 to 1. Table 4-4 lists the dimensions of specimens for both tensile and flexural properties testing.

Table 4-4 Details of specimens used for flexural and tensile properties testing.

Test	Specimen Replicate Number	Width in.	Thickness in.	Specimen Shape
Tensile Test (ASTM D638)	1	0.496	0.150	
	2	0.496	0.149	
	3	0.496	0.149	
	4	0.496	0.148	
Flexural Test (ASTM D790)	1	0.495	0.140	
	2	0.495	0.137	
	3	0.495	0.140	
	4	0.495	0.145	

#### 4.6 Soil Box Testing Loading Configuration and Operations

The CMP samples were loaded using a 330-kip MTS hydraulic actuator attached to a reaction steel frame located at the CUIRE Laboratory at the University of Texas at Arlington, as illustrated in Figure 4-30. In the first set of testing (CMP control test), a static load was applied on the soil surface, on top of the pipe at the middle section, through a 10 × 20 in. AASHTO H20 truck standard pad size (dimensions of 1 sets of

tires) for the intact circular CMP and a 20 × 40 in. load pad for the invert-cut samples, as it is illustrated in Figure 4-31. It is noteworthy that the load pad size was changed from 10 × 20 in. to 20 × 40 in. to prevent the occurrence of premature soil failure prior to the pipe failure. In case of the invert-cut CMP samples compared with intact CMP sample, the pipes were in a fully deteriorated invert condition (invert-cut) and a larger deflection was expected. Hence, a larger load pad size was used to distribute the stress at the connection area of the load pad and soil surface.



Figure 4-30 The 330-kip MTS actuator hydraulic actuator attached to a reaction steel frame located at the CUIRE Laboratory at the University of Texas at Arlington.

For the second and third sets of testing (SAPL renewed CMPs), a static load was applied on the soil surface, on top of the pipe at the middle section, through a rigid 20 × 40 in. steel load pad. Since a static loading regime causes a higher deformation on a pipe sample compared with dynamic loading (Yeau et al. 2009), it was selected for loading of the CMP samples. A continuous displacement-control loading method with a rate of 0.03 in./min was selected because of its advantage for obtaining the post-peak softening behavior of the CMP samples. The reason for choosing a continuous loading regime rather than an incremental loading regime was due to the insensitivity of the selected poorly graded sandy soil to the delayed deformation and settlement (Masada 2017a; Regier et al. 2016).



Figure 4-31 Steel load pad: (a) 10 × 20 in., and (b) 20 × 40 in. pad size.

#### **4.6.1 Live Load Distribution According to the AASHTO LRFD Bridge Design Specifications**

According to the AASHTO LRFD Bridge Design Specifications, the load through a vehicle on the pavement will be transferred as a uniform stress over a rectangular area equal to the contact area of the wheels. For an H20 truck, the contact area will be 10 × 20 in., as illustrated in Figure 4-32. Figure 4-33 illustrates the pattern of load distribution through top of the pavement to top of the pipe.

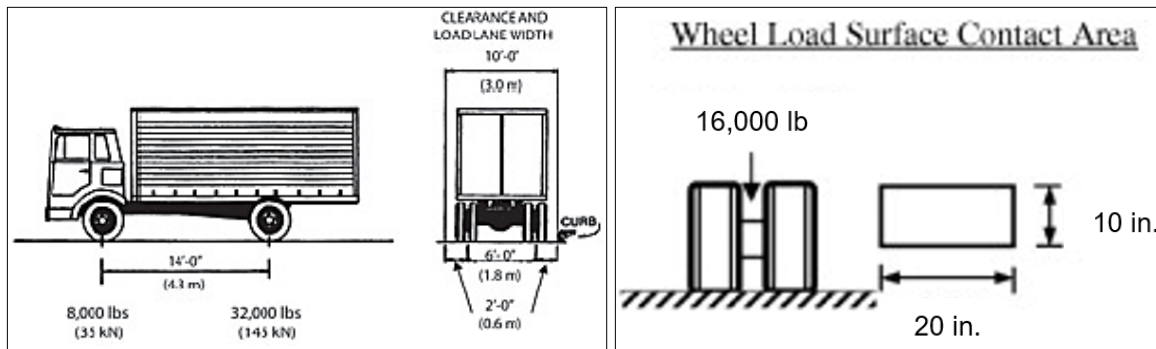


Figure 4-32 AASHTO-approved live loading specifications for standard H20 trucks  
(AASHTO LRFD Bridge Design Specifications 2020).

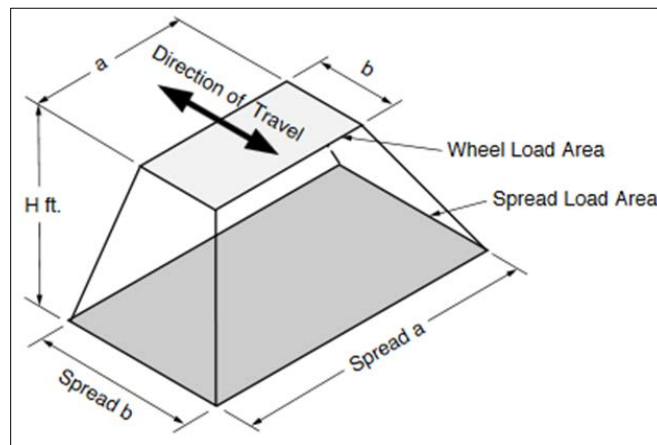


Figure 4-33 Load distribution below the wheel area (AASHTO LRFD Bridge Design Specifications 2020).

For flexible/asphalt pavements, there is no generally accepted theory to estimate the effects of pavement on load distribution. Therefore, these pavements can be considered as an additional layer of backfill. The spread load area is developed by increasing the length and width of the wheel contact area for a load configuration as illustrated in Figure 4-33. AASHTO LRFD Bridge Design Specifications Articles 3.6.1.2.6 a-c provides the calculation procedure for obtaining the dimensional increases to the wheel contact area are based on the height of earth cover over the top of the pipe for two types of soil, as listed in Table 4-5.

Table 4-5 LRFD wheel contact area dimensional increase factor (AASHTO LRFD Bridge Design Specifications 2020).

Soil Type	Dimensional Increase Factor
LRFD select granular	1.15 H
LRFD any other soil	1.00 H

The factors for calculating these areas can depend on the direction of traffic concerning the pipe span, height of fill and wheel load. For a 2-ft deep fill with 16,000 lb wheel load at the top traveling perpendicular to the pipe, the factors are obtained according to Table 4-6.

Table 4-6 Live load distribution of  $1.15 \times H$  for select granular fill.

Vehicle Traveling Perpendicular to Pipe				
	H (ft)	P (lbs)	Spread a (ft)	Spread b (ft)
Live Load Distribution of $1.15 \times H$ for Select Granular Fill	$H + 1.15D_o < 2.05$	16,000	$a + 1.15H$	$b + 1.15H$
	$2.05 - 1.15D_o < H < 5.5$	32,000	$a + 4 + 1.15H$	$b + 1.15H$
	$5.5 < H$	50,000	$a + 4 + 1.15H$	$b + 4 + 1.15H$

#### 4.7 Chapter Summary

To evaluate the structural capacity of renewed CMPs with polymeric spray applied pipe lining (SAPL), full scale laboratory soil box testing was conducted at the Center for Underground Infrastructure Research and Education (CUIRE) at the University of Texas at Arlington (UTA). Through the soil box testing, a total number of nine buried CMP culverts were tested with and without polymeric SAPL, by applying a static load on the soil surface. Details of soil box testing plan, procedure and test setups of buried rehabilitated CMPs, instrumentation, loading configuration, SAPL thickness measurement, and material property testing were explained in detail in this chapter.



## Chapter 5

### Soil Box Testing Results and Discussions

This chapter presents the results of soil box testing discussed in Chapter 4 for all three sets of CMP control test, SAPL renewed circular CMP and SAPL renewed arch CMP (Kohankar Kouchesfehni et al. 2020).

#### 5.1 Control Test Results

##### 5.1.1 *Invert Detachment Effect*

The invert-cut sections of both circular and arch CMPs were detached and removed prior to the loading of the pipe samples. Once the invert-cut sections were detached completely, the CMP samples suddenly moved and squeezed to the presence of active soil pressure on the sides of CMP walls, as illustrated in Figure 5-1. The CMP samples inside diameters were measured before and after the invert detachment. A laser distance meter was used for the pipe diameter measurement. As for the invert-detachment operation was a manual task and for the sake of safety, the utilization of CDS and LVDT was not possible in the confined space of CMP samples. The pipe diameter measurements revealed that the vertical and horizontal diameters of the circular CMP sample were reduced by 3.1 in. downward and 3 in. inward. The rise and span of CMP arch after the invert detachment were reduced by 2.23 in. downward and 5.24 in. inward. As the invert section of the arch CMP has a flat shape compared to the circular CMP, after the invert detachment and in the absence of the ring stiffness, the bottom of the arch CMP was slipped on the soil surface. Hence, due to the invert detachment, the arch CMP registered a smaller change in diameters compared with the circular CMP. With utilization of the digital image correlation (DIC) technique, it was measured that the circular CMP was rotated clockwise to a magnitude of approximately 0.45 in. (arc length) as illustrated in Figure 5-2.



Figure 5-1 CMP movement due to the invert detachment (without any end strips) before loading.

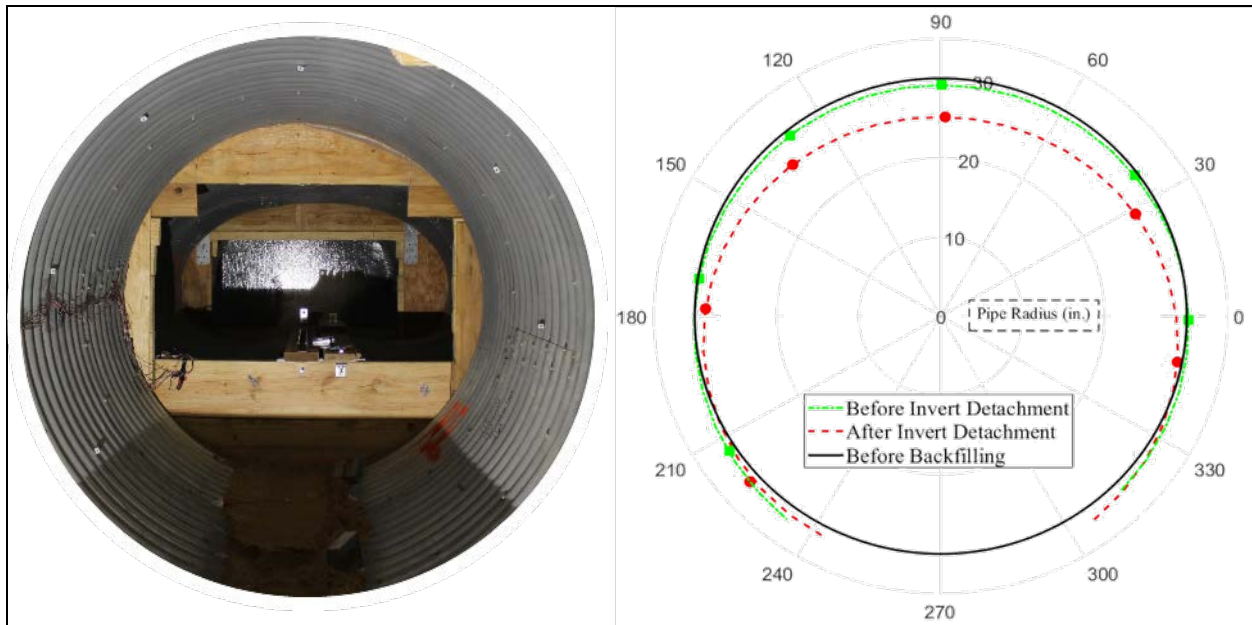


Figure 5-2 60 in. invert-cut circular bare CMP, pipe profiling using DIC technique.

### 5.1.2 Bare CMPs Behavior under the Static Load

The comparison of soil-pipe system settlement under the applied static load for the intact circular, invert-cut circular and invert-cut arch CMPs in terms of the load-displacement graphs are illustrated in Figure 5-3, Figure 5-4 and Figure 5-5. The applied pressures through the load pad on the soil surface at the middle section of the soil cells for intact circular, invert-cut circular and invert-cut arch CMP samples are illustrated in Figure 5-4. The registered pressures by the earth pressure cells on top of the CMP samples (within a 4 in. gap away the outer surface of the CMP) at the crown locations of the intact circular, invert-cut circular and invert-cut arch CMPs are illustrated in Figure 5-5.

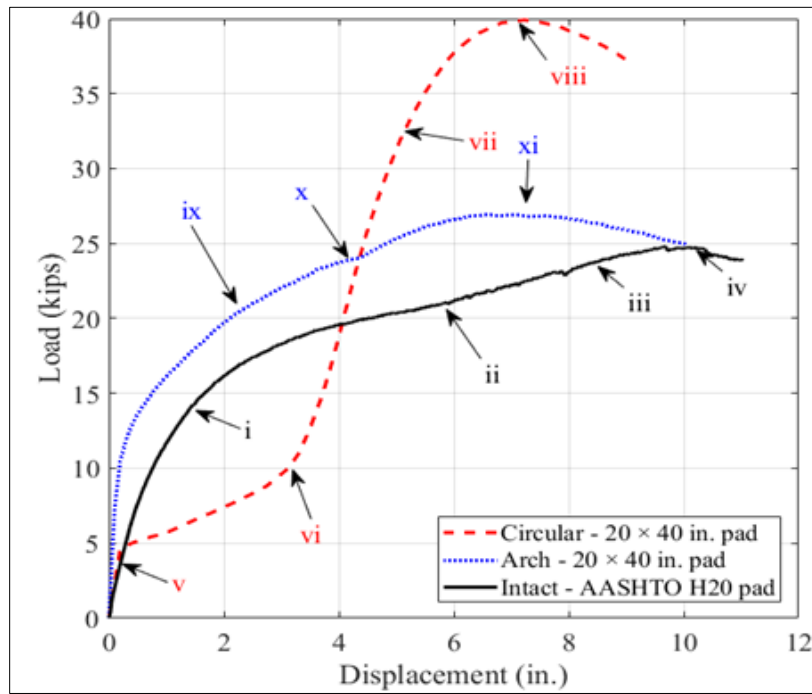


Figure 5-3 Control test - applied load through the steel load pad versus soil settlement.

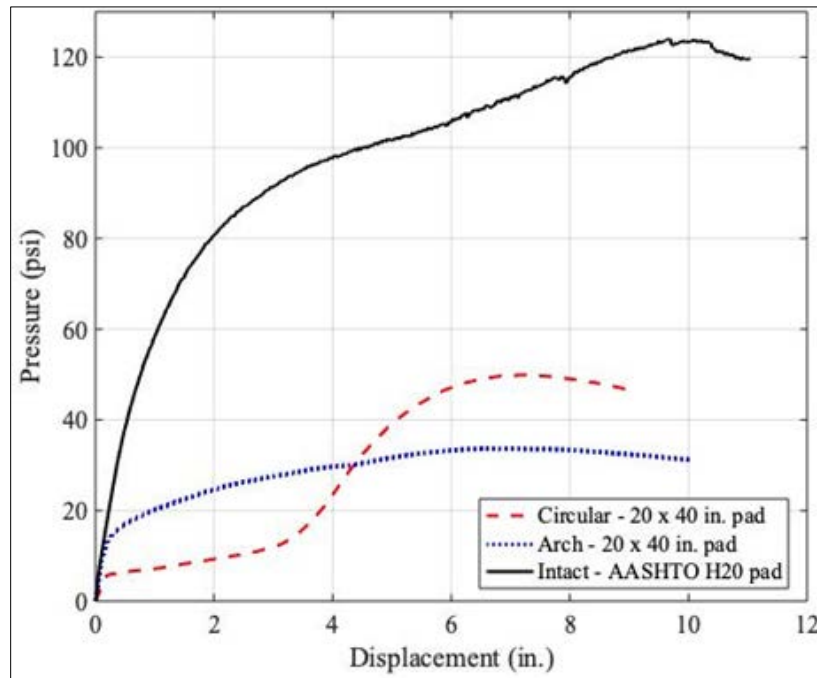


Figure 5-4 Control test - pressure on the soil surface under the load pad versus soil settlement.

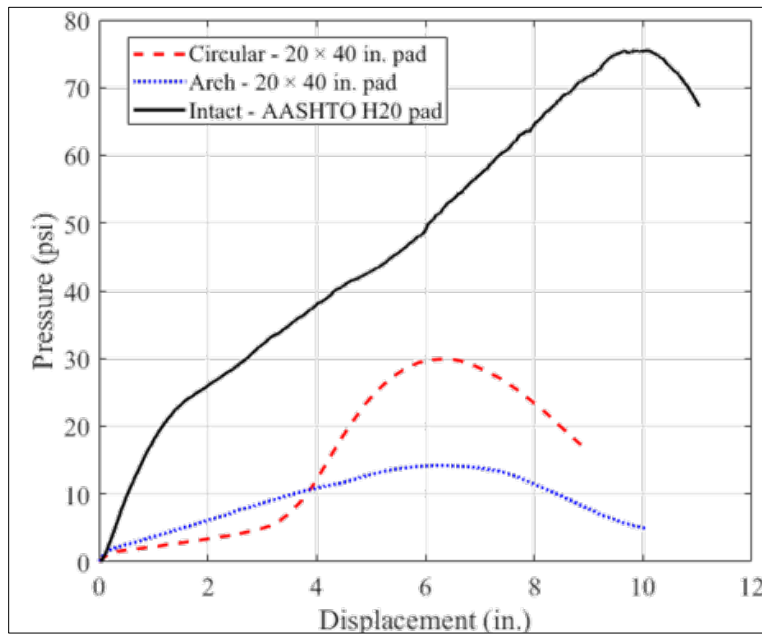


Figure 5-5 Control test - pressure on top of the CMP samples vs soil settlement.

As it is illustrated in Figure 5-3 and Figure 5-4, the bare intact CMP, invert-cut circular CMP and invert-cut arch CMP could withstand the ultimate load of 24.85, 39.9, and 26.9 Kips, respectively. Earth pressure cells registered the maximum pressure of 75.38, 29.95, and 14.23 psi for the intact, invert-cut circular and invert-cut arch CMPs at the crown location at the time of failure.

#### 5.1.2.1 Bare Intact Circular CMP

For the intact circular CMP, the soil-pipe system showed a stiff response to the AASHTO H20 truck service load up to 16 kips, with approximately 1.95 in. of soil displacement, as illustrated in Figure 5-3 by the notation of ‘i’. For the intact bare circular CMP after passing the service load, the soil-pipe system showed a softened response to the applied load until the occurrence of the soil failure at point (notation of “ii” in Figure 5-3). Once the soil failed, all the applied load was carried by the intact bare CMP that caused the stiffening of the system (notation of “iii” in Figure 5-3) and ultimately the failure at the load of 24.8 kips (notation of “iv” in Figure 5-3). The results of DIC measurement and pipe profiling for the 60 in. intact circular CMP is illustrated in Figure 5-6.

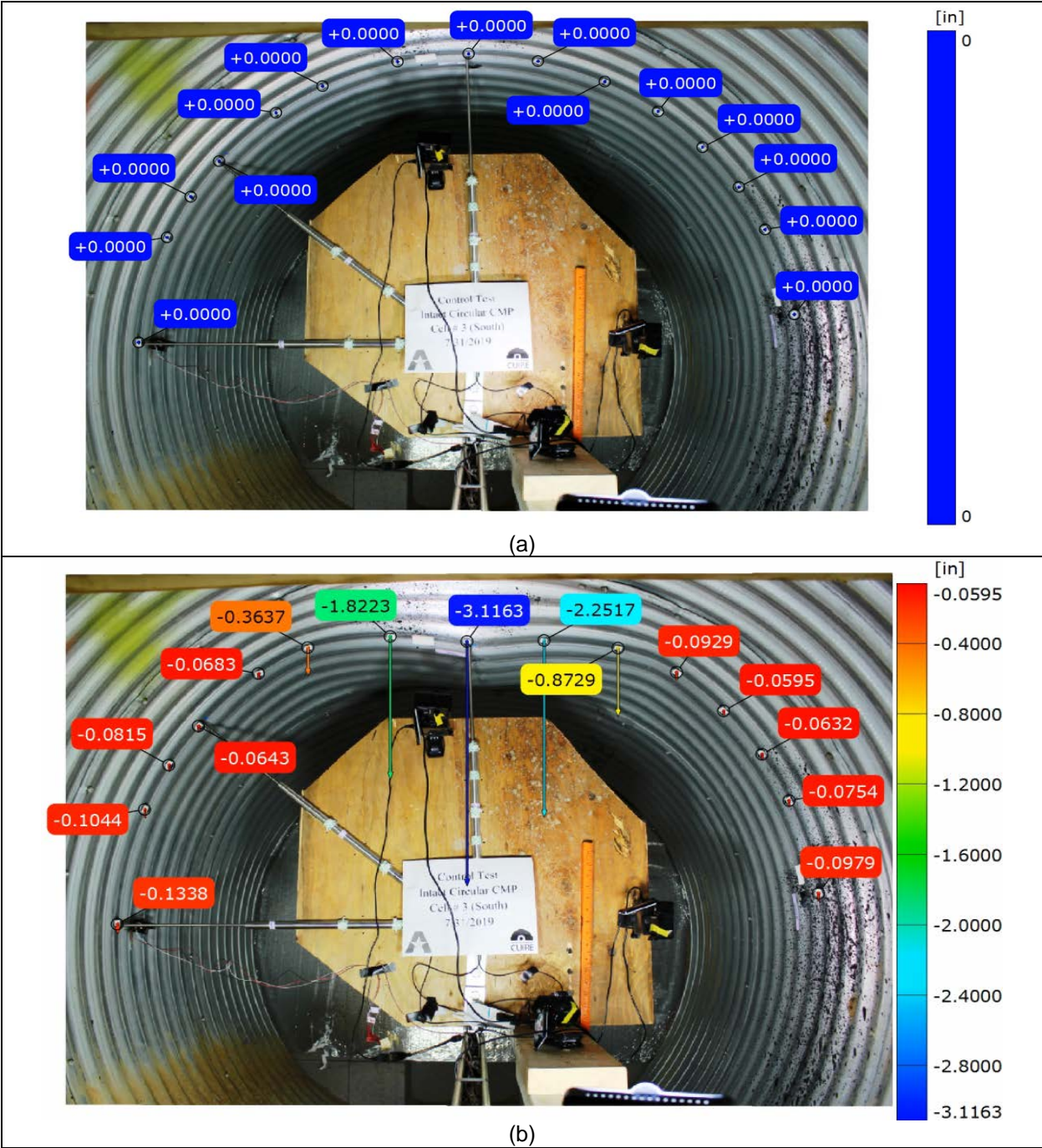


Figure 5-6 Results of DIC measurement for 60 in. intact circular CMP: (a) before loading, and (b) after loading at the end of the test.

### 5.1.2.2 Bare Invert-cut Circular CMP

The invert-cut circular bare CMP compared with intact circular bare CMP under the static live load showed a different behavior. The invert-cut circular bare CMP sample under the applied load initially showed a stiffer response (v), due to the friction resistance force of the soil-pipe system. After reaching the limit of 4.58 kips, in the absence of pipe ring stiffness, there was no other resisting force to prevent the circumferential movement of the CMP sample. Hence, the invert-cut circular bare CMP sample under the load after passing the load of 4.85 kips, continuously moved until both sides of the invert-cut sections meet each other and the pipe ring stiffness was recovered (vi). Due to the circumferential movement of the CMP sample, the vertical diameter of the pipe reduced by 3.1 in. After contacting both edges of the pipe at the invert-cut sections (vi), the system significantly showed a stiffer response to the applied load (vii) until the failure at the load of 39.9 kips. At the failure point the system registered the 7.22 in. soil settlement (viii). The structural failure mode of the invert-cut circular CMP sample was local buckling at the crown, as illustrated in Figure 5-8 (b).

The movement mechanism of the invert-cut circular CMP sample is illustrated in Figure 5-7 (a). The gap closure of the invert-cut circular CMP sample at the cut location due to vertical loading is illustrated in Figure 5-7 (b) and Figure 5-10. Figure 5-8 illustrates the invert-cut circular CMP sample before and after loading. Figure 5-9 illustrates the results of DIC measurement for the invert-cut circular CMP sample at the end of the test.

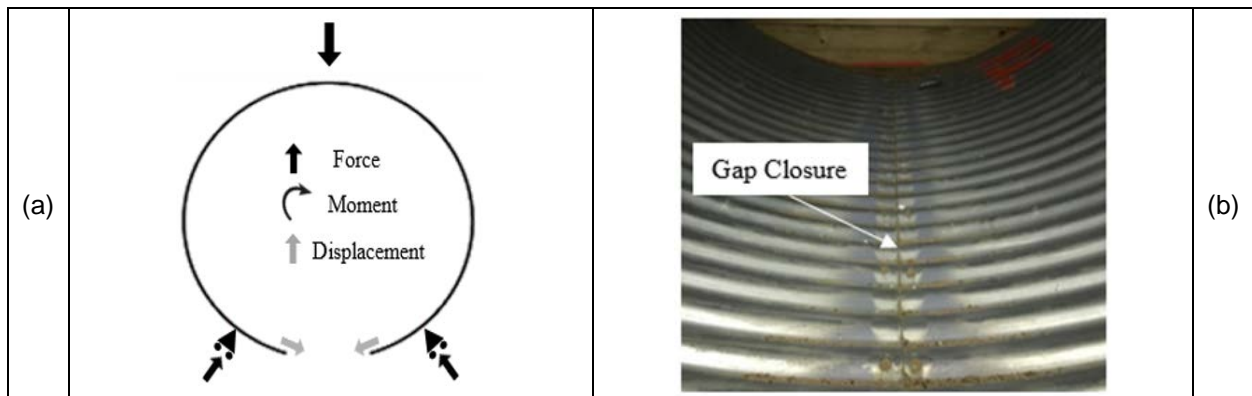


Figure 5-7 Circular CMP movement due to the invert detachment: (a) the movement mechanism, and (b) The gap closure at the cut location due to vertical loading.

The designed and explained laboratory soil box testing in this dissertation was a simulation of the worst-case scenario in the field condition. In the actual field condition, the magnitude of the pipe circumferential movement in a fully deteriorated invert condition, is lower than the laboratory condition. In the actual field condition, the soil-pipe system is stabilized and usually the existed pavement layer on top of the pipe soil cover significantly distresses the traffic load on the structure. Therefore, the circumferential movement of a fully deteriorated pipe happens at a very low pace compared to the laboratory condition. Moreover, the CMP external corrosion increases the pipe roughness as well as the circumferential friction between the pipe wall and surrounding soil. This friction has a direct relationship with the length of the pipe. Hence, in the actual field condition that pipes are much longer than a test pipe sample in a laboratory condition, the resistive frictional force between the pipe and soil reduces the circumferential movement of the pipe. Consequently, the probability of the local buckling occurrence will be increased.

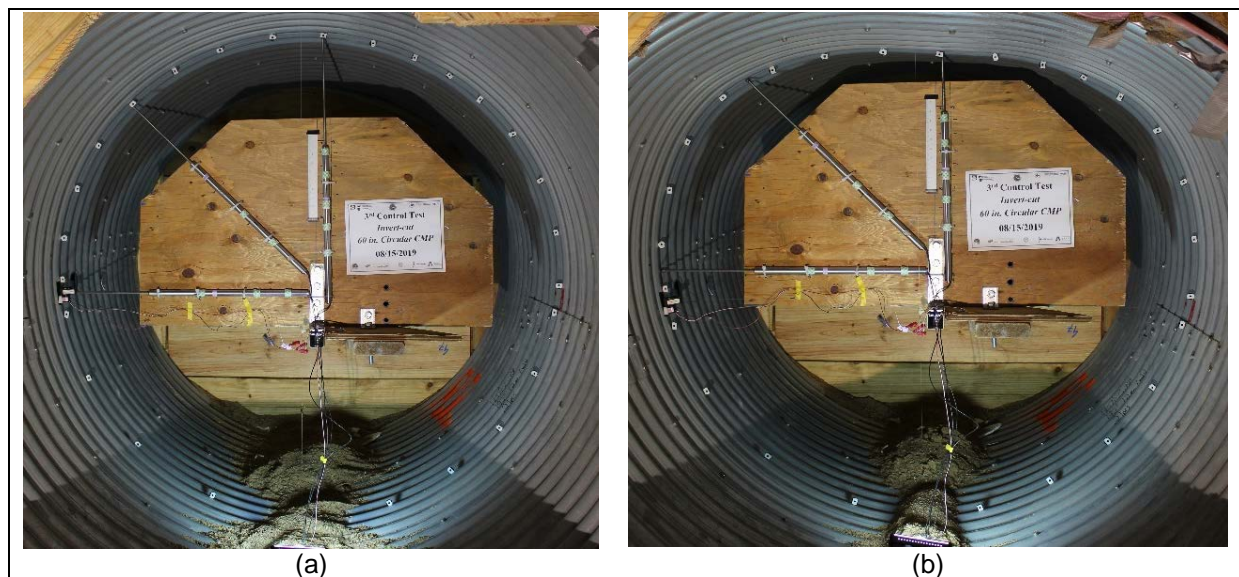


Figure 5-8 60 in. Invert-cut circular CMP soil box testing: (a) before loading, and (b) after loading.



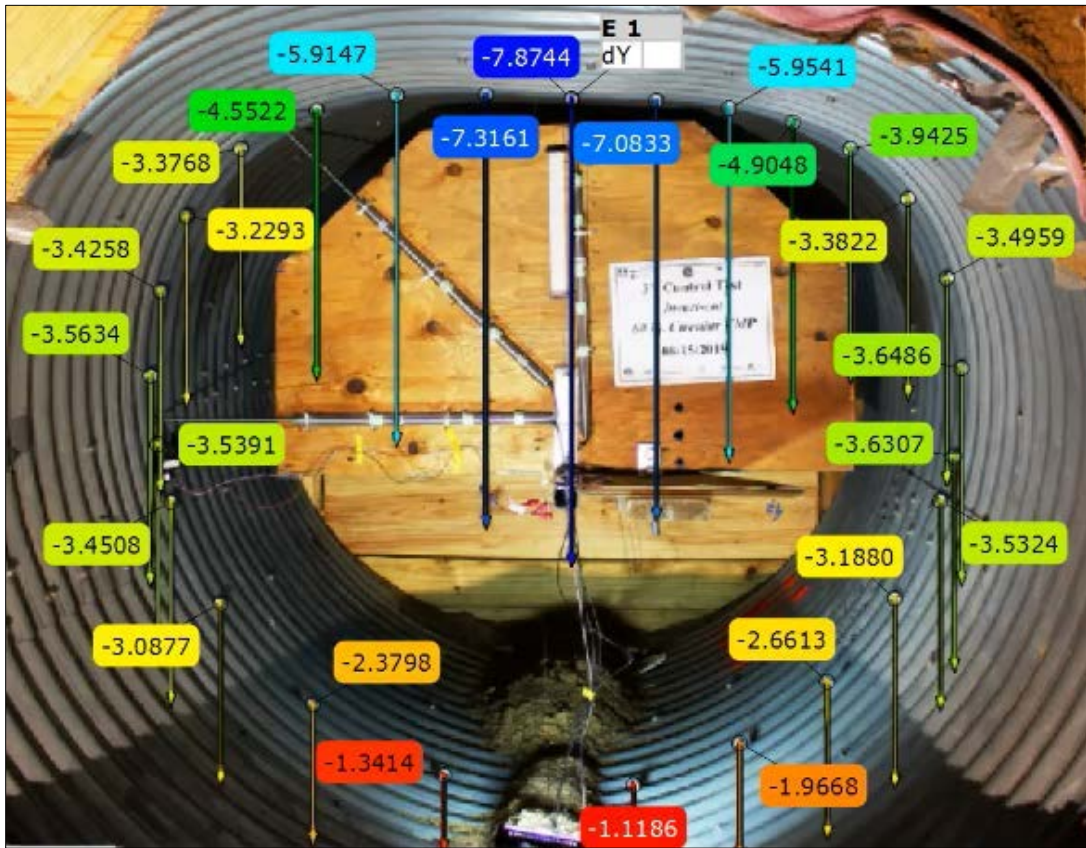


Figure 5-9 Results of DIC measurement at the end of the test – 60 in. invert-cut circular CMP.

### 5.1.2.3 Bare Invert-cut Arch CMP

The invert-cut arch CMP in the absence of ring stiffness maintained its stability under the applied loading. It could take the advantage of its geometry (flat bottom) and no significant horizontal displacement was observed, as illustrated in Figure 5-3 by the notation of “ix”. The low slope area at the arch CMP shoulder and the flat area at the bottom, enabled the CMP sample to resist the applied vertical load. The movement mechanism of the invert-cut arch CMP sample is illustrated in Figure 5-10 (a). Figure 5-10 (b) depicts the uplift of the invert-cut arch CMP after loading and soil compaction. As illustrated in Figure 5-10 (a), a positive movement and upward forces at the invert section of the arch CMP are generated due to the applied vertical force on top of the pipe sample. Hence, the movement of the invert-cut arch CMP sample at the free ends of the invert section with a uniform upward displacement of approximately 2.2 in. was

occurred, as illustrated in Figure 5-10 (c). A gap was generated due to this upward displacement at the invert-cut area of the arch CMP that previously its formation was interpreted as a result of soil erosion (Matthews et al. 2012). However, in the actual field condition this gap could be possibly due to the combination of both soil erosion and CMP upward movement at the invert location. The invert-cut arch CMP failed at the load of 26.9 kips with a 6.54 in. soil surface settlement. Same as the invert-cut circular CMP sample, the structural failure mode of the invert-cut arch CMP sample was also local buckling at the crown. The crown of the CMP sample was the critical location under the load pad that formation of the three-hinge plastic collapse mechanism was occurred there, as illustrated in Figure 5-11. The results of DIC measurement and pipe profiling for the invert-cut arch CMP at the end of the test is illustrated in Figure 5-12.

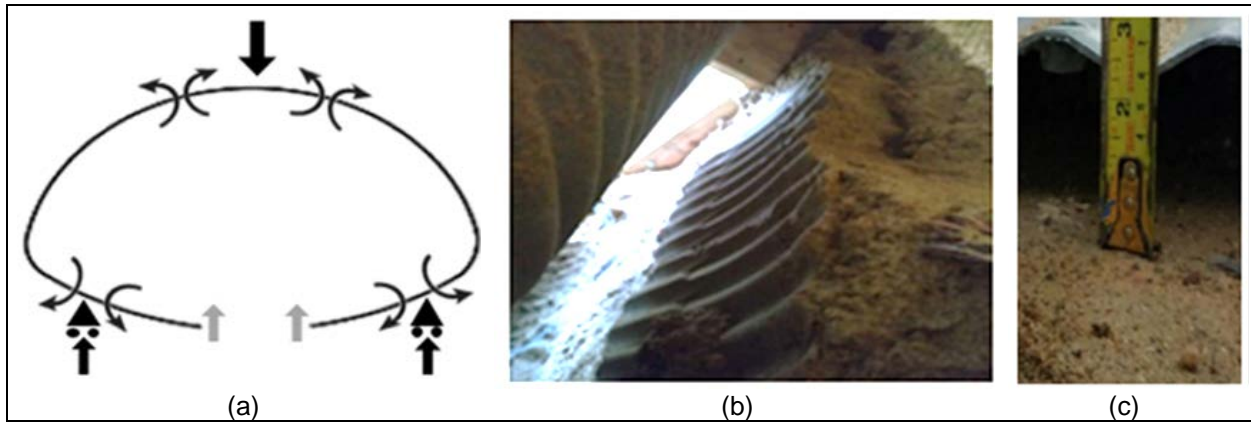
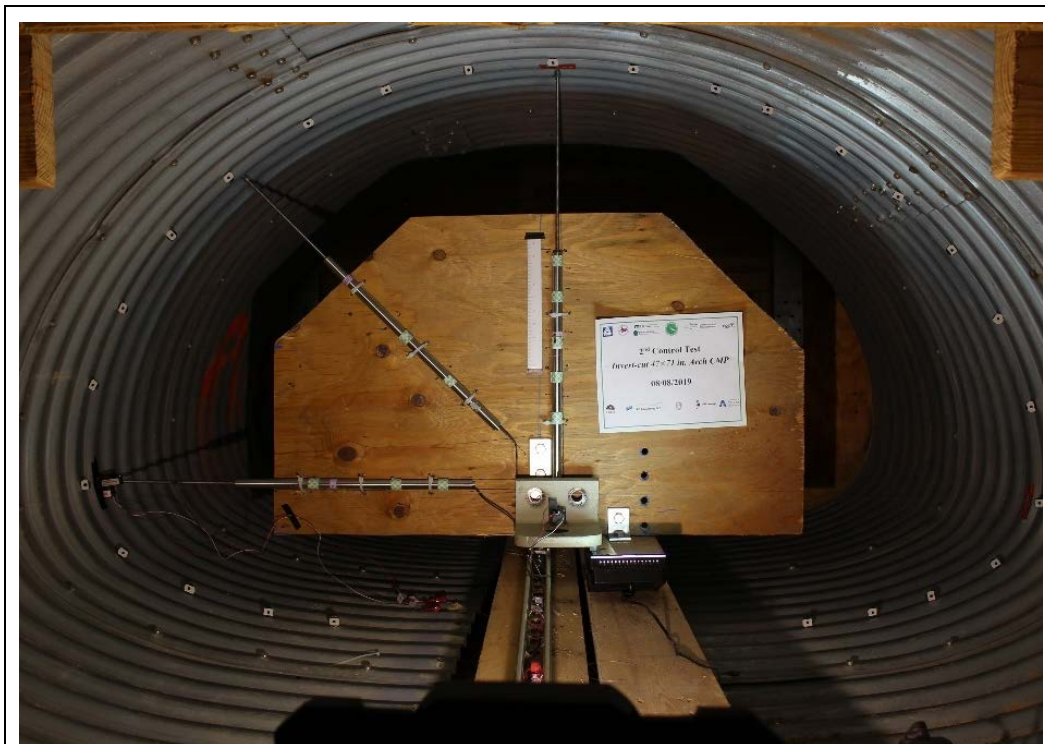


Figure 5-10 Arch CMP movement due to the invert detachment: (a) the movement mechanism, and (b) the uplift of the invert-cut arch CMP after loading and soil compaction. under the haunch area after exhuming the CMP.



(a)



(b)

Figure 5-11 47×71 in. invert-cut arch CMP soil box testing: (a) before loading, and (b) the local buckling failure of the pipe sample after loading.

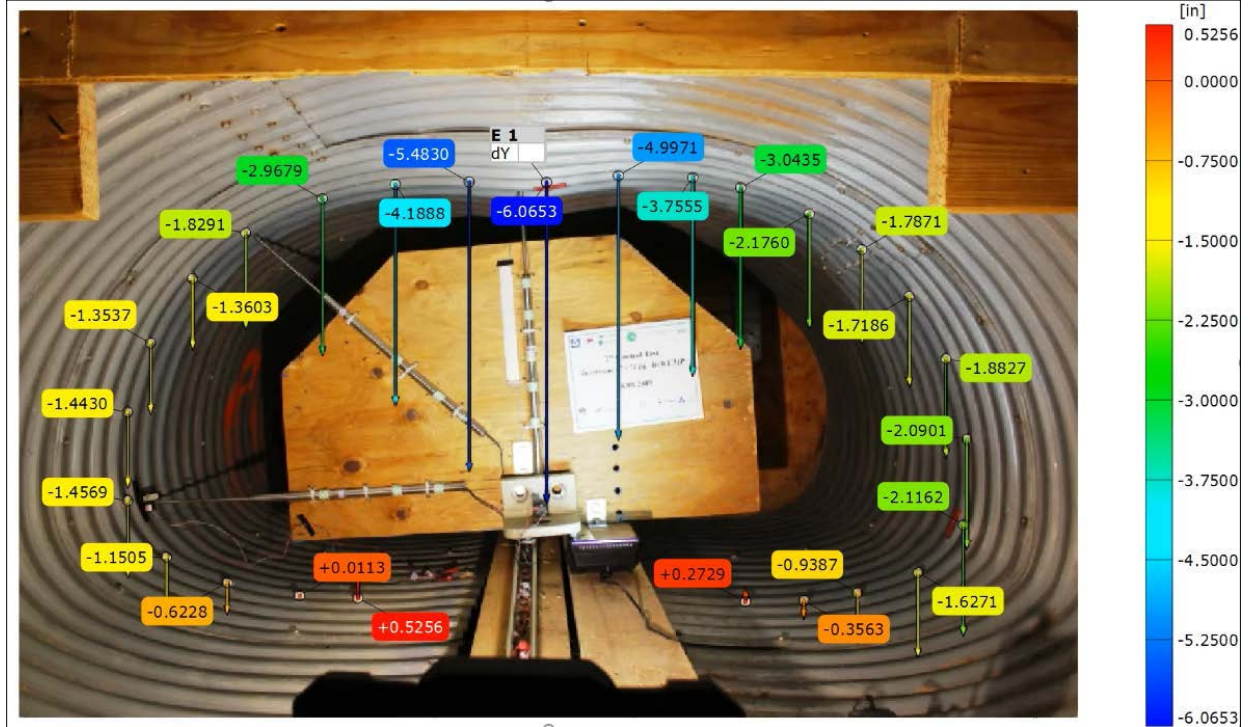
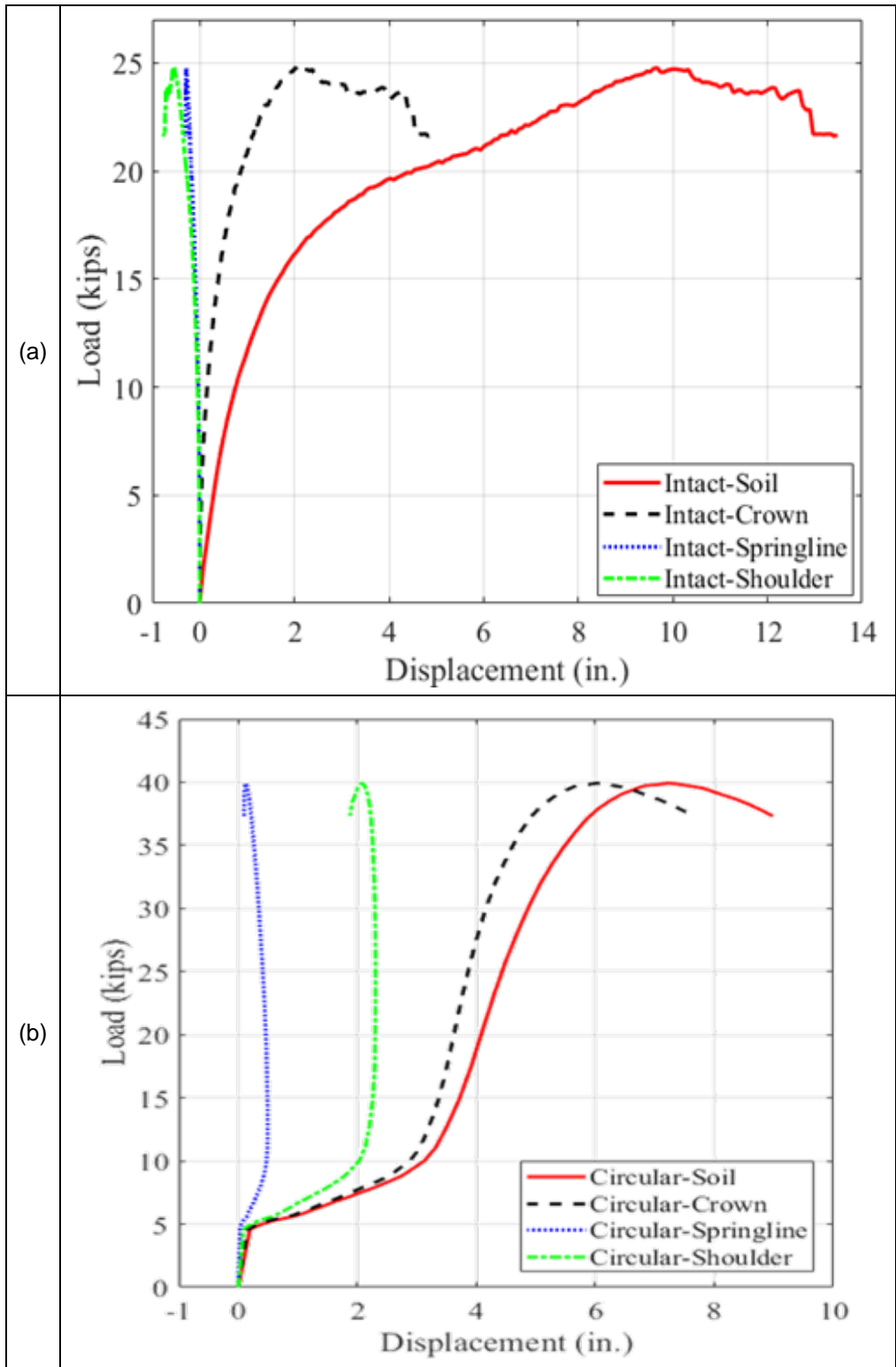


Figure 5-12 Results of DIC measurement at the end of the test – 47×71 in. invert-cut arch CMP.

### 5.1.3 Bare CMPs Load Carrying Capacity

Figure 5-13 illustrates the applied load on the soil surface versus the deflection of CMPs at different locations of crown, springlines and shoulder along with the soil settlement for the first set of soil box testing (CMP control test). It should be noted that in this figure, a negative displacement means the CMP sample upward movement.

The difference in the strength of CMP and soil materials caused a discrepancy between the obtained load-displacement graphs from the CMP samples and soil, as illustrated in Figure 5-13. The soil, as the softer material, deformed or compressed more than the CMP as the stronger material.



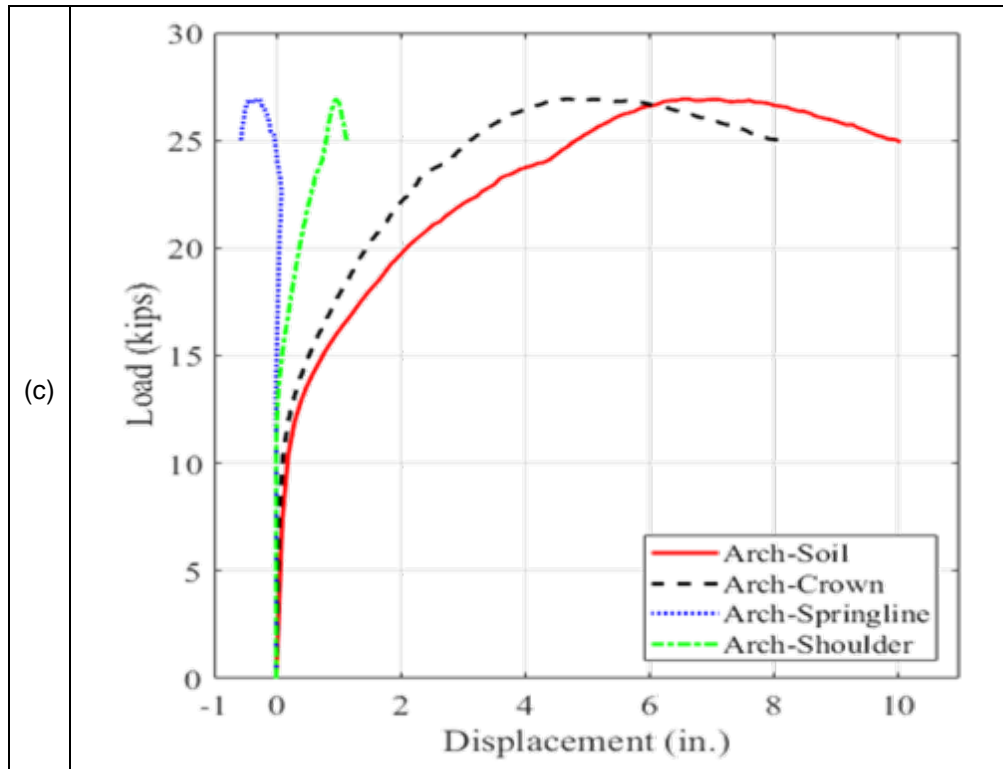


Figure 5-13 Load versus displacement of CMPs at different locations for the control test: (a) intact 60 in. circular CMP under a 10x20 in. steel load pad, (b) invert-cut 60 in. circular CMP under a 20x40 in. steel load pad, and (c) invert-cut 47x71 in. arch CMP under a 20x40 in. steel load pad.

### 5.1.3.1 Bare Intact Circular CMP

The intact circular CMP, under the AASHTO H20 truck load (under the steel load pad size of 10 x 20 in.), reached the service load of 16 kips with a vertical deflection of 0.46 in. at the crown of the pipe and soil settlement of 1.97 in. on the soil surface. The ultimate load carrying capacity of the intact circular CMP was reached to the load of 24.77 kips with the vertical deflection of 2.03 in. at the crown of the intact circular CMP and soil settlement of 9.96 in. on the soil surface. The soil box testing results of the intact circular CMP showed that the CMP sample did not reach the deflection limit of 5%, as specified in section 1.1.5.1.2, prior to the occurrence of the local buckling failure at the crown.

#### **5.1.3.2 Bare Invert-cut Circular CMP**

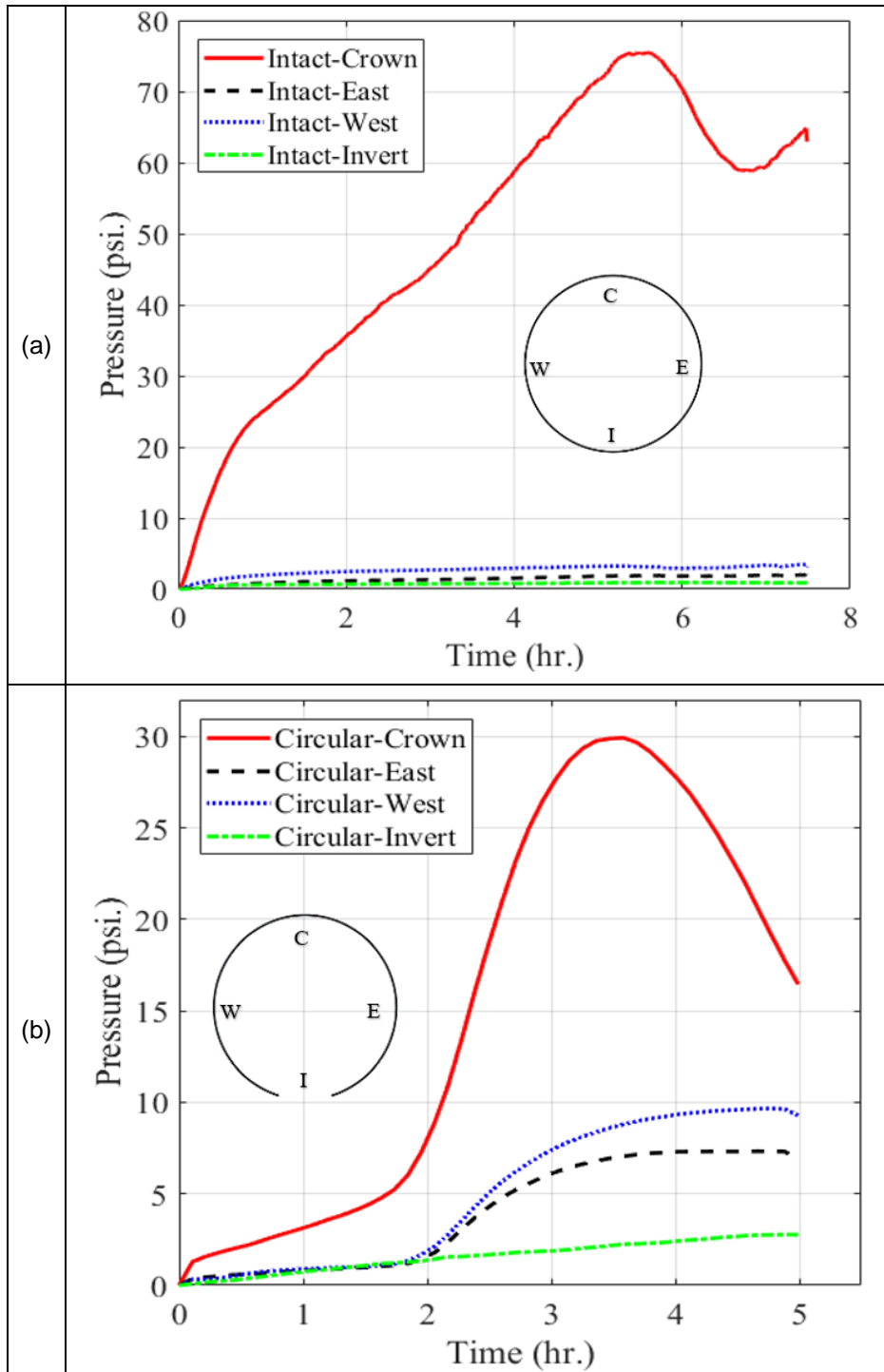
The invert-cut circular CMP registered the horizontal pipe deflection of 0.12 in. at the springline and the vertical deflection of recorded 6.03 in. at the crown for both LVDT and CDS. However, by disregarding the initial movement of the CMP sample, the absolute displacement of the invert-cut circular CMP sample pipe at the shoulder, springline, and crown are 0.07, -0.33, and -3.15 in., respectively.

#### **5.1.3.3 Bare Invert-cut Arch CMP**

The invert-cut arch CMP sample failed at approximately the load of 26.9 kips with the vertical deformation of 4.64 in. at the crown of CMP sample and the soil settlement of 6.54 in. on the soil surface under the steel load pad. LVDTs registered the horizontal inward displacement of -0.7 in. from the east side of the springline towards the center of the pipe and CDS registered a reduction of -1.35 in. in the span of the invert-cut arch CMP sample.

#### **5.1.4 Results of Earth Pressure Cells**

The earth pressure cell results are illustrated in Figure 5-14. The maximum pressure at the crown of the intact CMP, invert-cut circular CMP and invert-cut arch were registered 75.38, 29.95 and 14.23 psi, respectively. As it is observed by the pressure graphs, in each cell of testing the maximum pressure was carried out by the crown of CMP samples, and compared with the crown, no significant pressures were transferred to the springline and invert.





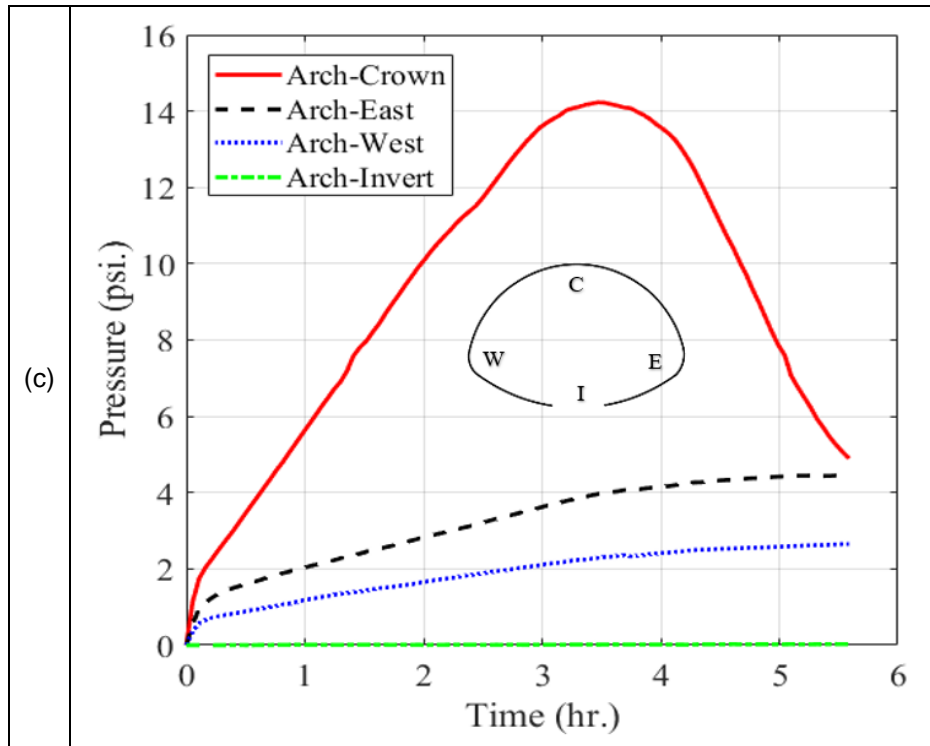


Figure 5-14 Results of earth pressure cells for the CMP control test: (a) intact circular CMP, (b) invert-cut circular CMP, and (c) invert-cut arch CMP.

The soil-structure interaction system of the invert-cut arch CMP, in compare with the invert-cut circular CMP, showed a stiffer response to the initial stages of loading. However, the invert-cut circular CMP after retrieving its ring stiffness showed a stiffer response which was almost twice of its initial stiffness in the absence of ring stiffness. The earth pressure cells located at East and West sides for both invert-cut circular CMP and invert-cut arch CMP samples, showed that the passive pressures applied on both sides for the invert-cut circular CMP were almost twice the invert-cut arch CMP. This comparison of pressure values on both sides of the invert-cut samples indicated that the invert-cut arch CMP had less tendency to horizontal expansion. The discrepancy between the results of the earth pressure cells located at East and West sides of the invert-cut samples, as illustrated in Figure 5-14, could be due to the uneven movement of the pipe samples after the invert-section detachment.

As it is illustrated in Figure 5-14 (c), the magnitude of pressure at the invert location shows a value of zero. The zero-pressure value indicates that in the absence of invert section no pressure was applied from the invert-cut arch CMP to the soil at the invert location. As it is illustrated in Figure 5-14 (b), the magnitude of the ultimate pressure in the existence of the pipe ring stiffness at the invert location for the invert-cut circular CMP sample showed a value of 2.7 psi that was not significant compared to the maximum registered pressure at the crown of the pipe sample. This could be due to a relatively larger movement of the circular CMP, in compare with the arch CMP, at the time of invert detachment and during the loading phase.

Table 5-1 as a summary presents the ultimate load and pressure and the maximum displacement of bare CMPs at the time of failure for the control test.

Table 5-1 Control test of bare CMPs - the ultimate load and pressure and the maximum displacement at the time of failure.

<b>Pipe Sample</b>	<b>Ultimate Load (kips)</b>	<b>Pressure on Crown (psi)</b>	<b>Crown Deflection (in.)</b>	<b>Soil Surface Settlement (in.)</b>
Intact CMP	24.8	75.38	4.87	9.68
Invert-cut Circular CMP	39.9	29.95	5.35	7.22
Invert-cut arch CMP	26.9	14.23	4.38	6.54

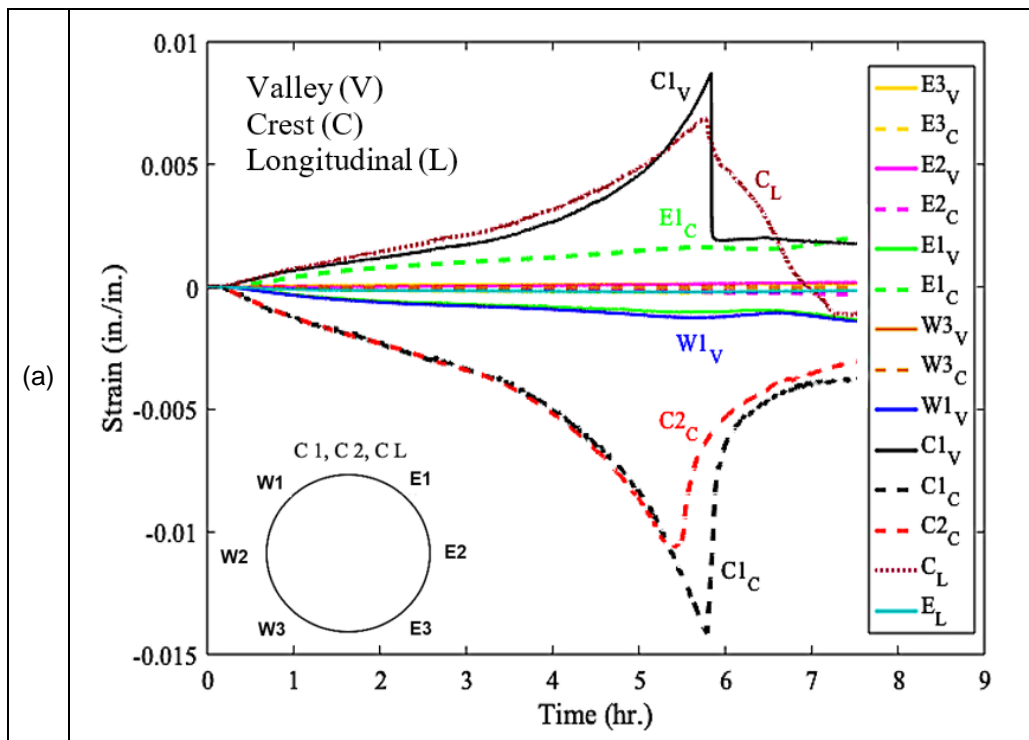
### **5.1.5 Results of Strain Gauges**

The results of strain gauges for the control test of CMPs are illustrated in Figure 5-15. The intact circular CMP under the loading through a smaller load pad, compared with the invert-cut CMP samples under a bigger lad pad, experienced relatively a larger longitudinal strain (noted by “CL” in the figure) at the crown of the pipe, as it is shown in Figure 5-15 (a). The exerted load on the pipe through a smaller load pad resulted in a larger buckling curvature in longitudinal direction at the crown of the pipe.

The invert-cut circular CMP experienced the same pattern of buckling failure at the crown of the pipe. However, the invert-cut circular CMP, unlike the intact circular CMP and the invert-cut arch CMP,

registered a lower strain value at the valley at the crown of the pipe compared to the shoulder locations. This could be resulted from the 2 in. circumferential movement due the invert detachment of the invert-cut circular CMP prior to the loading. Consequently, a tensile stress on the exterior extreme fiber of the crest and a compressive stress on the interior extreme fiber of the valley at the crown of the pipe were exerted. Due to the vertical displacement of the crown of the pipe under the static load, the crest and valley were subjected to compressive and tensile stresses, respectively. These stress reversions (the existed stress in the pipe due to the pipe circumferential movement and the applied stress due to the static load) counteracted each other that caused a lower strain value at the crown of the pipe.

The invert-cut arch CMP registered a large strain value at the crown of the pipe and both shoulder locations, as shown in Figure 12 (a), that indicates the formation of a three-hinge plastic collapse mechanism due to the local buckling at the crown. Same trend was also observed on the intact circular CMP sample.



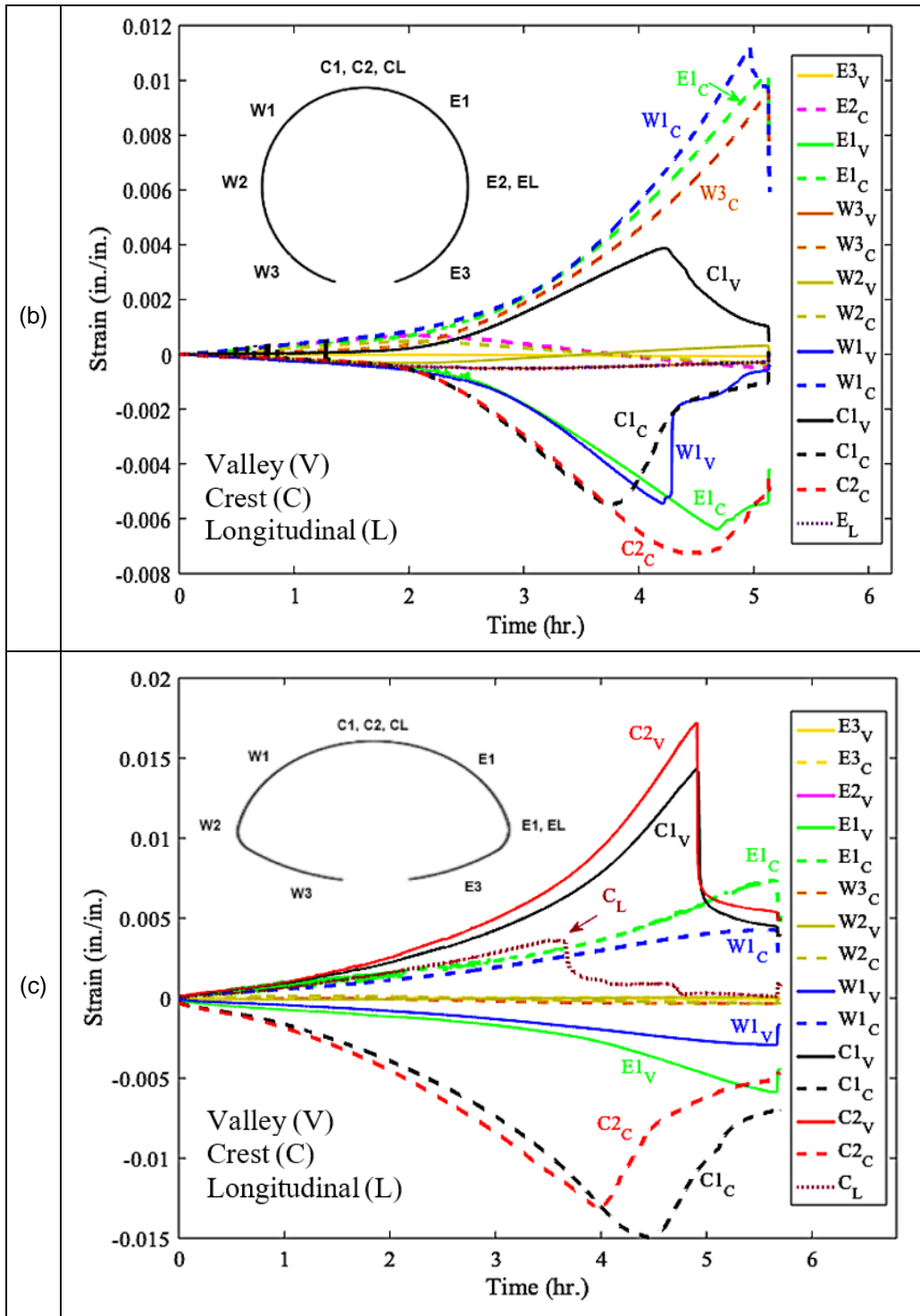


Figure 5-15 Results of strain gauges for the CMP control test: (a) intact circular CMP, (b) invert-cut circular CMP, and (c) invert-cut arch CMP.

### **5.1.6 Thrust Force and Bending Moment**

For each CMP sample, once the first strain gauge registered the yield strain value of  $1,138 \mu\epsilon$ , the thrust force and bending moment values were calculated at seven locations around the pipe. Figure 5-16 illustrates the thrust force and bending moment values around the CMP samples. It should be noted that a spline distribution was used to connect the seven available data points of bending moment and thrust force and estimate these values for other locations in between.

The intact circular CMP, invert-cut circular CMP and invert-cut arch CMP samples reached to the yield strain at the soil pressure values of 26, 14.9 and 5.2 psi, respectively, on top of the pipes. At these pressures and at the time of reaching the yield strain, the CMP samples registered the values of 0.448, 0.304 and 0.474 kip-in./in. on top of the pipes, respectively, for the maximum positive bending moments of intact circular CMP, invert-cut circular CMP and invert-cut arch CMP. However, the shoulder areas registered the negative values of -0.175, -0.339 and -0.236, respectively, for bending moments of intact circular CMP, invert-cut circular CMP and invert-cut arch CMP. These sign changes are in conformity with the formation of the three-hinge plastic collapse mechanism at the crown of the CMP samples.

The thrust force values of -0.416, -1.002 and -1.027 kip/in. were calculated at the crown of the pipe samples, respectively, for the intact circular CMP, invert-cut circular CMP, and invert-cut arch CMP. It is noted that some of the strain gauges were damaged due to the soil backfilling and compaction. Hence, it was impossible to report their results.

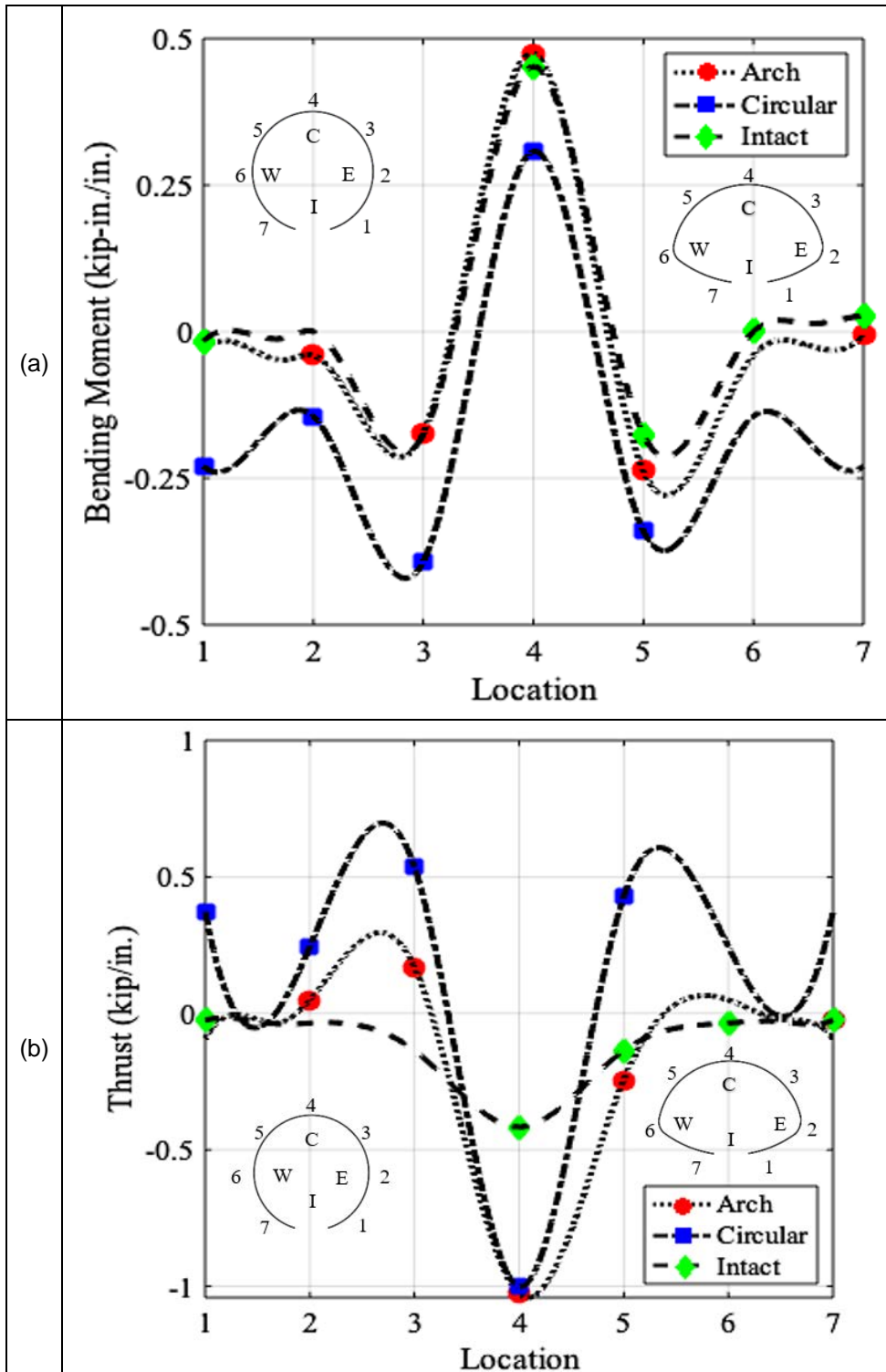
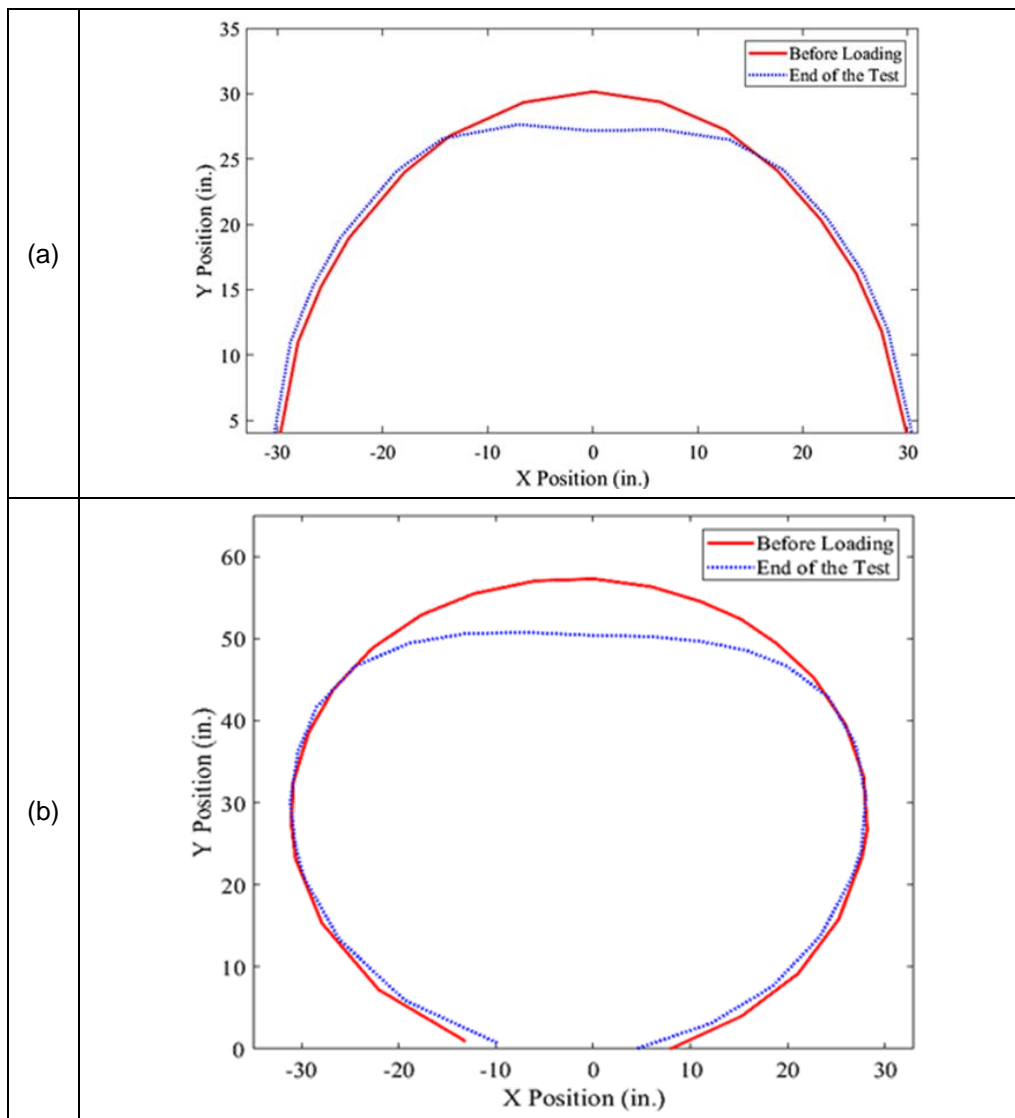


Figure 5-16 Internal forces on intact, invert-cut circular and invert-cut arch CMP samples: (a) bending moment, and (b) thrust forces for the invert-cut arch, invert-cut circular and circular intact CMPs.

### 5.1.7 Results of DIC Deflection Measurement

The pipe profiling and deflection measurement using digital image correlation (DIC) results are illustrated in Figure 5-16. The readings are obtained from the middle section of the CMP samples under the load pad area. The failure mode of all CMP samples was local buckling at the crown of the pipe as it is explicitly evident in Figure 5-16 as well. Due to the soil extrusion from the invert-cut section of the circular CMP sample under the loading (as a result of invert detachment), the installation of DIC targets was not possible at that location. Therefore, the invert gap closing is not captured with the DIC technique. The comparison of the DIC results and the results of LVDTs showed an excellent match of both methods.



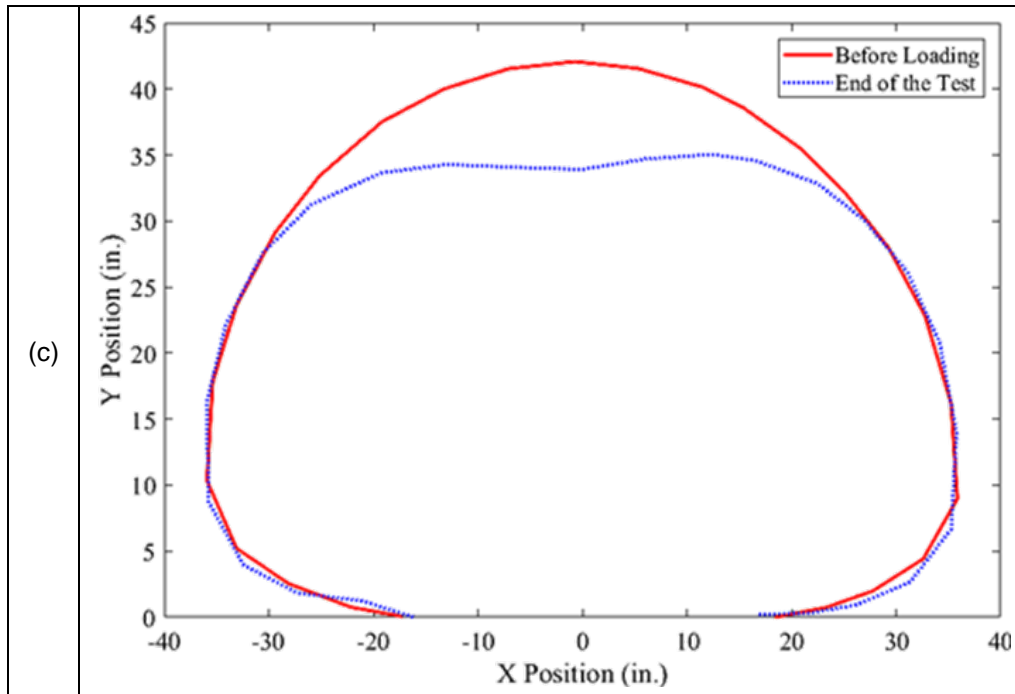


Figure 5-17 Pipe profiling using DIC results before loading and after loading at the ultimate load carrying capacity of the samples: (a) intact CMP, (b) invert-cut circular CMP, and (c) invert-cut arch CMP.

## 5.2 Soil Box Testing – SAPL Renewed Circular CMPs

### 5.2.1 SAPL Material Property Testing Results

The polymeric beam and dog-bone samples were tested according to the related ASTM standards. The results of the polymeric SAPL material property test are illustrated in Figure 5-18. The polymeric SAPL's uniaxial tensile test showed the averaged maximum tensile stress was 8,670.78 psi with the standard deviation of 623.94 psi. The samples failed with the averaged maximum tensile strain of 0.0443 with standard deviation of 0.0031. Averaged elastic modulus of 329,209.9 psi was calculated through calculation of slope of the stress-strain line at initial stage.

The averaged maximum force resisted by the polymeric SAPL samples under the flexural test using 3-point bending configuration was 53.99 lb with the standard deviation of 2.23 lb. Consequently, the calculated averaged flexural modulus was 855,639 psi. The results of the tests are close to the manufacturers specifications (Johnson and Hammon 2017; TRI / Environment 2012).



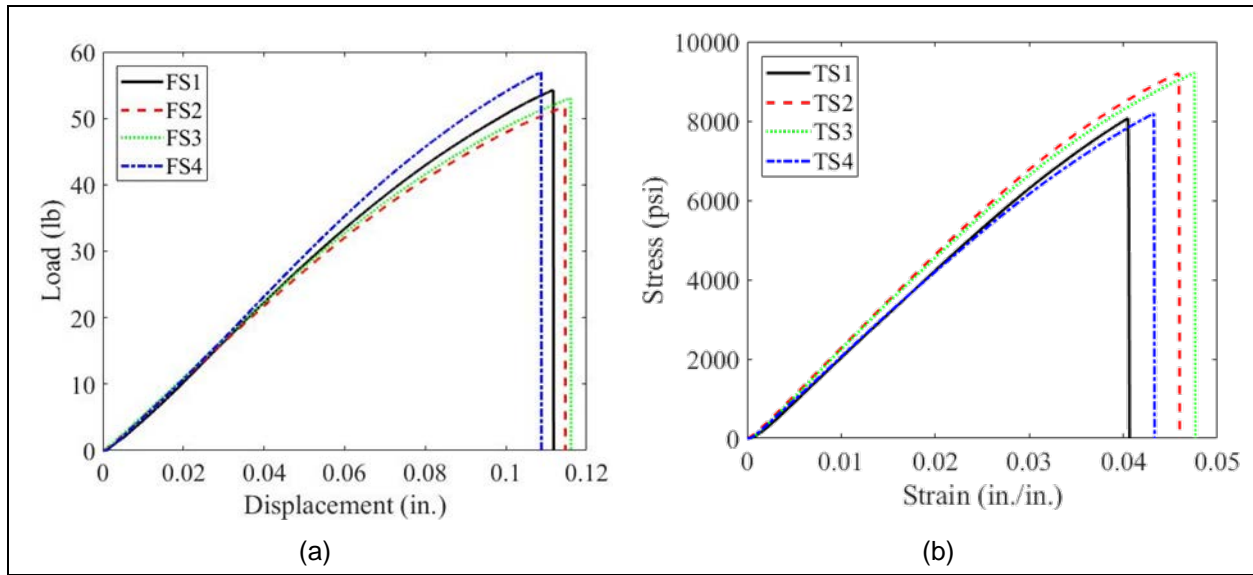


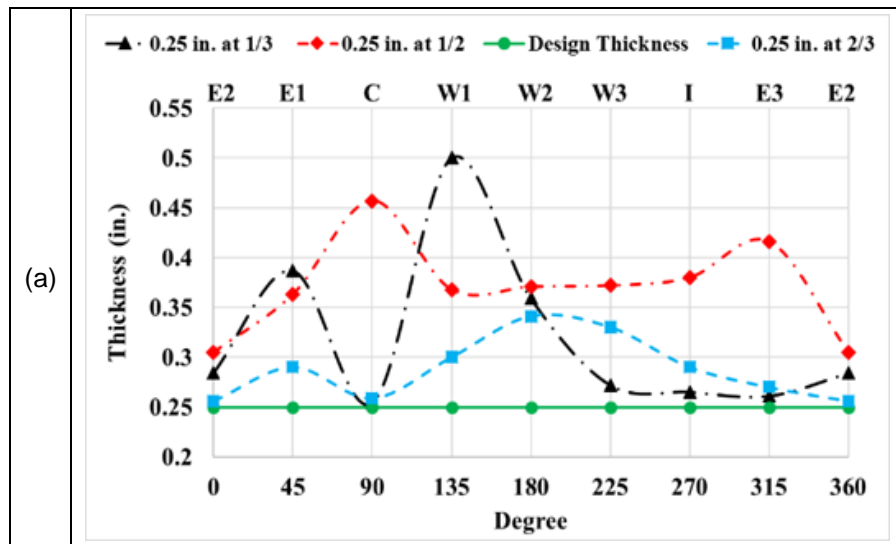
Figure 5-18 Polymer SAPL material property test results: (a) flexural test (ASTM D790), and (b) tensile test (ASTM D638).

### 5.2.2 SAPL Thickness Survey Installed Inside Circular CMPs

The thickness of the SAPL installed on the pipe samples were measured at three locations of approximately 1/3, 1/2, and 2/3 of the pipe sample's length. The measurement results showed that the applied thickness is usually higher at springline (i.e., locations W2 and E2 in Figure 5-19) than the design thickness. Opposite trend was observed at the crown locations (i.e., location C in Figure 5-19) where the thickness was lower than the required thickness. This alteration is more evident in the pipe sample with thicker SAPL which downward gravity force could result in the movement of the sprayed material toward the springline. Figure 5-19 (c) illustrates the thickness variation of SAPL on the 1.0 in. SAPL renewed CMP sample that shows the thickness was more uniformly applied at the center of the pipe in compare with the both ends of the CMP. The same trend was observed for the 0.5 in. and 0.25 in. SAPL renewed CMP samples that could stem from the nature of hand-spray installation method of the polymeric SAPL. On the other hand, the installer had more space and ease of movement at the center of the pipe in compare with the pipe ends where the partition walls were located.

Once the structural test was carried out, the measured thickness locations with the ultrasonic thickness measurement device were drilled down to the CMP surface. Then the manual thickness measurement was conducted using a digital caliper to verify the accuracy of the ultrasonic thickness measurement. The results comparison showed an excellent agreement between both measuring methods, especially for thicker liners. For the 0.25-in. thick SAPL renewed CMP sample, the ultrasonic device was not able to accurately measure the thickness at the location, 2/3 of the pipe's length, as illustrated in Figure 4-10 (a). One possible reason could be due to the received higher volume of backscattered waves in low thickness such as 0.25 in. or lower that made the device unable to calculate the thickness accurately. Therefore, for this location (i.e., 0.25 in. at 2/3) the results of manual thickness measurements are presented in Figure 5-19 (a).

The visual observation on 0.25 in. SAPL renewed CMP showed the applied SAPL thickness on the seams of CMP was not sufficient and, in many sections, there was discontinuity on the liner at the seams' locations. However, this issue was not observed on the 0.5 in., and 1.0 in. thick SAPL pipe samples, which implies the quarter inch thickness may not be sufficient or requires additional consideration on the seams' locations.



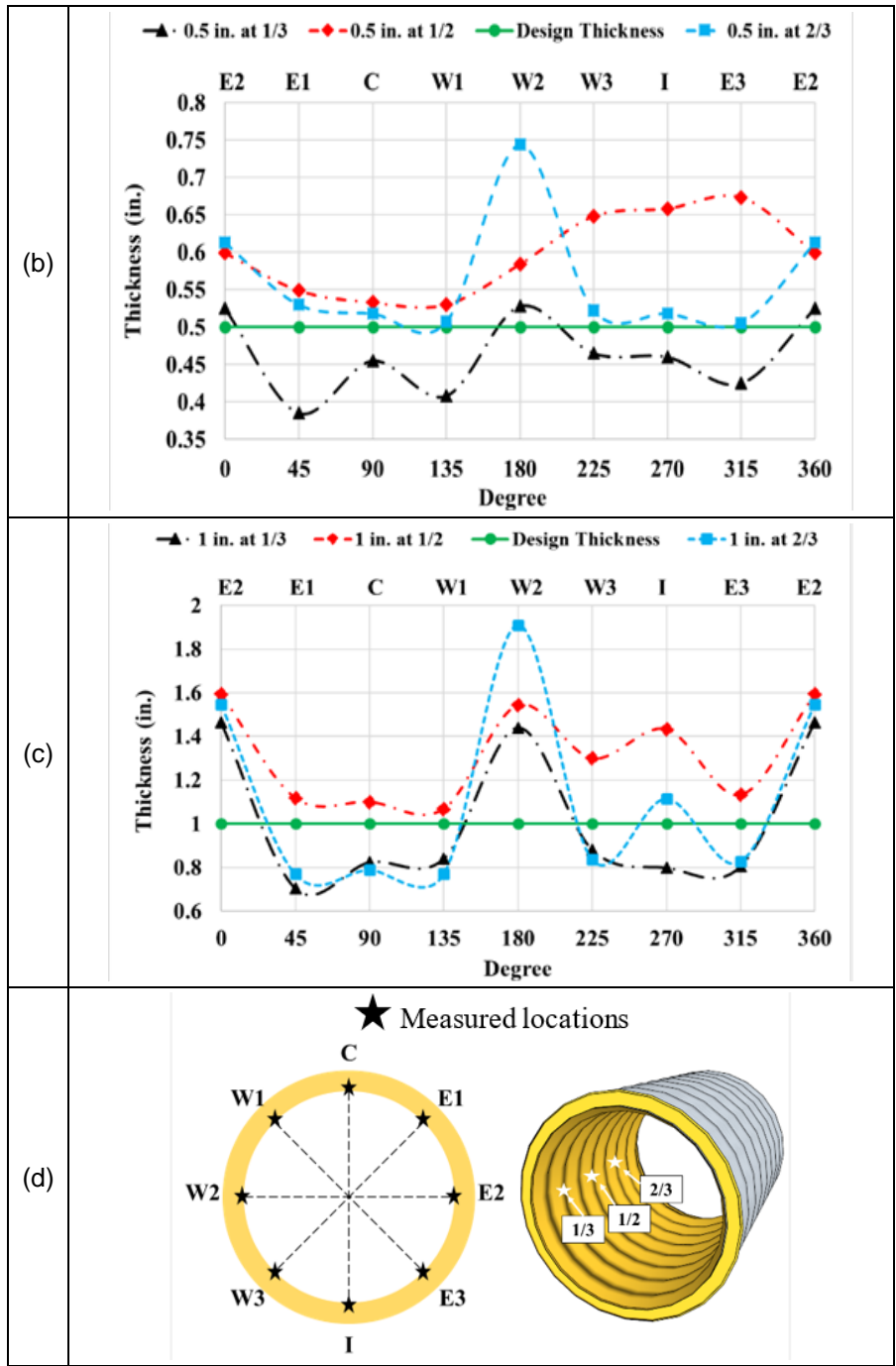


Figure 5-19 Thickness measurement results of polymeric SAPL renewed circular CMPs: (a) 0.25 in. thick SAPL, (b) 0.5 in. thick SAPL, (c) 1 in. thick SAPL, and (d) measured locations in circumferential and longitudinal direction.

### **5.2.3 Comparison of Bare and SAPL Renewed Circular CMPs Load Bearing Capacities**

#### ***(Responses to Static Load)***

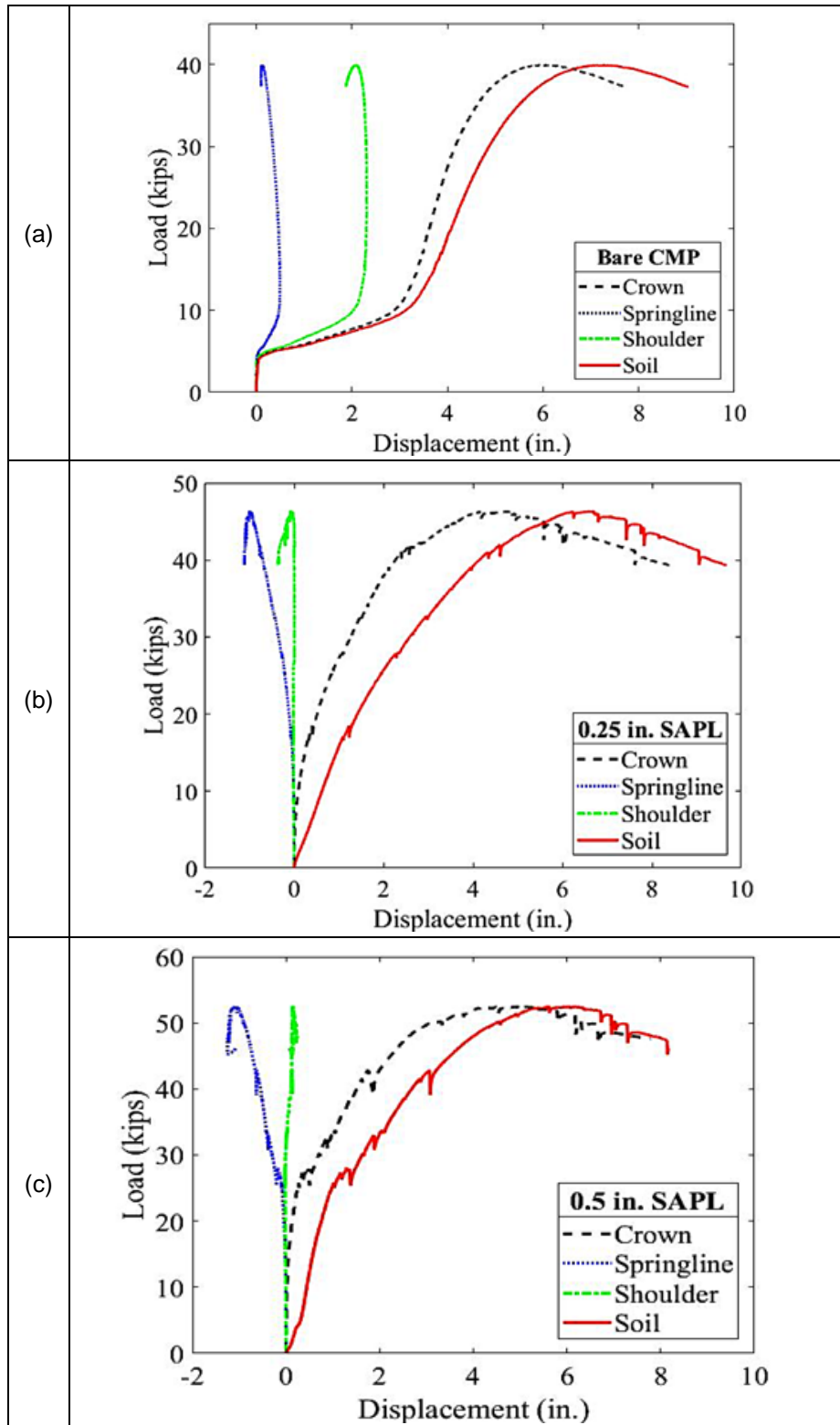
The static load was applied on the soil surface at the middle section of the CMPs through a 20×40 in. steel load pad. The load was continuously applied with a load rate of 0.03 in./min. Figure 5-20 illustrates the results of load-deflection of soil-CMP samples due to the applied load for the bare invert-cut CMP, and all three SAPL renewed circular CMPs. The invert-cut bare CMP, in the absence of the invert section and its ring stiffness, initially resisted the applied load on the soil surface until about 5 kips, which is believed to be due to the friction resistance force of the soil-pipe system. Once this limit was reached there was no other resisting force to prevent the pipe sample circumferential movement. Therefore with progression of the load, the CMP moved continuously until both sides of the invert-cut section contacted each other and as a result the CMP's ring stiffness was recovered. Afterward, the system showed a significantly stiffer response to the applied load and resisted until 39.9 kips of load. At this load, the corresponding soil surface settlement was with almost 7.22 in. and the crown's deflection was 5.8 in.

On the contrary, the SAPL renewed CMP samples were able to resist the applied load without any sign of cracking or fracture at the invert location, which is not protected or surrounded by the host pipe. This indicates that the polymeric SAPL was structurally capable to solely withstand the applied ring compression. In the 0.25 in. SAPL renewed CMP, the first structural crack was observed at the load of 39 kips with 2.12 in. of SAPL-CMP deflection at the crown. The CMP sample buckled at the crown, along with the SAPL crack that initiated and propagated in the longitudinal direction, as shown in Figure 5-21 (a). once the crack reached the interlocking seams of the CMP, it diverted towards the seams direction in the circumference of the CMP. This is due to the insufficient SAPL thickness at the seams location that cause SAPL discontinuity at these locations. The 0.25 in. renewed pipe sample failed at the load of 46.38 kips, as illustrated in Figure 5-20 (b).

The 0.5 in. SAPL renewed CMP showed a similar response to the applied surface load. The 0.5 in. SAPL cracked longitudinally at the crown when 42.78 kips of load was applied on the soil surface that induced 1.75 in. crown deflection. The SAPL-CMP system reached its ultimate load carrying capacity prior to the soil failure and eventually failed at the load of 52.43 kips. Although it was expected to observe larger

load carrying capacity enhancement from 0.25 in. SAPL to 0.5 in. SAPL, the ultimate load bearing capacity was improved by 13%. This can be due to the relatively small difference between the applied SAPL thicknesses on 0.25 and 0.5 in. SAPL renewed CMPs at the crown locations, as discussed in the SAPL thickness survey section. The 0.5 in. SAPL renewed CMP's response to the applied soil surface load is illustrated in Figure 5-20 (c). It is noteworthy that the initial drop in Figure 5-20 (c) between the loads 25 to 35 kips was due to the detachment of the over sprayed SAPL material between the CMP and the partition walls. Exercise were made to keep the renewed CMPs fully disconnected form the partition walls including installation of plastic sheets at the edges prior to the SAPL installation and make a thin notch after the installation. However a few points were remained connected at the shoulder area as it was highly concerned that a deep cut would tear the Styrofoam placed the CMP-partition wall area, which would cause soil ingress to the pipes. Therefore, it was decided to only have the notches instead of a full cut at those locations.

The 1 in. SAPL renewed CMP showed relatively stiffer response compared with the other renewed CMP samples. The 1 in. SAPL cracked longitudinally at the crown with the load of 66.26 kips and the 2.12 in. of pipe deflection that released relatively larger amount of energy. The energy release is also evident in Figure 5-20 (d), where a large drop in the load displacement graph at the time of the first crack initiation was registered by LVDT sensor. This phenomenon can be related to the lower diameter over thickness ratio of the SAPL-CMP system that provides higher stiffness to the system. On the contrary, the higher diameter to thickness ratio of the lower SAPL thickness (i.e., 0.25 and 0.5 in.) resulted in more flexible behavior of the SAPL-CMP system. The higher stiffness of the 1 in. SAPL resulted in an instantaneous crack throughout the crown, while in the quarter and half an inch SAPL samples a small crack initiated at the center of the pipe at the crown and propagated with the increase of the load, as shown in the Figure 5-21. The 1 in. SAPL renewed CMP eventually failed at the load 72.15 kips, which was about 20 kips higher than the 0.5 in. SAPL renewed sample. The circular CMPs' load bearing capacity, crown deflection at initial crack and failure as well as the soil displacement in both initial crack and failure stages are summarized in Table 5-2.



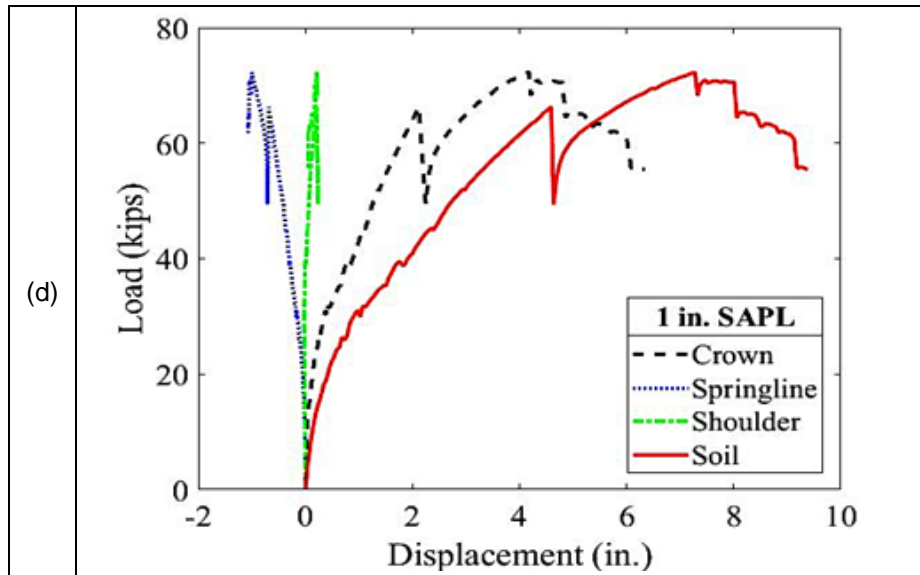
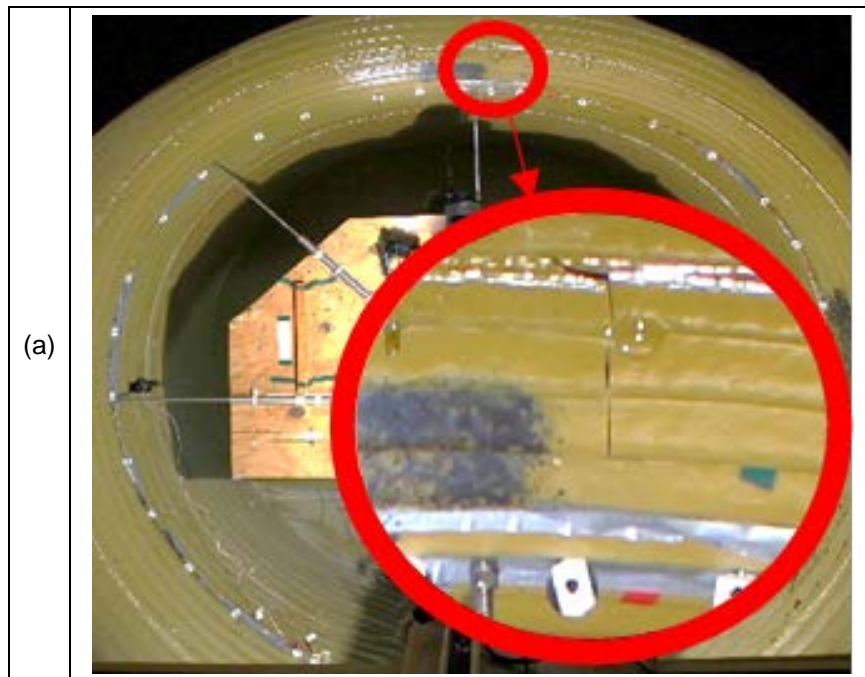


Figure 5-20 Load vs. displacement results for CMP samples and soil: (a) bare invert cut CMP, (b) 0.25 in. SAPL renewed CMP, (c) 0.5 in. SAPL renewed CMP, and (d) 1 in. SAPL renewed CMP.



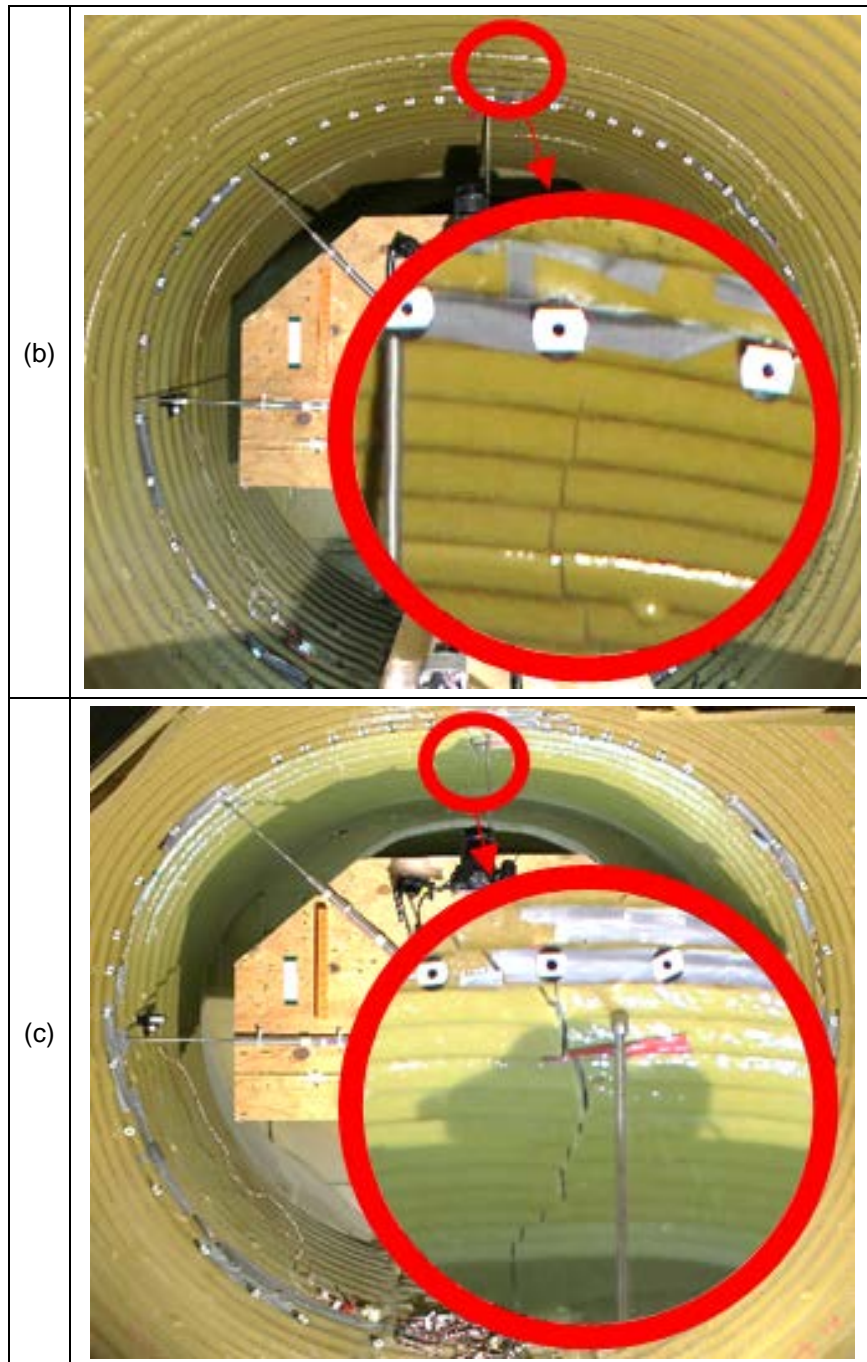


Figure 5-21 Formation of the first structural crack. It shows (a) 0.25 in. SAPL renewed circular CMP at 39 kips, (b) 0.5 in. SAPL renewed circular CMP at 42.78 kips, and (c) 1 in. SAPL renewed circular CMP at 66.26 kips.



The circular CMPs' load bearing capacity, crown deflection at initial crack and failure as well as the soil displacement in both initial crack and failure stages are summarized in Table 5-2.

Table 5-2 The circular CMPs' load bearing capacity, crown deflection and the soil displacement at initial crack and failure.

Test Setup		Initial Structural Cracking Stage			Failure Stage		
		Load (kips)	Pipe Deflection at Crown (in.)	Soil Displacement (in.)	Load kips	Pipe Deflection at Crown (in.)	Soil Displacement (in.)
<b>Bare Invert-cut CMP</b>		-	-	-	39.9	5.8	7.22
<b>SAPL Renewed CMP</b>	0.25 in. SAPL	39	2.12	3.95	46.38	4.83	6.69
	0.5 in. SAPL	42.78	1.75	3.06	52.43	4.43	5.61
	1 in. SAPL	66.26	2.12	4.58	72.15	4.17	7.27

Comparison between the ultimate loads of the SAPL renewed circular CMPs and the bare CMP showed that the application of SAPL increases the ultimate load bearing capacity of the invert corroded CMP. The improvement rate for the quarter, half, and one-inch thick SAPL is 16.24, 34.4, and 80.82% respectively, which is illustrated in Figure 5-22 (a). Considering the pipe deflection at the time of the first crack in Figure 5-20 shows all SAPL renewed pipes were cracked at about 2 in. of pipe deflection, which is 3% of pipe diameter. The bare CMP's load response at 2 in. deflection was 7.34 kips. Figure 5-22(b) illustrates that the application of 0.25 in., 0.5 in., and 1 in. polymeric SAPL increased the load carrying capacity at this pipe deflection for 471.7, 482.8, and 802.7% respectively.

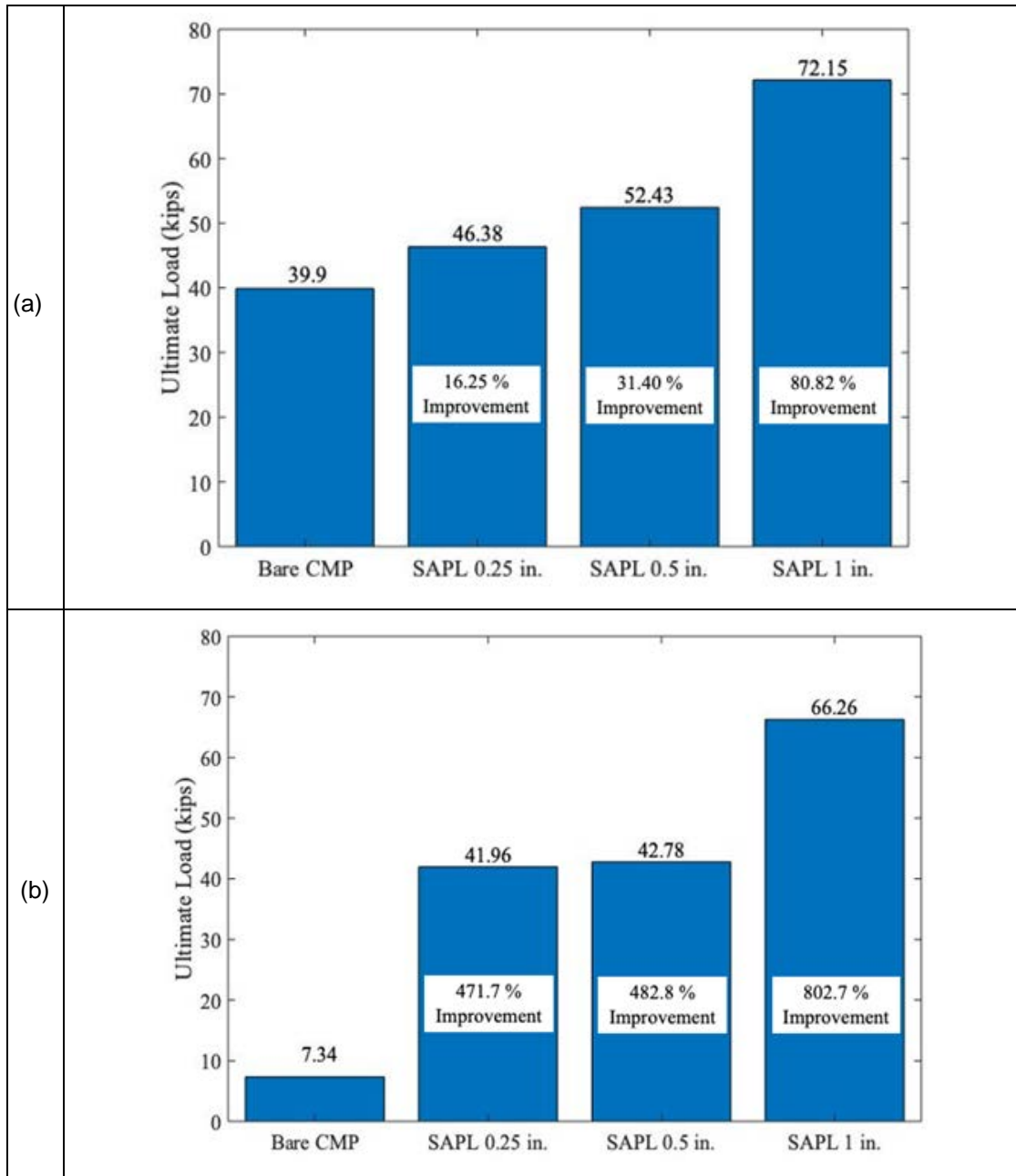


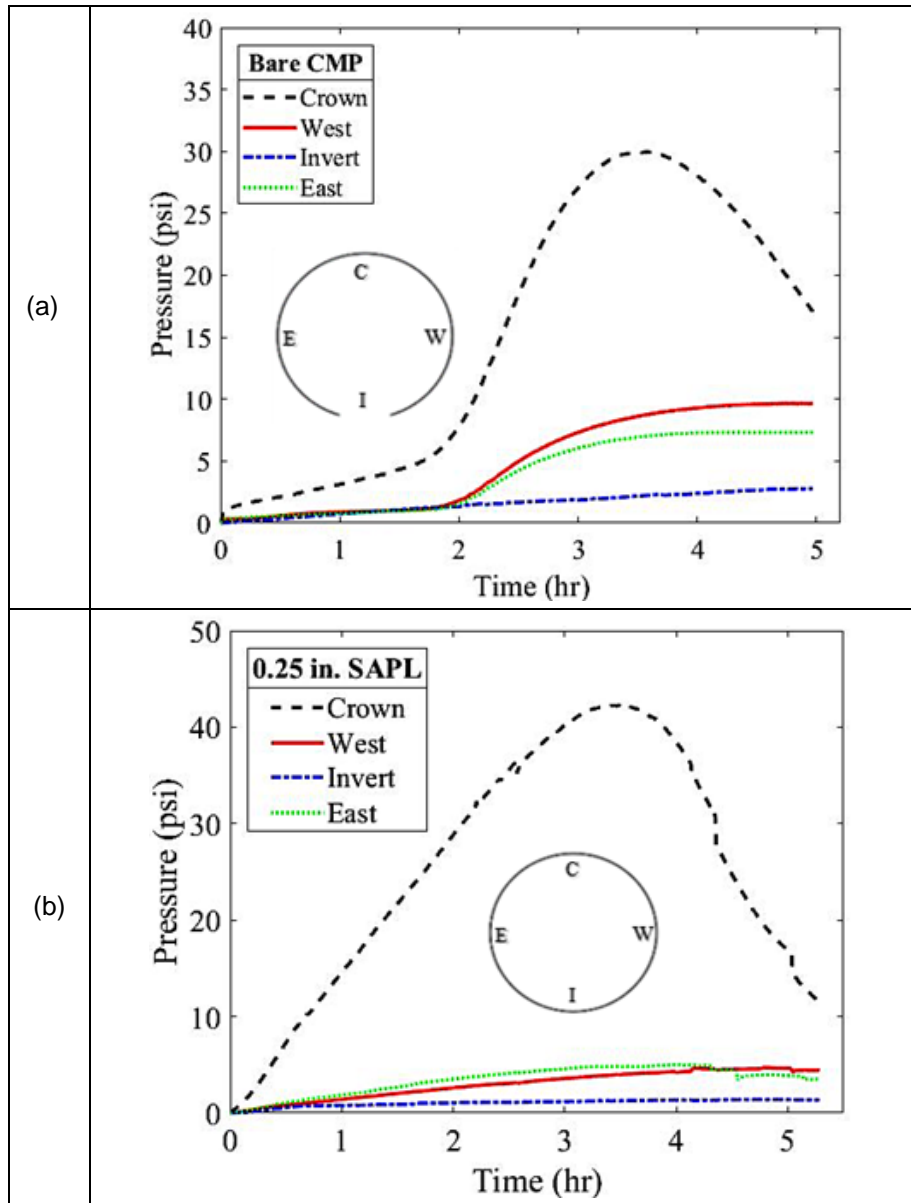
Figure 5-22 Load improvement by SAPL application: (a) ultimate load comparison of renewed SAPL circular CMPs with bare CMP, and (b) load comparison of renewed SAPL CMPs with bare CMP at 2 in. pipe deflection.

#### 5.2.4 Pressure around the circular CMPs (Earth Pressure Cell Results)

During the tests, the earth pressure cells recorded the applied pressure around the CMP samples. Figure 5-23 illustrates the applied pressure all around the pipes. The maximum pressure registered by the earth pressure cell on top (i.e., crown) of the bare CMP was 30 psi. The maximum pressure value for the 0.25 in., 0.5 in., and 1 in. SAPL renewed CMPs were 42, 42.11 and 71.61 psi, respectively. Similar to the load-deflection graphs, illustrated in Figure 5-29, there is no substantial pressure difference between the crown pressures of 0.25 in. and 0.5 in. SAPL renewed CMP samples. This could be due to the minimal thickness difference of both SAPL samples at the crown locations. However, the applied thickness at the both sides of the springline (i.e. East and West) in the 0.5 in. SAPL renewed samples was almost two times greater than the 0.25 in. SAPL renewed sample that could be the reason for the pressure difference between two CMPs. The 0.25 in. SAPL renewed CMP experienced 4.6 psi at the west location and 4.93 psi at the East location. While the applied pressures on the East and West locations of the 0.5 in. SAPL renewed CMP were 6.19 psi and 8.86 psi, respectively, which were relatively higher than the 0.25 in. sample. The pressure values for the East and West sides of the 1 in. SAPL renewed CMPs were 13.93 psi and 8.407 psi, respectively. The results of the earth pressure sensors at the crown of the CMPs implied that the pressure response of the soil-CMP system was directly affected by thickness of the applied SAPL. The soil pressure around the CMPs are recorded by the earth pressure cells and are summarized in Table 5-3.

Table 5-3 Soil pressure results around the circular CMPs at the time of failure.

Test Setup		Pressure (psi)			
		Crown	Invert	East	West
Bare CMP		30	2.78	7.33	9.66
SAPL Renewed CMP	0.25 in. SAPL	42	1.34	4.93	4.6
	0.5 in. SAPL	42.11	5.06	6.19	8.86
	1.0 in. SAPL	71.61	1.72	13.93	8.407



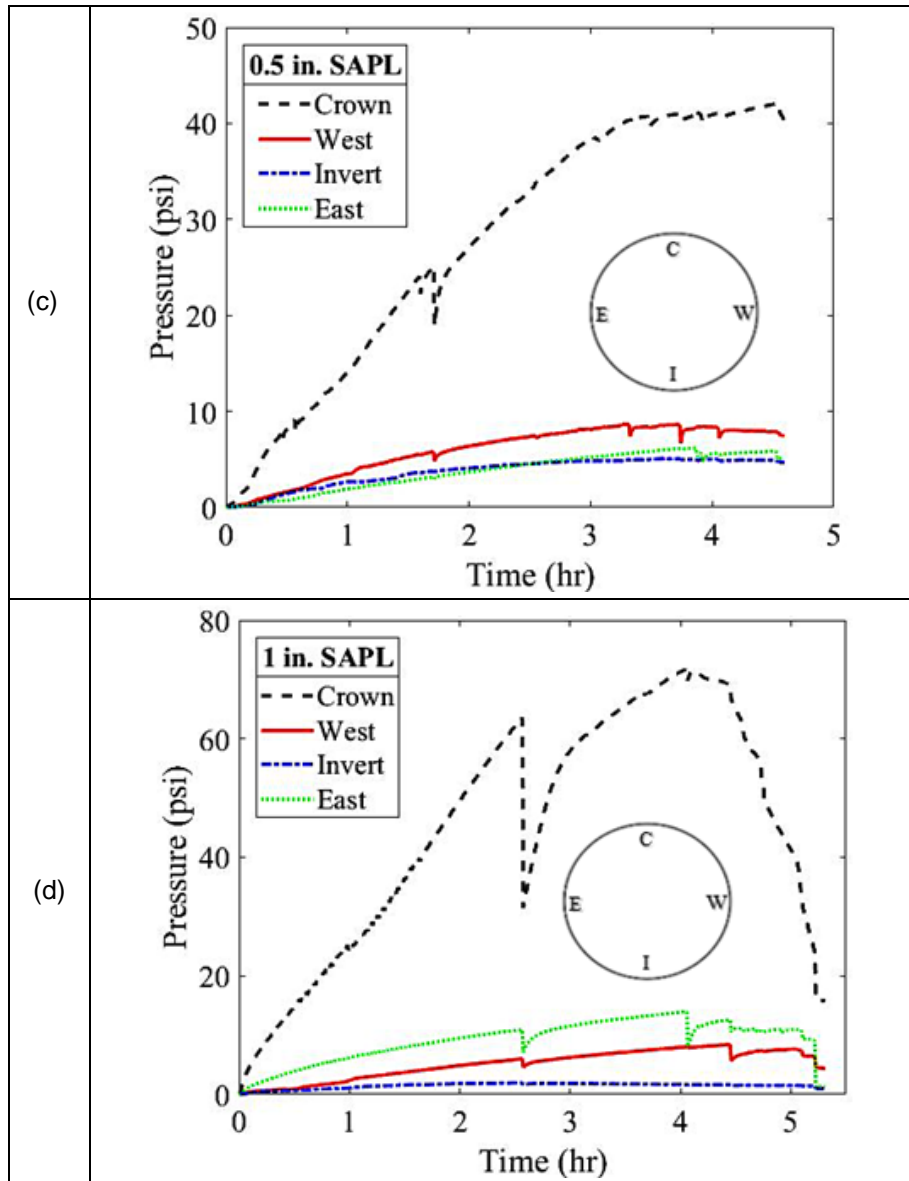
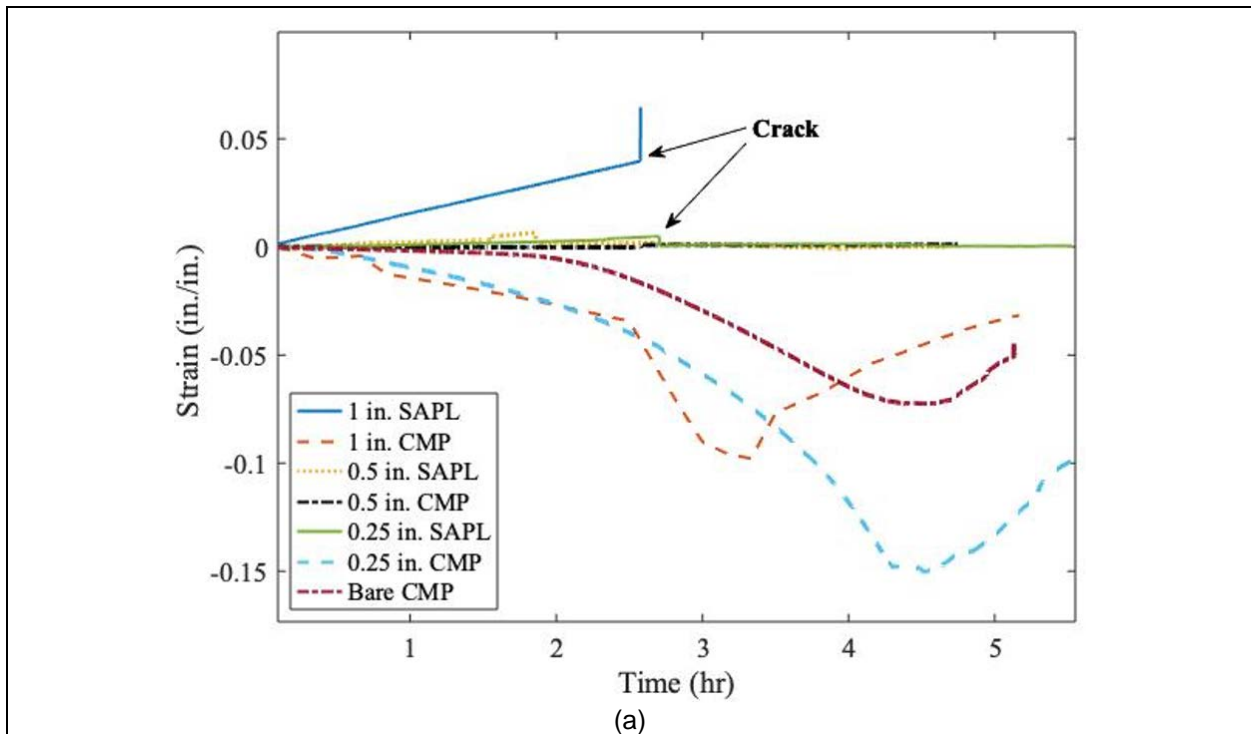


Figure 5-23 Earth pressure cells' results: (a) bare circular CMP, (b) 0.25 in. SAPL renewed circular CMP (c) 0.5 in. SAPL renewed circular CMP, and (d) 1 in. SAPL renewed circular CMP.

### 5.2.5 Strain Gauges Results for SAPL Renewed Circular CMPs

The strain values of the crown for circular CMPs and liners are illustrated in Figure 5-24 (a). The maximum strain was registered by the host pipe of the 0.25 in. SAPL sample at the time of failure. The 1 in. SAPL renewed CMP registered relatively lower strain value compared with the 0.25 in. SAPL renewed

CMP sample. However, the 1 in. SAPL sample registered the largest strain at the time of the first structural crack at the crown location. Figure 5-24 (b) illustrates the results of the SAPL strain values at time of first structural crack for other locations, such as shoulders, springline, haunches, and invert. The maximum strain occurred at the crown which is located directly under the load area. Also, it can be observed that the thicker SAPL resulted in higher strain value at the time of cracking. It should be noted that due to the aggressive environment of the soil box and existence of high moisture content, some strain gauges outside of host pipe, including the crown of 0.5 in. SAPL, were either damaged or not responsive.



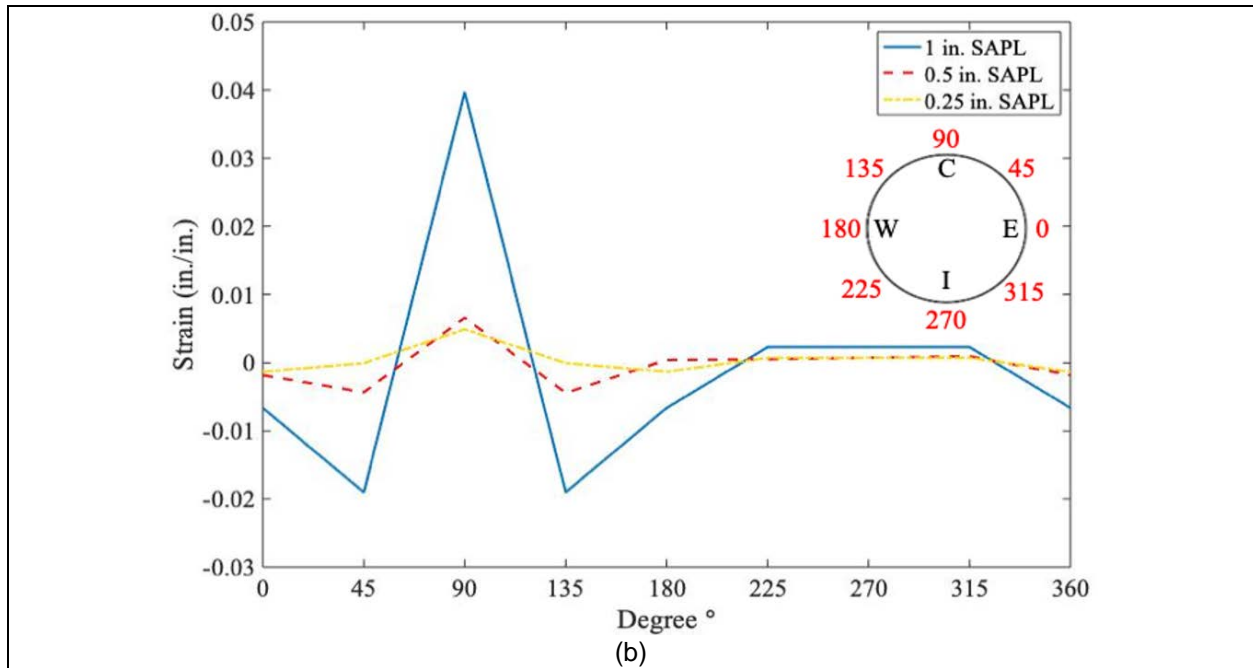


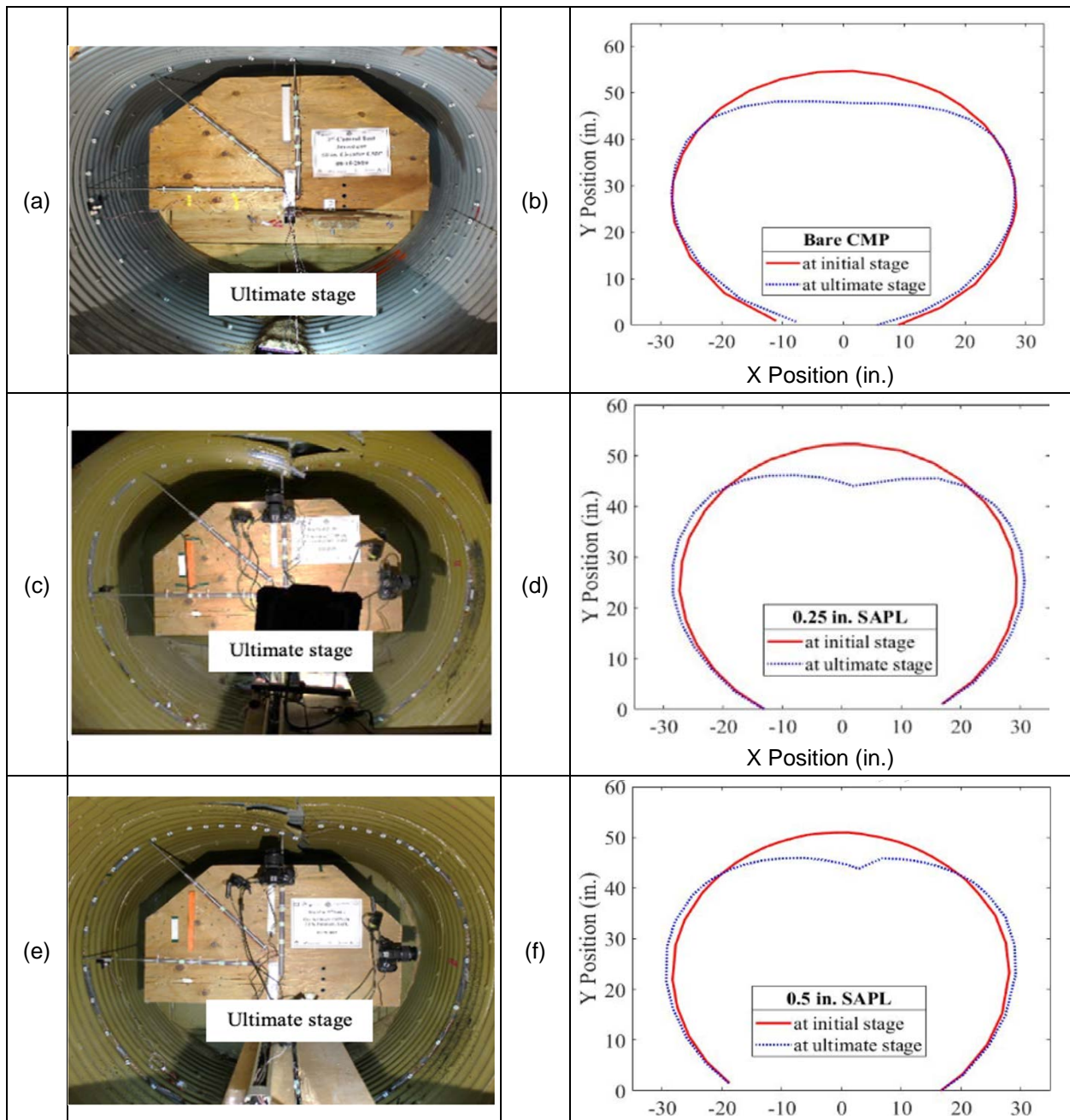
Figure 5-24 Strain gauge results for SAPL renewed circular CMP: (a) at the crown and (b) around the SAPL at the time of first structural crack.

### 5.2.6 Pipe Profile Measurement using DIC for SAPL Renewed Circular CMPs

The middle ring profile renewed pipe profile was measured during the test using digital image correlation (DIC) technique. Figure 5-25 illustrates the results of pipe deflection measurement before and after the loading. The comparison of crown deflection measurement DIC technique with mechanical sensors (i.e., LVDT & CDS) revealed that the both measuring methods have an excellent conformity (Darabnoush Tehrani et al. 2020b).

Pipe profiling showed that the bare CMP had movement in both horizontal and vertical directions during the loading. The bare CMP sample failed due to the buckling at the crown, which is evident in the invert of the plotted CMP profile in the Figure 5-25 (b). Application of SAPL sustained the pipe's ring stiffness and as the result, no movement in the invert of all three SAPL renewed samples was observed. In addition to that, the SAPL renewed samples had horizontal expansion at the springline and shoulder areas as well as vertical deflection. In addition, the fracture at the crown is evident in Figure 5-25 (d), (f), and (h). The

DIC results implied that for all CMP samples, the mode of failure was local buckling of the crown section, where in case of bare CMP the buckling caused CMP deformation and in case of SAPL samples it caused cracking and fracture of the crown. It is noteworthy that due to the existence of the instrumentation frame's beam and wires, illustration of the full pipe's ring was not possible. Figure 5-26 illustrates pipe profiling of SAPL renewed circular CMPs at the time of failure.





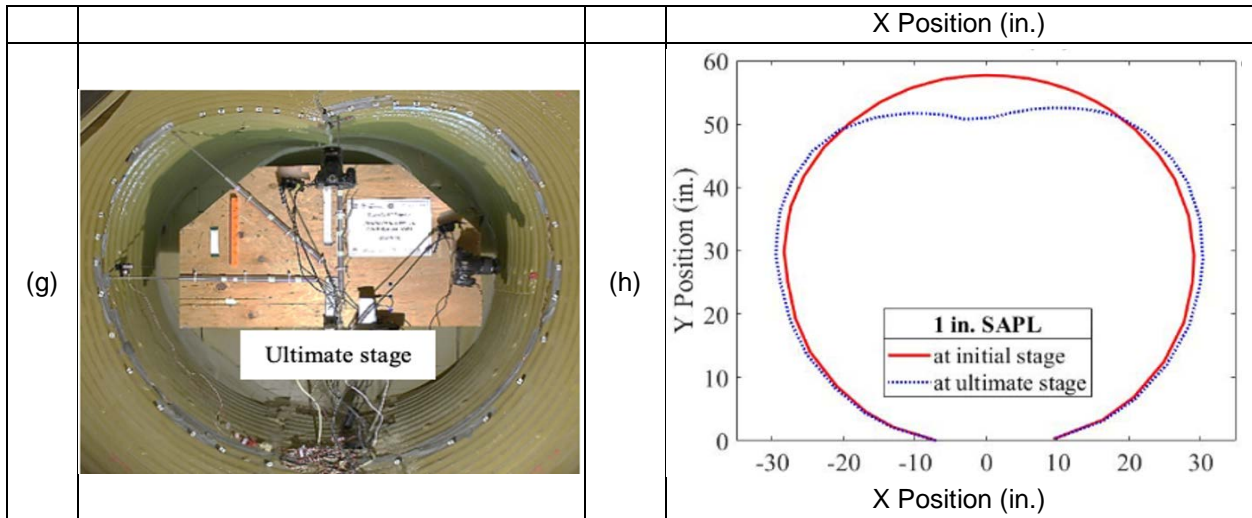
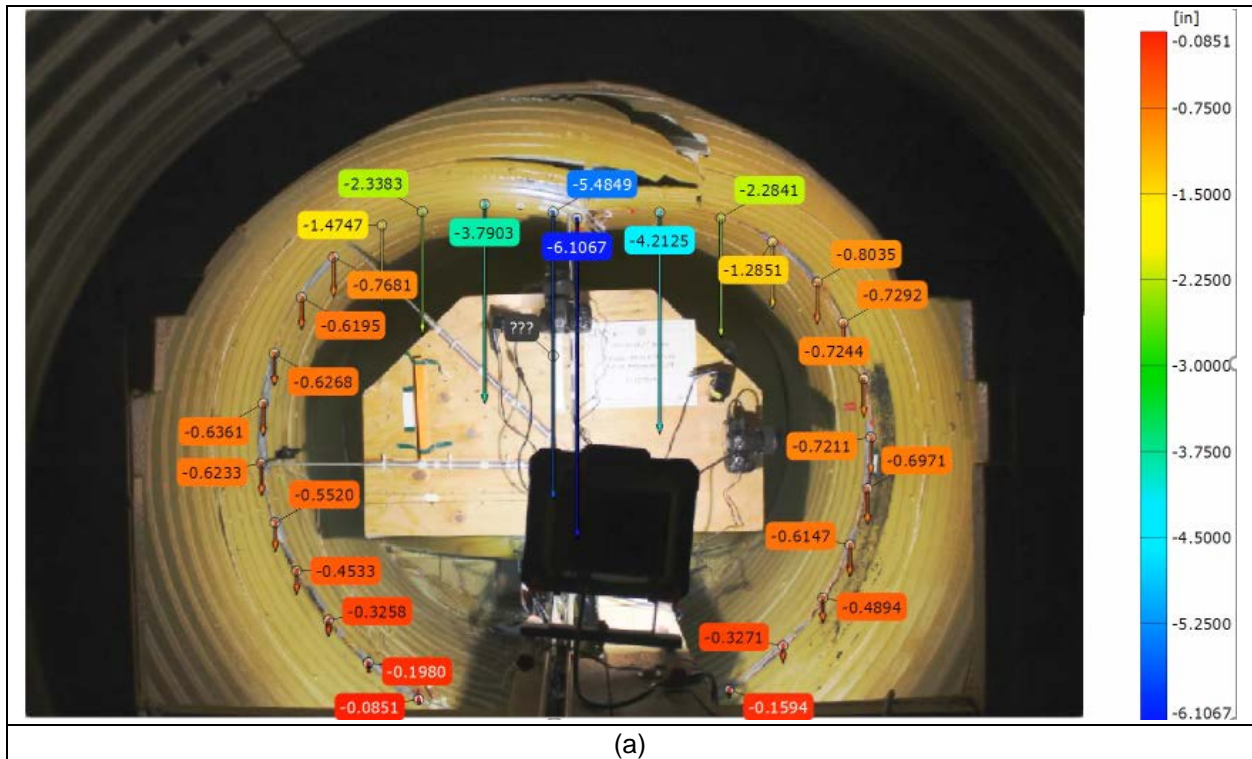
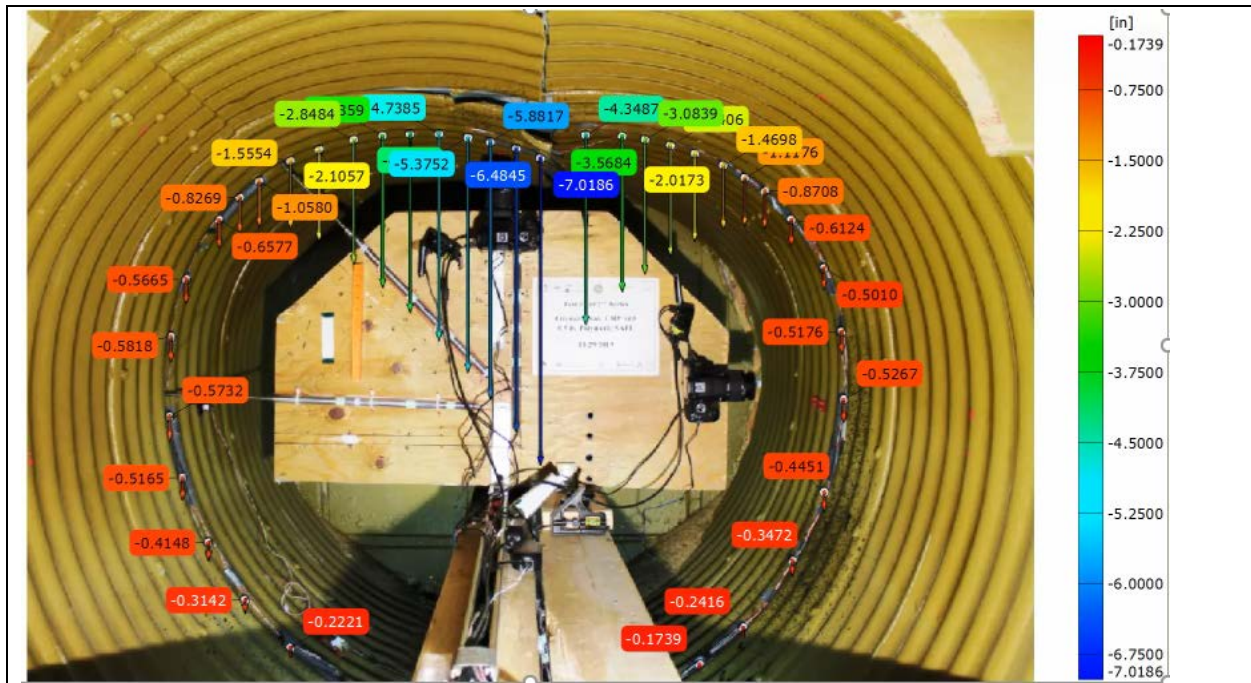
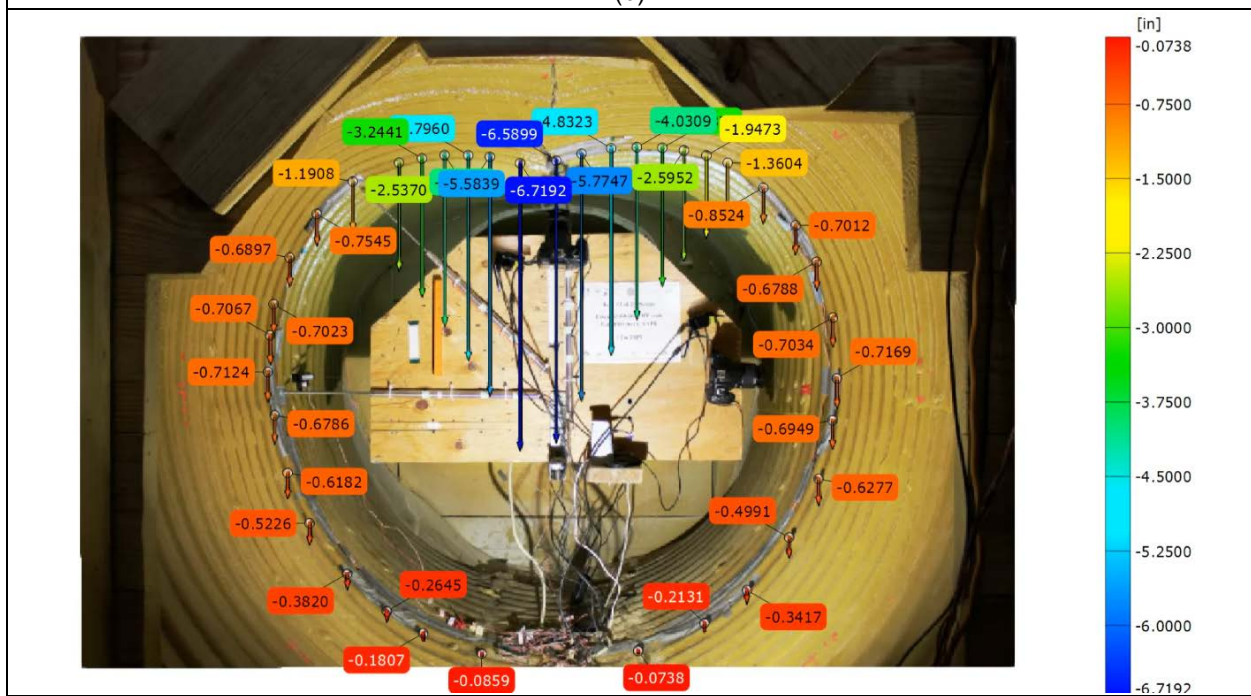


Figure 5-25 DIC results of SAPL renewed circular CMP: (a) and (b) bare CMP, (c) and (d) 0.25 in. SAPL renewed CMP, (e) and (f) 0.5 in. SAPL renewed CMP, (g) and (h) 1 in. SAPL renewed CMP.





(b)



(c)

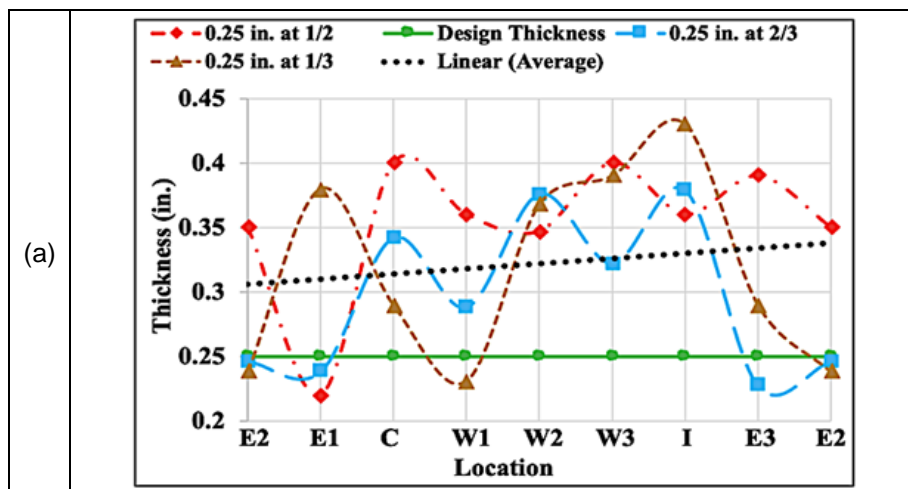
Figure 5-26 Pipe profiling using DIC technique at the time of failure: (a) 0.25 in. SAPL, (b) 0.5 in. SAPL, and (c) 1.0 in. SAPL renewed circular CMP.

### 5.3 Soil Box Testing – SAPL Renewed Arch CMPs

#### 5.3.1 SAPL Thickness Survey Installed Inside Arch CMPs

Figure 5-27. Illustrates the results of the SAPL thickness measurement that was conducted by an ultrasonic gauge at three locations of approximately 1/3, 1/2, and 2/3 of the pipe sample's length, and eight location on the pipe circumference. It was observed that in almost all locations, the applied thickness was higher than the design thickness could be due to the factor of safety, considered in the required SAPL quantity calculation presented in section 4.2. For the quarter inch SAPL renewed arch CMP the average thickness was approximately 0.33 in., where the liner thickness was higher on the invert section. The average thicknesses for half and one inch SAPL renewed arch CMP samples were 0.66 and 1.2 in., respectively.

A digital caliper was used to conduct a manual thickness measurement after the structural testing was and carried out. The results showed an excellent agreement between both manual and ultrasonic measurement methods. The visual observations on quarter inch SAPL renewed arch CMP showed the applied SAPL thickness on the seams locations were not sufficient and discontinuities were observed on the liner. For the half and one inch thick SAPL pipe samples, this issue was completely resolved that implies the 0.25 in. thickness requires additional consideration on the seams' locations.



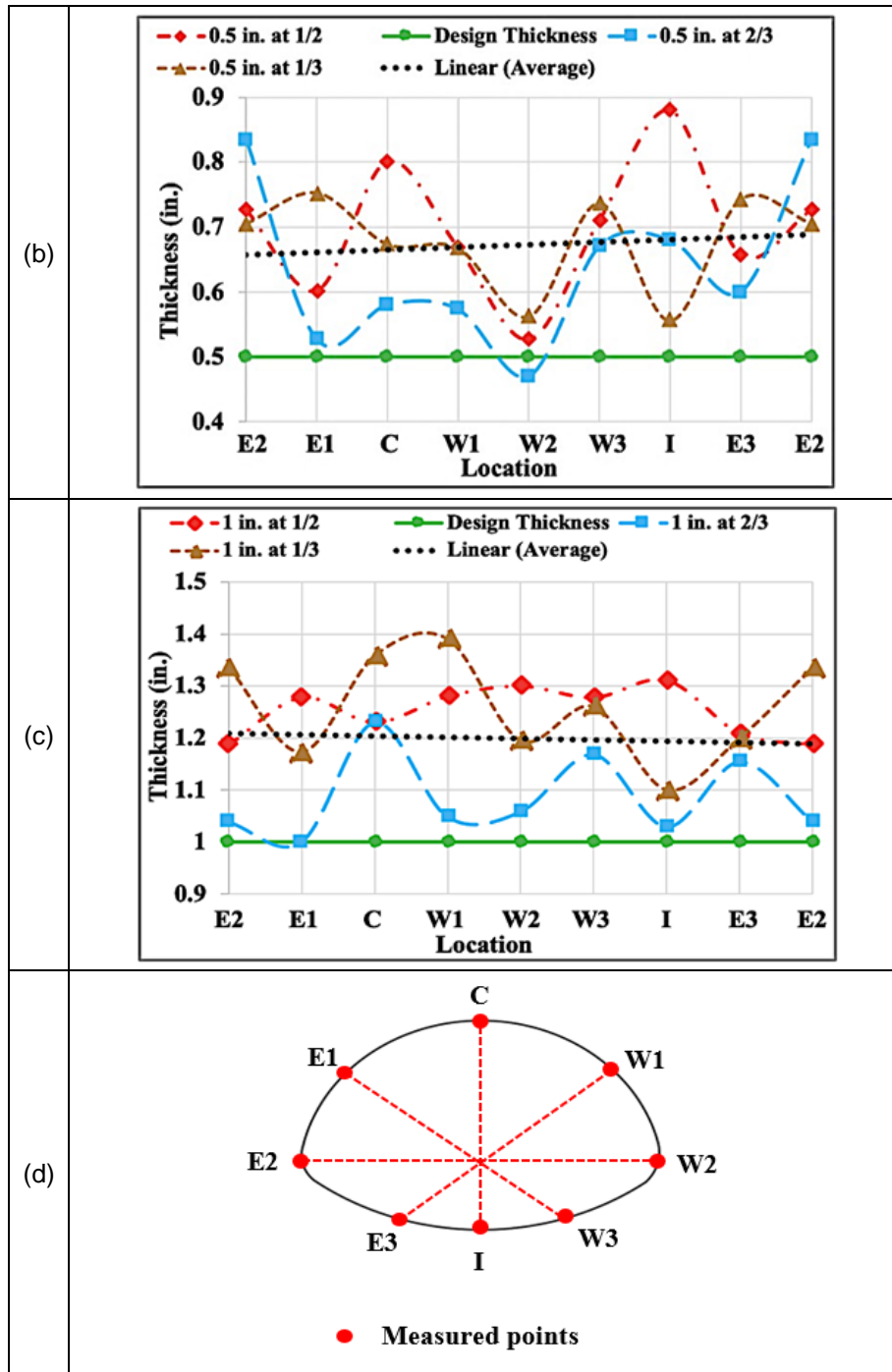


Figure 5-27 Thickness measurement results of polymeric SAPL renewed CMPAs: (a) quarter, (b) half, (c) one inch SAPL renewed arch CMPs, and (d) measured locations in circumferential direction.

### 5.3.2 Arch CMP Invert Detachment Response

For the SAPL renewed arch CMPs, the main parts of the inverts (i.e., the invert-cut and angle sections excluding the end-strips) were detached prior to the SAPL installation. The remaining two end-strips were kept bolted to maintain the pipes geometry at the time of SAPL installation. Once the SAPL was sprayed and cured, the end-strips were detached, as illustrated in Figure 5-28. This procedure was earlier discussed in the stage 4 of Figure 4-7. At this stage, no sign of CMP movement, SAPL crack or damage was observed.

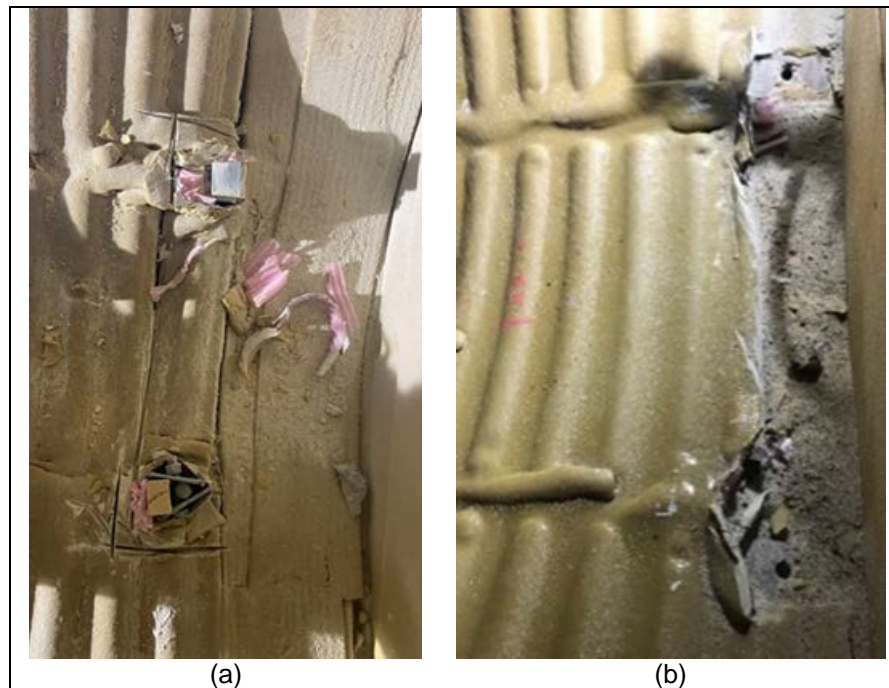


Figure 5-28 Invert-cut arch CMP end-strip detachment to remove the host pipe's ring stiffness: (a) over-sprayed SAPL and cutting process on the end-strip location, and (b) unbolted end-strip.

### 5.3.3 Comparison of Bare and SAPL Renewed Arch CMPs Load Bearing Capacities (Responses to Static Load)

The soil-CMP system was loaded through a 20×40 in. steel load pad. The continues static load was applied on the middle ring of the CMPs on the soil surface using a load rate of 0.03 in./min. Figure 4-29 illustrates the CMP deflection in both horizontal and vertical directions due to the applied load for the bare

invert-cut arch CMP, and all three SAPL renewed arch CMPs. In the absence of the invert section and ring stiffness, the bare invert-cut arch CMP showed a stiff response to the applied load which could be due to the arch CMP's low slope at the shoulder and large flat area at the invert section. The bare arch CMP softening initiated from 12.5 kips and ultimately the soil-CMP system failed at 26.97 kips with about a 4 in. of CMP's crown deflection.

The quarter inch SAPL renewed arch CMP sample showed a stiff response to the applied load initially and showed softening behavior starting at 15 kips of load. The first crack formed in longitudinal direction at the load at the load of 29.32 kips at the crown with a 2.1 in. of crown displacement. The crack was further propagated with the load progression until it reached to the seams of the CMP, where the SAPL's thickness was not covered the seams and as a result, the crack was diverted in circumferential direction. The formation of the first crack is illustrated in Figure 5-30 (a). The renewed arch CMP ultimately failed at 33.2 kips of load with 4.75 in. of crown deflection.

The one inch SAPL renewed arch CMP showed relatively stiffer response compared with the quarter and half an inch renewed CMP samples. The first crack formed on the crown of the SAPL at 41.08 kips of load with 0.33 in. of pipe vertical deflection and released relatively larger amount of energy than the quarter inch SAPL renewed arch CMP. This is evident in Figure 5-29 (d), where a large drop in the load displacement graph at the time of the first crack initiation was registered by the crown's LVDT. This can be related to the more stiffness of thicker SAPL due to its lower diameter over thickness ratio. As illustrated in Figure 5-30 (c), the one inch SAPL renewed arch CMP cracked instantaneously throughout the length of the pipe at the crown. The pipe ultimately failed at 53.66 kips of static load with a 5.2 in. of crown deflection.

The half inch SAPL renewed arch CMP had relatively lower structural capacity than expected and cracked at 26.27 kips of load with a 0.838 in. of pipe's crown deflection. This could be due to the reason that the renewed arch CMP at this thickness is neither a fully flexible pipe like the quarter inch SAPL renewed CMP sample, nor a fully rigid pipe like the one inch SAPL renewed arch CMP.

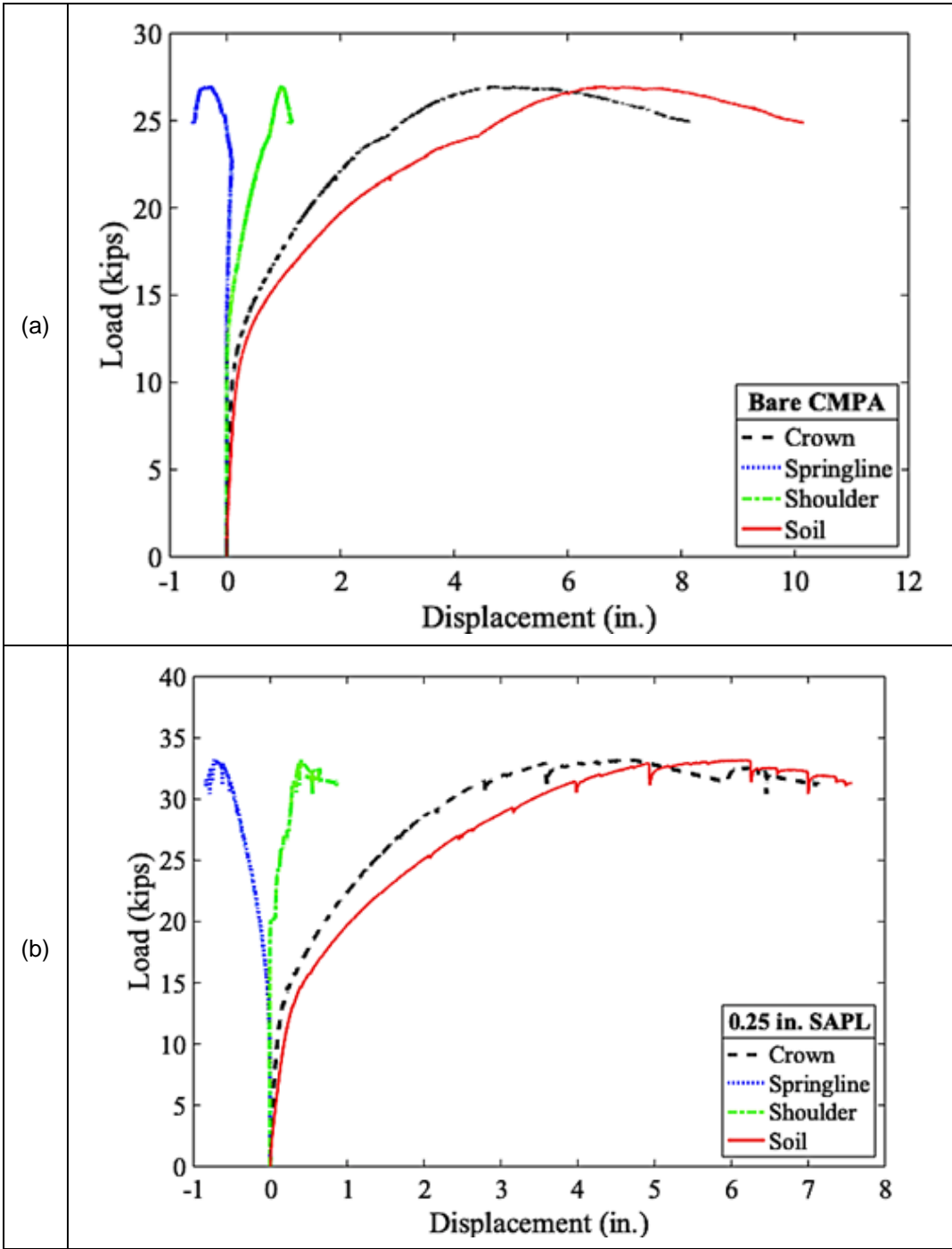
In the case of the half inch SAPL renewed arch CMP, the pipe had a 1.26 in. less crown deflection than the quarter inch SAPL renewed arch CMP and a 0.5 in. more crown deflection than the one inch SAPL renewed arch CMP at the time of first structural crack. This comparison implies that the half inch SAPL

renewed CMP might fall in the transition zone between a flexible pipe to a rigid pipe behavior, where the renewed arch CMP did not received stiffness from the passive pressure activation nor the SAPL wall stiffness.

The other possible reason for the relative low cracking load of the half inch SAPL renewed arch CMP could be due to the unrepaired circumferential crack's effect on the structural bearing capacity of the renewed arch CMP, as discussed earlier in section 4.2.2. However, the likelihood of a structural capacity lose due to the a circumferential crack located at the end of a pipe is low.

The structural crack (i.e., due to loading) of the half inch SAPL renewed arch CMP occurred throughout the crown instantaneously, as shown in Figure 5-30 (b), similar to the both 1 in. SAPL renewed circular and arch CMP samples. The renewed half inch SAPL- arch CMP failed eventually at the load of 35.62 kips with a 5.07 in. of crown's deflection.

At the end of the tests, many hairline cracks were observed in circumferential, longitudinal, and 45° directions (similar to shear crack) at both shoulder areas. All of these cracks were formed after the first crack initiation at the crown that could be due the formation of three-point bending failure mechanism. In addition, no crack was observed at the invert-cut area, where the invert of host pipe was cut entirely. This can imply that the SAPL was a fully structural liner. It should be mentioned that during the load application no sign of crack was observed in the patched (repaired) area, which demonstrates the repair worked perfectly.





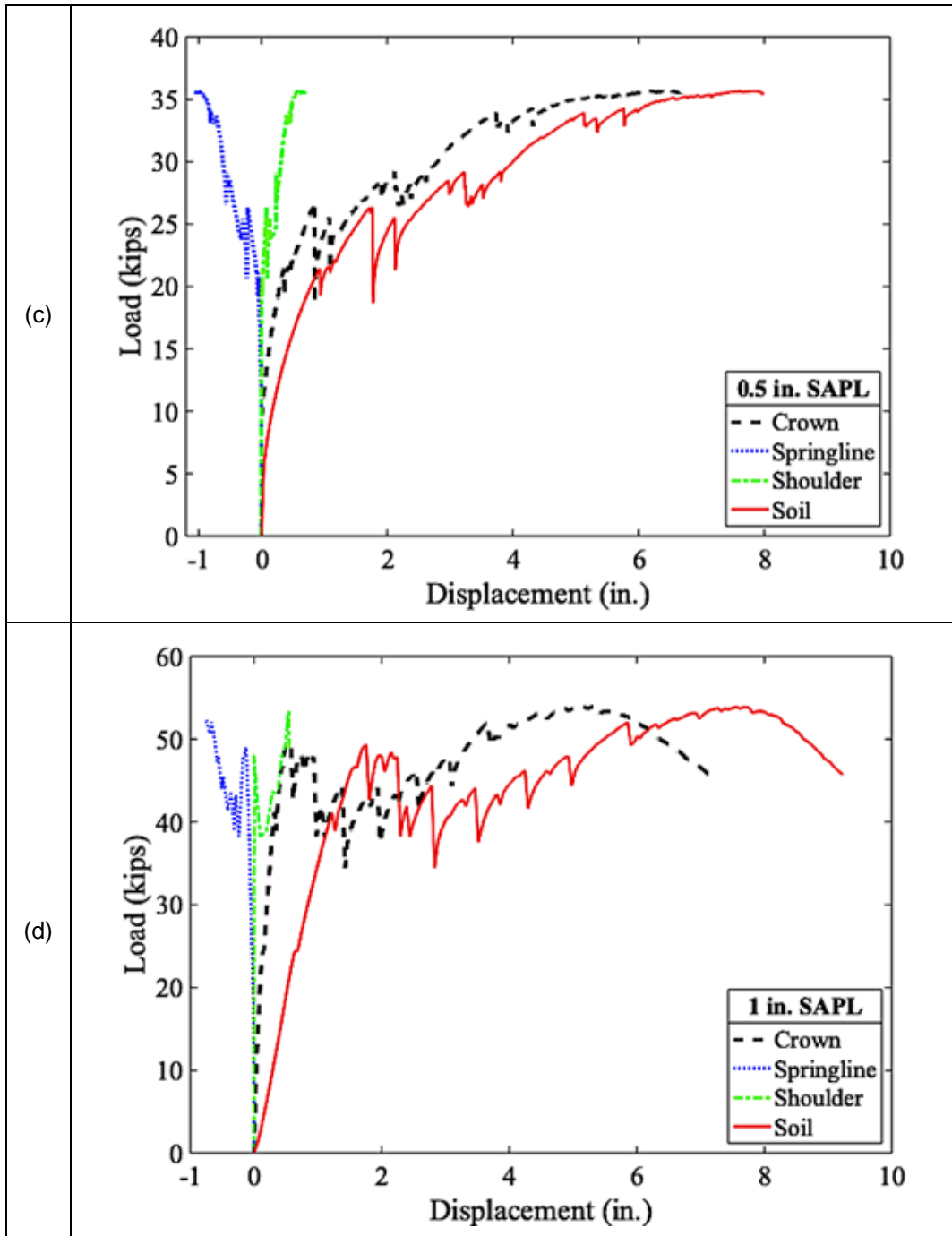
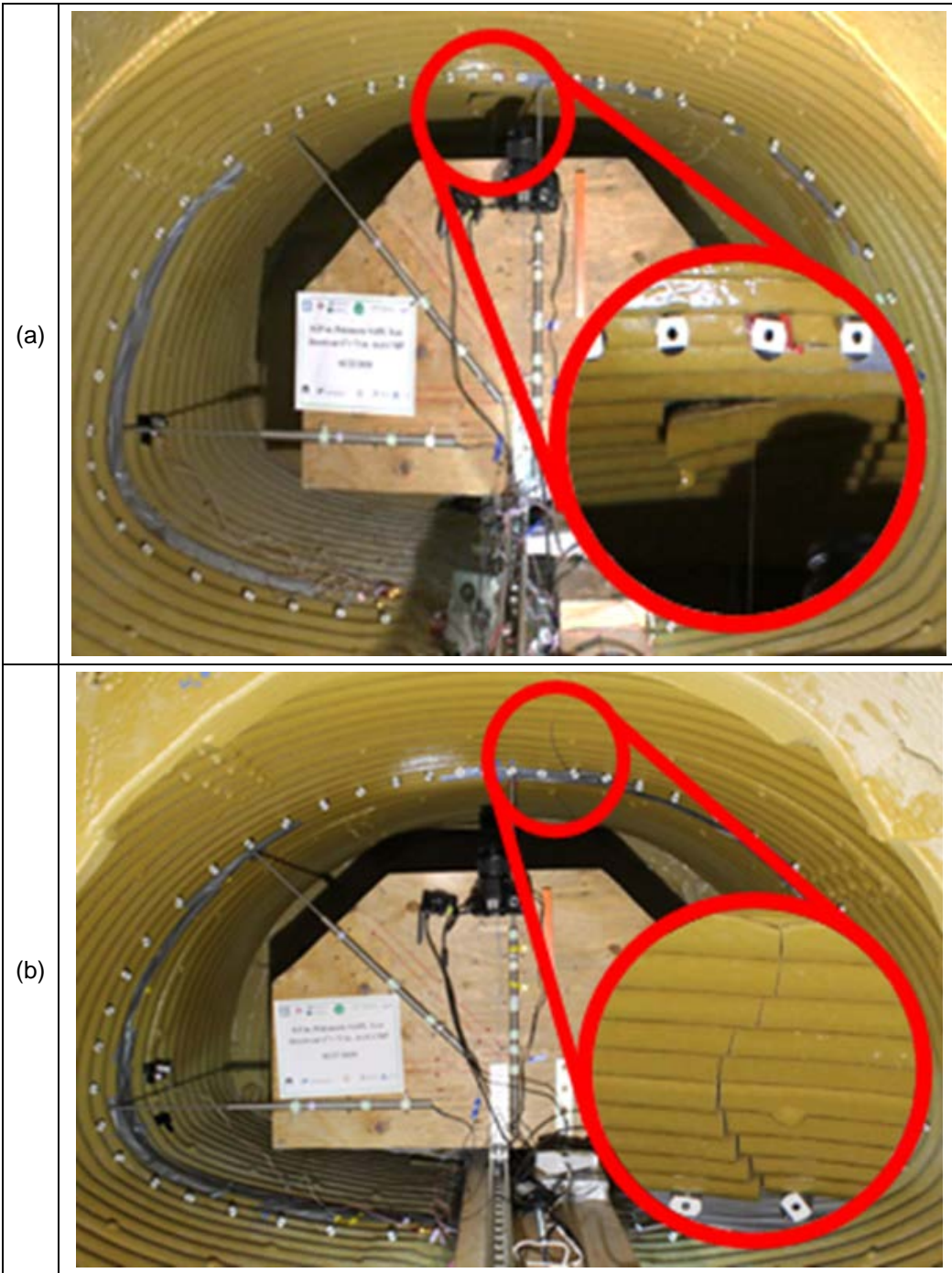


Figure 5-29 Bare and SAL renewed arch CMPs Load-Displacement graphs: (a) invert-cut bare arch CMP, (b) 0.25 in. SAPL renewed arch CMP, (c) 0.5 in. SAPL renewed arch CMP, and (d) 1 in. SAPL renewed arch CMP.



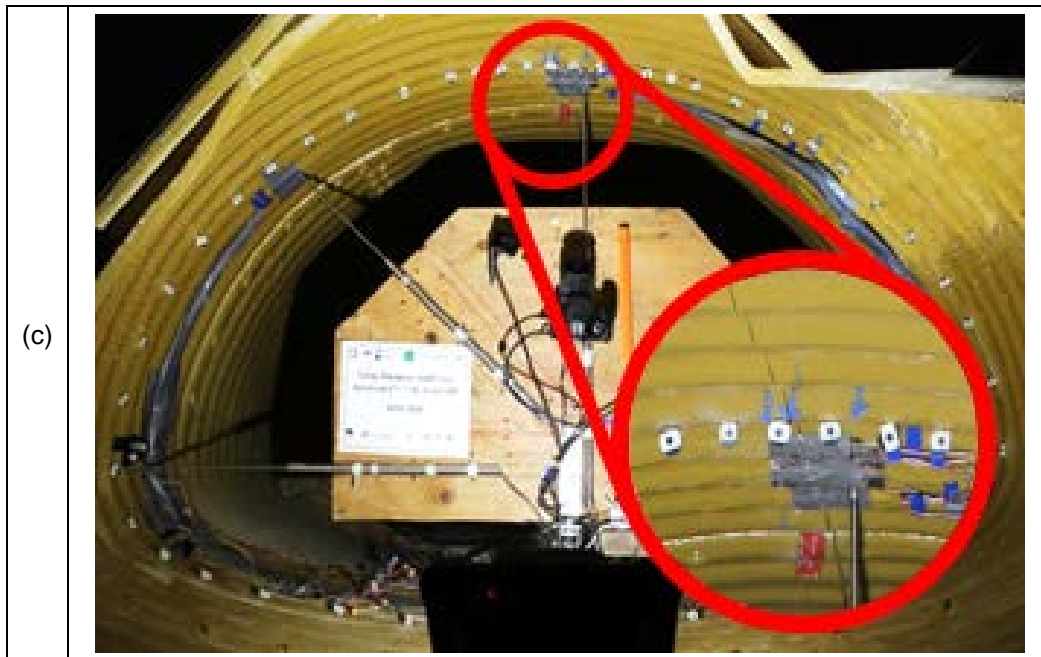


Figure 5-30 Formation of the first structural crack: (a) 0.25 in. SAPL renewed arch CMP at 29.32 kips, (b) 0.5 in. SAPL renewed arch CMP at 26.27 kips, and (c) 1 in. SAPL renewed arch CMP at 41.08 kips.

Figure 5-31 illustrates the ultimate load comparison between the bare arch CMP (i.e., control test) and all three SAPL renewed arch CMPs. It was observed that the application of polymeric SAPL increased the ultimate load bearing capacity of the invert corroded arch CMP. The SAPL improvement rates for the 0.25, 0.5, and 1-in. thick SAPLs were 23.1, 32.1, and 98.9 %, respectively.

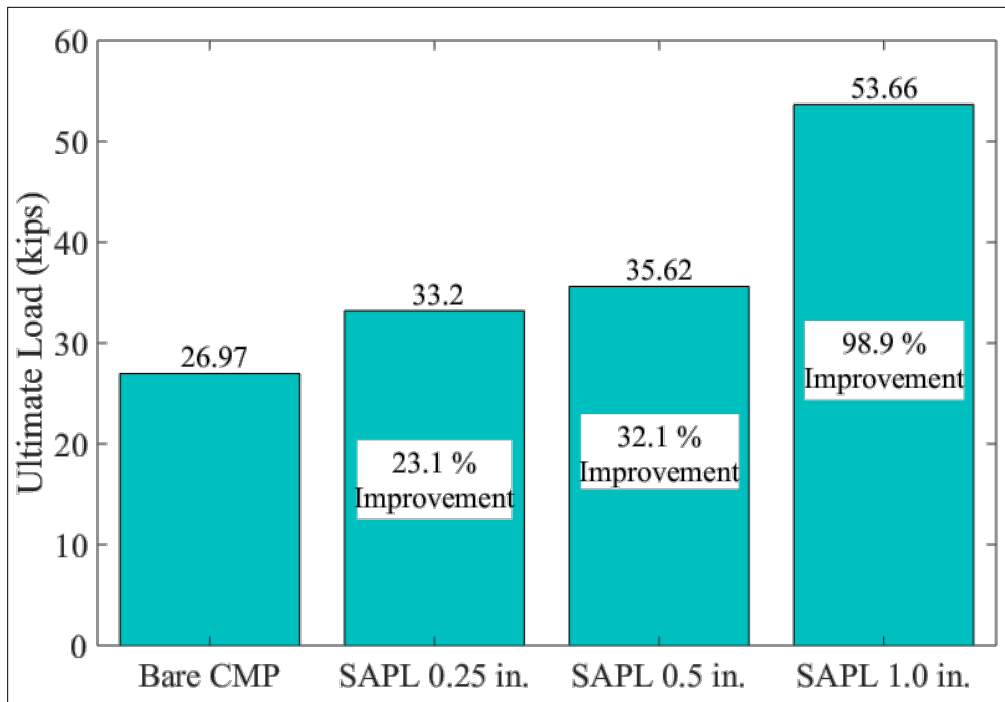


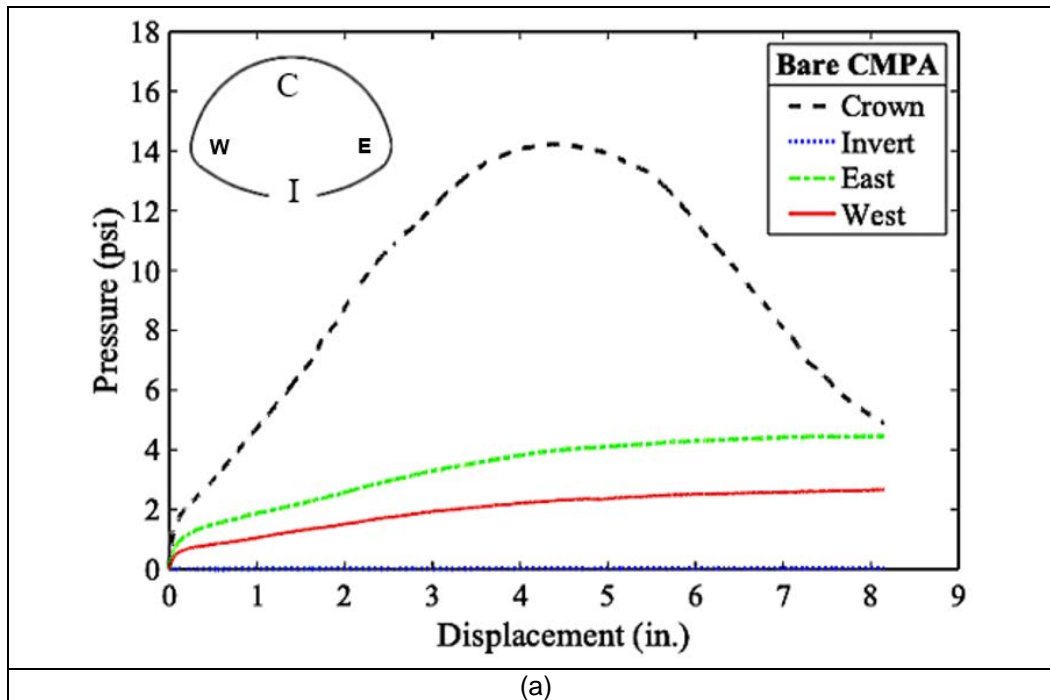
Figure 5-31 Fully Invert deteriorated arch CMPs ultimate load carrying capacity improvement through SAPL application.

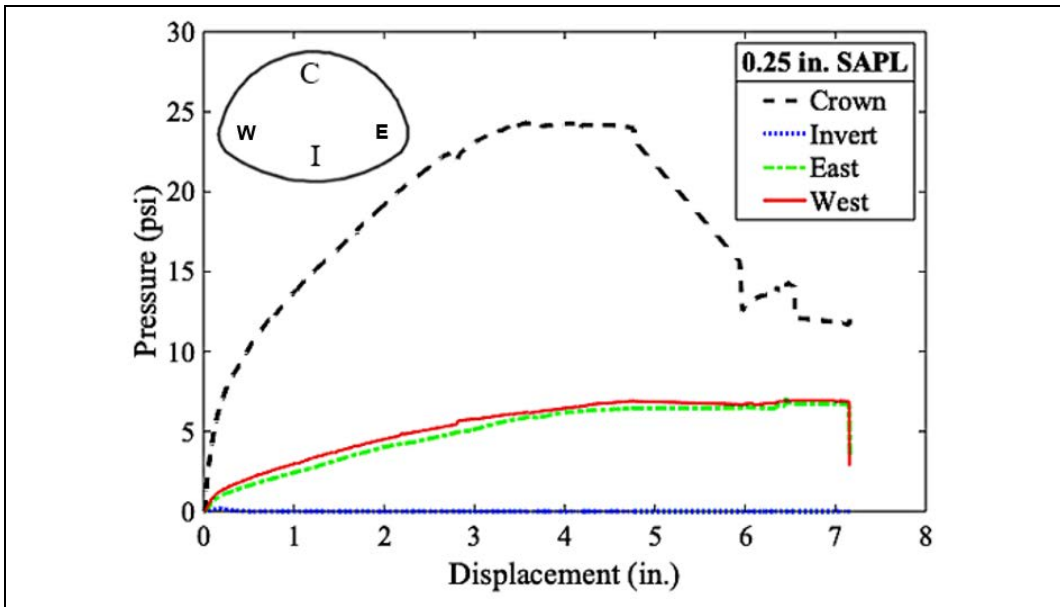
#### 5.3.4 Pressure around the Arch CMPs (Earth Pressure Cell Results)

Figure 5-32 shows the applied pressures around the arch CMPs, measured by earth pressure cells. In all four arch CMP samples the maximum pressures were registered at top of the pipes, where the pressure cells were buried 20 in. deep under the steel load pad. The maximum applied pressure on top of the bare arch CMP was 14.23 psi. The side pressures on West and East locations were 1.9 and 4 psi, respectively. No pressure was registered at the bottom of the arch CMP since in the absence of the invert section no pressure was applied on the soil underneath of that area.

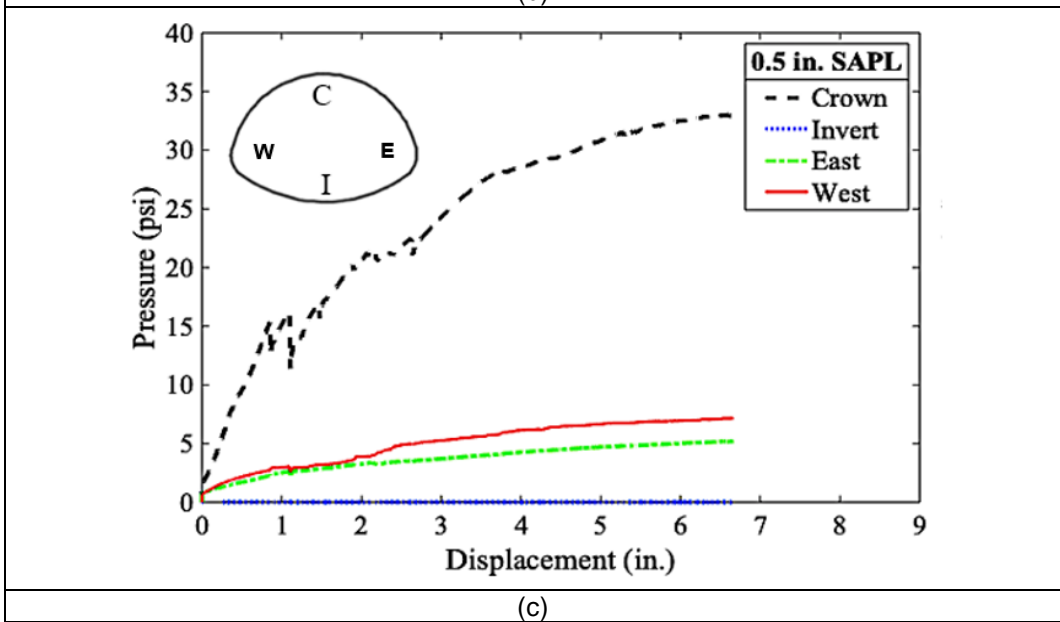
The quarter, half, and one in. SAPL renewed arch CMPs reached the failure pressure on top of the CMP at 24.32, 32.92, and 51.23 psi, respectively. Figure 5-32 illustrates the pressure-displacement graphs for bare, and all three SAPL renewed arch CMPs. In the all arch CMPs no pressure was registered by earth pressure cells on the bottom of the pipes. This was expected for the bare arch CMP since its invert section

was entirely removed. However, for the SAPL renewed samples where the invert section was rehabilitated the pressure on the bottom of the pipe was still zero. This is due to the closed-arch behavior under a vertical load which produced an uplift force on the bottom and consequently no pressure was applied to the soil below. The free body diagram of an arch CMP subjected to a vertical load on its top is illustrated in Figure 5-33. The load developed positive bending moment on the crown and negative bending moment on the invert section of the CMP. Therefore, an upward force is generated that uplifted the invert section as a result of the negative bending moment. This upward movement was also observed in the soil box tests through measuring the gap between the arch CMPs invert at the cut end-strip location and the soil below. Figure 5-33 also illustrates the arch CMP's invert uplift after loading. DIC also capture the renewed arch CMPs' invert upward movement.





(b)



(c)

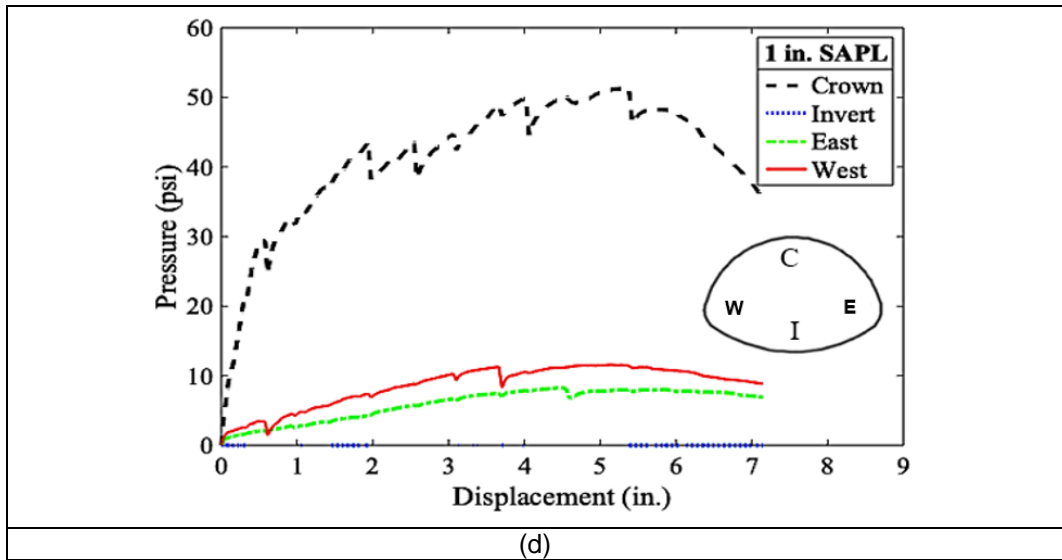


Figure 5-32 Pressure vs. crown displacement graphs: (a) invert-cut bare arch CMP, (b) 0.25 in. SAPL renewed arch CMP, (c) 0.5 in. SAPL renewed arch CMP, and (d) 1 in. SAPL renewed arch CMP.

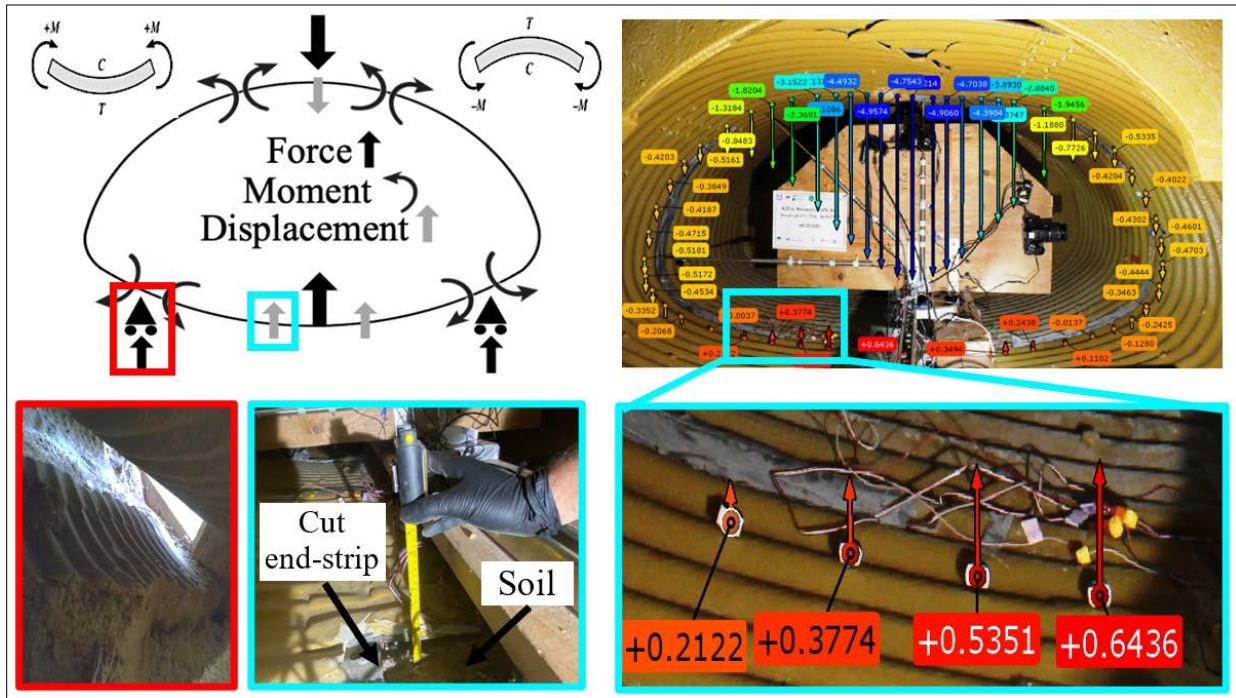


Figure 5-33 Arch CMP behavior due to the vertical load, where the red boxes show the soil support under the pipe on the west haunch area and the blue boxes illustrates the pipe upward movement.

The arch CMPs' load carrying capacity, crown deflection at initial crack and failure as well as the soil displacement in both initial crack and failure stages are summarized in Table 5-4.

Table 5-4 The circular CMPs' load bearing capacity, crown deflection and the soil displacement at initial crack and failure.

Test Setup		Initial Structural Cracking Stage				Failure Stage		
		Load (kips)	Pipe Deflection at Crown (in.)	Soil Displacement (in.)	Pressure at Crown (psi)	Load kips	Pipe Deflection at Crown (in.)	Soil Displacement (in.)
<b>Bare Invert-cut CMP</b>		-	-	-	-	26.97	4	6.47
<b>SAPL Renewed CMP</b>	0.25 in. SAPL	29.32	2.1	3.15	20.01	33.2	4.75	6.23
	0.5 in. SAPL	26.27	0.838	1.71	15.23	35.62	5.07	7.61
	1 in. SAPL	41.08	0.33	1.22	21.85	53.66	5.2	7.56

The soil pressure around the arch CMPs are recorded by the earth pressure cells and are summarized in Table 5-5 for the time of failure at the ultimate load.

Table 5-5 Soil pressure results around the arch CMPs at the time of failure.

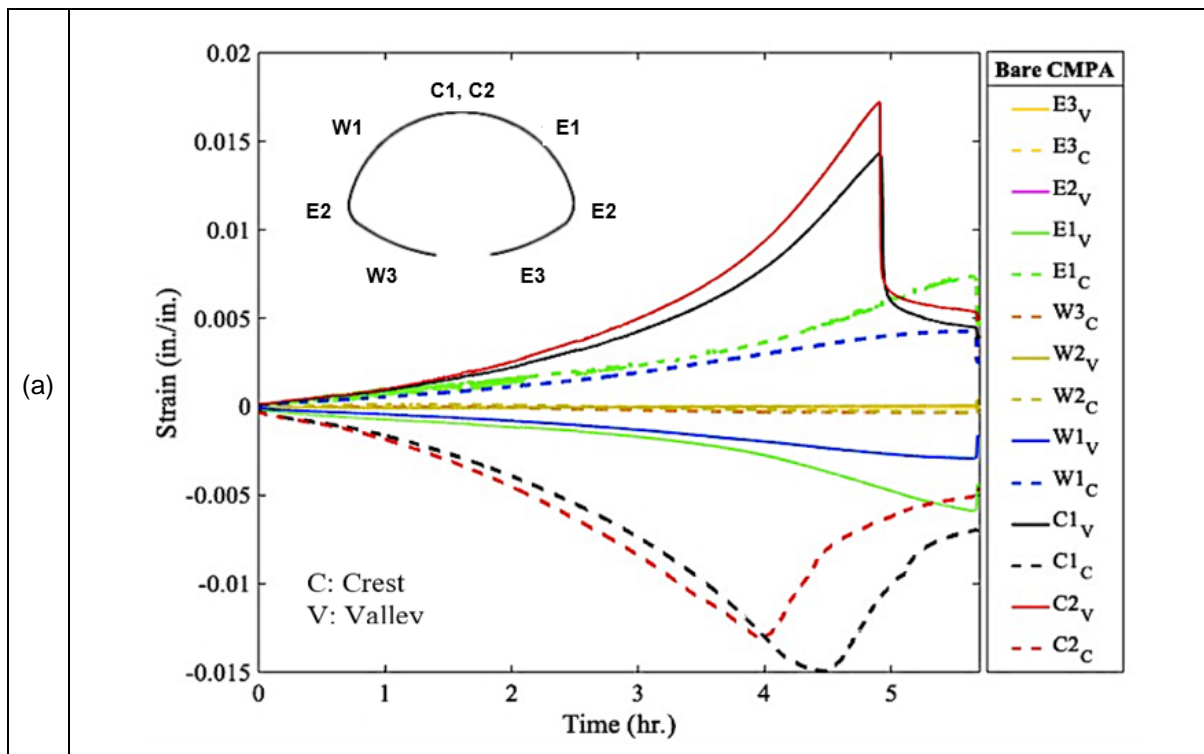
Test Setup		Pressure (psi)			
		Crown	Invert	East	West
<b>Bare CMP</b>		14.23	0	4.05	2.34
<b>SAPL Renewed CMP</b>	0.25 in. SAPL	24.32	0	6.45	6.9
	0.5 in. SAPL	32.92	0	5.05	6.99
	1.0 in. SAPL	51.23	0	8.01	11.53

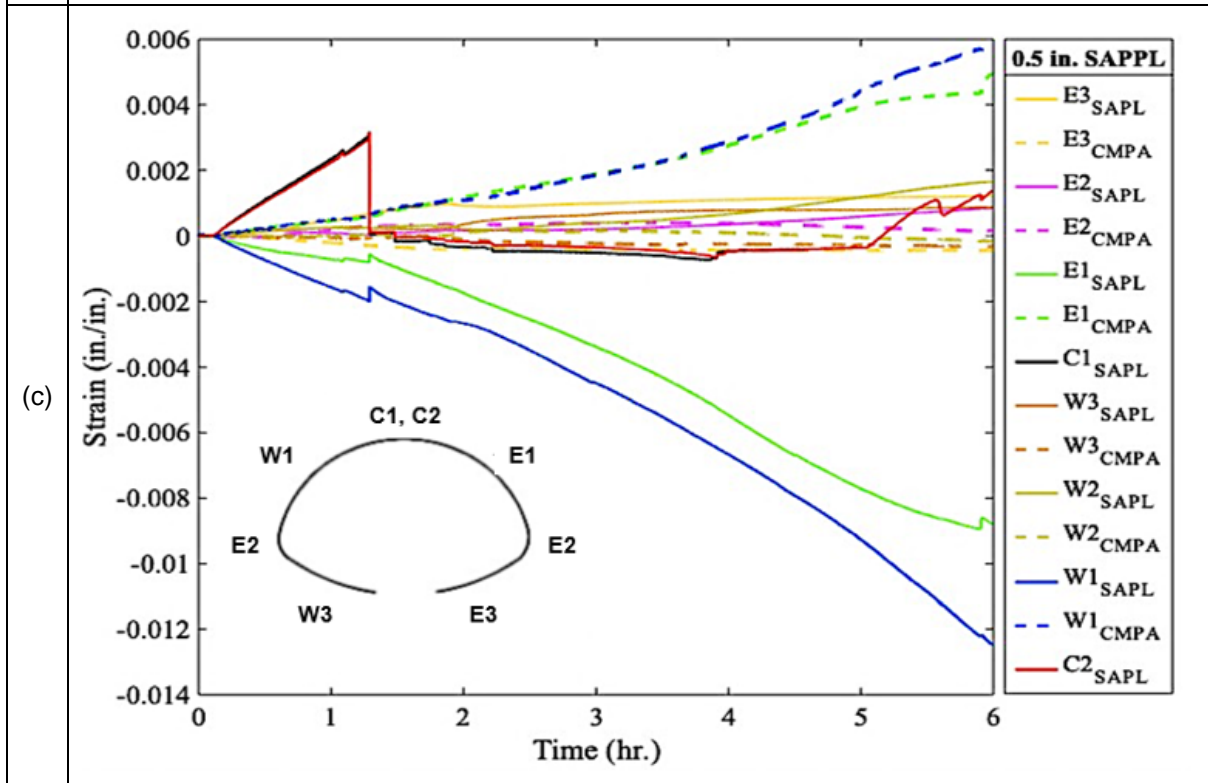
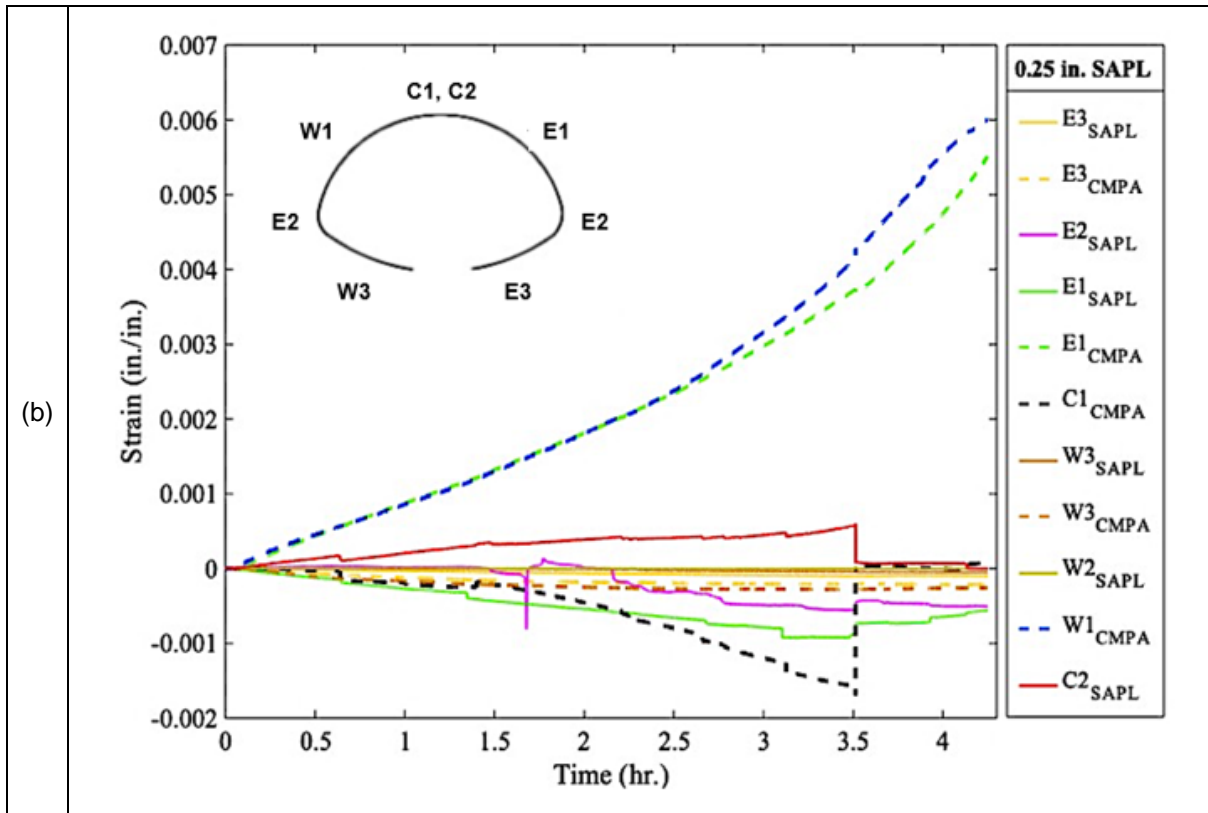


### 5.3.5 Strain Gauges Results for SAPL Renewed Arch CMPs

Figure 5-34 illustrates the results of strain values. The bare arch CMP experienced a large strain at the crown and both shoulder locations which indicates the formation of a three-hinge plastic mechanism (i.e., local buckling) at the crown. Likewise, the host arch CMPs of SAPL were subjected to large amount of strains at the crown and both shoulder locations. Strain results comparison at the crown and shoulder of the arch CMPs indicate that the sprayed polymeric material increased the stiffness of the fully invert deteriorated (i.e., invert-cut) arch CMPs. Cracking of the half and one inch SAPL renewed arch CMPs at the crown locations with a large drop are evident in Figure 5-34 (c) and (d) respectively. The arch SAPLs were cracked with the strain values of approximately 0.003 in./in.

In Figure 5-34, some strain gauges' values are not illustrated which were due to the harsh abrasive nature of the soil-pipe system.





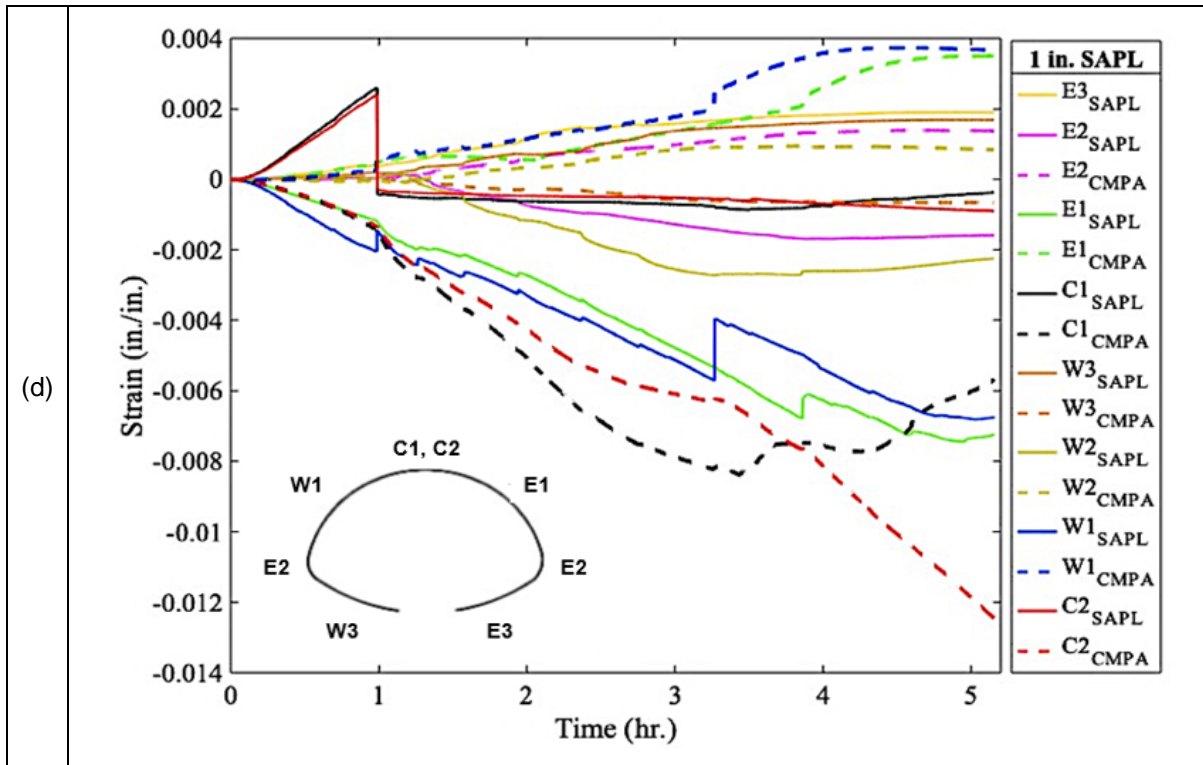
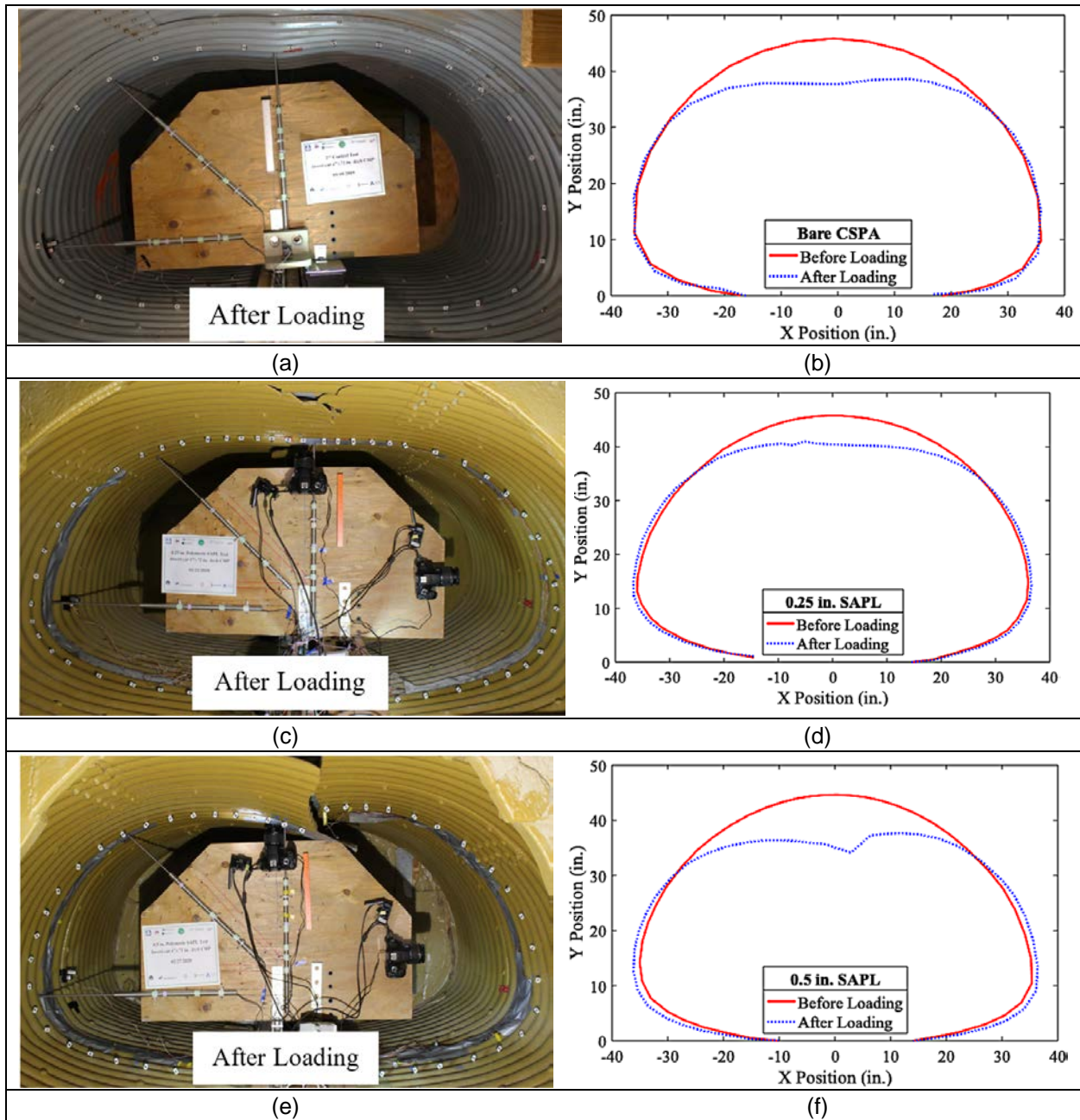


Figure 5-34 Strain gauge results: (a) invert-cut bare arch CMP, (b) 0.25 in. SAPL renewed arch CMP, (c) 0.5 in. SAPL renewed arch CMP, (d), 1 in. SAPL renewed arch CMP.

### 5.3.6 Pipe Profile Measurement using DIC for SAPL Renewed Arch CMPs

Figure 5-35 illustrates the results of pipe deflection measurements at the middle ring of the arch CMP using DIC technique prior and after the loading. The accuracy of the DIC measurement was investigated by direct comparison with mechanical sensors (i.e., LVDT & CDS) that revealed both techniques are in an excellent conformity (Darabnoush Tehrani et al. 2020b). The SAPL renewed arch CMPs had movement in both vertical and horizontal directions that the movements are evident in the DIC profiling. The pipe profiling for the after the test stage shows that the SAPL renewed pipe samples had horizontal expansion at springline due to the vertical load. The magnitude of this horizontal expansion in the bare arch CMP was inconsequential. This is due to the fully detached invert section which released the restraint from the pipe. The modes of failure for all arch CMP samples were local buckling at the crown locations, which is evident in the DIC results. In case of the bare arch CMP the buckling caused pipe

deformation (i.e., ductile failure) and in case of SAPL renewed arch CMPs it caused cracking and fracture at the crown locations (i.e., brittle failure). It should be noted that, due to the existence of the mechanical sensors' frame and its holding wooden beam, implementation of DIC and illustration of the invert section of pipes' profile were not possible. Figure 5-36 illustrates pipe profiling of SAPL renewed circular CMPs at the time of failure.



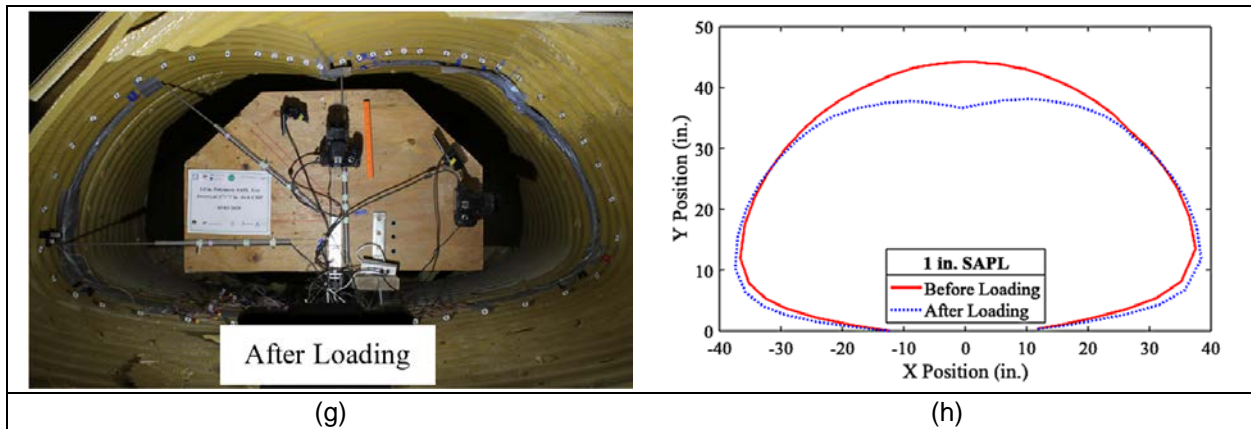
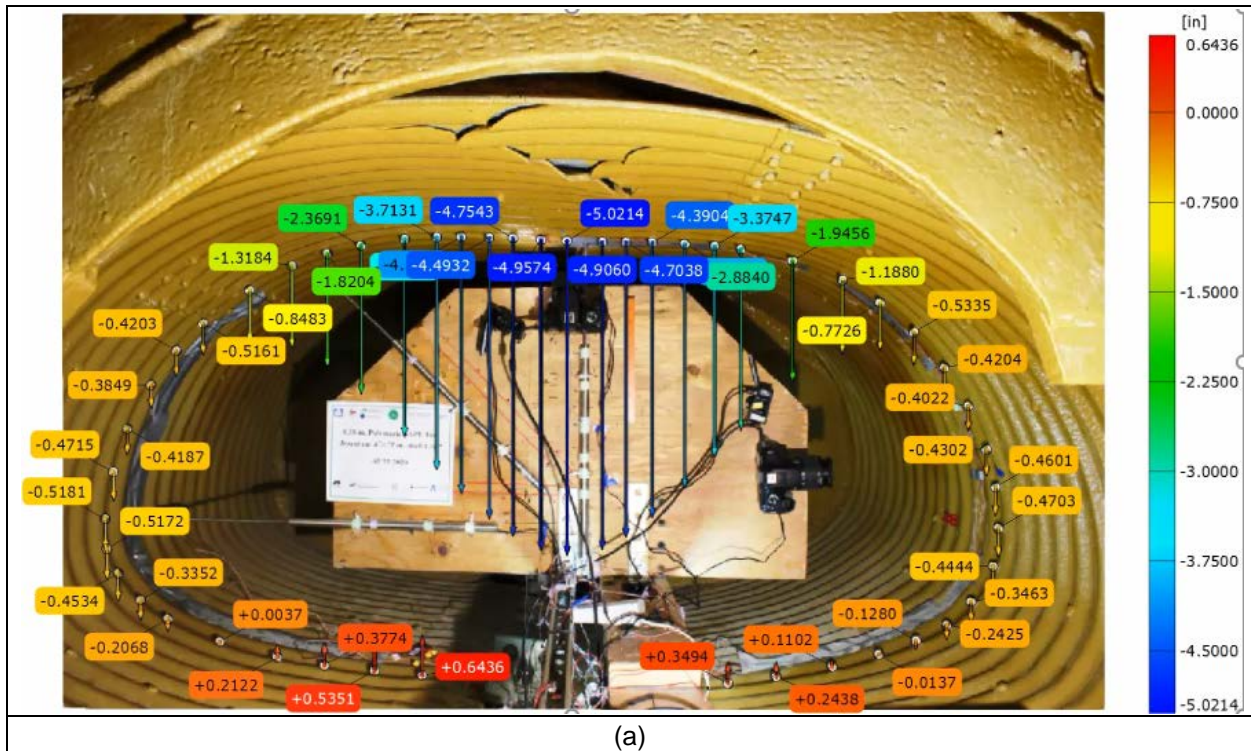
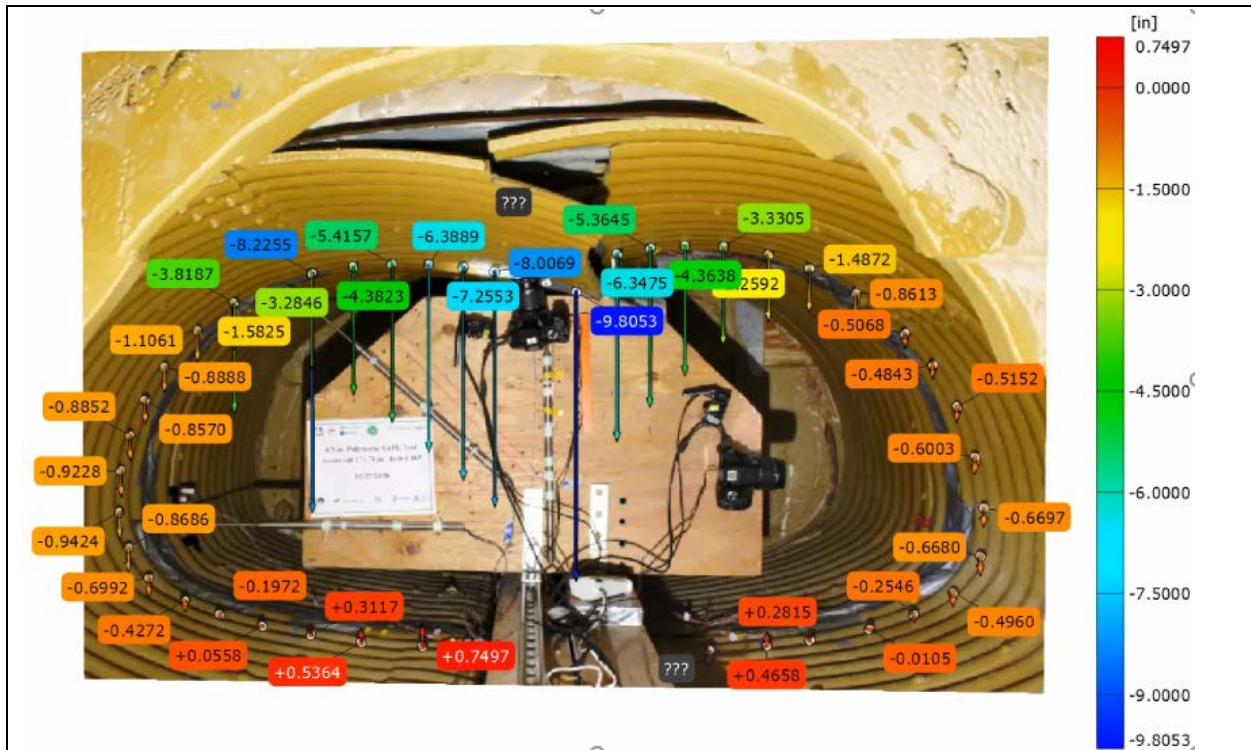
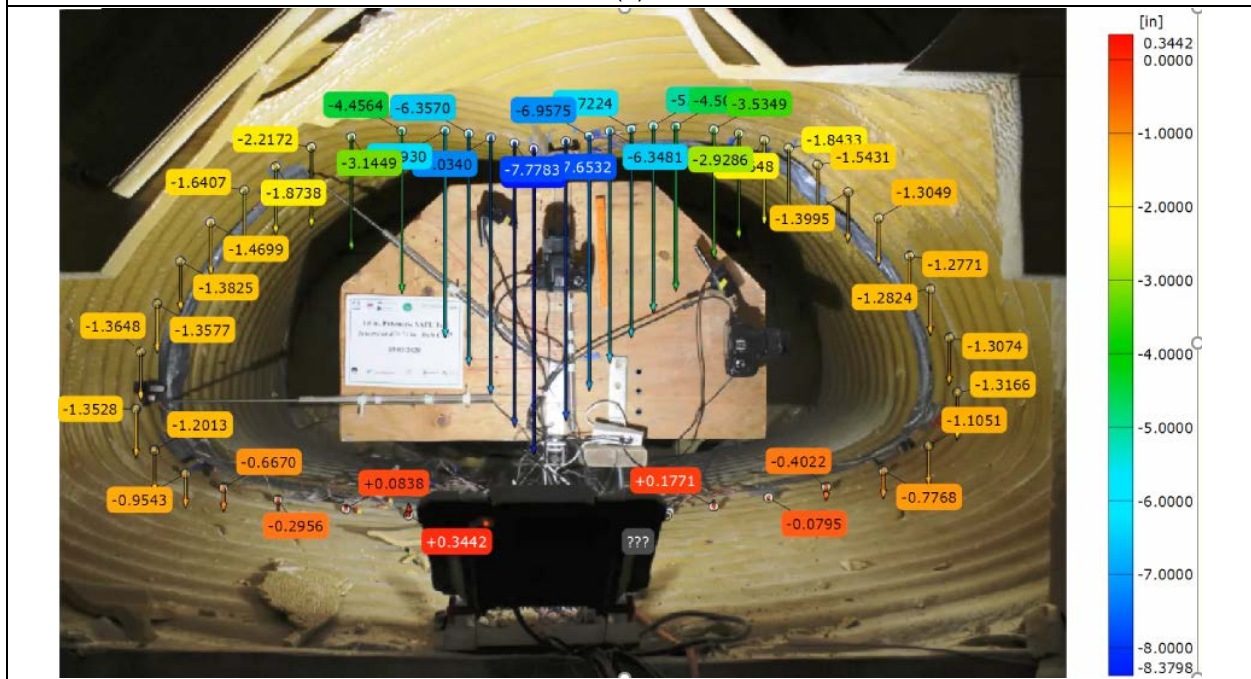


Figure 5-35 Pipe profiling using DIC results: (a) and (b) bare arch CMP, (c) and (d) 0.25 in. SAPL renewed arch CMP, (e) and (f) 0.5 in. SAPL renewed arch CMP, and (g) and (h) 1 in. SAPL renewed arch CMP.





(b)



(c)

Figure 5-36 Pipe profiling using DIC technique at the time of failure: (a) 0.25 in. SAPL, (b) 0.5 in. SAPL, and (c) 1.0 in. SAPL renewed arch CMPs.

## 5.4 Chapter Summary

Chapter 5 presented the results of nine full scale soil box testing including examining the structural capacity of bare CMPs, SAPL renewed circular CMPs and SAPL renewed arch CMPs. One bare intact circular, one bare invert-cut (simulating a fully deteriorated invert CMP) circular and one bare invert cut arch CMPs, three invert-cut circular and three invert-cut arch CMPs renewed with polymeric spray applied pipe liner (SAPL) were buried in three different test setups in a soil box of 25 × 12 × 10 in. The burial configuration included 2-ft of soil cover, backfilling, bedding, and foundation layers. TxDOT 247 grade 1 type D aggregates was used for the top one foot layer of soil cover and poorly graded sand (SP) were used for the rest of layers. A displacement-control static load with a load rate of 0.03 in./min was continuously applied on the soil surface through a rigid steel plate (load pad) of 20x40 in. The results of the soil box testing and discussions were presented in this chapter and are summarized as following:

### 5.4.1 Control Test of Bare CMPs

- The intact circular CMP could withstand the AASHTO H20 truck load and ultimately failed with a local buckling at the crown.
- The invert-cut circular CMP could withstand the equivalent AASHTO H20 truck load.
- The invert-cut circular CMP at the failure registered a larger horizontal movement in the absence of its ring stiffness compared with the invert-cut arch CMP that did not exhibit a significant horizontal movement.
- The invert-cut arch CMP could not reach the equivalent AASHTO H20 truck load prior to the ultimate failure. The ultimate load of the invert-cut arch CMP was 47% lower than the ultimate load of invert-cut circular CMP.
- The invert-cut arch CMP carried the superimposed loads by taking advantage of its flat area at the bottom for transferring the vertical loads to the soil, while the strength of invert-cut circular CMP was dependent on its ring stiffness.
- The initial load carrying capacity of the invert-cut circular CMP was due to the existence of frictional

resistance between the outer surface of the CMP and soil. The frictional resistance is a function of the contact area between the CMP and soil, as well as the length of the pipe. A culvert in the actual field condition is longer than tested CMPs in the laboratory condition. Hence, a longer CMP in the field will experience a higher frictional resistance which can lock the pipe in place and therefore, it may reduce or eliminate the circumferential movement of the pipe. Resistance to circumferential movement of the CMP may facilitate or increase the chance of local buckling failure.

- Considering the pipe sample length in the actual field condition along with the existence of frictional resistance factor, and a higher load carrying capacity for the circular CMP sample compared with arch CMP, it can be inferred that in a fully deteriorated condition a circular CMP has less risk of collapse compared with an arch CMP.

#### **5.4.2 SAPL Renewed Circular CMPs**

- The physical property test results demonstrated that the polymeric SAPL had the averaged maximum tensile stress of 8,670.78 psi, elastic modulus of 489,500 psi, and flexural modulus of 855,639 psi.
- The results of thickness measurement showed that the utilization of hand spray for installation of the polymeric SAPL resulted in a thicker liner at the springline for all renewed CMPs than the designated thickness. However, the SAPL was installed closer to the required thickness at crown and both shoulders. One of the possible reasons for the inconsistent thickness installation could be due to the sagging and movement of the SAPL material at the initial stage (i.e., before hardening) of installation due to gravity.
- All SAPL renewed pipes cracked at about 3% of the SAPL-CMP system deflection, where at this deflection the application of 0.25 in., 0.5 in., and 1 in. polymeric SAPL increased the load carrying capacity for 471.7, 482.8, and 802.7% respectively.
- Application of the polymeric SAPL increased the stiffness of the invert-cut CMP. The SAPL renewed CMPs with the thicknesses of 0.25 in., 0.5 in., and 1 in. increased the ultimate load bearing



capacity of the invert deteriorated CMPs for 16.24, 31.4, and 80.82%, respectively.

- The CMP with thinner liner (i.e., 0.25 in.) was susceptible to crack at the seam's locations, where the liner's thickness was not sufficient to prevent cracking. Although the first crack was initiated in the longitudinal direction, once it reached the seam locations, it diverted towards the circumferential direction.
- The CMP with 1 in. thick SAPL showed stiffer response to the applied load in compare with thinner SAPL renewed pipe samples. In contrast with the other samples, no circumferential crack was observed in the pipe sample.
- The SAPL renewed CMP samples with the thicknesses of 0.25 in., 0.5 in., and 1 in. cracked at 3.52, 2.9, and 3.65% of crown deflection, respectively.
- In the absence of the host pipe's ring stiffness, the SAPL was able to resist the ring compression solely. Therefore, the polymeric SAPL can be considered structurally sufficient to withstand the applied load and improve the overall load bearing capacity of the fully deteriorated host pipe.

#### **5.4.3 SAPL Renewed Arch CMPs**

Three invert-cut arch corrugated metal pipe samples (CMPs) renewed with polymeric spray applied pipe liner (SAPL) application and one invert-cut bare arch CMP were buried under 2-ft of soil cover including layers of poorly graded sand (SP), and TxDOT 247 grade 1 type D aggregates. The invert of arch CMPs were cut before SAPL application to simulate a fully deteriorated invert condition. Static load in a displacement-control regime was continuously applied with a load rate of 0.03 in./min through a rigid 20 × 40 in. steel load pad. The experimental test simulated a poor pipe installation condition (i.e., uncompacted soil) in the absence of pavement to maximize the applied load on the renewed pipe. The results and discussions were presented in this chapter and the conclusions are summarized as follow:

- The results of thickness measurements showed that the utilization of hand spray installation method for the polymeric SAPL resulted in about 0.2 in. thicker liner than the design thickness, which could be due to the inclusion of a factor of safety in SAPL's quantity calculation.

- Under the shallow cover condition, the invert-cut bare arch CMP, in the absence of ring stiffness, was able to resist the vertical load up to the 26.97 kips of the applied static load.
- Application of the polymeric SAPL increased the stiffness of the invert-cut arch CMP. The SAPL renewed arch CMPs with the thicknesses of 0.25 in., 0.5 in., and 1 in. increased the ultimate load bearing capacity of the invert deteriorated CMPs for 23.1, 32.1, and 98.9%, respectively.
- The arch CMP with 0.25 in. of SAPL was susceptible to crack at the seam's locations, where the SAPL was either discontinued or the thickness was not as thick as design thickness. Although, the first crack was initiated in the longitudinal direction, once it reached the seam locations, it diverted towards the circumferential direction.
- In compare with the bare arch CMP, the application of SAPL reduced the strain of the host pipes, especially at the crown and shoulder locations.
- The DIC results implied that for all arch CMP samples the modes of failure were local buckling at the crown locations, where in case of the bare arch CMP the buckling caused pipe deformation (i.e., ductile failure) and in case of SAPL renewed arch CMP samples it caused cracking and fracture at the crown sections (i.e., brittle failure).
- The 0.25, 0.5, and 1 in. SAPL renewed arch CMPs were cracked at the pressures of 19.77, 16.26, and 21.95 psi, respectively. All the SAPL renewed arch CMPs cracking pressures were higher than the applied pressure by the AASHTO H20 truck, calculated through AASHTO LRFD, AWWA, and NCSPA design guidelines.
- In the absence of the host pipe's ring stiffness, the SAPL was able to resist the ring compression solely. No sign of crack was observed at the invert area, where the host pipe was entirely cut and detached. Therefore, the polymeric SAPL can be considered structurally sufficient to withstand the applied load and improve the overall load bearing capacity of the fully invert deteriorated host arch CMP.

## Chapter 6

### Finite Element Modeling (FEM)

This chapter presents a full size three-dimensional finite element modeling (FEM) simulation of the full scale SAPL soil box testing performed at CUIRE laboratory. The ABAQUS 6.14-3 software was used to perform FEM simulations and analyses. The FEM simulation in this chapter is generated by CUIRE based on the soil box testing setup developed by the author at CUIRE, presented in Chapters 4 and 5 of this dissertation. The FEM simulation results are prepared by research team at CUIRE and reported by Raut (2020) for the purpose of verification with the test results that were obtained from the soil box testing as described in Chapter 5 of this dissertation.

#### 6.1 Model setup

The soil box test model, simulated in ABAQUS, included three solid parts of soil, corrugated metal pipe (CMP) and SAPL. The geometry of the corrugated metal pipes were generated in AutoCAD software and imported to ABAQUS for meshing and modeling. The boundary conditions of models were defined according to the soil box test setup. All the vertical soil faces were defined as restricted in their normal directions and free in their tangential directions. The bottom surface of the soil was restricted. Figure 6-1 illustrates the boundary conditions of the FEM used for calibration of soil box testing. The load was applied on the soil surface at the middle section of the pipe using a master node in the loading area. The soil used for the experimental soil box testing, as presented in Chapter 4 of this dissertation, included poorly graded sand (SP) for foundation, bedding and backfilling layers, and TxDOT specified grade D sub-base layer classified according to ASTM D-2487 for the top 1 ft of soil cover. Hence, the “Drucker Prager Model Soil” was used for soil simulation in ABAQUAS. Table 6-1 presents the soil properties used in ABAQUS.

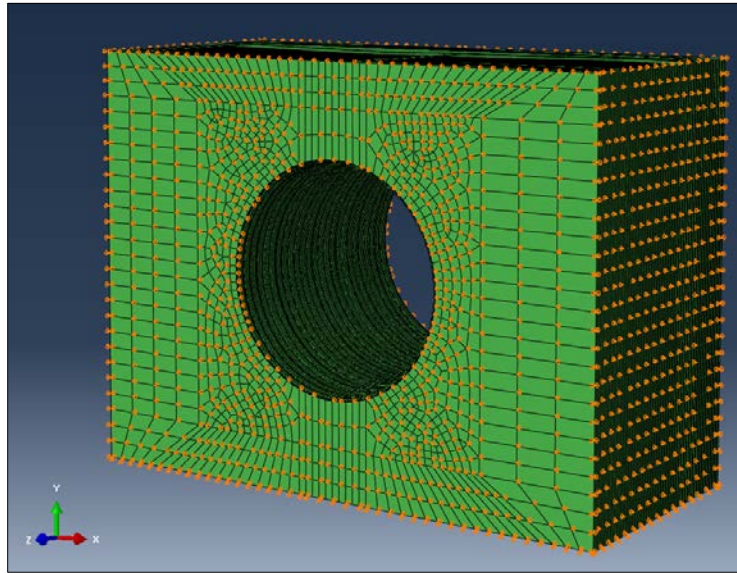


Figure 6-1 FEM of the SAPL soil box testing showing the boundary conditions (Source: CUIRE).

Table 6-1 Soil properties used in ABAQUS (Source: CUIRE FEM report).

Soil Parameters	Density (pcf) (Max. dry density)	Young's Modulus (psi)	Poisson Ratio	Angle of Friction (°)	Dilation Angle (°)
Sand	115	510	0.3	32	1
RCA	130	1,100	0.3	39	1

The material properties of CMP samples and polyurethane SAPL are presented in Chapter 4 of this dissertation. To simulate the CMP samples and SAPL in ABAQUS, the elastic-plastic model was used. In the FEM simulation, the occurrence of a crack in the SAPL was assumed by appearance of its plastic strain in ABAQUS.

The interface of soil and CMP was modeled using a surface-to-surface interaction, considering the CMP as the master surface and the soil as the slave with a friction coefficient of 0.5. A hard contact was defined between the soil and CMP that allowed the soil to displace the pipe without piercing it.

The interface of CMP and SAPL was modeled using a surface-to-surface interaction, considering the CMP as the master surface and SAPL as the slave, with a friction coefficient of 1.0 to simulate a stronger tangential bonding.

In the FEM simulation, the solid linear C3D8R mesh was used for the soil element (an eight-node brick element with reduced integration). The mesh size of the soil was optimized to be 2.4 in. Solid linear hexagonal C3D8R mesh was used for the CMP and SAPL elements. The mesh size of the CMP used was selected to be 1.8 in.

## 6.2 Comparison of the Soil Box Testing Results Presented in Chapter 5 and FEM Results of Fully Deteriorated Invert Circular CMPs Renewed with Polymeric 0.25 SAPL.

### 6.2.1 0.25 in. SAPL Renewed CMP Sample

As it is explained in Chapter 5 of this dissertation, in all SAPL renewed soil box testing, the first crack occurred at the middle section of the pipe samples at the crown location. This crack was predicted in the FEM simulation as a plastic strain initiation at the same place, as illustrated in Figure 6-2.

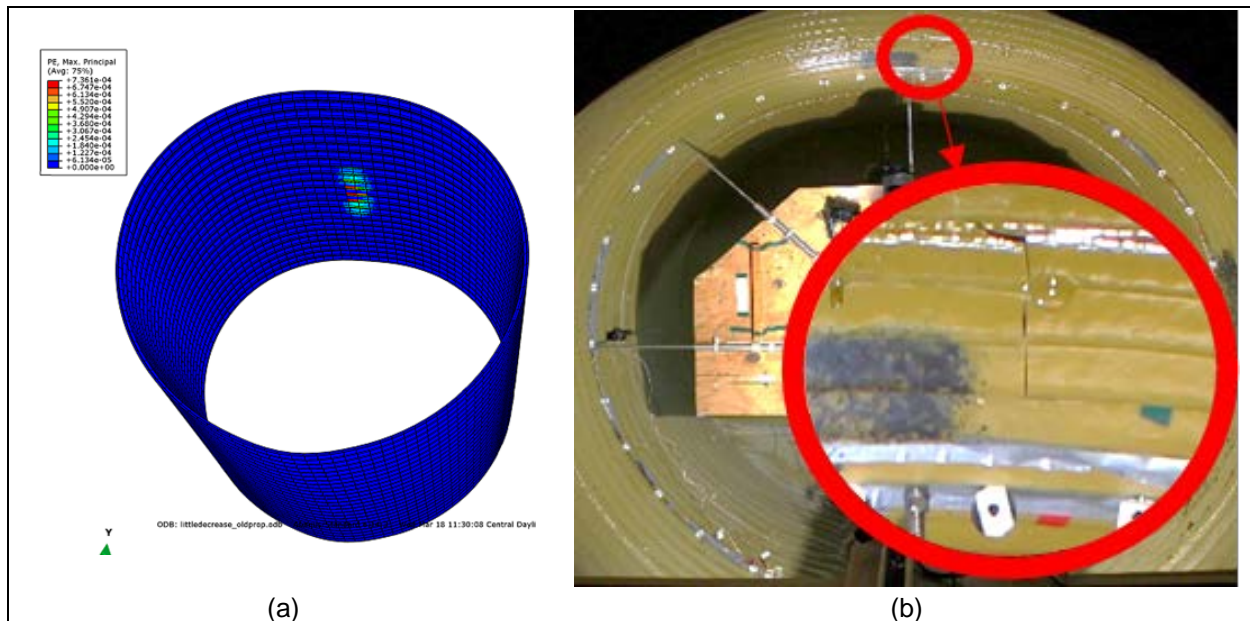


Figure 6-2 Comparison of the soil box testing results and FEM with respect to the occurrence of the first crack: (a) plastic strain predicted by FEM (Source: CUIRE FEM report), and (b) 0.25 in. SAPL first crack at the crown location.

As it is presented in Chapter 5 of this dissertation, the initial crack at the crown location propagated longitudinally along the pipe and created a wide fracture by the end of the test at the ultimate load. The same pattern was predicted by the FEM, as illustrated in Figure 6-3.

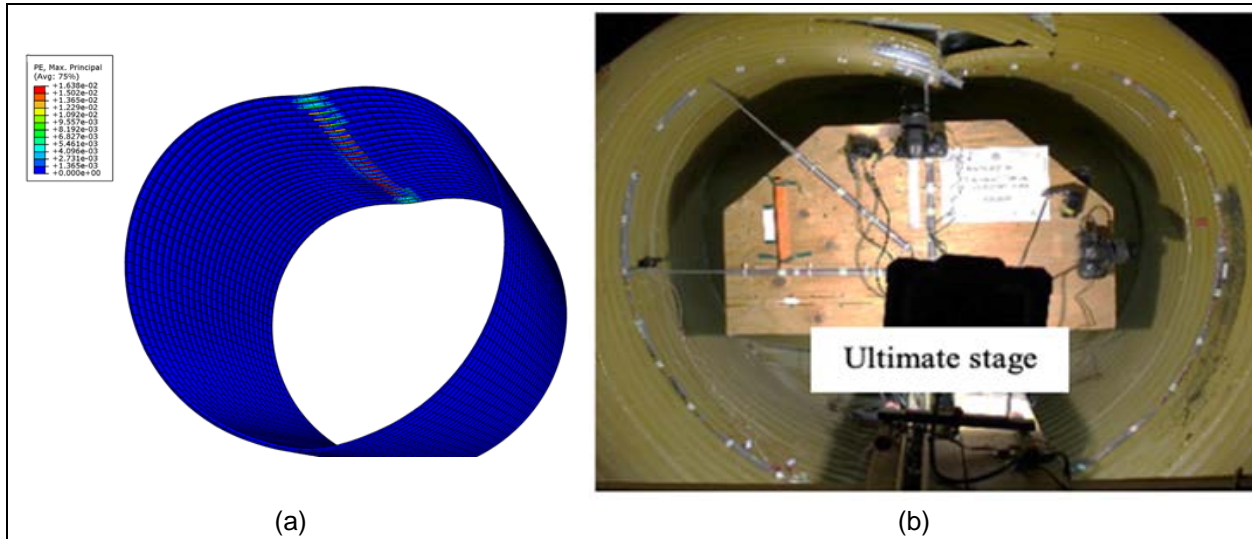


Figure 6-3 Crack propagation and fracture in 0.25 SAPL at the crown of the pipe at the ultimate load: (a) FEM (Source: CUIRE FEM report), and (b) SAPL soil box testing results.

The comparison of the soil box testing results (using DIC technique) and the FEM simulation with respect to the SAPL deflection at the ultimate load condition at the crown of the pipe is illustrated in Figure 6-4.

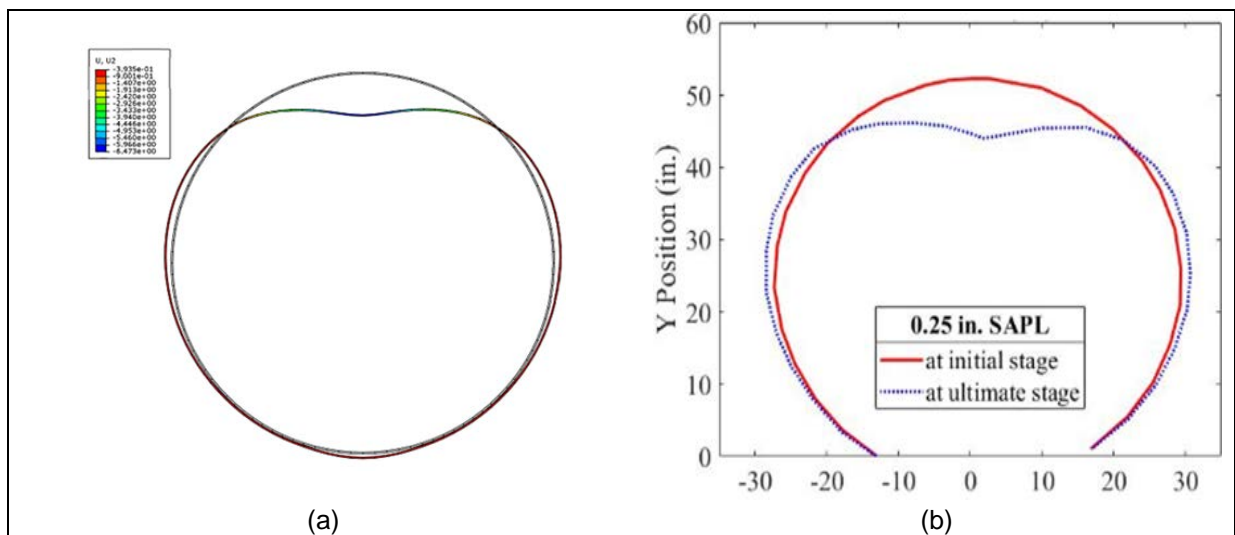


Figure 6-4 SAPL Deflection at the ultimate load at the crown of the pipe: (a) FEM results (Source: CUIRE FEM report), and (b) DIC results of pipe profiling (0.25 in. SAPL).

The comparison of the soil box testing results and FEM results for the applied static load versus displacement changes at the crown of the pipe are illustrated in Figure 6-5.

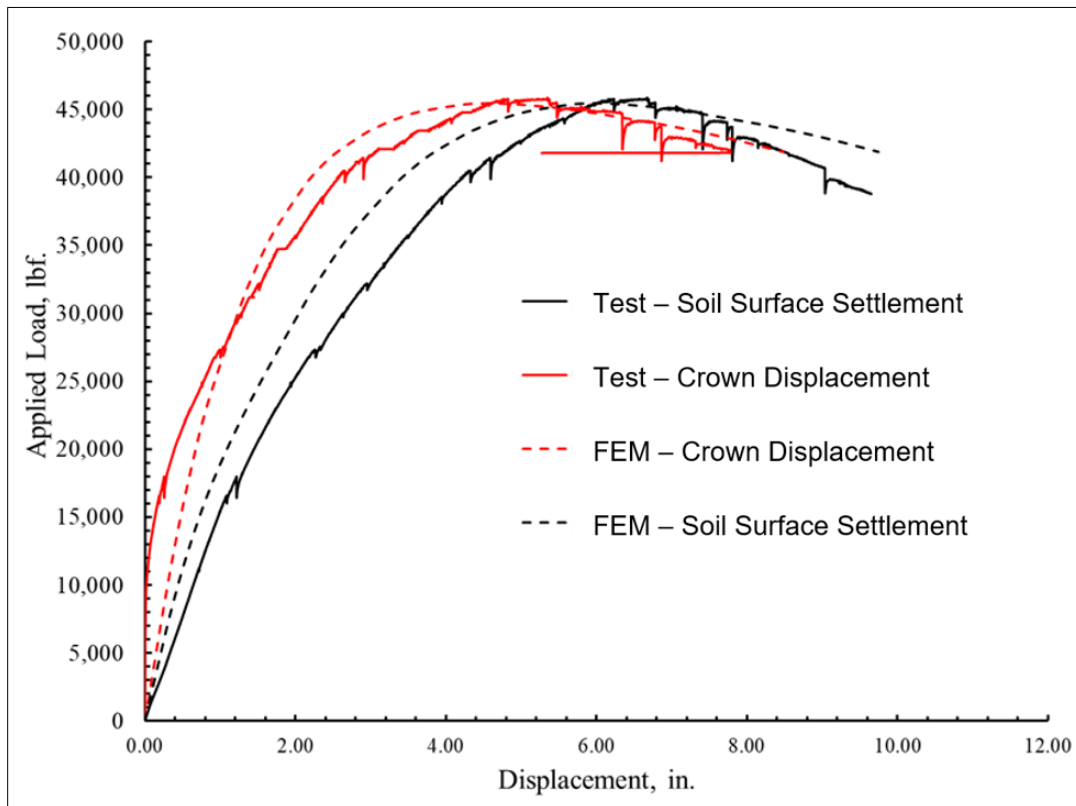


Figure 6-5 Load versus displacement – comparison of soil box testing results and FEM (Source: CUIRE FEM report) results (0.25 in. SAPL).

The comparison of the soil box testing results and the FEM simulation at the time of first crack initiation and the ultimate load are presented in Table 6-2. As the values of this table shows, there is 8% difference between the results.

Table 6-2 Load-displacement results – comparison of SAPL soil box testing and FEM (Source: CUIRE FEM report) at the time of first crack and ultimate load (0.25 in. SAPL).

Description \ Time	Initiation of 1 <sup>st</sup> crack (1 <sup>st</sup> plastic strain)			Ultimate Load		
	Test	FEM	Difference FEM vs. Test (%)	Test	FEM	Difference FEM vs. Test (%)
Crown Displacement (in.)	2.12	3.13	47.64% increase	4.83	4.98	3.1% increase
Soil Settlement (in.)	3.95	4.79	21.26% increase	6.69	6.48	3.13% increase
Load (kips) on the Soil Surface	39	44.40	13.84% increase	46.38	45.78	1.3% increase

The comparison of the soil box testing results (presented in Chapter 5 of this dissertation) and FEM results for distributed pressure on top of the pipe versus displacement at the crown location is illustrated in Figure 6-6. The comparison of soil box testing results and FEM results for the applied load on the soil surface versus distributed pressure on top of the pipe at the middle cross section is illustrated in Figure 6-7. The soil box testing results revealed a pressure of 31 psi on top of the pipe at the middle cross section at the time of first crack along with 2.12 in. of SAPL displacement of the crown. The FEM results for the same location and the same time (first crack) showed a pressure of 36.16 psi and SAPL crown displacement of 3.13 in., as presented in Table 6-3. Hence, the FEM predicted a higher value of pressure on top of the pipe with 16.64% difference from the actual value obtained through the soil box testing (as presented in Chapter 5 of this dissertation).

Table 6-3 The comparison of soil box testing results and the FEM predicted pressure value at the time of first crack on top of the pipe (0.25 in. SAPL).

Description \ Time	Time of Initiation of 1 <sup>st</sup> crack (1 <sup>st</sup> plastic strain)		
	Test	FEM	Difference FEM vs. Test (%)
Crown Displacement (in.)	2.12	3.13	47.64% increase
Pressure on Top of the Pipe (psi)	31	36.16	16.64% increase



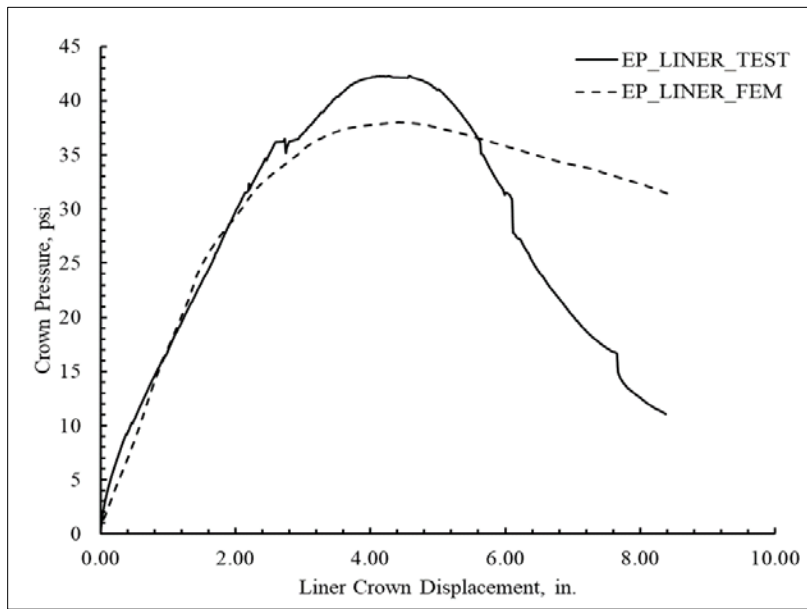


Figure 6-6 The comparison of soil box testing results and FEM (Source: CUIRE FEM report) results for distributed pressure on top of the pipe versus displacement at the crown location (0.25 in. SAPL).

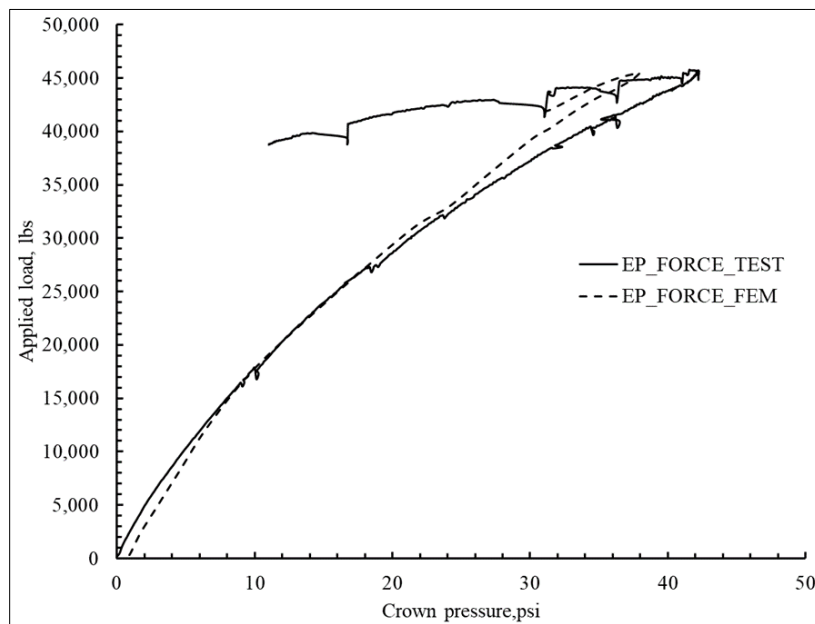


Figure 6-7 The comparison of soil box testing results and FEM (Source: CUIRE FEM report) results for the applied load on the soil surface versus distributed pressure on top of the pipe at the middle cross section (0.25 in. SAPL).

### 6.2.2 0.5 in. SAPL Renewed CMP Sample

In both SAPL soil box testing, as presented in Chapter 5 of this dissertation, and the FEM simulation the first crack in the SAPL occurred at the crown location at the middle section of the pipe. As it is discussed in Chapter 5, the initiated crack at the crown propagated longitudinally along the pipe and became a fracture at the ultimate load. The same pattern was predicted by the FEM simulation. The longitudinal fracture of 0.5 in. SAPL at the crown of the pipe is illustrated in Figure 6-8 along with a picture of FEM simulation at the same time.

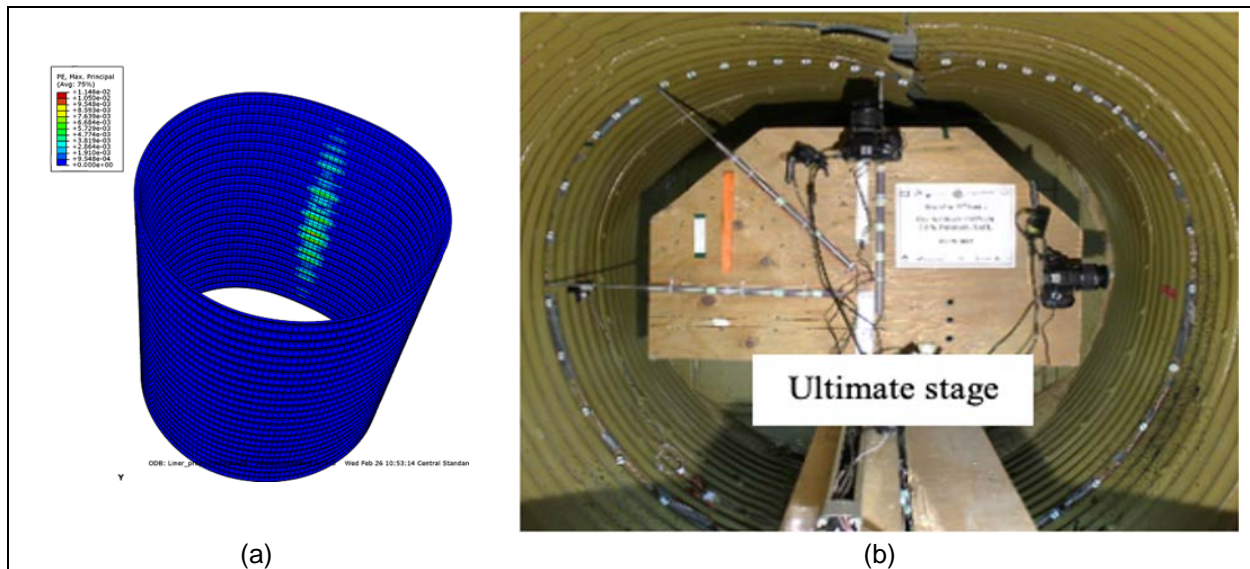


Figure 6-8 Crack propagation and fracture in 0.5 SAPL at the crown of the pipe at ultimate load condition:

(a) FEM (Source: CUIRE FEM report), and (b) SAPL soil box testing results.

The pipe profiling of the 0.5 in. SAPL CMP renewed sample using DIC technique, presented in Chapter 5 of this dissertation, and the FEM results, showing the pipe deflection at the crown at the time ultimate load is illustrated in Figure 6-9.

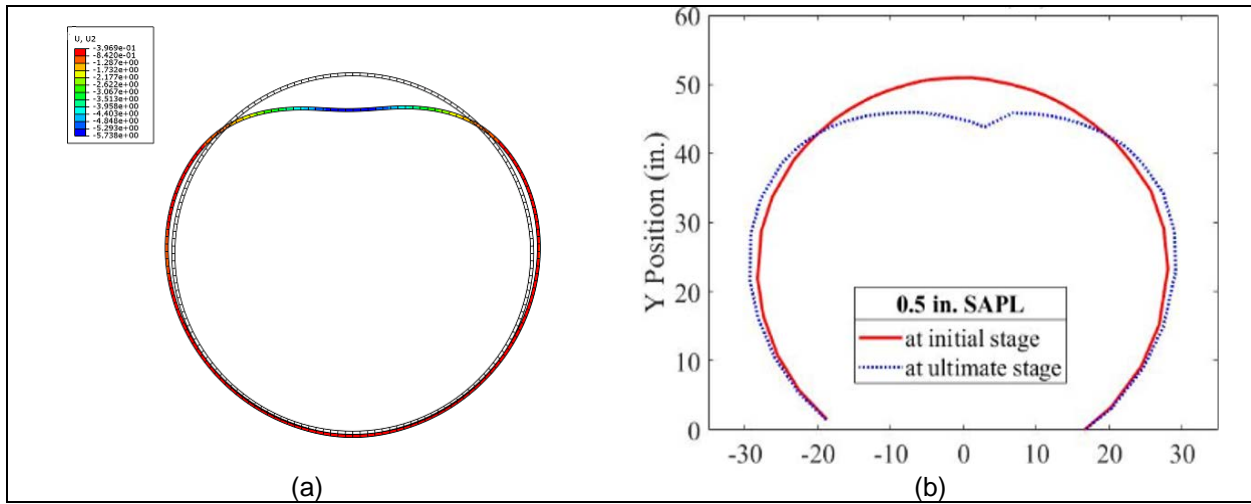


Figure 6-9 SAPL Deflection at the ultimate load at the crown of the pipe: (a) FEM results (Source: CUIRE FEM report), and (b) DIC results (0.5 in. SAPL).

The comparison of the soil box testing results and FEM results for the applied load versus displacement changes at the crown of the pipe are illustrated in Figure 6-10.

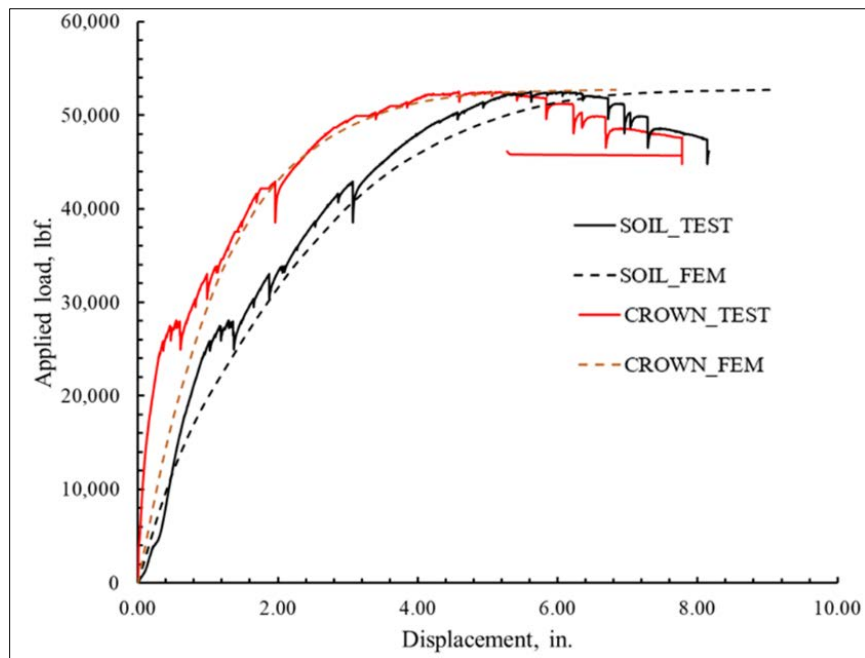


Figure 6-10 Load versus displacement – comparison of soil box testing and FEM results (0.5 in. SAPL).

The comparison of the load versus displacement plots obtained from the results of the 0.5 in. SAPL soil box testing and FEM are presented in Table 6-4.

Table 6-4 Load-displacement results – comparison of SAPL soil box testing and FEM (Source: CUIRE FEM report) at the time of first crack and ultimate load (0.5 in. SAPL).

Time Description	Initiation of 1 <sup>st</sup> crack (1 <sup>st</sup> plastic strain)			Ultimate Load		
	Test	FEM	Difference FEM vs. Test (%)	Test	FEM	Difference FEM vs. Test (%)
Crown Displacement (in.)	1.75	2.01	14.85% increase	4.43	5.08	14.67% increase
Soil Settlement (in.)	3.06	3.45	12.74% increase	5.61	7.17	27.81% increase
Load (kips) on the Soil Surface	42.78	43.11	1% increase	52.43	52.09	1% increase

The comparison of soil box testing results and FEM results for distributed pressure on top of the pipe versus displacement at the crown location is illustrated in Figure 6-11. The comparison of soil box testing results and FEM results for the applied load on the soil surface versus distributed pressure on top of the pipe at the middle cross section is illustrated in Figure 6-12.

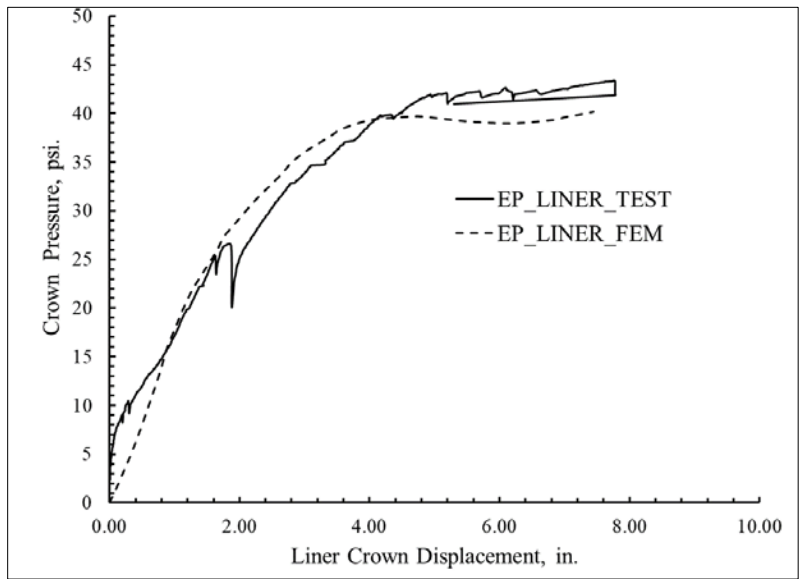


Figure 6-11 The comparison of soil box testing results and FEM (Source: CUIRE FEM report) results for distributed pressure on top of the pipe versus displacement at the crown location (0.5 in. SAPL).

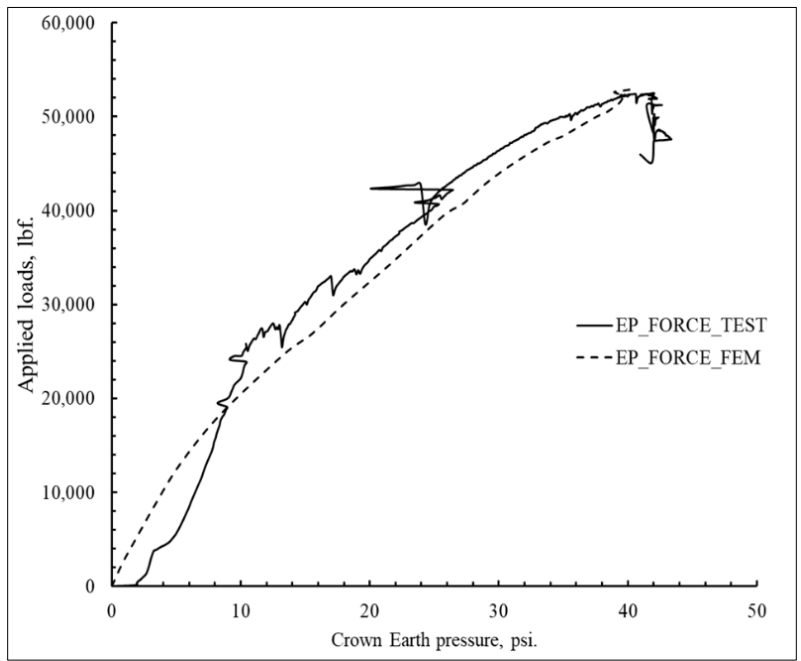


Figure 6-12 The comparison of soil box testing results and FEM (Source: CUIRE FEM report) results for the applied load on the soil surface versus distributed pressure on top of the pipe at the middle cross section (0.5 in. SAPL).

### 6.2.3 1.0 in. SAPL Renewed CMP Sample

In both SAPL soil box testing and the FEM simulation the first crack in the SAPL occurred at the crown location at the middle section of the pipe, as illustrated in Figure 6-13. In both soil box testing and FEM simulation the first crack (plastic strain) propagated longitudinally along the crown of the pipe.

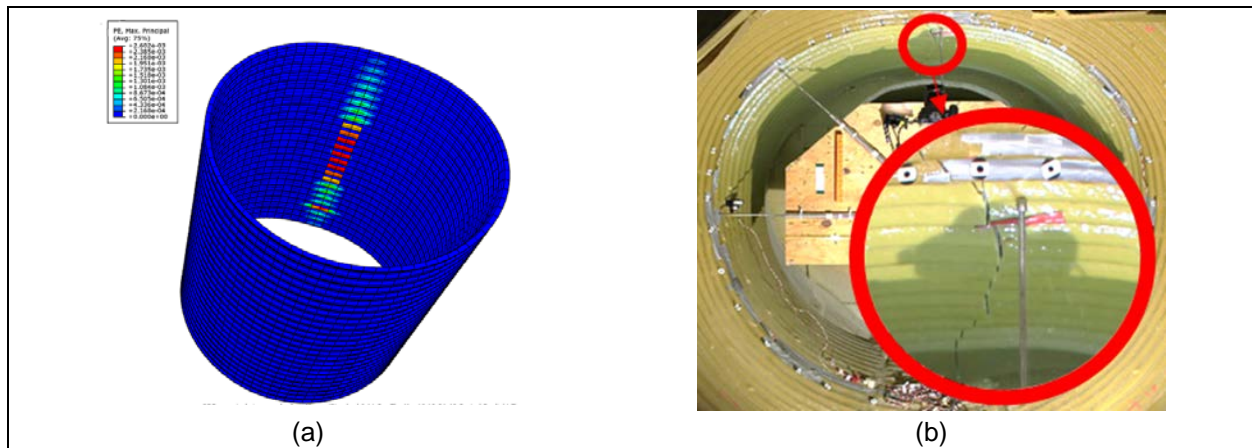


Figure 6-13 Occurrence of first plastic strain in 1.0 in. SAPL at the crown of the pipe: (a) FEM (Source: CUIRE FEM report), and (b) SAPL soil box testing results.

As the soil box testing results presented in Chapter 5 of this dissertation revealed, the initial crack at the crown of the pipe propagated longitudinally along the pipe and became a fracture at the ultimate load. The same pattern was predicted by the FEM simulation, as illustrated in Figure 6-14.

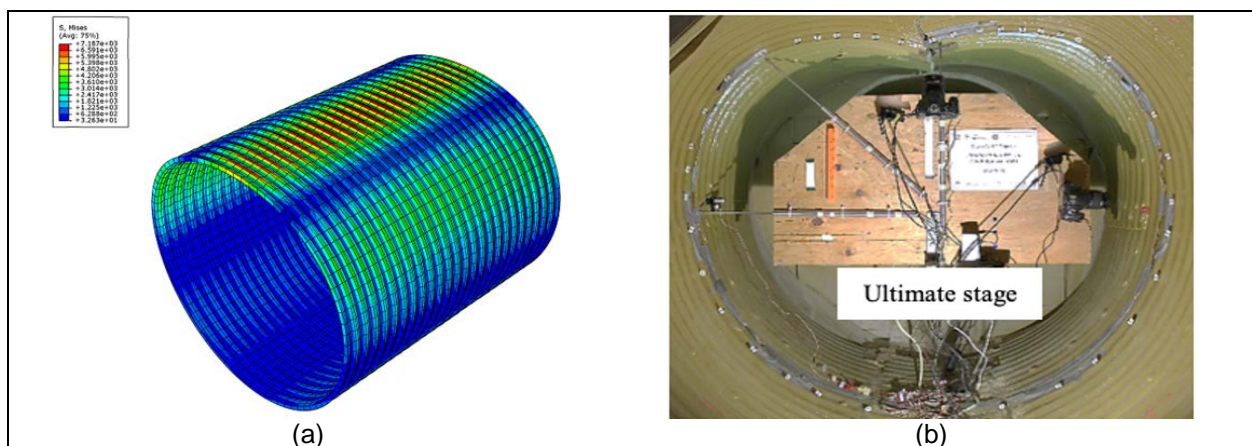


Figure 6-14 SAPL Ultimate load condition: (a) Von Mises stress around the SAPL (Source: CUIRE FEM report), and (b) crack propagation and fracture at the crown of the pipe (1.0 in. SAPL).

The pipe profiling of the 1.0 in. SAPL CMP renewed sample using DIC technique, presented in Chapter 5 of this dissertation, and the FEM results, showing the pipe deflection at the crown at the time ultimate load is illustrated in Figure 6-15.

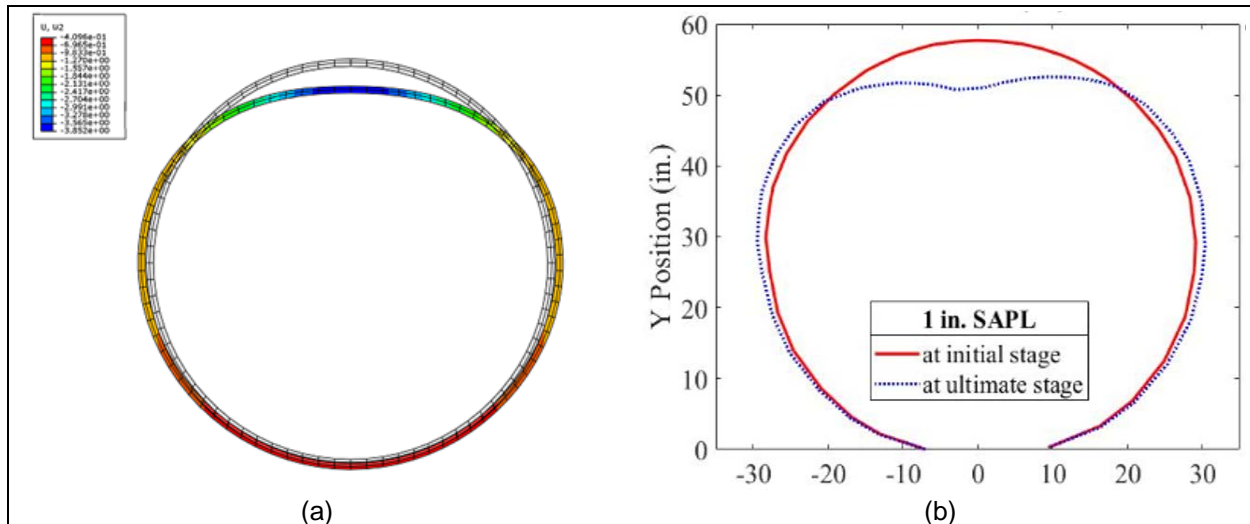


Figure 6-15 SAPL Deflection at the ultimate load at the crown of the pipe:

(a) FEM results (Source: CUIRE FEM report), and (b) DIC results (1.0 in. SAPL).

The comparison of the soil box testing results and FEM results for the applied load versus displacement changes at the crown of the pipe are illustrated in Figure 6-16. The comparison of the load versus displacement plots obtained from the results of the 1.0 in. SAPL soil box testing and FEM are presented in Table 6-5. The comparison of soil box testing results and FEM results for distributed pressure on top of the pipe versus displacement at the crown location is illustrated in Figure 6-17. The comparison of soil box testing results and FEM results for the applied load on the soil surface versus distributed pressure on top of the pipe at the middle cross section is illustrated in Figure 6-18.

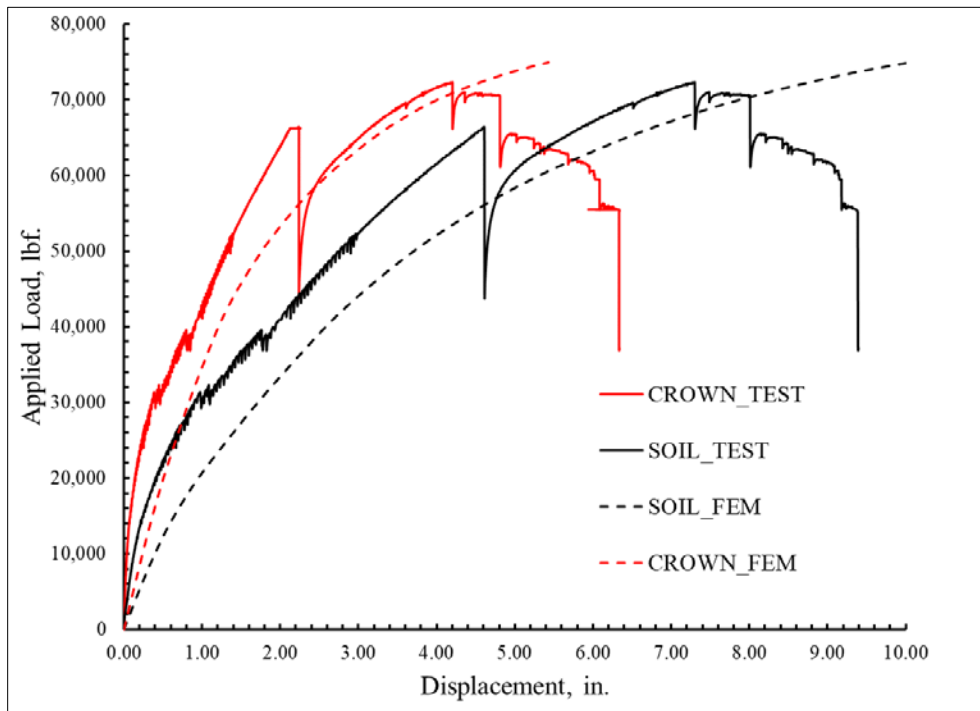


Figure 6-16 Load versus displacement – comparison of soil box testing results and FEM (Source: CUIRE FEM report) results (0.1 in. SAPL).

Table 6-5 Load-displacement results – comparison of SAPL soil box testing and FEM (Source: CUIRE FEM report) at the time of the first crack and the ultimate load (1.0 in. SAPL).

Time Description	Initiation of 1 <sup>st</sup> crack (1 <sup>st</sup> plastic strain)			Ultimate Load		
	Test	FEM	Difference FEM vs. Test (%)	Test	FEM	Difference FEM vs. Test (%)
Crown Displacement (in.)	2.12	3.05	43.86% increase	4.17	3.85	7.67% decrease
Soil Settlement (in.)	4.58	5.42	18.34% increase	7.27	8.0	10% increase
Load (kips) on the Soil Surface	66.26	64.97	2% increase	72.15	73.27	1.55% increase



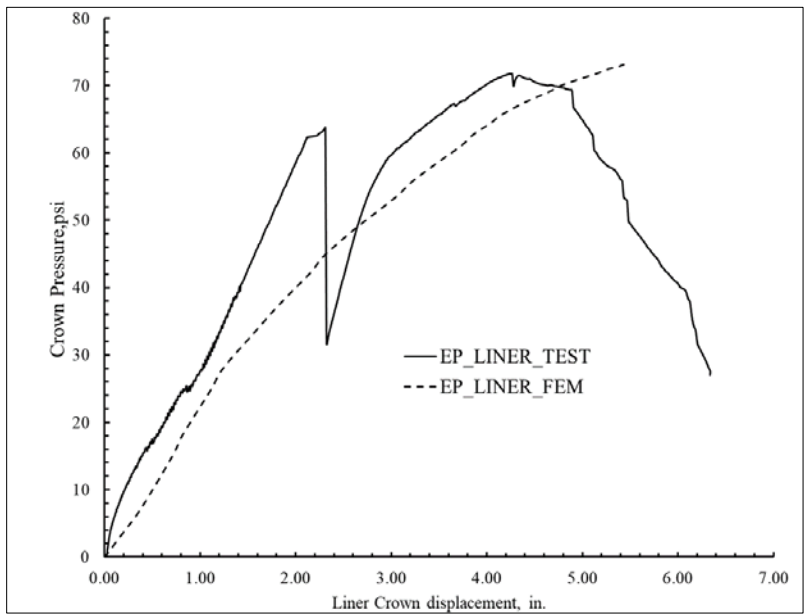


Figure 6-17 The comparison of soil box testing results and FEM (Source: CUIRE FEM report) results for distributed pressure on top of the pipe versus displacement at the crown location (1.0 in. SAPL).

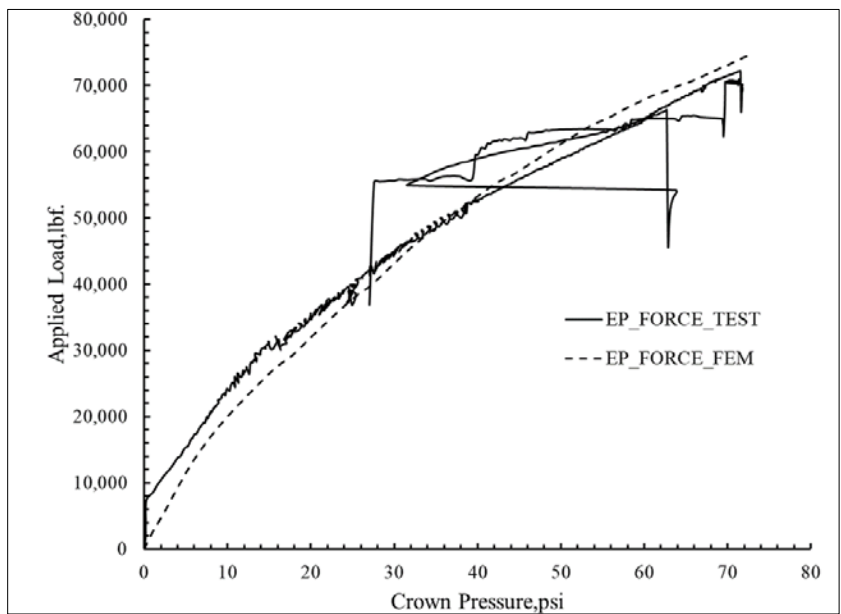


Figure 6-18 The comparison of soil box testing results and FEM (Source: CUIRE FEM report) results for the applied load on the soil surface versus distributed pressure on top of the pipe at the middle cross section (1.0 in. SAPL).

#### 6.2.4 FEM Simulation of 0.75, 1.5, and 2.0 in. SAPLs

FEM simulation of fully deteriorated invert circular CMPs renewed with 0.75, 1.5, and 2.0 in. of SAPLs showed that the first crack occurred at the crown location of the pipe same as the other tested thicknesses of SAPL, as illustrated in Figure 6-19.

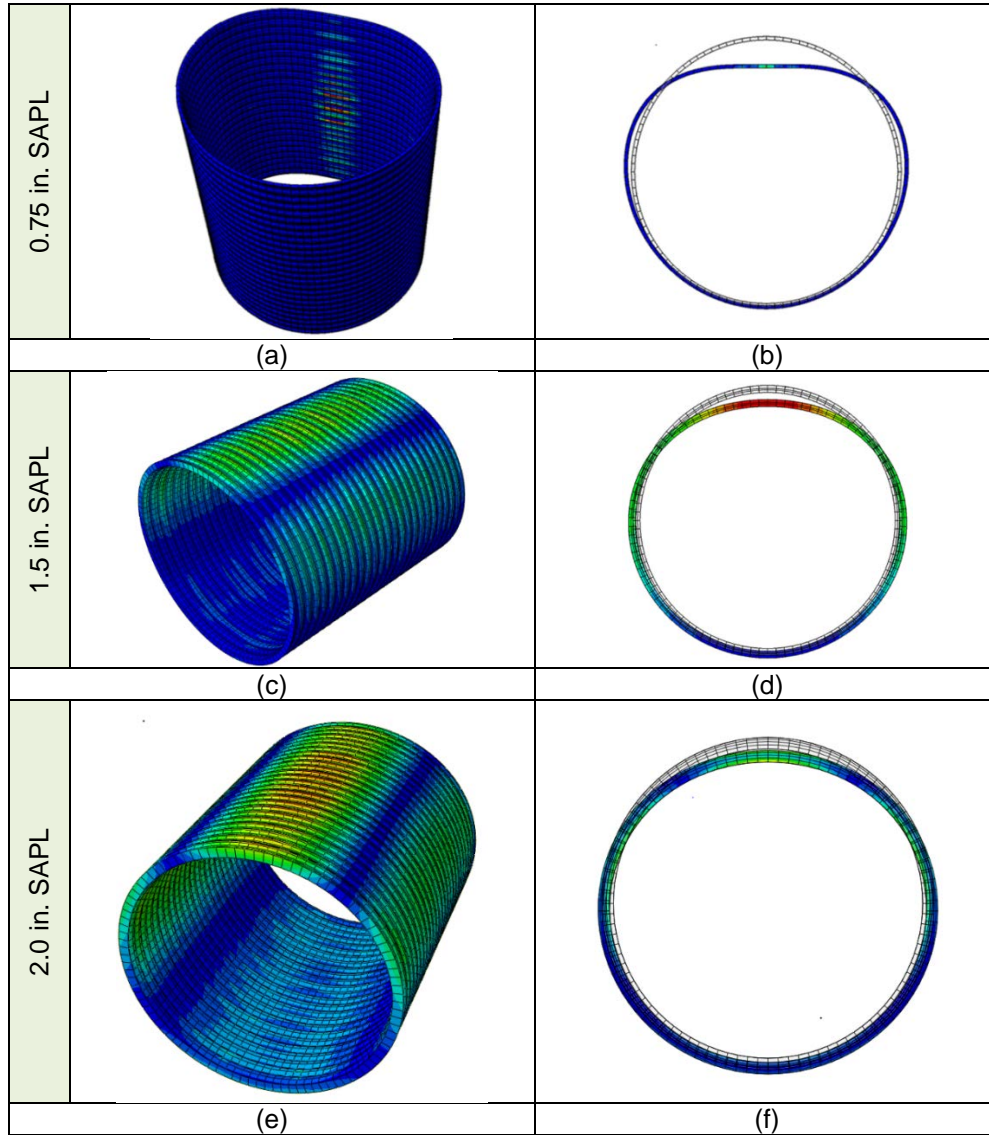
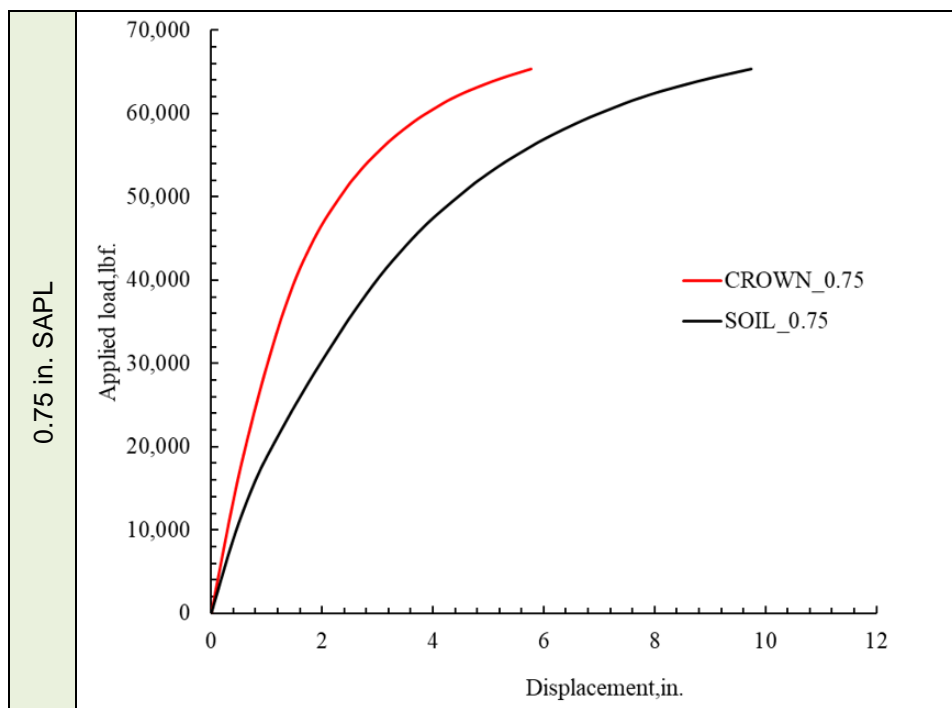


Figure 6-19 the fully deteriorated invert circular CMP renewed with SAPL: (a), (c) and (e) formation of the plastic strain at the crown of the pipe, and (b), (d) and (f) SAPL. Deflection at the crown of the pipe (Source: CUIRE FEM report).

The applied load, crown displacement and soil surface settlement at the time of first crack and the ultimate load for the simulated 0.75, 1.5, and 2.0 in. thicknesses of SAPL are listed in Table 6-6.

Table 6-6 FEM results for the simulated 0.75, 1.5, and 2.0 in. thicknesses of SAPL (Source: CUIRE FEM report).

Time Description	Initiation of 1 <sup>st</sup> crack (1 <sup>st</sup> plastic strain)			Ultimate Load		
	SAPL Thickness (in.)			SAPL Thickness (in.)		
	0.75	1.5	2.0	0.75	1.5	2.0
Crown Displacement (in.)	2.6	2.76	2.06	5.77	2.76	2.06
Soil Settlement (in.)	4.91	7.47	6.91	9.7	7.47	6.91
Load (kips) on the Soil Surface	52.47	78.98	80.50	65.37	78.98	80.50



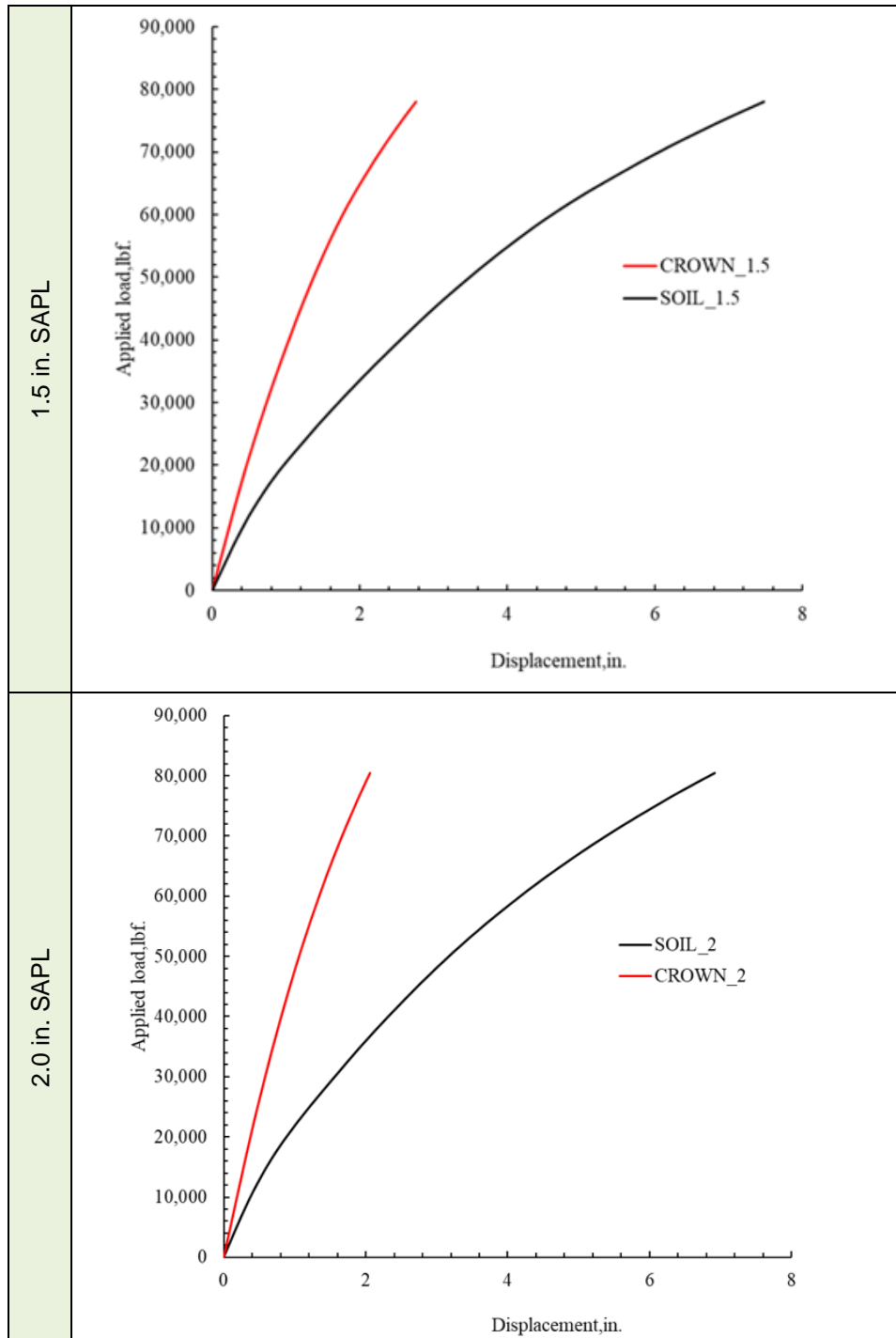


Figure 6-20 Load versus displacement – FEM results for 0.75, 1.5, and 2.0 in. SAPLs

(Source: CUIRE FEM report).

## 6.2.5 Comparison of Different SAPL Thicknesses Installed Inside the Fully Invert Deteriorated Circular CMPs

The comparison of applied load on top the soil surface versus displacement of SAPL at the crown at the middle section of the pipe for different SAPL thicknesses installed inside the fully deteriorated invert circular CMPs are illustrated in Figure 6-21.

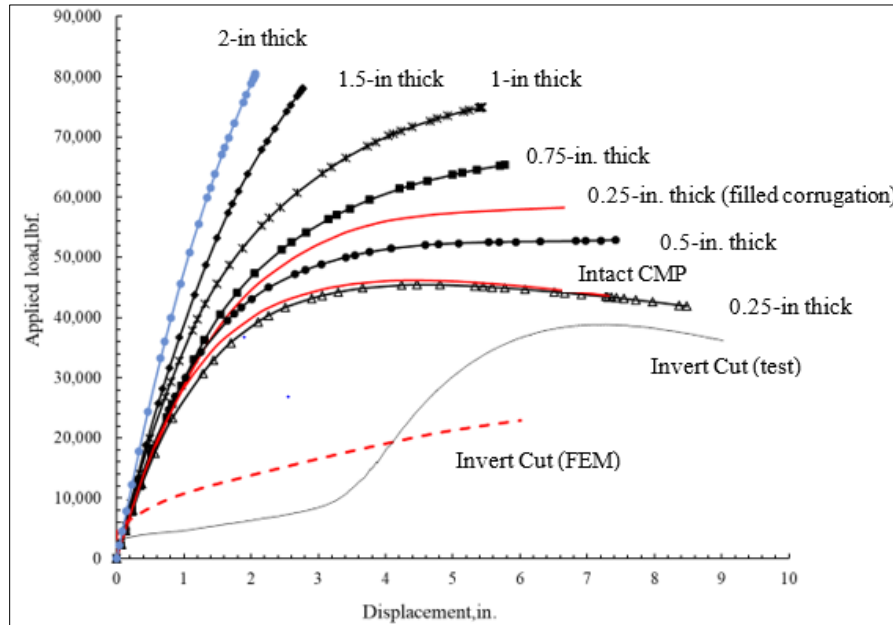


Figure 6-21 Load versus displacement plots – comparison of different SAPL thicknesses installed inside the fully deteriorated invert circular CMPs (Source of FEM: CUIRE FEM report).

## 6.3 Comparison of the Soil Box Testing Results Presented in Chapter 5 and FEM Results of Fully Deteriorated Invert Circular CMPs Renewed with Polymeric 0.5 SAPL.

### 6.3.1 0.25 in. SAPL Renewed CMP Sample

As it is explained in Chapter 5 of this dissertation, in all SAPL renewed soil box testing, the first crack occurred at the middle section of the pipe samples at the crown location. This crack was predicted in the FEM simulation as a plastic strain initiation at the same place. The deflection comparison of FEM simulation and soil box testing results for 0.25 in. SAPL in two stages of first crack and ultimate load is illustrated in Figure 6-22.

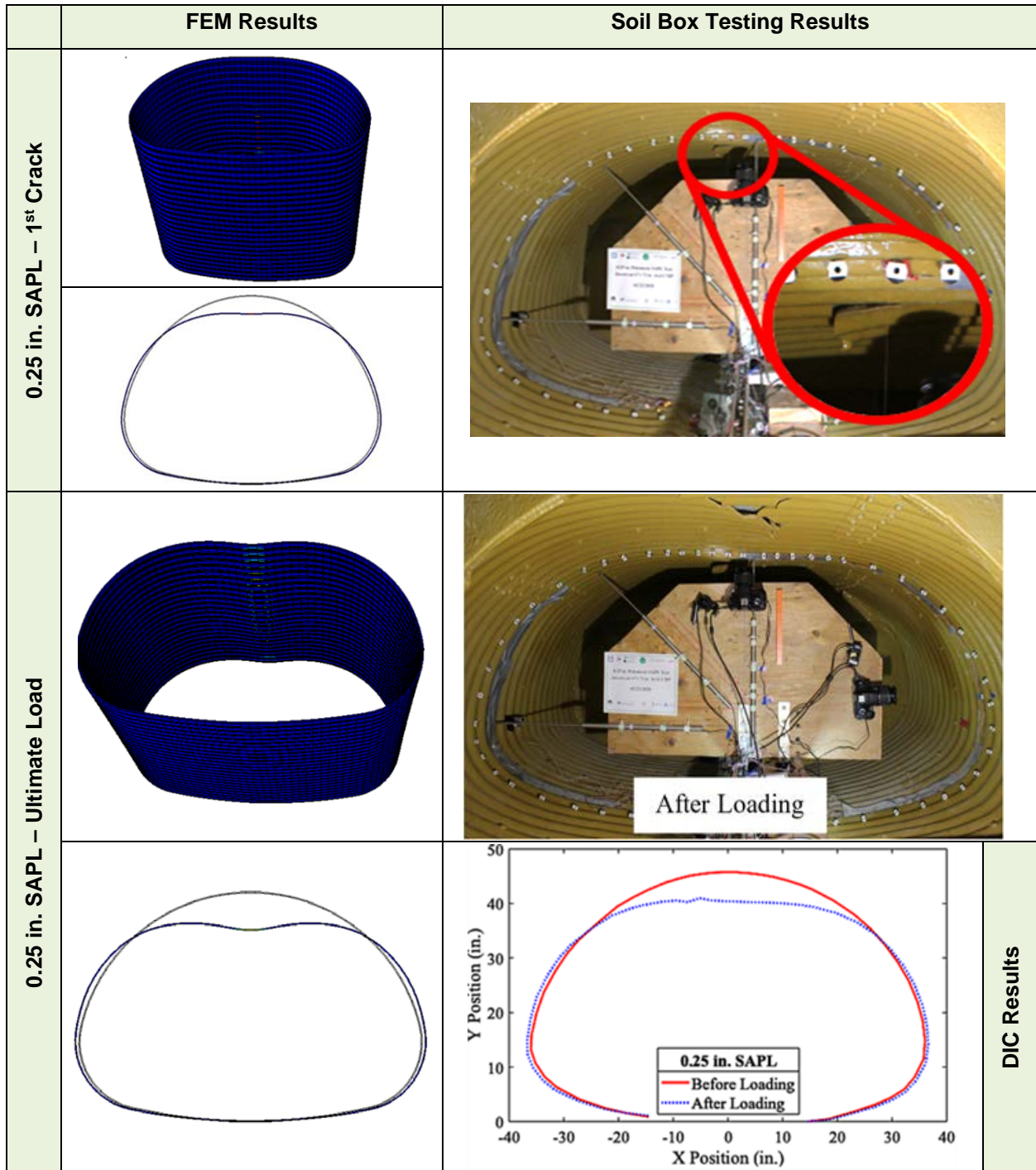


Figure 6-22 The deflection comparison soil box testing results and FEM (Source: CUIRE FEM report) for 0.25 in. SAPL, installed inside the fully deteriorated invert arch CMP, in two stages of first crack and ultimate load.

The initiated crack at the crown of the pipe propagated longitudinally and became a fracture at the ultimate load. Figure 6-23 illustrates the stress distribution concentrated on the soil below the load pad, hunch area and springlines of the arch CMP.

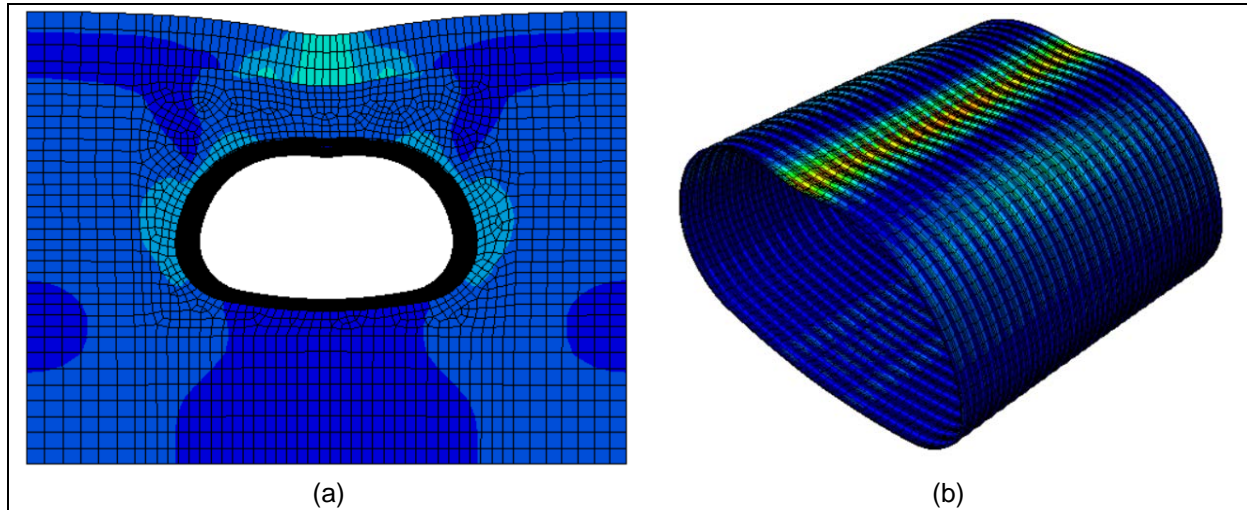


Figure 6-23 FEM results – stress distribution at the ultimate load for 0.25 in. SAPL:

(a) soil mass, and (b) SAPL (Source: CUIRE FEM report).

The load versus displacement changes in both SAPL soil box testing and FEM simulation had the same trend. However, the FEM simulation predicted higher loads by around 25% for the first crack and 10% for the ultimate stage of the 0.25 in. SAPL, as illustrated in Figure 6-24. The comparison of SAPL soil box testing and FEM results for the applied load and displacements at the time of the first crack and the ultimate load are presented in Table 6-7 for 0.25 in. SAPL.

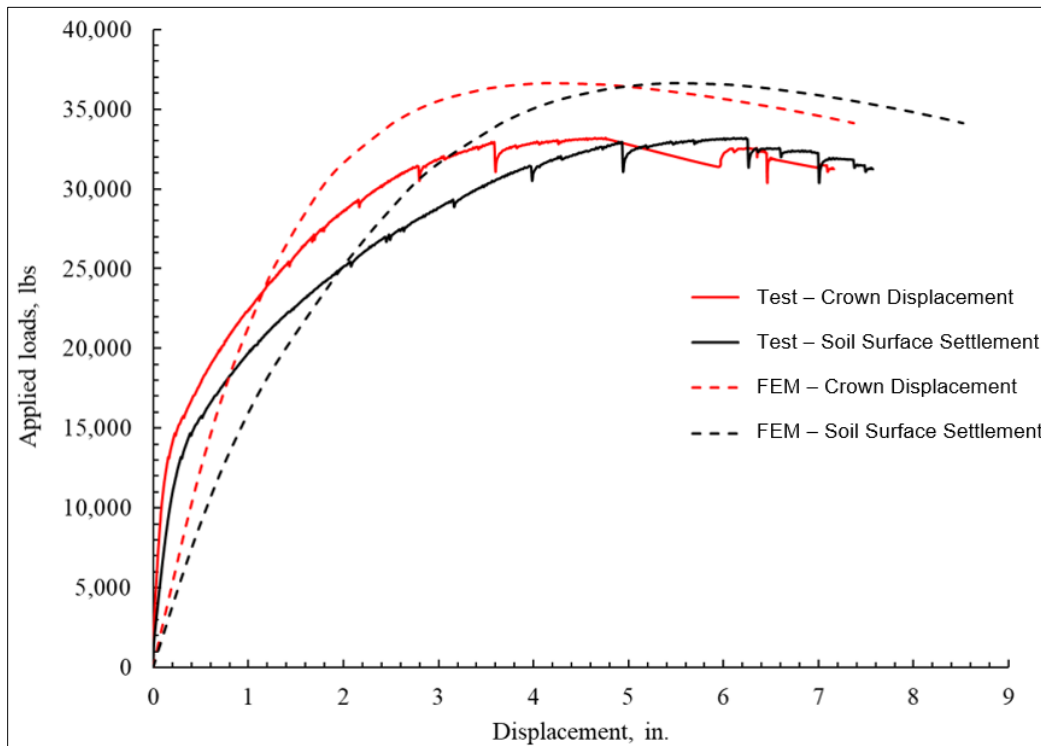


Figure 6-24 Load versus displacement – comparison of SAPL soil box testing and the FEM (Source: CUIRE FEM report) results for 0.25 in. SAPL installed inside the fully invert deteriorated arch CMP sample.

Table 6-7 Load-displacement results – comparison of SAPL soil box testing and FEM (Source: CUIRE FEM report) at the time of the first crack and the ultimate load (0.25 in. SAPL).

Description	Initiation of 1 <sup>st</sup> crack (1 <sup>st</sup> plastic strain)			Ultimate Load		
	Test	FEM	Difference FEM vs. Test (%)	Test	FEM	Difference FEM vs. Test (%)
Crown Displacement (in.)	2.18	3.82	75.22% increase	4.75	4.15	12.63% decrease
Soil Settlement (in.)	3.16	5.13	62.34% increase	6.24	5.48	12.18% decrease
Load (kips) on the Soil Surface	29.32	36.5	24.48% increase	33.2	36.61	10.27% increase



The comparison of the soil box testing results and FEM results for distributed pressure on top of the pipe versus displacement at the crown location is illustrated in Figure 6-25. The comparison of soil box testing results and FEM results for the applied load on the soil surface versus distributed pressure on top of the pipe at the middle cross section is illustrated in Figure 6-26.

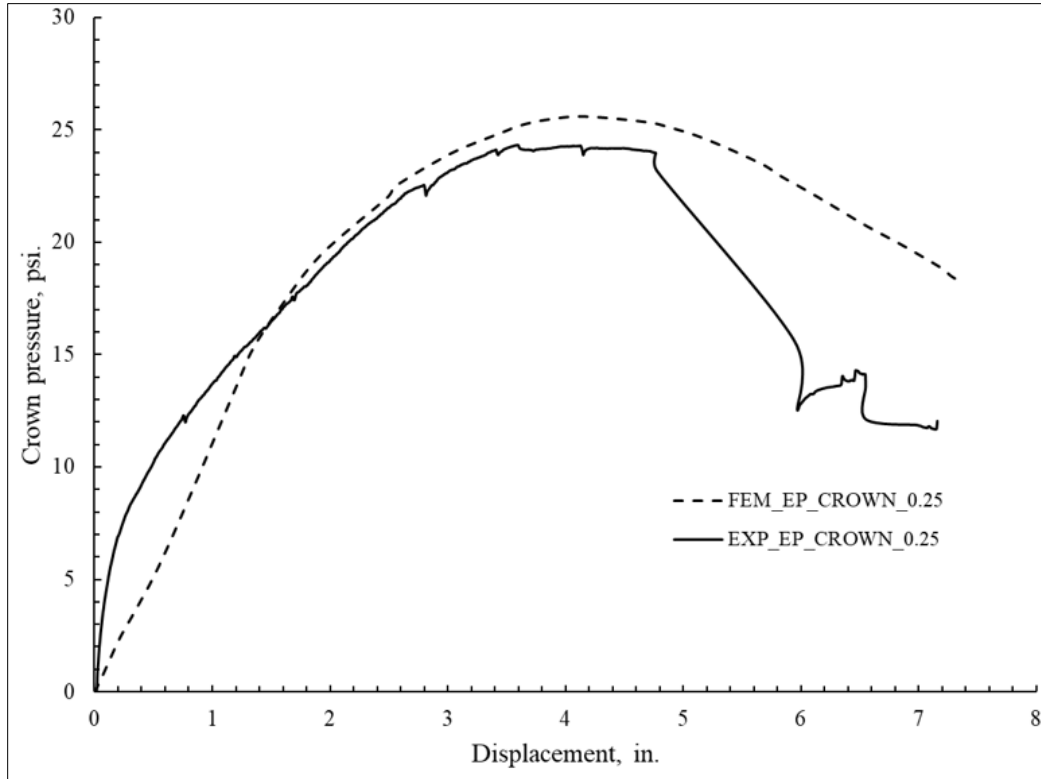


Figure 6-25 The comparison of soil box testing results and FEM (Source: CUIRE FEM report) results for distributed pressure on top of the pipe versus displacement at the crown location (0.25 in. SAPL).

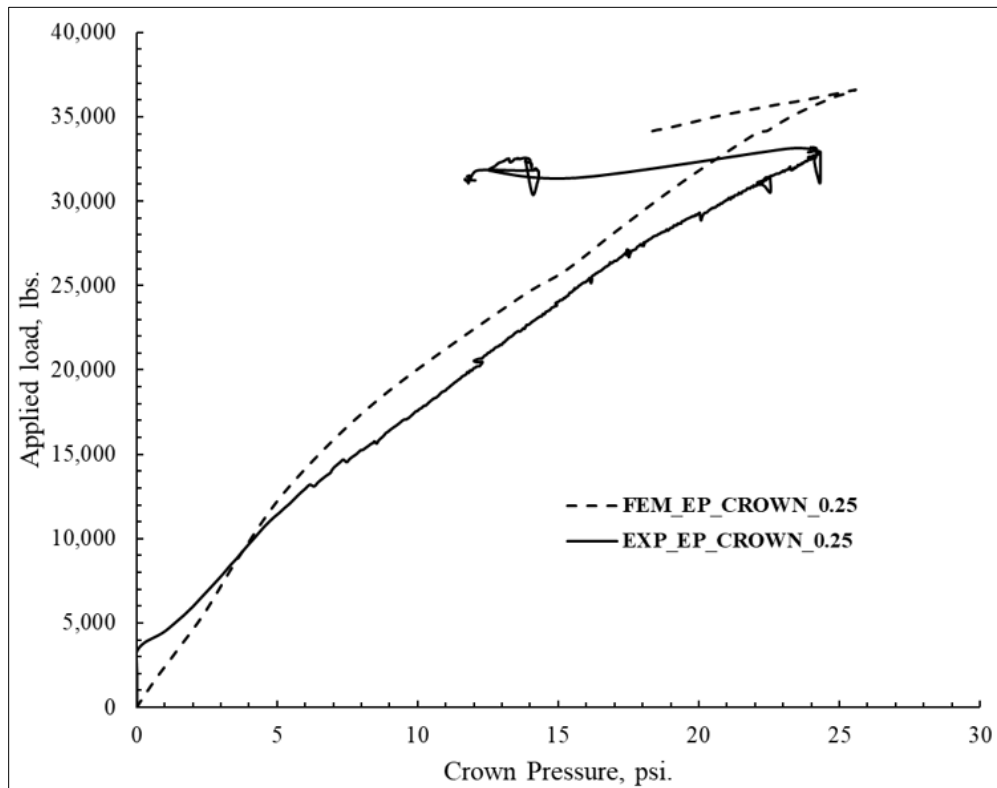


Figure 6-26 The comparison of soil box testing results and FEM (Source: CUIRE FEM report) results for the applied load on the soil surface versus distributed pressure on top of the pipe at the middle cross section (0.25 in. SAPL).

### 6.3.2 0.5 in. SAPL Renewed CMP Sample

In both SAPL soil box testing, as presented in Chapter 5 of this dissertation, and the FEM simulation the first crack in the SAPL occurred at the crown location at the middle section of the pipe. As it is discussed in Chapter 5, the initiated crack at the crown propagated longitudinally along the pipe and became a fracture at the ultimate load. The same pattern was predicted by the FEM simulation. The deflection comparison of soil box testing results and FEM for 0.5 in. SAPL in two stages of first crack and ultimate load is illustrated in Figure 6-27. The comparison of SAPL soil box testing and FEM results for the applied load and displacements at the time of the first crack and the ultimate load are presented in Table 6-8 for 0.5 in. SAPL.

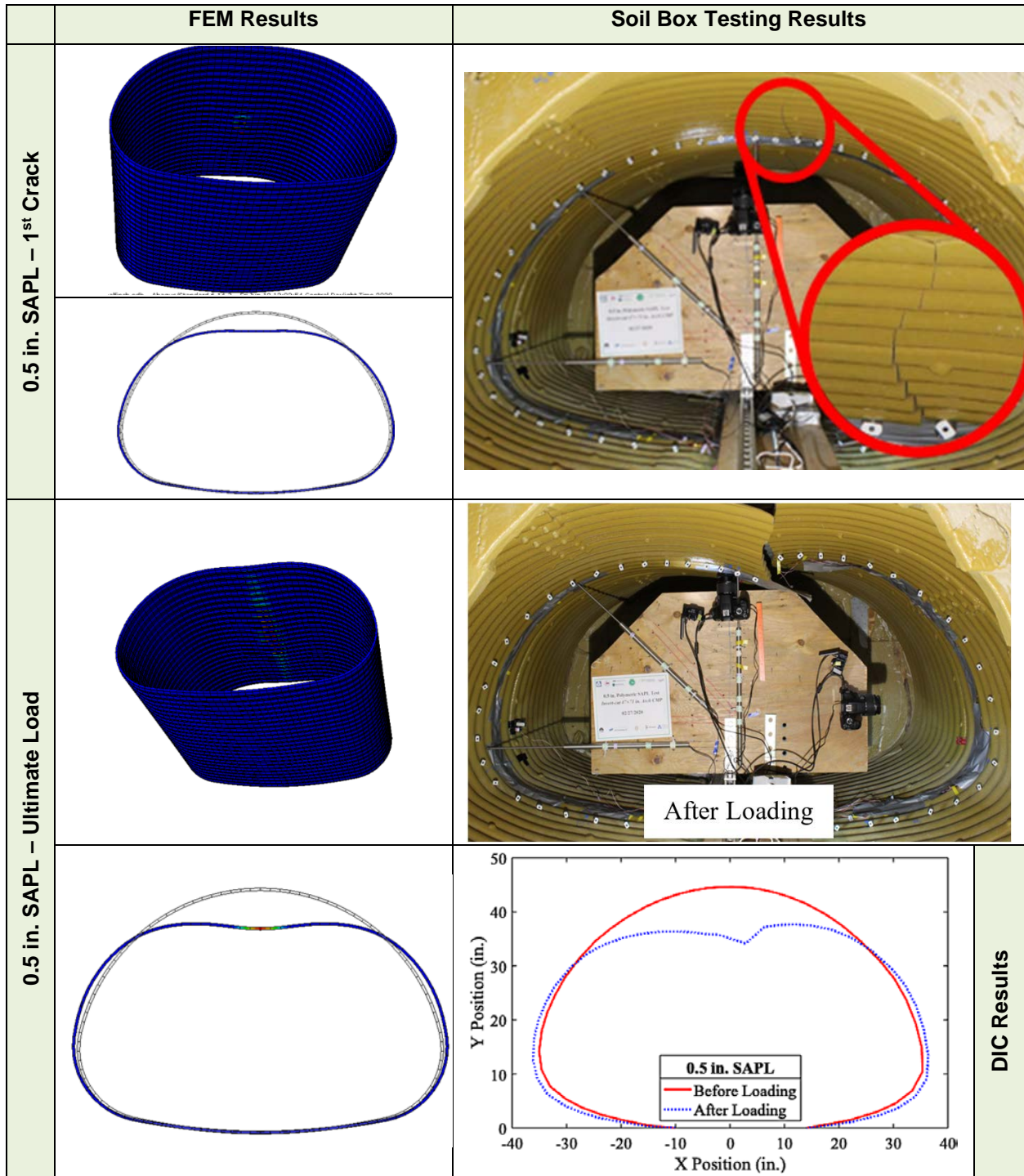


Figure 6-27 The deflection comparison of FEM simulation (Source: CUIRE FEM report) and soil box testing results for 0.25 in. SAPL, installed inside the fully deteriorated invert arch CMP, in two stages of first crack and ultimate load.

The load versus displacement changes in both SAPL soil box testing and FEM simulation had the same trend. However, the FEM simulation predicted higher loads for the first crack and the ultimate stage of the 0.5 in. SAPL, as illustrated in Figure 6-28. Although there is a big difference between the FEM prediction of the displacement and load and the SAPL soil box testing results at the time of the first crack, for the ultimate load, FEM predicted a load of 39.98 kips along with a crown displacement of 6.13 in. which are 12.24% and 21%, respectively, higher than the actual testing results obtained through soil box testing, as presented in Chapter 5 of this dissertation. The comparison of the soil box testing results and FEM results for distributed pressure on top of the pipe versus displacement at the crown location is illustrated in Figure 6-29. The comparison of soil box testing results and FEM results for the applied load on the soil surface versus distributed pressure on top of the pipe at the middle cross section is illustrated in Figure 6-30.

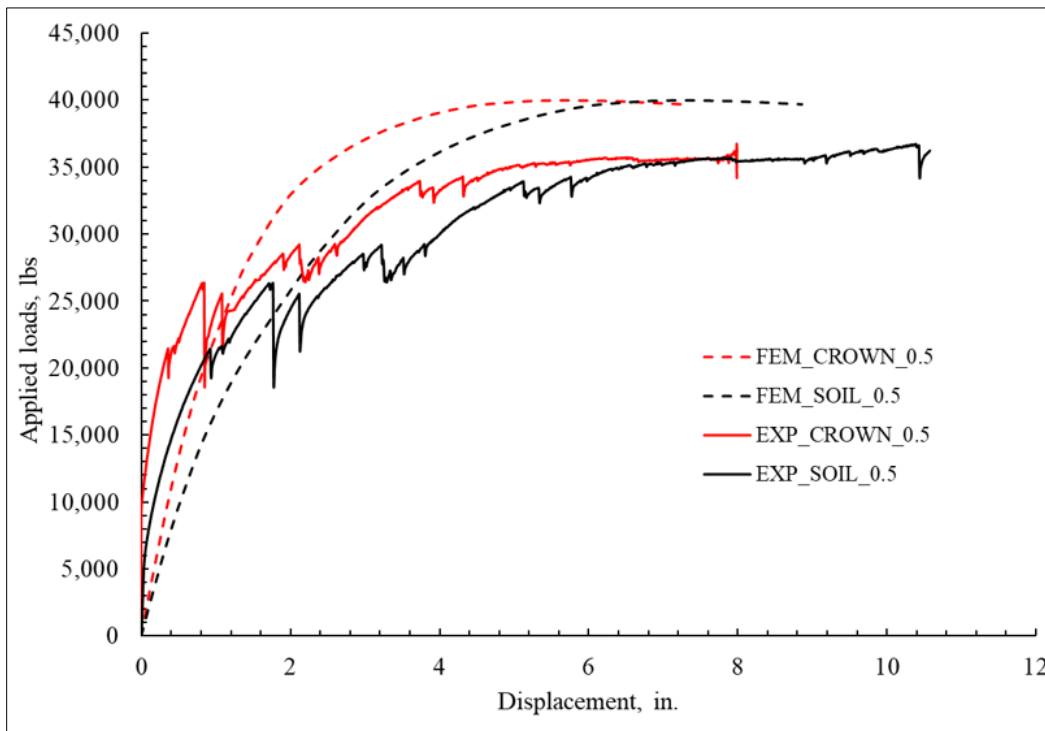


Figure 6-28 Load versus displacement – comparison of SAPL soil box testing and the FEM (Source:

CUIRE FEM report) results for 0.5 in. SAPL installed inside the fully

invert deteriorated arch CMP sample.

Table 6-8 Load-displacement results – comparison of SAPL soil box testing results and FEM (Source: CUIRE FEM report) results at the time of the first crack and the ultimate load (0.5 in. SAPL).

Time Description	Initiation of 1 <sup>st</sup> crack (1 <sup>st</sup> plastic strain)			Ultimate Load		
	Test	FEM	Difference FEM vs. Test (%)	Test	FEM	Difference FEM vs. Test (%)
Crown Displacement (in.)	0.83	4.57	450% increase	5.07	6.13	21% increase
Soil Settlement (in.)	1.77	6.13	246% increase	7.28	6.98	4.12% decrease
Load (kips) on the Soil Surface	26.27	39.68	51% increase	35.62	39.98	12.24% increase

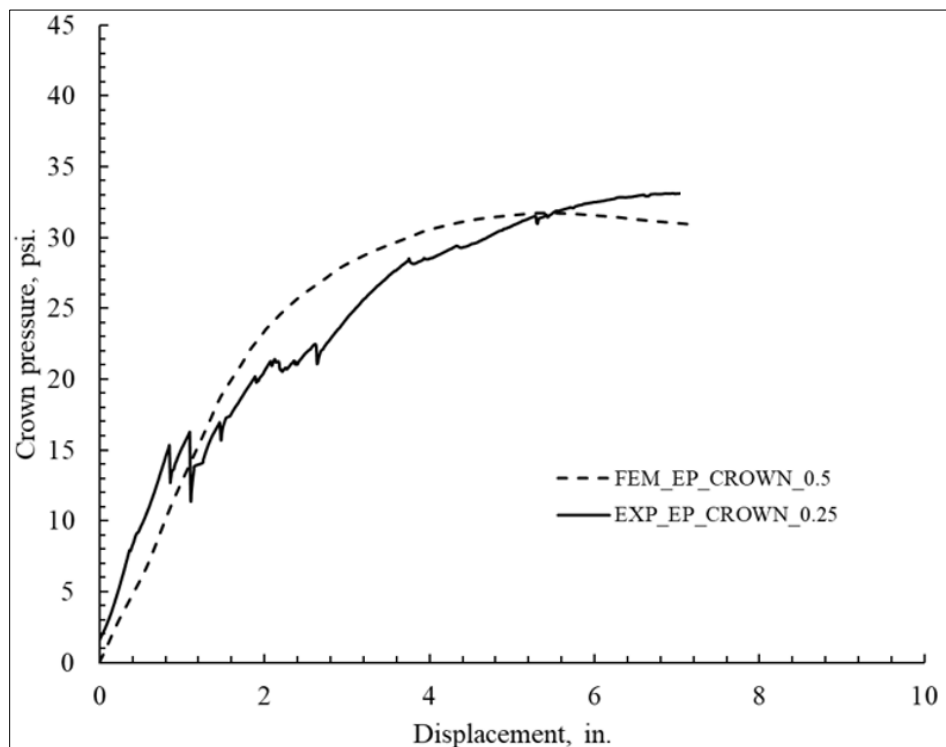


Figure 6-29 The comparison of soil box testing results and FEM (Source: CUIRE FEM report) results for distributed pressure on top of the pipe versus displacement at the crown location (0.5 in. SAPL).

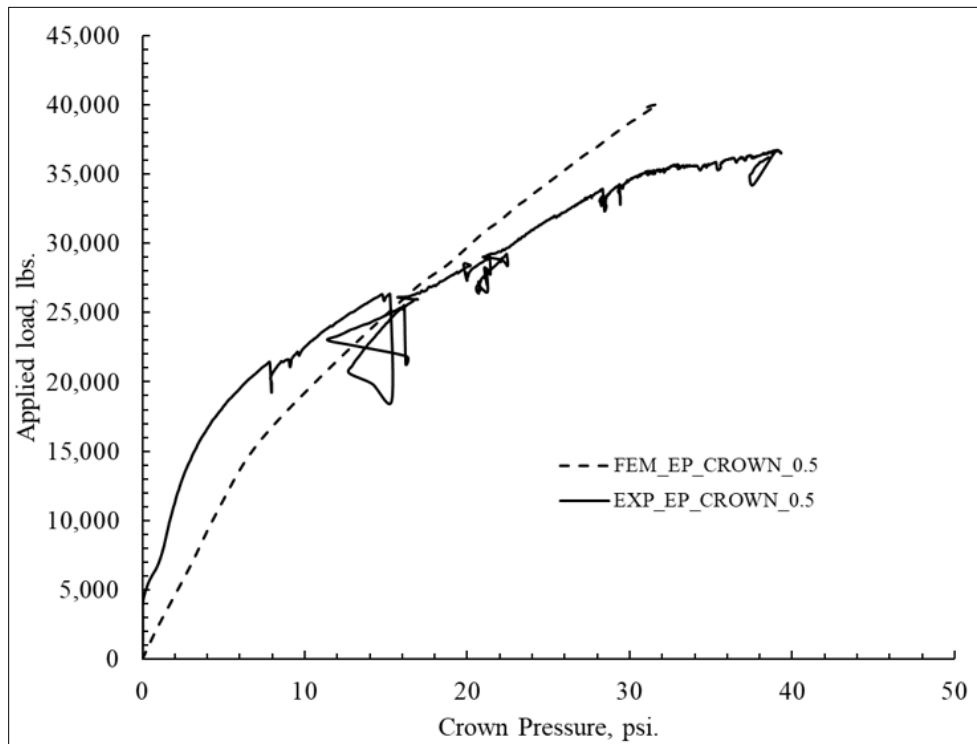


Figure 6-30 The comparison of soil box testing results and FEM (Source: CUIRE FEM report) results for the applied load on the soil surface versus distributed pressure on top of the pipe at the middle cross section (0.5 in. SAPL).

### 6.3.3 1.0 in. SAPL Renewed CMP Sample

The deflection comparison of FEM simulation and soil box testing results for 1.0 in. SAPL in two stages of first crack and ultimate load is illustrated in Figure 6-31. The comparison of SAPL soil box testing results and FEM for the applied load and displacements at the time of the first crack and the ultimate load are presented in Table 6-9 for 1.0 in. SAPL.

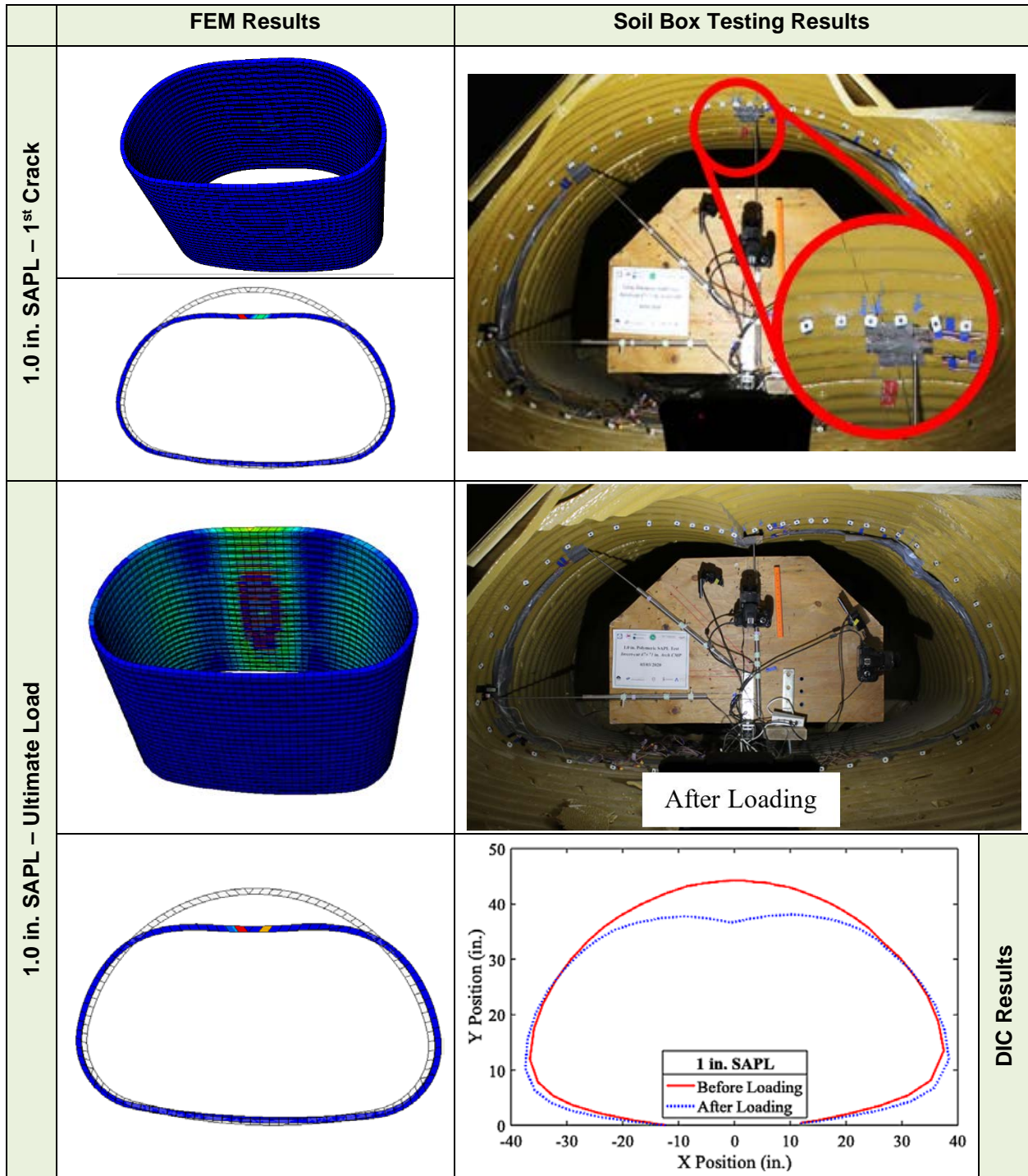


Figure 6-31 The deflection comparison of FEM simulation (Source: CUIRE FEM report) and soil box testing results for 0.25 in. SAPL, installed inside the fully deteriorated invert arch CMP, in two stages of first crack and ultimate load.

The load versus displacement changes in both SAPL soil box testing and FEM simulation had the same trend. However, the FEM simulation predicted higher loads for the first crack and the ultimate stage of the 1.0 in. SAPL, as illustrated in Figure 6-32. Although there is a big difference between the FEM prediction of the displacement and load and the SAPL soil box testing results at the time of the first crack, for the ultimate load FEM predicted a load of 54.78 kips along with 7.2 in. of crown displacement which is 2.08% and 38.46%, respectively, more than the actual soil box testing results presented in Chapter 5 of this dissertation.

Table 6-9 Load-displacement results – comparison of SAPL soil box testing results and FEM (Source: CUIRE FEM report) results at the time of the first crack and the ultimate load (1.0 in. SAPL).

Time Description	Initiation of 1 <sup>st</sup> crack (1 <sup>st</sup> plastic strain)			Ultimate Load		
	Test	FEM	Difference FEM vs. Test (%)	Test	FEM	Difference FEM vs. Test (%)
Crown Displacement (in.)	0.32	6.08	1800% increase	5.2	7.2	38.46% increase
Soil Settlement (in.)	1.22	8.3	580% increase	7.71	9.66	25.29% increase
Load (kips) on the Soil Surface	41.08	53.3	29.75% increase	53.66	54.78	2.08% increase

The comparison of soil box testing results and FEM results for the applied load on the soil surface versus distributed pressure on top of the pipe at the middle cross section is illustrated in Figure 6-32. The comparison of the soil box testing results and FEM results for distributed pressure on top of the pipe versus displacement at the crown location is illustrated in Figure 6-33. The comparison of the soil box testing results and FEM results for the applied load versus the distributed pressure on top of the pipe at the crown location is illustrated in Figure 6-34.



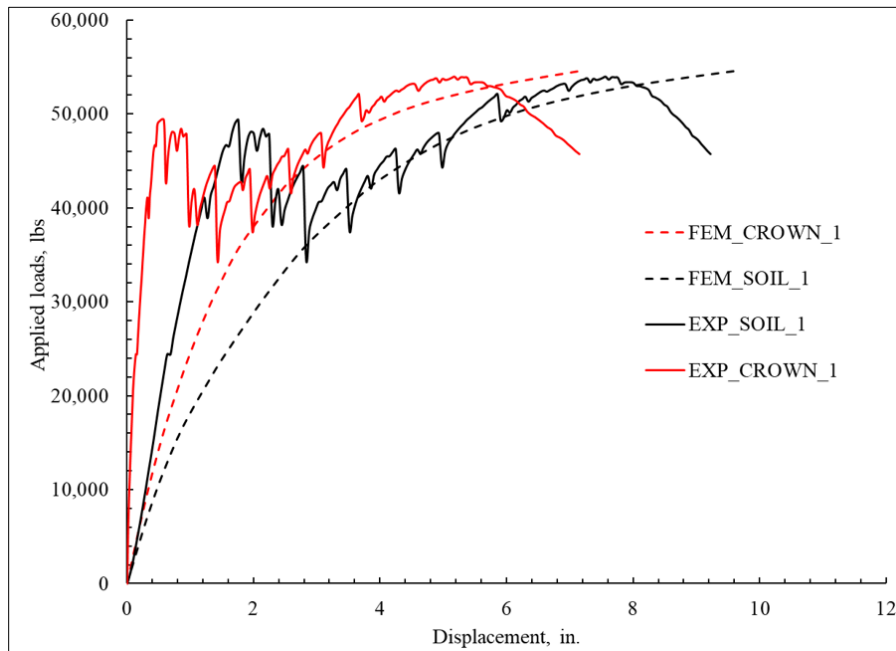


Figure 6-32 Load versus displacement – comparison of SAPL soil box testing and the FEM (Source: CUIRE FEM report) results for 1.0 in. SAPL installed inside the fully invert deteriorated arch CMP sample.

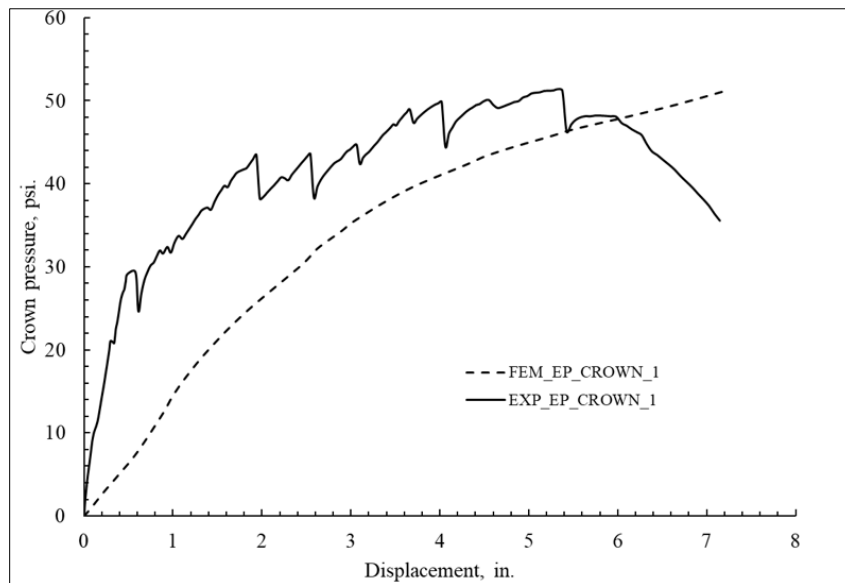


Figure 6-33 The comparison of soil box testing results and FEM (Source: CUIRE FEM report) results for distributed pressure on top of the pipe versus displacement at the crown location (1.0 in. SAPL).

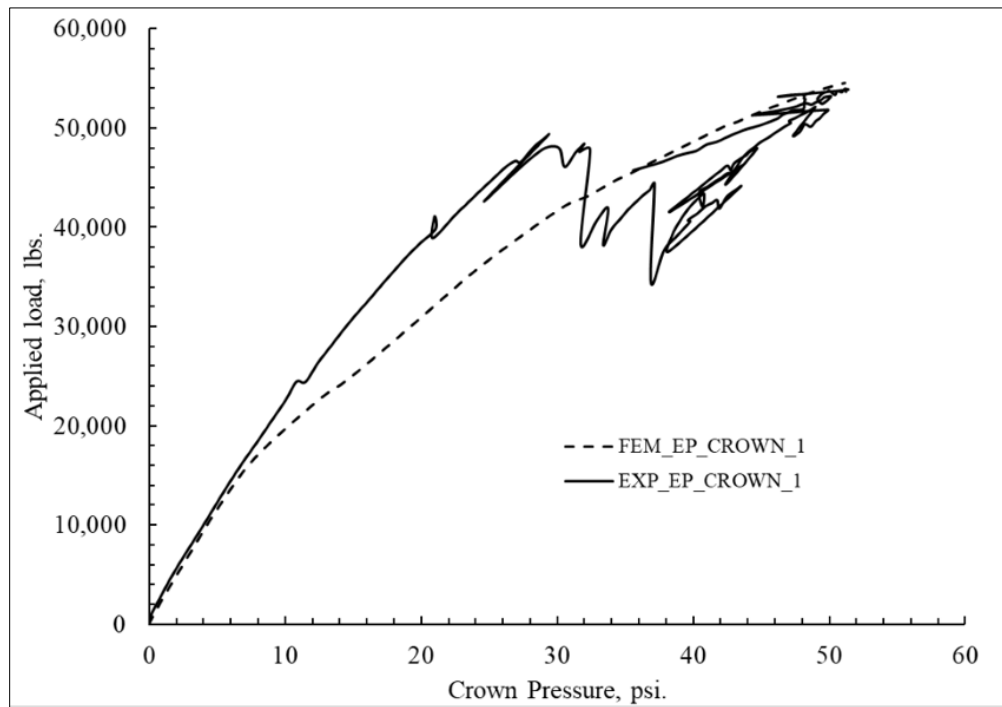


Figure 6-34 The comparison of soil box testing results and FEM (Source: CUIRE FEM report) results for the applied load on the soil surface versus distributed pressure on top of the pipe at the middle cross section (1.0 in. SAPL).

#### 6.3.4 FEM Simulation of 0.75, 1.5, and 2.0 in. SAPLs

FEM simulation of the fully deteriorated invert arch CMP samples renewed with 0.75, 1.5, and 2.0 in. of SAPLs showed that the first crack occurred at the crown location of the pipe, as illustrated in Figure 6-35. The applied load, crown displacement and soil surface settlement at the time of ultimate load for the simulated 0.75, 1.5, and 2.0 in. thicknesses of SAPL are listed in Table 6-10. The FEM results for the applied load versus displacement for 0.75, 1.5 and 2 in. SAPLs are plotted in Figure 6-36.

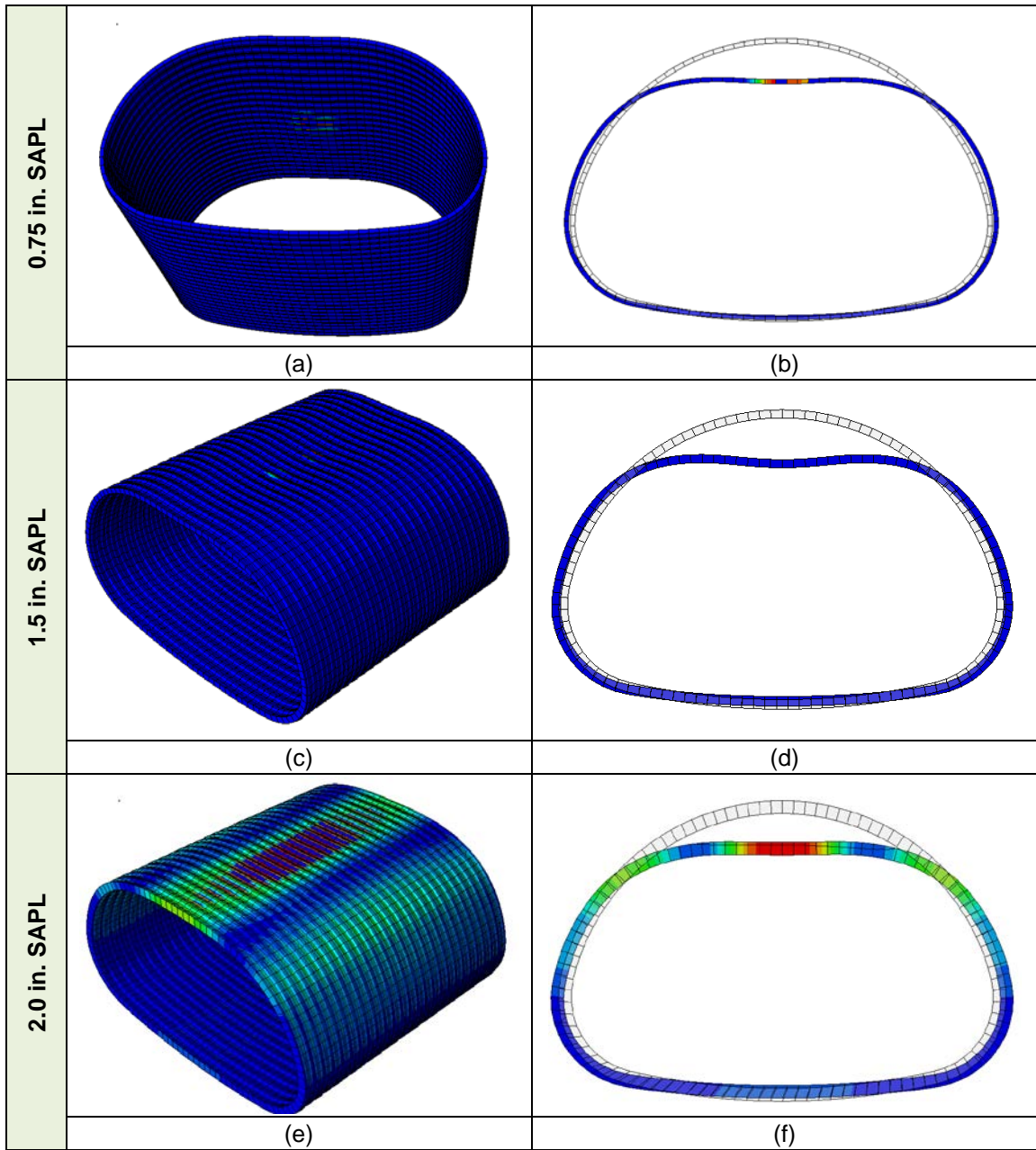
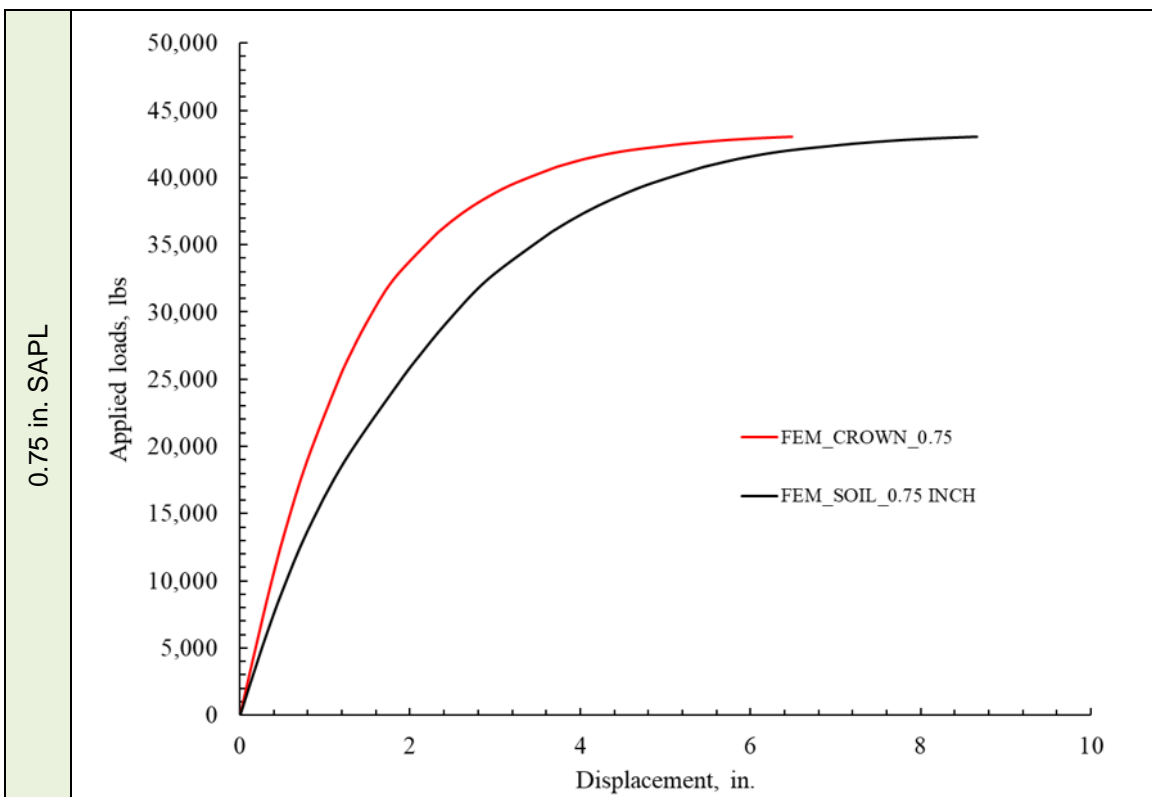


Figure 6-35 the fully deteriorated invert arch CMP samples renewed with SAPL: (a), (c) and (e) formation of the plastic strain at the crown of the pipe, and (b), (d) and (f) SAPL deflection at the crown of the pipe (Source: CUIRE FEM report).

Table 6-10 FEM results for the simulated 0.75, 1.5, and 2.0 in. thicknesses of SAPL (Source: CUIRE FEM report).

Description	Time		Ultimate Load		
			SAPL Thickness (in.)		
	0.75	1.5	2.0		
Crown Displacement (in.)	6.54	7.5	6.11		
Soil Settlement (in.)	8.66	9.66	9.66		
Load (kips) on the Soil Surface	43.08	52	66.87		



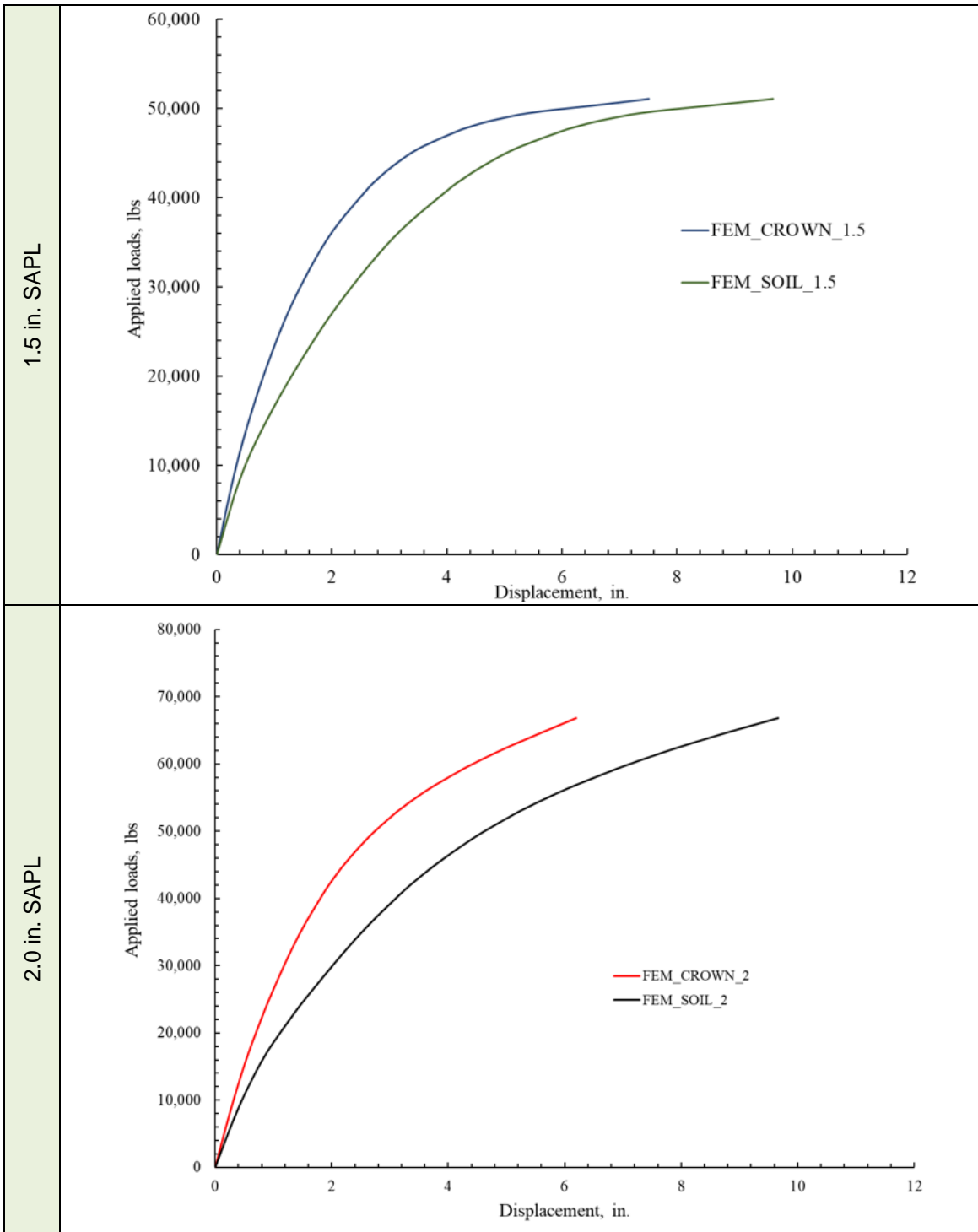


Figure 6-36 Load versus displacement – FEM results for 0.75, 1.5, and 2.0 in. SAPLs

(Source: CUIRE FEM report).

### 6.3.5 Comparison of Different SAPL Thicknesses Installed Inside the Fully Invert Deteriorated Circular CMPs

The comparison of applied load on top the soil surface versus displacement of SAPL at the crown at the middle section of the pipe for different SAPL thicknesses installed inside the fully deteriorated invert circular CMPs are illustrated in Figure 6-37.

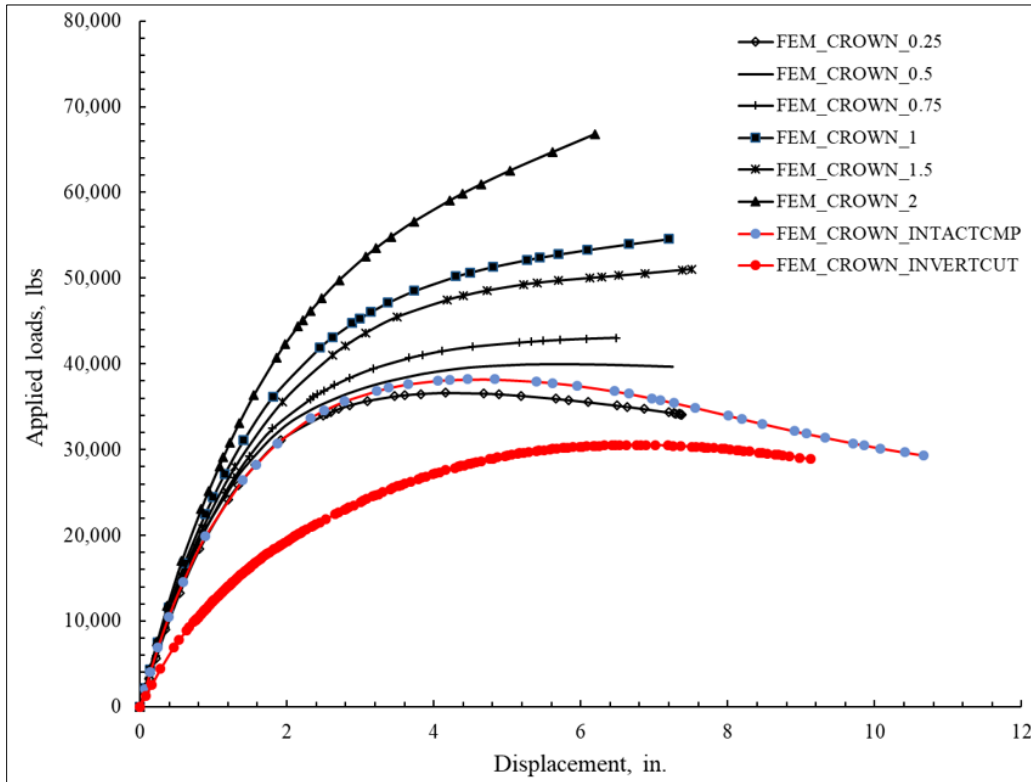


Figure 6-37 Load versus displacement plots – comparison of different SAPL thicknesses installed inside the fully deteriorated invert arch CMP samples (Source: CUIRE FEM report).

## 6.4 Chapter Summary

The results of SAPL soil box testing for both circular and arch shapes of fully deteriorated invert CMPs, presented in Chapter 5 of this dissertation, were compared with the FEM results conducted by Raut (2020) at CUIRE. The implicit FEM simulation could not predict the post-cracking behavior of the SAPL. However, the FEM simulations could approximately predict the first crack and ultimate loads of the examined SAPL thicknesses in the laboratory soil box testing. The FEM model was not used to simulate

different soil conditions, pipe sample sizes, embedment types, and depth of cover, as these parameters were out of scope of this dissertation.

The comparison of soil box testing results and FEM are summarized at the following sections:

#### **6.4.1 Fully Deteriorated Invert Circular CMP Renewed with SAPL**

- FEM simulations of fully deteriorated invert circular CMPs renewed with different thicknesses of polymeric SAPL could predict the load versus displacement changes, pressure versus displacement changes, the first crack load and the ultimate load with around 10-30% difference from the soil box testing results, presented in Chapter 5.
- Both SAPL soil box testing and FEM simulation showed that increasing the thickness of SAPL resulted in an increase in the rigidity of the samples and a reduction in the crown displacement.

#### **6.4.2 Fully Deteriorated Invert Arch CMP Renewed with SAPL**

- FEM simulations of the fully deteriorated invert arch CMP samples renewed with different thicknesses of polymeric SAPL could predict the ultimate load and displacements with around 10-20% difference from the soil box testing results, presented in Chapter 5. The initial formed cracks in the SAPLs prior to the loading could not be accurately predicted by the FEM.
- The SAPL attachment to the end walls due to the over spraying was not simulated by the FEM.
- The SAPL soil box testing had a stiffer response compared with the FEM simulation.
- From both SAPL soil box testing, presented in Chapter 5, and the FEM simulation, it was observed a higher load carrying capacity for the SAPL renewed circular CMPs compared with the SAPL renewed arch CMP samples.

#### **6.4.3 FEM Limitations**

- The implicit FEM simulation was unable to predict the SAPL post-cracking behavior.
- Using a simple elastic-plastic model for simulation of the brittle SAPL material, the FEM could not predict the immediate load drop at the time of first crack initiation.

## Chapter 7

### Development of a Design Methodology

#### 7.1 Existing Rehabilitation/Renewal Lining Design Theory

Design of a liner material, as a pipeline renewal application, is affected by its relationship to the host pipe which, in turn, is acting in concert with the surrounding soil and to the above applied surface live loads, or to the external hydrostatic pressure when the pipe is below the phreatic surface.

Table 7-1 presents a list of existing design theories to calculate the critical buckling pressure on a flexible pipe (liner) that were discussed in detail in Chapter 2. The applicability of all the listed theories for the design of SAPL is discussed and examined in this chapter.

Table 7-1 Existing design equations and theories to calculate the critical buckling pressure on flexible pipes.

Potential Equations	Equation	Applicability for SAPL	Rational
ASTM F1216-Partially Deteriorated Condition	$P_w = \frac{2KE_L}{(1-\nu^2)} \times \frac{1}{(DR-1)^3} \times \frac{C}{N}$	Not Applicable	Designed just for Hydrostatic Pressure
Timoshenko and Gere (1961)	$P_{cr} = \frac{3EI}{(1-\nu^2)R^3}$	Not Applicable	Designed just for Hydrostatic Pressure
ASTM F1216-Fully Deteriorated Condition	$q_t = \frac{1}{N} [32R_w B' E'_s \cdot C (E_L I / D^3)]^{1/2}$	Maybe	Designed for all Superimposed Loads
AWWA C950	$P = \left( 0.593 \frac{R_w E_s EI}{0.149 r^3} \right)^{1/2}$	Maybe	Designed for all Superimposed Loads
G.H. Bryan (1888)	$P_{cr} = \frac{2E}{(1-\nu^2)} \left( \frac{t}{D} \right)^3$	Not Applicable	Designed just for Hydrostatic Pressure
Glock (1977)	$P_{cr} = \frac{E}{1-\nu^2} \left( \frac{t}{D} \right)^{2.2}$	Not Applicable	Designed just for Hydrostatic Pressure
Bresse (1866)	$P_{cr} = \frac{3EI}{R^3}$	Not Applicable	Designed just for Hydrostatic Pressure



As this table presents, the ASTM F1216 design equation for partially deteriorated pipe condition (F1216-16 2016), the Timoshenko and Gere (1961), the G.H. Bryan (1888), the Glock (1977) and the Bresse (1866) theories are not applicable to be checked against the SAPL soil box testing results. These equations can design a liner to withstand the hydrostatic pressure in a partially deteriorated condition. While the conducted soil box testing in this dissertation was a simulation of a fully deteriorated pipe condition in the absence of host pipe ring stiffness.

### 7.1.1 Vehicle and Earth Loads for Liner Designs

The first step in the design process is to accurately estimate the vehicular and earth loads applied on the renewed pipe after completion of the liner installation. For traffic parallel to the span, culverts shall be analyzed for a single loaded lane with the single lane multiple presence factor. For traffic Perpendicular to the culvert span, analysis shall include consideration of multiple lane loadings with appropriate multiple presence factors (*AASHTO LRFD Bridge Design Specifications 2020*).

According to the AASHTO LRFD Bridge Design Specifications, the loads from truck wheel pairs on the ground surface attenuate with depth based on a Live Load Distribution Factor (LLDF) for concrete pipes of 1.15 (for a cover depth of 2.0 feet or less) to 1.75 for pipes 8 feet in diameter and larger. For all other pipe materials, it recommends 1.15 for coarse grained soils (SC1 and SC2) and 1.00 in other backfill materials, as listed in Table 7-2.

Table 7-2 Live load distribution factor for buried structures (*AASHTO LRFD Bridge Design Specifications 2020*).

Structure Type	LLDF Transverse or Parallel to Span
Concrete Pipe with fill depth 2.0 ft or greater	1.15 for pipe diameters of 2.0 ft or less 1.75 for pipe diameters of 8.0 ft or greater Linearly interpolate for LLDF between these limits
All other culverts and buried structures	1.15

As the depth of cover on the pipe increases the load widths increase. The standard axle has a distance of 72 in. between the wheels (center to center). The depth at which load from the wheels begins

to interact is known as the  $H_{int}$ . For live load distribution transverse to culvert spans, the wheel/axle load interaction depth  $H_{int-t}$  shall be determined as:

$$H_{int} = \frac{S_w \frac{W_t}{12} \frac{0.06D_j}{12}}{LLDF} \quad \text{Eq. 7-1}$$

in which:

- where,  $H < H_{int-t}$ :

$$W_w = \frac{W_t}{12} + LLDF (H) + 0.06 \frac{D_i}{12} \quad \text{Eq. 7-2}$$

- where,  $H \geq H_{int-t}$ :

$$W_w = \frac{W_t}{12} + S_w + LLDF (H) + 0.06 \frac{D_i}{12} \quad \text{Eq. 7-3}$$

For live load distribution parallel to culvert span, the wheel/axle load interaction depth  $H_{int-p}$  shall be determined as:

$$H_{int-p} = \frac{S_a \frac{l_t}{12}}{LLDF} \quad \text{Eq. 7-4}$$

in which:

- where,  $H < H_{int-p}$ :

$$l_w = \frac{l_t}{12} + LLDF (H) \quad \text{Eq. 7-5}$$

- where,  $H \geq H_{int-p}$ :

$$l_w = \frac{l_t}{12} + S_a + LLDF (H) \quad \text{Eq. 7-6}$$

where,

$A_{LL}$  = rectangular area at depth  $H$  (ft<sup>2</sup>),

$l_w$  = live load patch length at depth  $H$  (ft),

$w_w$  = live load patch width at depth  $H$  (ft),

$H_{int-t}$  = wheel interaction depth transverse to culvert span (ft),

$s_w$  = wheel spacing, 6.0 ft,

$w_t$  = tire patch width, 20 (in.),

$D_i$  = inside diameter or clear span of the culvert (in.),  
 $LLDF$  = live load distribution factor as specified in Table 7-2,  
 $H$  = depth of fill over culvert (ft),  
 $H_{int-p}$  = axle interaction depth parallel to culvert span (ft),  
 $s_a$  = axle spacing (ft),  
 $l$  = tire patch length (in.) = 10 in.

For traffic crossing perpendicular to the alignment of the culvert, which applies to vast majority of highway culverts, using Article 3.6.1.2.6b of the ASSHTO LRFD Bridge Design Manual, live load calculations are made considering a single-axle truck travelling perpendicular to the pipe (parallel to the span) on an unpaved surface or a roadway with a flexible pavement as shown below (equation 35). The live load vertical crown pressure shall be determined as Eq. 7-7.

$$P_L = \frac{P \left(1 + \frac{IM}{100}\right) (m)}{A_{LL}} \quad \text{Eq. 7-7}$$

where,

$P_L$  = live load vertical crown pressure (ksf)

$P$  = live load applied at surface on all interacting wheels (kip).  $P = 16$  kip for AASHTO H20 truck.

$IM$  = dynamic load allowance,

$m$  = multiple presence factor specified in Eq. 7-8, typically equal to 1.2,

$A_{LL}$  = rectangular area at depth  $H$  (ft<sup>2</sup>).

$$IM = 33(1.0 - 0.125D_E) \geq 0\% \quad \text{Eq. 7-8}$$

where,

$D_E$  = the minimum depth of earth cover above the structure (ft).

According to the AASHTO LRFD Bridge Specifications article 3.6.1.2.6a, for single span culverts, the effects of live load may be neglected where the depth of fill (cover) to the top of the pipe is more than 8.0 feet and the spread of the load exceeds the span length. For multiple span culverts, the effects may be neglected where the depth of fill exceeds the distance between inside faces of end walls.

Further, since lining is taking place in an existing pipe with an existing pavement structure in place, it is important to note that rigid pavements are known to dramatically reduce any live load effects on buried pipes (American Concrete Pipe Association 1987).

In calculating the earth loads to be supported by the liner it should be noted that before the culvert is lined, the earth loads are already being supported by the existing deteriorated structure. Therefore, it may be excessively conservative to design liners in deeply buried culverts (those more than two diameters from the ground surface) to support the full weight of the overlying soil (i.e. soil prism load). In fact, some researchers suggest that no earth loads need to be considered when designing the liner (Gumbel 1998). However, this approach is only reasonable if there is no subsequent deterioration of the culvert structure and/or the soil surrounding it during the service life of the lining, which could result in some of the earth loads reaching the liner. For tunnel design, it is known that the maximum amount of ground that can come to bear on the tunnel structure is limited to an overburden depth of two culvert pipe diameters, since stresses coming from further overhead tend to be redistributed around the tunnel opening. Therefore, the maximum earth load that the liner is likely to experience over its service life,  $P_E$ , is assumed to be as Eq. 7-9.

$$P_E = \left( \frac{\delta_{soil}}{144} \right) \cdot (H_{net}) \quad \text{Eq. 7-9}$$

where,

$P_E$  = earth load acting on the horizontal soil plane at the top of the pipe (psi),

$\delta_{soil}$  = soil cover unit weight (pcf)

$H_{net}$  = the actual cover depth or 2.0 times Diameter of the Liner, whichever is the smaller value (ft.).

## 7.2 Design of Liner Thickness Using Polymeric SAPL Materials

According to ASHTO LRFD Bridge Design Specifications, Article 12.5.1, buried structures shall be designed by appropriate methods to resist load combinations for the service limit state and the strength limit state. For service limit state the polymeric liner structure would be evaluated for the critical buckling pressure.

Any proposed design methodology for a flexible polymeric material to produce a pipe within a pipe to be fully structural on its own requires recognizing the current state of the stresses in the existing soil-

structure interaction system, the differences in the types of loading that can come onto the new pipe within a pipe, and the pipe within a pipe's load response behavior.

The potential SAPL design equations presented in Table 7-1 were checked against the results obtained from the SAPL soil box testing. Curve fitting was conducted on the experimental results using the presented base equation model presented in this table and the comparisons are illustrated in Figure 7-8.

### **7.2.1. CIPP Design Equations for Fully Deteriorated Pipe Condition**

The CIPP design equation for a fully deteriorated pipe condition is presented in section 2.5.1.2 of this dissertation and is given in this chapter by Eq. 7-10. All the parameters of this equation are explained in detail in section 2.5.1.2. This equation is checked against the results obtained from the SAPL soil box testing and the conducted curve fitting is illustrated in Figure 7-8. From the results of soil box testing, the applied pressure on the SAPL at the crown of the pipe at time of first crack is used to be compared with the  $q_t$  calculated by Eq. 7-10.

$$q_t = \frac{1}{N} [32R_w B' E_s' C (E_L I / D^3)]^{1/2} \quad \text{Eq. 7-10}$$

As Figure 7-8 depicts, it is observed that this equation cannot predict the critical buckling pressure on SAPL.

### **7.2.2 AWWA C950 Design Equations**

The AWWA C950 design equations, Eq. 7-11, presented in section 2.5.1.2 of this dissertation, is the origin of the CIPP design equation in a fully deteriorated pipe condition. Hence, the AWWA C950 equation was checked against the results obtained from the soil box testing, and the conducted curve fitting is illustrated in Figure 7-8. All the parameters of the Eq. 7-11 are explained in section 2.5.1.2. From the results of soil box testing, the applied pressure on the SAPL at the crown of the pipe at time of first crack is used to be compared with the  $q_t$  calculated by Eq. 7-11.

$$P = \left( 0.593 \frac{R_w E_s E I}{0.149 r^3} \right)^{1/2} \quad \text{Eq. 7-11}$$

As Figure 7-8 depicts, it is observed that this equation cannot predict the critical buckling pressure on the SAPL.

### 7.2.3 Modified CIPP Design Equations for Fully Deteriorated Pipe Condition

#### 7.2.3.1. Calculation of the Moment of Inertia

For the CIPP design equation, in both partially and fully deteriorated pipe conditions, the moment of inertia ( $I$ ) in this formula is defined as  $t^3/12$  which is applicable to a rectangular section. However, the moment of inertia for a corrugated plate, as illustrated in Figure 7-1, is given by the Eq. 7-12 (El-Atrouzy 1969).

$$I = C_1 \cdot b \cdot d^2 \cdot t \quad \text{Eq. 7-12}$$

where,

$b$  = width of the corrugated sheet (not the developed width), in.,

$d$  = depth of corrugation, in.,

$t$  = thickness of the sheet (gauge), in.,

$$C_1 = \frac{2}{15} \left[ 1 + \frac{8}{3} \left( \frac{1}{K} \right)^2 \right], \text{ a constant,}$$

$$K = \frac{e}{d},$$

$e$  = pitch of corrugation (distance from ridge to ridge), in.

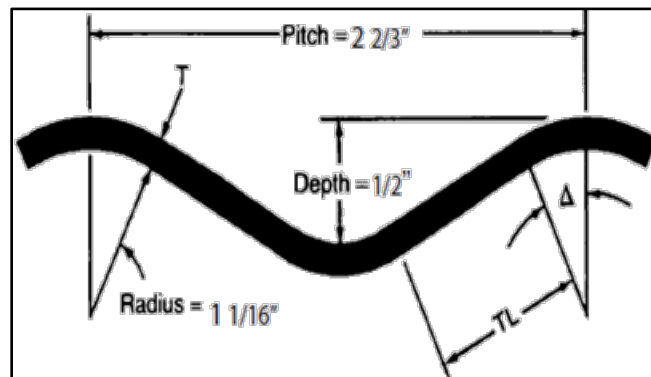


Figure 7-1 Details of corrugated metal pipe for calculation of the moment of inertia ( $I$ ).

Hence, the moment of inertia for the SAPL was calculated using the Eq. 7-12 and the ( $I$ ) value for the tested SAPL thicknesses of 0.25, 0.5 and 1.0 in. are presented in Table 7-3.

Table 7-3 SAPL moment of inertia for the tested SAPL thicknesses.

<b>t = SAPL Thickness (in.)</b>	<b>I = Moment of Inertia (in.<sup>3</sup>/12)</b>
0.25	0.0091125
0.5	0.018225
0.75	0.0273375
1.0	0.03645
1.25	0.0455625
1.5	0.054675
1.75	0.0637875
2.0	0.0729

The CIPP design equation for a fully deteriorated pipe condition was adapted using the new calculation for the SAPL moment of inertia (given by Eq. 7-12) and the results obtained from this modified equation were checked against the results obtained from the soil box testing. The adapted equation still predicted lower values compared with the results of soil box testing. However, through the statistical analysis using a linear regression with an  $R^2$  of 0.99304, it is found that multiplying a new enhancement factor of 2.738 could predict the same results as the soil box testing data. The modified equation using a new coefficient of 2.738 was checked with the results of soil box testing using the residual analysis, as illustrated in Figure 7-2, Figure 7-3 and Figure 7-4. Figure 7-2 shows that the Y (values obtained from the adapted CIPP design equation using ( $I$ ) for the corrugated geometry) and the predicted Y (test results) are pretty close to each other. As it is depicted in Figure 7-3, no specific pattern can be observed in this graph. The normal probability distribution illustrated in Figure 7-4 depicts a straight line that is well acceptable. The statistical analysis presented by these figures implies that the enhancement factor of 2.738 could predict very well the results obtained from the soil box testing.

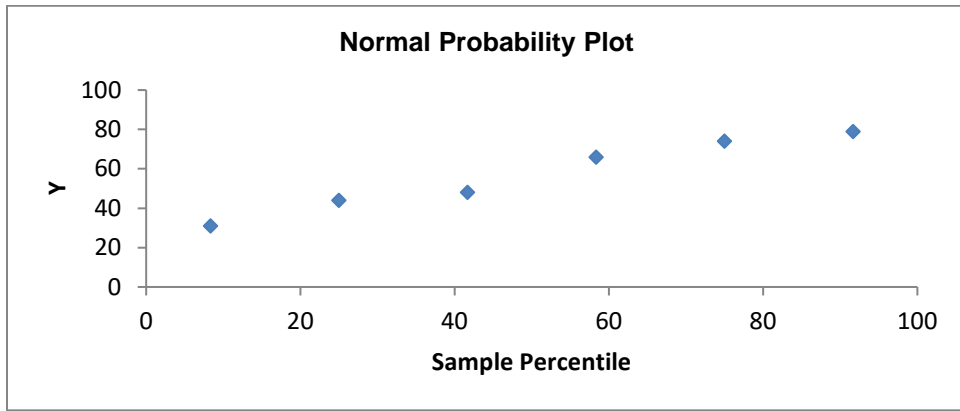


Figure 7-2 Normal probability plot of the linear regression predictive model to obtain the coefficient enhancement factor of 2.738.

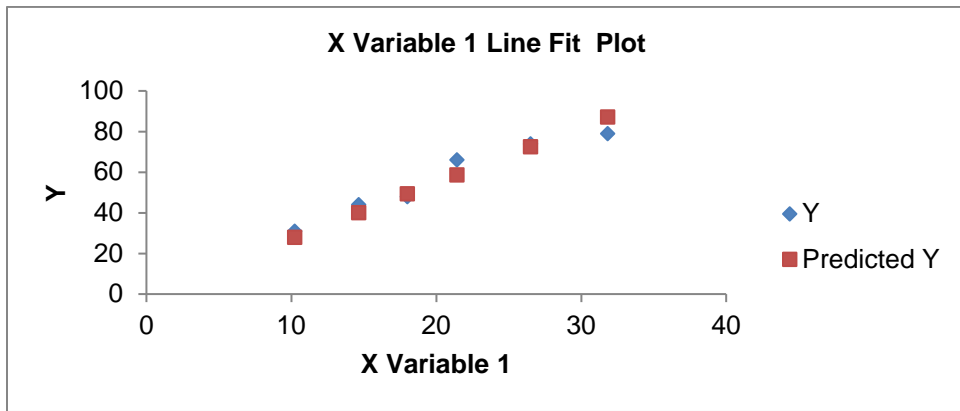


Figure 7-3 The Y (values obtained from the adapted CIPP design equation using  $I$ ) for the corrugated geometry) and the predicted Y (test results) using the predictive model.

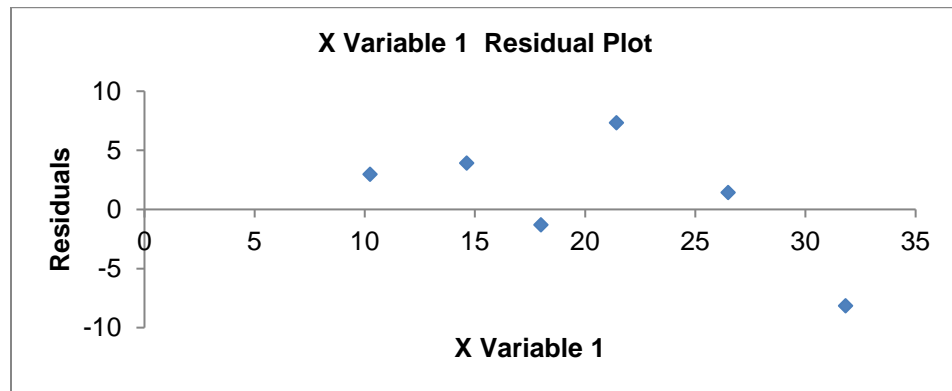


Figure 7-4 Residual analysis using a linear regression compared to the test data.



#### 7.2.4 Adapted AWWA C950 Design Equations

For the AWWA C950 design equation, the moment of inertia ( $I$ ) in the formula is defined as  $t^3/12$ , which is applicable to a rectangular section. However, the moment of inertia for a corrugated plate is given by the Eq. 7-12, as illustrated in Figure 7-1. Therefore, the critical buckling pressure on the SAPL was calculated by the AWWA C950 design equation, using the ( $I$ ) value for a corrugated geometry, and the results obtained from the adapted equation were checked against the soil box testing results. Statistical analysis using a linear regression was conducted on the new model of the AWWA C950 and an R square of 0.9944 was obtained. The adapted AWWA C950 equation model was checked using a residual analysis, as it is illustrated in Figure 7-5, Figure 7-6 and Figure 7-7. Figure 7-5 shows that the Y (values obtained from the adapted AWWA C950 design equation using ( $I$ ) for the corrugated geometry) and the predicted Y (test results) are pretty close to each other. As it is depicted in Figure 7-6, no specific pattern can be observed in this graph. The normal probability distribution illustrated in Figure 7-7 depicts a straight line that is well acceptable. The statistical analysis presented by these figures implies that the adapted AWWA C950 equation could predict very well the same results as obtained from soil box testing. Figure 7-8 illustrates the comparison of the modified AWWA C950 design equation and the soil box testing results.

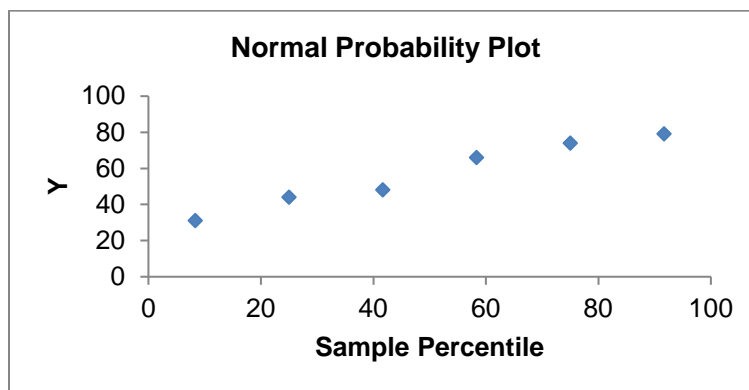


Figure 7-5 Normal probability plot of the linear regression predictive model.

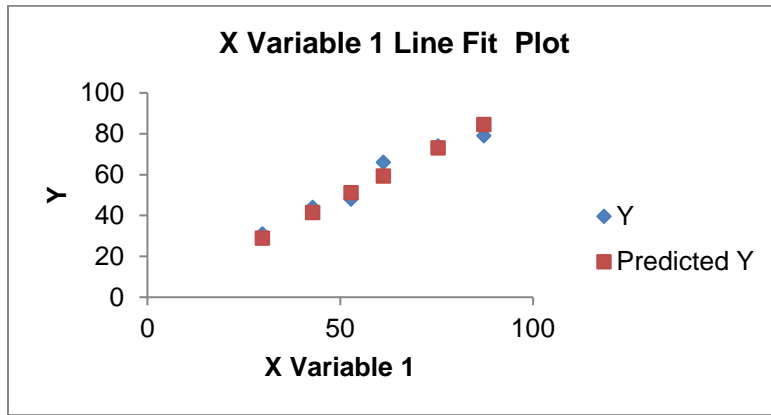


Figure 7-6 The Y (values obtained from the adapted AWWA C950 design equation using  $I$  for the corrugated geometry) and the predicted Y (test results) using the predictive model.

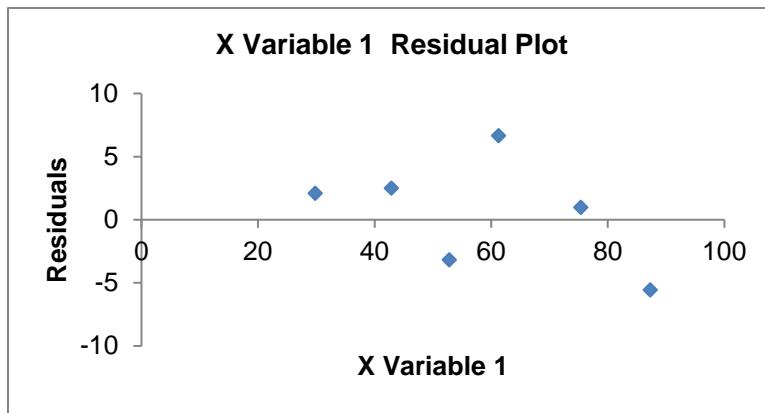


Figure 7-7 Residual analysis using a linear regression compared to the test data.

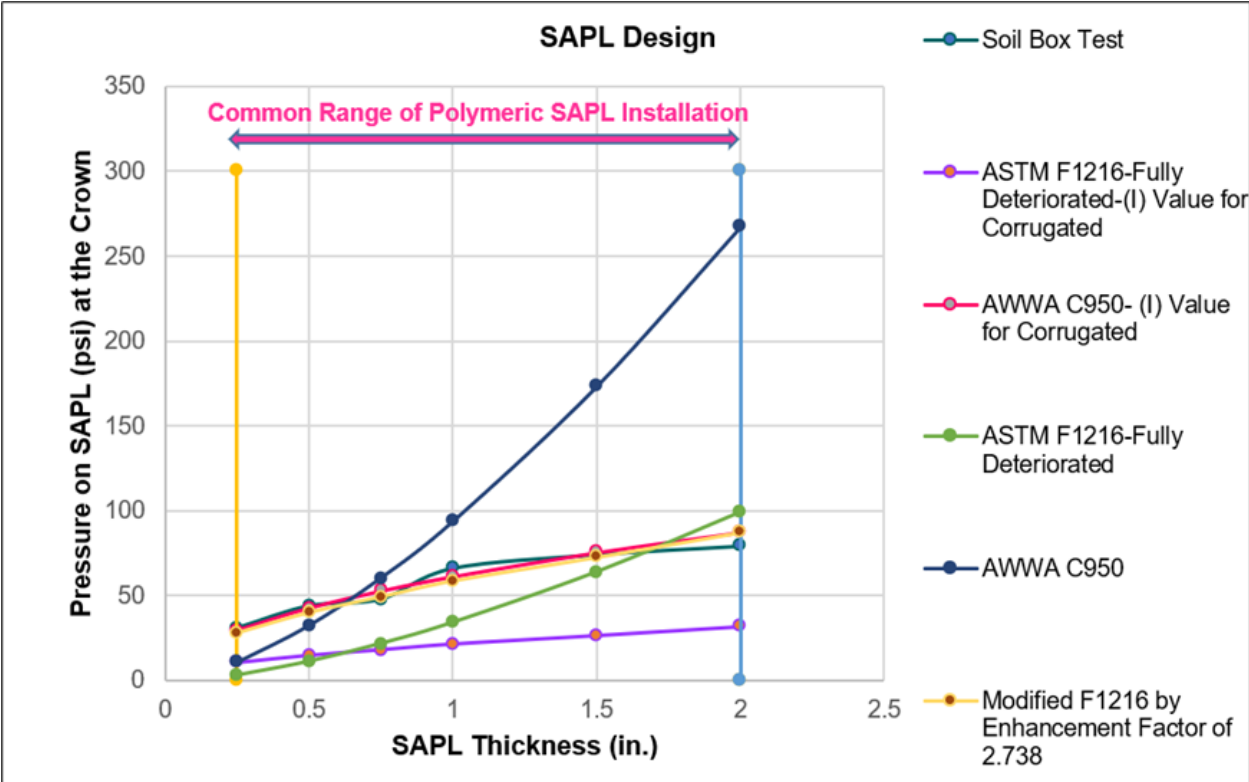


Figure 7-8 Comparison of the potential design equations, modified design equations and test data of the polymeric SAPL.

7.3 Proposed Design Method for Polymeric Materials

Eq. 7-13 and Eq. 7-14 for calculation of buckling pressure can predict the circular SAPL soil box testing results and are presented here as base design models for the design thickness of polymeric SAPL. It is noted that these equations do not include any safety factor, and are predictive models of the results of soil box testing conducted in this dissertation.

$$q_t = Z \cdot [32R_w B' E'_s C (E_L I / D^3)]^{1/2} \tag{Eq. 7-13}$$

where,

Z = coefficient enhancement factor of 2.738,

q<sub>t</sub> = critical buckling pressure of unconstrained pipe (psi),

R<sub>w</sub> = the buoyancy factor (0.67 minimum) = 1 – 0.33(H<sub>w</sub>/H), dimensionless,

B' = the empirical coefficient of elastic support = 1/(1 + 4e<sup>-0.065H</sup>) (inch-pound units, dimensionless),

$E'_s$  = the modulus of elasticity of adjacent soils or soil reaction, psi,

$E_L$  = long-term modulus of elasticity for liner, psi,

$E$  = modulus of elasticity at operating temperature of the pipe (psi),

$C$  = ovality reduction factor,

$D$  = inside diameter of original pipe, in.,

$I$  = moment of inertia (in.<sup>4</sup>/in.),

where,

$$I = C_1 \cdot b \cdot d^2 \cdot t$$

$b$  = width of the corrugated sheet (not the developed width), in.,

$d$  = depth of corrugation, in.,

$t$  = thickness of the sheet (gauge), in.,

$$C_1 = \frac{2}{15} \left[ 1 + \frac{8}{3} \left( \frac{1}{K} \right)^2 \right], \text{ a constant,}$$

$$K = \frac{e}{d},$$

$e$  = pitch of corrugation (distance from ridge to ridge), in.

$$P = \left( 0.593 \frac{R_w E_s E I}{0.149 r^3} \right)^{1/2}$$

Eq. 7-14

where,

$P$  = collapse pressure of unconstrained pipe (psi),

$R_w$  = the buoyancy factor (0.67 minimum) =  $1 - 0.33(H_w/H)$ , dimensionless,

$E_s$  = the modulus of elasticity of adjacent soils or soil reaction (psi),

$E$  = modulus of elasticity at operating temperature of the pipe (psi),

$r$  = radius assume no ovalization (in.).

$I$  = moment of inertia (in.<sup>4</sup>/in.),

where,

$$I = C_1 \cdot b \cdot d^2 \cdot t$$

$b$  = width of the corrugated sheet (not the developed width), in.,

$d$  = depth of corrugation, in.,

$t$  = thickness of the sheet (gauge), in.,

$$C_1 = \frac{2}{15} \left[ 1 + \frac{8}{3} \left( \frac{1}{K} \right)^2 \right], \text{ a constant,}$$

$$K = \frac{e}{d},$$

$e$  = pitch of corrugation (distance from ridge to ridge), in.

## 7.4 Chapter Summary

The objective of this dissertation was to develop a set of equations for polymeric spray applied pipe lining materials for installing pipes within the existing pipes given their current in-situ conditions for SAPL to act as a standalone pipe in the site-specific embedment soil.

The design methods presently in use for polymeric materials consisted design appendix X1 of the ASTM Standard F1216. The fully deteriorated design case (standalone pipe) follows a design methodology originally used for the installation of fiberglass pipe by the AWWA Committee C950 in 1987. As the AWWA committee evolved and the fiberglass pipe design was put into a Manual of Practice (M45), it has undergone numerous improvements over the years and has become the state of the art for these type pipe installations.

The modified CIPP design equation for a pipe in fully deteriorated condition (Eq. 7-13) and the adapted AWWA C950 design equation (Eq. 7-14) for calculation of buckling pressure can predict the circular SAPL soil box testing results and are presented here as base design models for the design thickness of polymeric SAPLs used for renewal of culverts. It is noted that these equations do not include any safety factor, and are predictive models of the results of soil box testing conducted in this dissertation.

Currently polymeric non-circular liners are designed using 3R2014 (Structural Design for Non-Circular Linings Under Groundwater Pressure), which is the proposed at the ASCE Manual of Practice for Design of Flexible Liners that is known to be under review. In this manual, live loads can be added as an equivalent external hydrostatic load acting on the liner. In this design method, soil is assumed in equilibrium with the pipe diameter and structurally sufficient to take long-term groundwater loading. This design concept also looks at the long-term effects of the axial compression applied to liner, the circumferential deflection

that will occur due to creep, and the final buckling of the liner in the area of the largest radius. This method does not consider any bonding of the liner to the host pipe material.

## Chapter 8

### Conclusions and Recommendations for Future Research

#### 8.1 Summary

Spray applied pipe lining (SAPL) is a trenchless renewal methodology to renew the deteriorated corrugated metal pipes (CMPs) or reinforced concrete pipes (RCPs) to provide a new design life. Currently, there is no design methodology specifically for structural applications of SAPLs. Hence, this dissertation presented the results and analysis of nine full-scale laboratory soil box testing in three different setups to investigate the structural load carrying capacity of bare CMPs, fully deteriorated invert circular CMPs, and fully deteriorated invert arch CMPs. To simulate the actual field condition, where the CMPs are mostly corroded at the invert, the invert section of CMP samples was removed and the actual capacity of SAPL was tested in the absence of the host pipe ring stiffness. Due to lack of standard for the SAPL design and installation, this dissertation discussed the common issues with the SAPL installation and provided some recommendations to help with the performance of the SAPL. A literature search was conducted on the available buckling pressure theories and design equations used for other renewal methods (such as ASTM F1216 for CIPP) and their applicability for SAPL design was examined. Based on the numerical and statistical analysis, two base equations for the design of polymeric SAPL for renewal of deteriorated culverts were selected and modified based on results of soil box testing.

#### 8.2 Conclusions

The conclusion of this dissertation is summarized as following:

- Polymeric spray applied pipe linings (SAPLs) have potentials to inhibit further deterioration of culverts and drainage structures and structurally renew the existing host culverts.
- The SAPL installation process must have a uniform thickness of SAPL to achieve structural application.
- Polymeric SAPL is a fully structural solution as it can restore and even increase the load carrying capacity of fully deteriorated invert culverts.

- Circular CMP renewed with polymeric SAPL has a higher load carrying capacity than a SAPL renewed arch CMP.
- All the soil box tests of renewed CMPs revealed that the maximum pressure on SAPLs occurred at the crown of the pipe, where in the initiation of first crack and the failure occurred as well. In contrast, zero pressures or negligible values were recorded for the invert location and springline. Hence, in shallow cover burial condition, a reinforcement or a higher thickness is recommended for the crown location of the pipes.
- Under conditions of testing performed, the modified CIPP design equation, with an enhancement factor of 2.738, for fully deteriorated condition is applicable for polymeric SAPLs.
- The adapted AWWA C950 design equation is applicable for polymeric SAPLs. The moment of inertia in this equation needs to be calculated based on the corrugated geometry.
- The tested polymeric SAPL exhibited a stiff fracture propagation that was clearly audible, which is called a plastic phase.

### **8.2.1 Bare CMP Control Tests (First Soil Box Test Setup)**

- The intact circular CMP could withstand the AASHTO H20 truck load and ultimately failed with a local buckling at the crown.
- The invert-cut circular CMP could withstand the equivalent AASHTO H20 truck load.
- The invert-cut circular CMP at the failure registered a larger horizontal movement in the absence of its ring stiffness compared with the invert-cut arch CMP that did not exhibit a significant horizontal movement.
- The invert-cut arch CMP could not reach the equivalent AASHTO H20 truck load prior to the ultimate failure. The ultimate load of the invert-cut arch CMP was 47% lower than the ultimate load of invert-cut circular CMP.
- The invert-cut arch CMP carried the superimposed loads by taking advantage of its flat area at the bottom for transferring the vertical loads to the soil, while the strength of invert-cut circular CMP was dependent on its ring stiffness.



- The initial load carrying capacity of the invert-cut circular CMP was due to the existence of frictional resistance between the outer surface of the CMP and soil. The frictional resistance is a function of the contact area between the CMP and soil, as well as the length of the pipe. A culvert in the actual field condition is longer than tested CMPs in the laboratory condition. Hence, a longer CMP in the field will experience a higher frictional resistance which can lock the pipe in place and therefore, it may reduce or eliminate the circumferential movement of the pipe. Resistance to circumferential movement of the CMP may facilitate or increase the chance of local buckling failure.
- Considering the pipe sample length in the actual field condition along with the existence of frictional resistance factor, and a higher load carrying capacity for the circular CMP sample compared with arch CMP, it can be inferred that in a fully deteriorated condition a circular CMP has less risk of collapse compared with an arch CMP.

### **8.2.2 SAPL Renewed Circular CMPs (Second Soil Box Test Setup)**

- The material properties of polymeric SAPL used in the soil box testing had an averaged maximum tensile stress of 8,670.78 psi, elastic modulus of 489,500 psi, and flexural modulus of 855,639 psi.
- The results of thickness measurement showed that the utilization of hand spray for installation of the polymeric SAPL resulted in a thicker liner at the springline for all renewed CMPs than the designated thickness. However, the SAPL was installed closer to the required thickness at crown and both shoulders. One of the possible reasons for the inconsistent thickness installation could be due to the sagging and creep movement of the SAPL material at the initial stage (i.e., before hardening) of installation due to gravity.
- All SAPL renewed pipes cracked at about 3% of the SAPL-CMP system deflection, where at this deflection the application of 0.25 in., 0.5 in., and 1 in. polymeric SAPL compared with bare CMP, increased the load carrying capacity for 471.7, 482.8, and 802.7% respectively.
- Application of the polymeric SAPL increased the stiffness of the bare invert-cut CMP. The SAPL renewed CMPs with the thicknesses of 0.25 in., 0.5 in., and 1 in. increased the ultimate load bearing capacity of the invert deteriorated CMPs for 16.24, 31.4, and 80.82%, respectively.

- The CMP with thinner liner (i.e., 0.25 in.) was susceptible to crack at the seam's locations, where the liner's thickness was not sufficient to prevent cracking. In this location, although the first crack was initiated in the longitudinal direction, once it reached the seam locations, it diverted towards the circumferential direction. The failure and fracture mode of renewed pipes are described in sections 5.2.3 and 5.3.3 of this dissertation.
- The CMP with 1 in. thick SAPL showed stiffer response to the applied load compared with thinner SAPL renewed pipe samples. In contrast with 0.25 and 0.5 thicknesses, no circumferential crack was observed in the pipe sample.
- The SAPL renewed CMP samples with the thicknesses of 0.25 in., 0.5 in., and 1 in. cracked at 3.52, 2.9, and 3.65% of crown deflection, respectively.
- In the absence of the host pipe's ring stiffness, the SAPL was able to resist the ring compression solely. Therefore, the polymeric SAPL can be considered structurally sufficient to withstand the applied load and improve the overall load bearing capacity of the fully deteriorated host pipe.

### **8.2.3 SAPL Renewed Arch CMPs (Third Soil Box Test Setup)**

- The results of thickness measurements showed that the utilization of hand spray installation method for the polymeric SAPL resulted in about 0.2 in. thicker liner than the design thickness, which could be due to the inclusion of a factor of safety in SAPL's quantity calculation.
- Application of the polymeric SAPL increased the stiffness of the fully deteriorated invert arch CMP. The SAPL renewed arch CMPs with the thicknesses of 0.25 in., 0.5 in., and 1 in. increased the ultimate load bearing capacity of the fully invert deteriorated CMPs by 23.1, 32.1, and 98.9%, respectively.
- The arch CMP with 0.25 in. of SAPL was susceptible to crack at the seam's locations, where the SAPL was either discontinued or the thickness was not as thick as design thickness. Although, the first crack was initiated in the longitudinal direction, once it reached the seam locations, it diverted towards the circumferential direction.

- Compared with the bare arch CMP, the application of SAPL reduced the strain of the host pipes, especially at the crown and shoulder locations.
- The DIC results showed that for all arch CMP samples the modes of failure were local buckling at the crown locations, where in case of the bare arch CMP the buckling caused pipe deformation (i.e., ductile failure) and in case of SAPL renewed arch CMP samples it caused cracking and fracture at the crown sections (i.e., brittle failure).
- The 0.25, 0.5, and 1 in. SAPL renewed arch CMPs were cracked at the pressures of 19.77, 16.26, and 21.95 psi, respectively, at the crown of the pipes. All the SAPL renewed arch CMP cracking pressures were higher than the applied pressure required by the AASHTO H20 truck, calculated through AASHTO LRFD, AWWA, and NCSPA design guidelines.
- In the absence of the host pipe's ring stiffness, the SAPL was able to resist the ring compression solely. No sign of crack was observed at the invert area, where the host pipe was entirely cut and detached. Therefore, the polymeric SAPL can be considered structurally sufficient to withstand the applied load and improve the overall load bearing capacity of the fully invert deteriorated host arch CMP.

### **8.3 Limitations and Recommendations for Future Research**

The equation obtained in this dissertation is based on the presented soil box test results for a SAPL range of installation between 0.25 in. to 2.0 in. It is recommended additional investigations be conducted using finite element modeling simulating different conditions for a buried pipe soil box testing such as:

- Different heights of soil cover,
- Different types of backfill soil material,
- Different pipe diameters,
- Different SAPL materials,
- Different types of reinforcement material in the SAPL mixture,
- Effects of dynamic loads (earthquake),
- Performance of existing culverts to verify design equations.

## References

- American Association of State Highway and Transportation Officials (AASHTO) LRFD bridge design specifications*, 8<sup>th</sup> Edition. (2017). LRFD-8 • ISBN: 978-1-56051-654-5.
- Al-Lami, B. (2020). "Performance of Cracked Reinforced Concrete Pipes Subjected to Different Environmental Conditions." The University of Texas at Arlington.
- American Concrete Pipe Association. (1987). *Concrete pipe design manual*. American Concrete Pipe Association.
- American Concrete Pipe Association. (2008). *Concrete Pipe Stays in Shape!*
- Arnoult, J. D. (1986). "FHWA Culvert Inspection Manual." U.S. Department of Transportation, Federal Highway Administration.
- ASTM D2412 - 11. (2018). "*Standard Test Method for Determination of External Loading Characteristics of Plastic Pipe by Parallel-Plate Loading.*" American Society for Testing and Materials. *ASTM International, West Conshohocken, PA.*
- ASTM A760 A760/A760M - 15. (2020). "*Standard Specification for Corrugated Steel Pipe, Metallic-Coated for Sewers and Drains.*" American Society for Testing and Materials. *ASTM International, West Conshohocken, PA.*
- ASTM A796 A796/A796M - 17a. (2017). "*Standard Practice for Structural Design of Corrugated Steel Pipe, Pipe-Arches, and Arches for Storm and Sanitary Sewers and Other Buried Applications.*" American Society for Testing and Materials. *ASTM International, West Conshohocken, PA.*
- ASTM B745/B745M - 15. (2015). "*Standard Specification for Corrugated Aluminum Pipe for Sewers and Drains.*" American Society for Testing and Materials. *ASTM International, West Conshohocken, PA.*
- ASTM D1633 - 17. (2017). "*Standard Test Methods for Compressive Strength of Molded Soil-Cement Cylinders.*" American Society for Testing and Materials. *ASTM International, West Conshohocken, PA.*
- ASTM D6913 / D6913M - 17. (2017). "*Standard Test Methods for Particle-Size Distribution (Gradation) of Soils Using Sieve Analysis.*" American Society for Testing and Materials. *ASTM International, West Conshohocken, PA.*

- ASTM F1216 - 16. (2016). "Standard Practice for Rehabilitation of Existing Pipelines and Conduits by the Inversion and Curing of a Resin-Impregnated Tube." American Society for Testing and Materials. *ASTM International, West Conshohocken, PA.*
- ASTM D790 - 17. (2017). "Standard Test Methods for Flexural Properties of Unreinforced and Reinforced Plastics and Electrical Insulating Materials." American Society for Testing and Materials. *ASTM International, West Conshohocken, PA.*
- Banthia, N., Chokri, K., Ohama, Y., and Mindess, S. (1994). "Fiber-reinforced cement based composites under tensile impact." *Advanced Cement Based Materials*, Elsevier, 1(3), 131–141.
- Banthia, N., Zanotti, C., and Sappakittipakorn, M. (2014). "Sustainable fiber reinforced concrete for repair applications." *Construction and Building Materials*, Elsevier, 67, 405–412.
- Bednar, L. (n.d.). "Plain Galvanized Steel Drainage Pipe Durability Estimation with a Modified California Chart." 70–79.
- Berney, E. S., and Smith, D. M. (2008). *Mechanical and Physical Properties of ASTM C33 Sand. U.S. Army Corps of Engineers.*
- Boot, J. C., and Gumbel, J. E. (1997). "Structural analysis of sewer linings by B. Falter (Trenchless Technology Research 11 (2), 27–41, 1996)." *Tunnelling and underground space technology*, Elsevier, 12, 49–52.
- Boot, J. C., and Javadi, A. A. (1998). "Experimental determination of buckling capacities for cured-in-place pipe linings." *Proceedings of 11th International Conference on Experimental Mechanics, Oxford, August, 1998*, Balkema Rotterdam, 327–332.
- Boot, J. C., and Welch, A. J. (1996). "Creep buckling of thin-walled polymeric pipe linings subject to external groundwater pressure." *Thin-walled structures*, Elsevier, 24(3), 191–210.
- Broekaen, M. (2002). "Polyurea spray coatings, the technology and latest developments, polyurethanes for high—Performance coatings ii." *ECC, Berlin, March*, 14(1), 5.
- Cain, A. (2016). "Make the right choice for metal coating for the right application." <<https://www.designworldonline.com/make-right-choice-metal-coating-right-application/>>.

- Chaallal, O., Arockiasamy, M., and Godat, A. (2014). "Field Test Performance of Buried Flexible Pipes under Live Truck Loads." *Journal of Performance of Constructed Facilities*, 29(5), 04014124.
- Chiaia, B., Fantilli, A. P., and Vallini, P. (2009). "Combining fiber-reinforced concrete with traditional reinforcement in tunnel linings." *Engineering Structures*, Elsevier, 31(7), 1600–1606.
- Center for Underground Infrastructure Research and Education (CUIRE). (2020). "*CUIRE SAPL FEM Report*." The University of Texas at Arlington.
- Darabnoush Tehrani, A. (2016). "FINITE ELEMENT ANALYSIS FOR ASTM C-76 REINFORCED CONCRETE PIPES WITH REDUCED STEEL CAGE."
- Darabnoush Tehrani, A. (2020). "Development of a Structural Design Methodology for Cementitious Sprayed Applied Pipe Linings in Gravity Storm Water Conveyance Conduits." The University of Texas at Arlington.
- Darabnoush Tehrani, A., Kohankar Kouchesfehaneh, Z., Chimaurya, H. R., Raut, S., Najafi, M., and Yu, X. (2020a). "Structural evaluation of invert-cut circular and arch shape corrugated steel pipes through laboratory testing." *Canadian Journal of Civil Engineering*, NRC Research Press, (999), 1–15.
- Darabnoush Tehrani, A., Kohankar Kouchesfehaneh, Z., and Najafi, M. (2020b). "Pipe Profiling using Digital Image Correlation." *Pipelines 2020*, American Society of Civil Engineers (ASCE), San Antonio, TX.
- Darabnoush Tehrani, A., Kohankar Kouchesfehaneh, Z., Najafi, M., Syar, J. E., and Kampbell, N. E. (2019). "Evaluation of Filling the Valleys of Corrugated Metal Pipes by Trenchless Spray Applied Pipe Linings." *Pipelines*, American Society of Civil Engineers.
- Darabnoush Tehrani, A., Kouchesfehaneh Kohankar, Z., and Najafi, M. (2020c). "Review and Recommendations for Structural Testing of Buried Gravity Storm Drain Pipes and Culverts." *Canadian Journal of Civil Engineering*, (Soil–structure interaction of buried structures).
- Dawood, E. T., and Ramli, M. (2011). "High strength characteristics of cement mortar reinforced with hybrid fibres." *Construction and building materials*, Elsevier, 25(5), 2240–2247.
- El Debs, M. K., and Naaman, A. E. (1995). "Bending behavior of mortar reinforced with steel meshes and polymeric fibers." *Cement and Concrete Composites*, Elsevier, 17(4), 327–338.

- El-Atrouzy, M. N. (1969). "Structural properties of corrugated sheets used in cylindrical shells." University of Windsor.
- Ellison, D., Sever, F., Oram, P., Lovins, W., Romer, A., Duranceau, S. J., and Bell, G. (2010). "Global review of spray-on structural lining technologies." *Water Research Foundation, Denver*, 1–184.
- Entezarmahdi, A. (2015). "TESTING, ANALYSIS AND CLASSIFICATION OF NO-DIG MANHOLE REHABILITATION MATERIALS." The University of Texas at Arlington.
- F1216-16, A. (2016). "ASTM F1216." *Standard Practice for Rehabilitation of Existing Pipelines and Conduits by the Inversion and Curing of a Resin-Impregnated Tube*, 1–8.
- F3182-16, A. (2016). "Standard Practice for the Application of Spray-Applied Polymeric Liners Inside Pipelines for Potable Water." 1–6.
- Falter, B. (1996). "Structural analysis of sewer linings." *Tunnelling and Underground Space Technology*, Elsevier, 11, 27–41.
- FHWA. (2012). *Hydraulic design of highway culverts*. United States. Federal Highway Administration.
- Garcia, D. B., and Moore, I. D. (2015). "Performance of deteriorated corrugated steel culverts rehabilitated with sprayed-on cementitious liners subjected to surface loads." *Tunnelling and Underground Space Technology*, 7, 222–232.
- García, D. B., and Moore, I. D. (2015). "Performance of deteriorated corrugated steel culverts rehabilitated with sprayed-on cementitious liners subjected to surface loads." *Tunnelling and Underground Space Technology*, Elsevier, 47, 222–232.
- GEOKON. (2019). "Pressure Cells."
- Glock, D. (1977). "Post-critical behavior of a rigidly encased circular pipe subject to external water pressure and temperature rise." *Der Stahlbau*, 46(7), 212–217.
- Guan, S. W. (2003). "100% solids polyurethane and polyurea coatings technology." *Coatings World*, 49–58.
- Guan, S. W., Liu, D., Moreno, M., and Garneau, R. (2004). "100% solids rigid polyurethane coatings technology for corrosion protection of ballast tanks." *CORROSION 2004*, NACE International.
- Gumbel, J. (1998). "NEW APPROACH TO DESIGN OF CIRCULAR LINER PIPE." 1–18.

- Ha, S. K., Lee, H.-K., and Kang, I. S. (2016). "Structural behavior and performance of water pipes rehabilitated with a fast-setting polyurea–urethane lining." *Tunnelling and Underground Space Technology*, Elsevier, 52, 192–201.
- Ham, S., and Darabnoush Tehrani, A. (2019). "2D Random Shape of Aggregate Model using Image Processing and Convex Combination Theory." *Transportation Research Board (TRB)*.
- Heavens, J., and Gumbel, J. (2004). "Gravity and pressure pipe liner design issues." *Proceedings of North-American No-Dig Conference. New Orleans LA*.
- Hsie, M., Tu, C., and Song, P. S. (2008). "Mechanical properties of polypropylene hybrid fiber-reinforced concrete." *Materials Science and Engineering: A*, Elsevier, 494(1–2), 153–157.
- Internasional, A. (2014). "ASTM D638-14 Standard Test Methods for Tensile Properties of Plastic." *America Society for Testing and Material*.
- Iucolano, F., Liguori, B., and Colella, C. (2013). "Fibre-reinforced lime-based mortars: A possible resource for ancient masonry restoration." *Construction and Building Materials*, Elsevier, 38, 785–789.
- Izaguirre, A., Lanas, J., and Alvarez, J. I. (2011). "Effect of a polypropylene fibre on the behaviour of aerial lime-based mortars." *Construction and Building Materials*, Elsevier, 25(2), 992–1000.
- Johnson, C., and Hammon, J. (2017). "Structural Polyurethane and Rehabilitation of America's Infrastructure." Department of Defence - Allied Nations Technical Corrosion Conference.
- Jozaghi, A., Nabatian, M., Noh, S., Seo, D.-J., Tang, L., and Zhang, J. (2019). "Improving Multisensor Precipitation Estimation via Adaptive Conditional Bias–Penalized Merging of Rain Gauge Data and Remotely Sensed Quantitative Precipitation Estimates." *Journal of Hydrometeorology*, 20(12), 2347–2365.
- Khatri, D. K., Han, J., Corey, R., Parsons, R. L., and Brennan, J. J. (2015). "Laboratory evaluation of installation of a steel-reinforced high-density polyethylene pipe in soil." *Tunnelling and Underground Space Technology*, Elsevier Ltd, 49, 199–207.
- Klöppel, K., and Glock, D. (1970). *Theoretische und experimentelle Untersuchungen zu den Traglastproblemen biegeweicher, in die Erde eingebetteter Rohre. 1.[Text]*. Techn. Hochsch., Inst. f. Statik u. Stahlbau.



- Kohankar Kouchesfehiani, Z., Darabnoush Tehrani, A., Najafi, M., and Syar, J. (2020). "Laboratory testing of invert-cut corrugated metal pipes renewed with polymeric spray applied pipe lining." *Transportation Geotechnics*, Elsevier, 100413.
- Kohankar Kouchesfehiani, Z., Darabnoush Tehrani, A., Najafi, M., Syar, J. E., and Ed Kampbell, P. E. (2019). "Adding Additional Reinforcement to Improve the Structural Performance of Spray Applied Pipe Lining Rehabilitation Technology: A Review." *Pipelines 2019: Multidisciplinary Topics, Utility Engineering, and Surveying*, ASCE, Nashville.
- Kohankar Kouchesfehiani, Z., Tabesh, A., and Najafi, M. (2017). "Risk Identification for Pipeline Installation by Horizontal Directional Drilling." *Proc. International Congress on Underground Infrastructure, Water Management and Trenchless Technology (ICUWT)*, 85–92.
- Kohankar Kouchesfehiani, Z. (2013). "Investigating the Feasibility of a Proposed Model for Geometric Design of Deployable Arc Structures." The University of Sistan and Baluchestan.
- Kohankar Kouchesfehiani, Z., Ghasemi M. R. (2013). "Investigating the Cross-Section and Structural Geometry Effects on Response of Flat Scissor-Type Structures in Deployed Configuration." 7th National Congress on Civil Engineering-University of Sistan and Baluchestan (7NCCE).
- Kohankar Kouchesfehiani, Z., Ghasemi M. R. (2013). "Investigating the Effects of Joint Size and Members' Flexural Rigidity on Response of Flat Scissor-Type Structures in Deployed Configuration." 7th National Congress on Civil Engineering-University of Sistan and Baluchestan (7NCCE).
- Kouchesfehiani, Z. K., Paggioli, K., Najafi, M., and Miglio, A. (2018). "Evaluation of Structural Design Methodologies for Large Diameter Pipeline Renewal Design." *Pipelines 2018: Condition Assessment, Construction, and Rehabilitation*, American Society of Civil Engineers Reston, VA, 327–332.
- Kunecki, B., and Kubica, E. (2004). "Full-scale laboratory tests and FEM analysis of corrugated steel culverts under standardized railway load." *Archives of Civil and Mechanical Engineering*, 4(4), 41–53.
- Leonards, G. A., and Stetkar, R. E. (1978). "Performance of buried flexible conduits: Interim report." Purdue University.
- Lougheed, A. C. (2008). "Limit States Testing of A Buried Deep corrugated Large-Span Box Culvert." Queen's University.

- Luk, G. K. (2001). "Pipeline rehabilitation with fiber-reinforced mortar lining." *Journal of infrastructure systems*, American Society of Civil Engineers, 7(3), 116–122.
- Luo, J., Li, Q., Zhao, T., Gao, S., and Sun, S. (2013). "Bonding and toughness properties of PVA fibre reinforced aqueous epoxy resin cement repair mortar." *Construction and Building Materials*, Elsevier, 49, 766–771.
- Luscher, U. (1966). "Buckling of Soil-surrounded Tubes, ASCE, Vol. 92." No. SM6.
- Mai, V. T., Hout, N. A., and Moore, I. D. (2013). "Effect of deterioration on the performance of corrugated steel culverts." *Journal of Geotechnical and Geoenvironmental Engineering*, 141(4), 1–11.
- Masada, T. (2017a). *Structural Benefits of Concrete Paving of Steel Structural Benefit of Concrete Paving of Steel Culvert Inverts*.
- Masada, T. (2017b). *Structural Benefit of Concrete Paving of Steel Culvert Inverts*. Ohio.
- Masada, T., Sargand, S. M., Tarawneh, B., Mitchell, G. F., and Gruver, D. (2007). "Inspection and risk assessment of concrete culverts under Ohio's highways." *Journal of Performance of Constructed Facilities*, 21(3), 225–233.
- Matthews, J., Simicevic, J., Kestler, M., and Piehl, R. . (2012). *Decision analysis guide for corrugated metal culvert rehabilitation and replacement using trenchless technology*. United States Department of Agriculture, Forest Service.
- Mitchell, G. F., Masada, T., Sargand, S. M., and Tarawneh, B. (2005). *Risk assessment and update of inspection procedures for culverts*. United States. Federal Highway Administration.
- Moore, I. D., and Garcia, D. B. (2015). "Ultimate Strength Testing of Two Deteriorated Metal Culverts Repaired with Spray-On Cementitious Liners." (2522), 139–147.
- Moser, A. P., and Folkman, S. L. (2008). *Buried pipe design*. McGraw-Hill New York.
- Najafi, M. (2008). *An asset management approach for drainage infrastructure and culverts*. Midwest Regional University Transportation Center, University of Wisconsin.
- Najafi, M. (2010). *Trenchless Technology Piping: Installation and Inspection: Installation and Inspection*. McGraw Hill Professional.
- Najafi, M. (2016). *Pipeline infrastructure renewal and asset management*. McGraw Hill Professional.

- Najafi, M., and Bhattachar, D. V. (2011). "Development of a culvert inventory and inspection framework for asset management of road structures." *Journal of King Saud University - Science*, 23(3), 243–254.
- Najafi, M., and Gokhale, S. (2005). *Trenchless technology: Pipeline and utility design, construction, and renewal*. McGraw-Hill New York.
- Najafi, M., Sever, V. F. (2019). "D-Load Strength of Concrete Pipes with Epoxy Linings." 10(4), 1–11.
- National Association of Sewer Service Companies (NASSCO). (2019). "*Certification Program (PACP) Reference Manual*."
- NCSPA. (2017). "Spiral Rib Pipe." North Carolina State Ports Authority. The National Corrugated Steel Pipe Association.
- ODOT. (2018). "Culvert Management Manual." (September).
- Olympus. (2020). "Olympus - Non Destructive Ultrasonic Test Equipment, Ultrasonic, Phased Array, Microscopes, Thickness Gages, Flaw Detectors, Innov-X, NDT, Remote Visual Inspection, Eddy Current, X-ray Fluorescence, X-ray Diffraction."
- Omara, A.-A. M. (1997). "Analysis of cured-in-place pipes (CIPP) installed in circular and oval deteriorated host pipes."
- OMEGA. (2019). "LVDT."
- PCPIPE. (2016). "Types of Corrugation." <[www.pcpipes.com/products/typesofcorrugation.html](http://www.pcpipes.com/products/typesofcorrugation.html)>.
- Piratla, K. R., Pang, W., Jin, H., and Stoner, M. (2017). *Best Practices for Assessing Culvert Health and Determining Appropriate Rehabilitation Methods*.
- Primeaux, I. I. (n.d.). "D.(1989). Spray Polyurea–Versatile High Performance Elastomer for the Polyurethane Industry." *Polyurethanes 89, Proceedings of the SPI–32nd Annual Technical/Marketing Conference*, 126–130.
- Rakitin, B., and Xu, M. (2014). "Centrifuge modeling of large-diameter underground pipes subjected to heavy traffic loads." *Canadian Geotechnical Journal*, 51(4), 353–368.
- Regier, C., Hoult, N. A., and Moore, I. D. (2016). "Laboratory Study on the Behavior of a Horizontal-Ellipse Culvert during Service and Ultimate Load Testing." *Journal of Bridge Engineering*, 22(3), 04016131.

- Royer, J., and Iseley, T. (2017). "Laboratory testing and analysis of geopolymer pipe-lining technology for rehabilitation of sewer & storm water conduits, part II - CMP culvert analysis." *NASTT's No-Dig Show and ISTT's 35th International No-Dig*, 1–10.
- Sargand, S. M., Khoury, I., Hussein, H. H., and Masada, T. (2018). "Load Capacity of Corrugated Steel Pipe with Extreme Corrosion under Shallow Cover." *Journal of Performance of Constructed Facilities*, American Society of Civil Engineers, 32(4), 4018050.
- Schluter, J. C., and Shade, J. W. (1999). "Flexibility factor or pipe stiffness: Significant stiffness considerations." *Transportation research record*, SAGE Publications Sage CA: Los Angeles, CA, 1656(1), 45–50.
- Schrock, B. J., and Gumbel, J. (1997). "Pipeline Renewal–1997." *North American No-Dig*, 97.
- Seemann, R. K., Hall, D. E., and Straughan, W. T. (2001). *Buckling Experiments for CIPP Liners Installed in Ovalized Host Pipes: Report*. Louisiana Tech University, College of Engineering and Science, Trenchless.
- Sehn, A. L., and Duncan, J. M. (1994). "Investigation of large deformations of a corrugated metal pipe in silty soil: Culvert distress and failures." *Transportation research record*, (1431), 3–12.
- Siavash G. Motlagh, Jain, A., and Najafi, M. (2013). "Comparison of Spray-on Linings for Water Pipeline Renewal Applications." 1114–1126.
- Spadea, S., Farina, I., Carrafiello, A., and Fraternali, F. (2015). "Recycled nylon fibers as cement mortar reinforcement." *Construction and Building Materials*, Elsevier, 80, 200–209.
- Spangler, M. G. (1941). "The structural design of flexible pipe culverts. Bulletin, XL (153)." Iowa State College Ames, IA.
- Spangler, M. G. (1960). "Engineering Characteristics of Soils and Soil Testing." *Highway Engineering Handbook, 1st Edition*. McGraw-Hill, 8.
- Straughan, W. T., Guice, L. K., and Mal-Duraipandian, C. (1995). "Long-term structural behavior of pipeline rehabilitation systems." *Journal of Infrastructure Systems*, American Society of Civil Engineers, 1(4), 214–220.

- Syar, J. E., Najafi, M., Kohankar Kouchesfehiani, Z., Korky, S., and Darabnough Tehrani, A. (2019). "Use of Spray Applied Pipe Linings as a Structural Renewal for Gravity Storm Water Conveyance Conduits." North American Society for Trenchless Technology (NASTT), Chicago, Illinois, WM-T5-05.
- Syar, J. E., Najafi, M., Kouchesfehiani Kohankar, Z., and Darabnough Tehrani, A. (2020). "Soil Box Testing Details of Spray Applied Pipe Linings as a Structural Renewal for Gravity Storm Water Conveyance Conduits." *NASTT's 2020 No-Dig Show*, North American Society for Trenchless Technology (NASTT), Denver, WM-T4-03.
- Szafran, J., and Matusiak, A. (2017). "STRUCTURAL BEHAVIOUR AND COMPRESSIVE STRENGTH OF CONCRETE RINGS STRENGTHENED WITH A POLYUREA COATING SYSTEM." *XXIII LSCE, Bydgoszcz*.
- Thepot, O. (2000). "A new design method for non-circular sewer linings." *Tunnelling and Underground Space Technology*, Elsevier, 15, 25–41.
- Thepot, O., Bergue, J.-M., Joussin, J.-M., and Orditz, D. (2015). "Systematic comparison of the four main national methods ASTM F1216, WRc-SRM, DWA-A 143-2 and 3R-2014 applicable to flexible liners of both circular and non-circular cross-sections." *No-Dig 2015*.
- Timoshenko, S., and Gere, J. M. (1961). *Theory of elasticity stability*. McGraw.
- Walker, D., and Guan, S. (1997). "Protective linings for steel pipe in potable water service." *NACE Northern Area International Conference Corrosion Prevention*, 10–11.
- Watkins, R. K., and Anderson, L. R. (1999). *Structural mechanics of buried pipes*. CRC press.
- Wisconsin DOT. (1997). *Facilities Development Manual, Hydraulic Design of Culverts*.
- WSDOT. (2019). "Pipe Classification and Materials, Hydraulics Manual M 23-03.06, WSDOT." (April), 1–42.
- Wyant, D. C. (2002). *SYNTHESIS 303 Assessment and Rehabilitation of Existing Culverts*.
- Yeau, K. Y., Sezen, H., and Fox, P. J. (2009). "Load performance of in situ corrugated steel highway culverts." *Journal of Performance of Constructed Facilities*, American Society of Civil Engineers, 23(1), 32–39.

Zanotti, C., Banthia, N., and Plizzari, G. (2014). "A study of some factors affecting bond in cementitious fiber reinforced repairs." *Cement and Concrete Research*, Elsevier, 63, 117–126.

## Appendix A

### Field Inspection and Data Collection

Table A- 1 Ohio DOT, site 1, SAPL inspection information and photos.


Ohio, Site 1: Warren County		
 <p>Bolt Heads Are Visible</p>	 <p>Circumferential Crack</p>	 <p>Iron Oxidation, Longitudinal and Circumferential Crack</p>
 <p>Circumferential Crack Through the Invert Iron Oxidation</p>	 <p>Efflorescence Circumferential Crack</p>	 <p>Multiple Hairline Cracks</p>

Table A- 2 Ohio DOT, site 2, SAPL inspection information and photos.

**Ohio Site 2: Muskingum County, Ohio**



**Inconsistent Thickness  
Concrete Patching on the Liner Surface**



**Corrosion of Metal pipe with Iron Oxidation on Liner Surface**



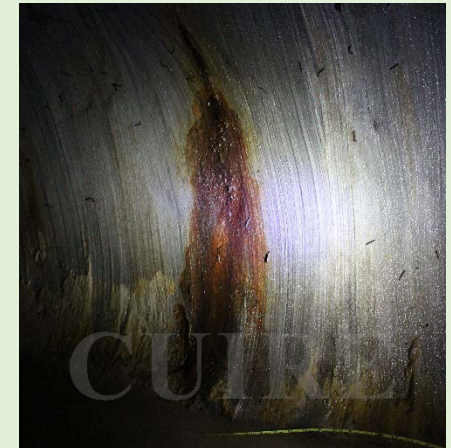
**Aggregate Deposits**



**Corrosion of Metal pipe with Iron Oxidation on Liner Surface, Aggregate Deposits at Invert**



**Worms on the Liner Surface (Vermin)**



**Circumferential Crack**



Table A- 3 Ohio DOT, site 3, SAPL inspection information and photos.




Ohio Site 3: Guernsey County, Ohio		
		
<b>Hand Spray Application with Troweling</b>	<b>Vermin (Frog)</b>	<b>Circumferential Crack</b>

Table A- 4 Ohio DOT, site 4, SAPL inspection information and photos.




Ohio, Site 4: Guernsey County, Ohio		
		
<b>Multiple Cracks</b>	<b>Circumferential Crack through the Invert</b>	<b>CMP Coating</b>

Table A- 5 Ohio DOT, site 5, SAPL inspection information and photos.

Ohio, Site 5: Warren County		
 <p><b>Shadowing</b></p>	 <p><b>Longitudinal Crack</b></p>	 <p><b>Deep Corrugation at The Crown and Thicker Thickness in the Valleys Above Springline</b></p>
 <p><b>Corrosion of Metal pipe with Iron Oxidation on SAPL Surface</b></p>	 <p><b>Aggregate Deposits at Invert</b></p>	 <p><b>Circumferential Crack</b></p>

Table A- 6 PennDOT, site 6, SAPL inspection information and photos.

**Pennsylvania, Site 6: Warren County**



**SAPL Irregularities at the Crown, Iron Oxidation on SAPL Surface below the Springline**



**Circumferential Crack**



**Multiple Cracks**



**Disturbed SAPL Surface**



**SAPL Irregularities (Problem with Application Process)**



**Invert Problem (Installation Problem)**

Table A- 7 NYSDOT, site 7, SAPL inspection information and photos.

New York, Site 7: Warren County		
 <p>Active Leakage from Pinhole Iron Oxidation on SAPL Surface</p>	 <p>Circumferential Shrinkage Cracks Efflorescence</p>	 <p>Infiltration Dripper</p>
 <p>SAPL Irregularities</p>	 <p>SAPL Irregularities</p>	 <p>360 degrees Infiltration Dripper Efflorescence, Iron Oxidation</p>

Table A- 8 DeIDOT, site 8, SAPL inspection information and photos.



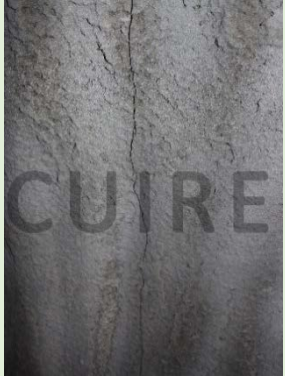



Delaware, Site 8: New Castle County		
 <p>Multiple Cracks Active Leakage</p>	 <p>Infiltration Dripper Circumferential Crack</p>	 <p>Circumferential Fracture</p>
 <p>Multiple Cracks Iron Oxidation, Efflorescence</p>	 <p>Circumferential Crack Iron Oxidation, Efflorescence</p>	 <p>Multiple Cracks Iron Oxidation</p>

Table A- 9 DeIDOT, site 9, SAPL inspection information and photos.

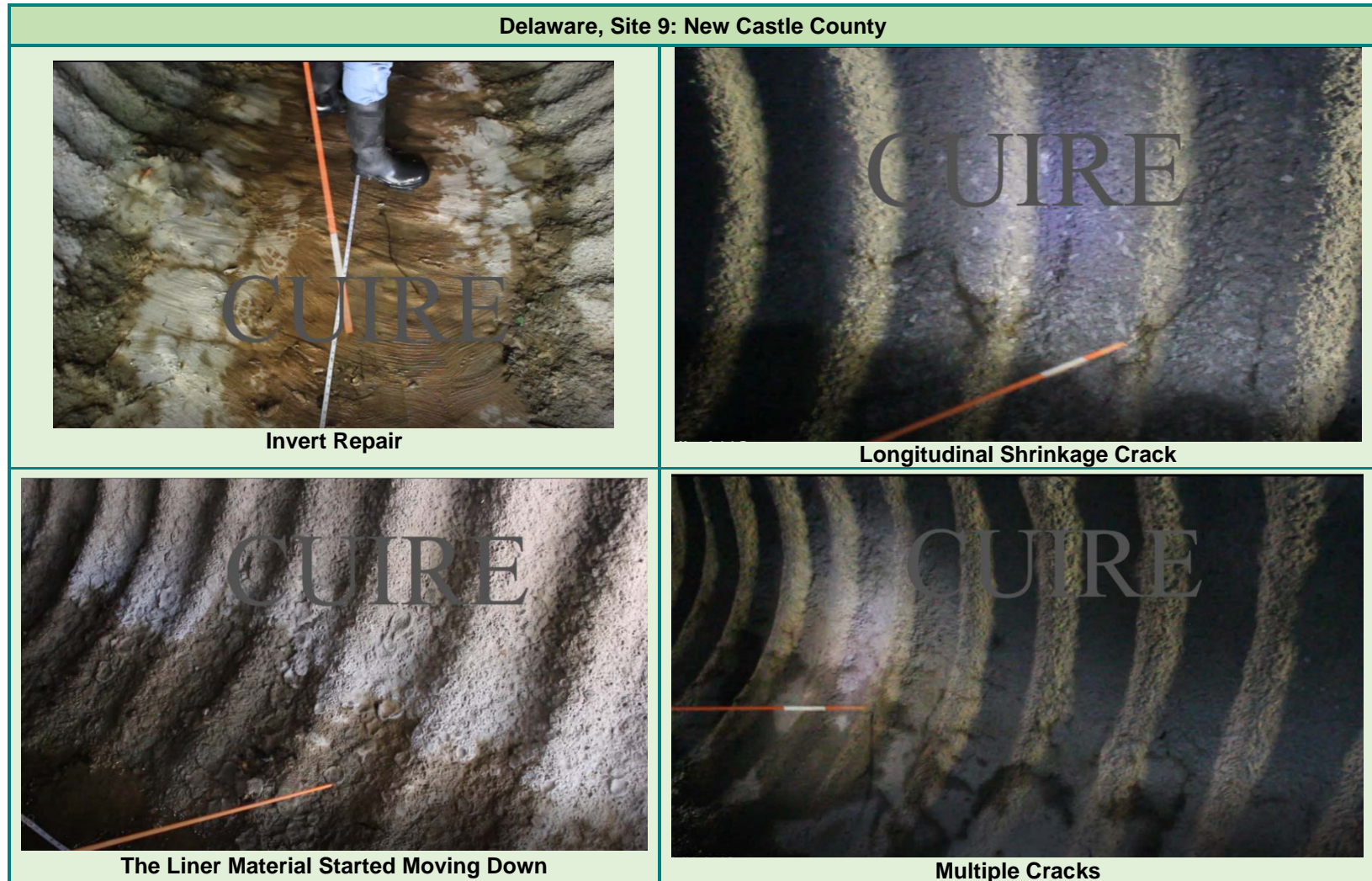


Table A- 10 NCDOT, site 10, SAPL inspection information and photos.

**North Carolina, Site 10: Buncombe County, SR 3479 Pole Creasman Rd**



**Delamination at the Crown**



**Settled Deposits (Hard/Compacted)**

Table A- 11 NCDOT, site 11, SAPL inspection information and photos.




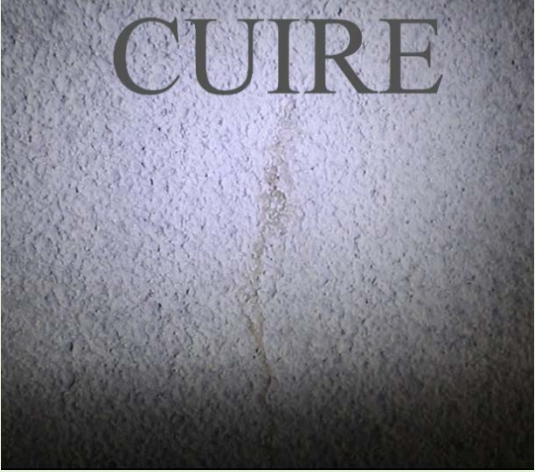
North Carolina, Site 11: Buncombe County	
 <p>CUIRE</p>	 <p>CUIRE</p>
 <p>CUIRE</p>	 <p>CUIRE</p>



Table A- 12 NCDOT, site 12, SAPL inspection information and photos.

North Carolina, Site 12: Buncombe County		
 <p>Irregular Installation</p>	 <p>The Bolts are not Completely Covered</p>	 <p>The Material is not Bonded Completely</p>
 <p>Irregular Installation</p>	 <p>The Bolts are not Completely Covered</p>	 <p>The Material is not Bonded Completely</p>

Table A- 13 NCDOT, site 13, SAPL inspection information and photos.

North Carolina, Site 13: Buncombe County		
 <p>CUIRE</p>	 <p>CUIRE</p>	 <p>CUIRE</p>
<b>Inconsistent Filling of Corrugation</b>	<b>Efflorescence from Pinhole, Iron Oxidation</b>	<b>The Material is not well Bonded</b>

Table A- 14 NCDOT, site 14, SAPL inspection information and photos.

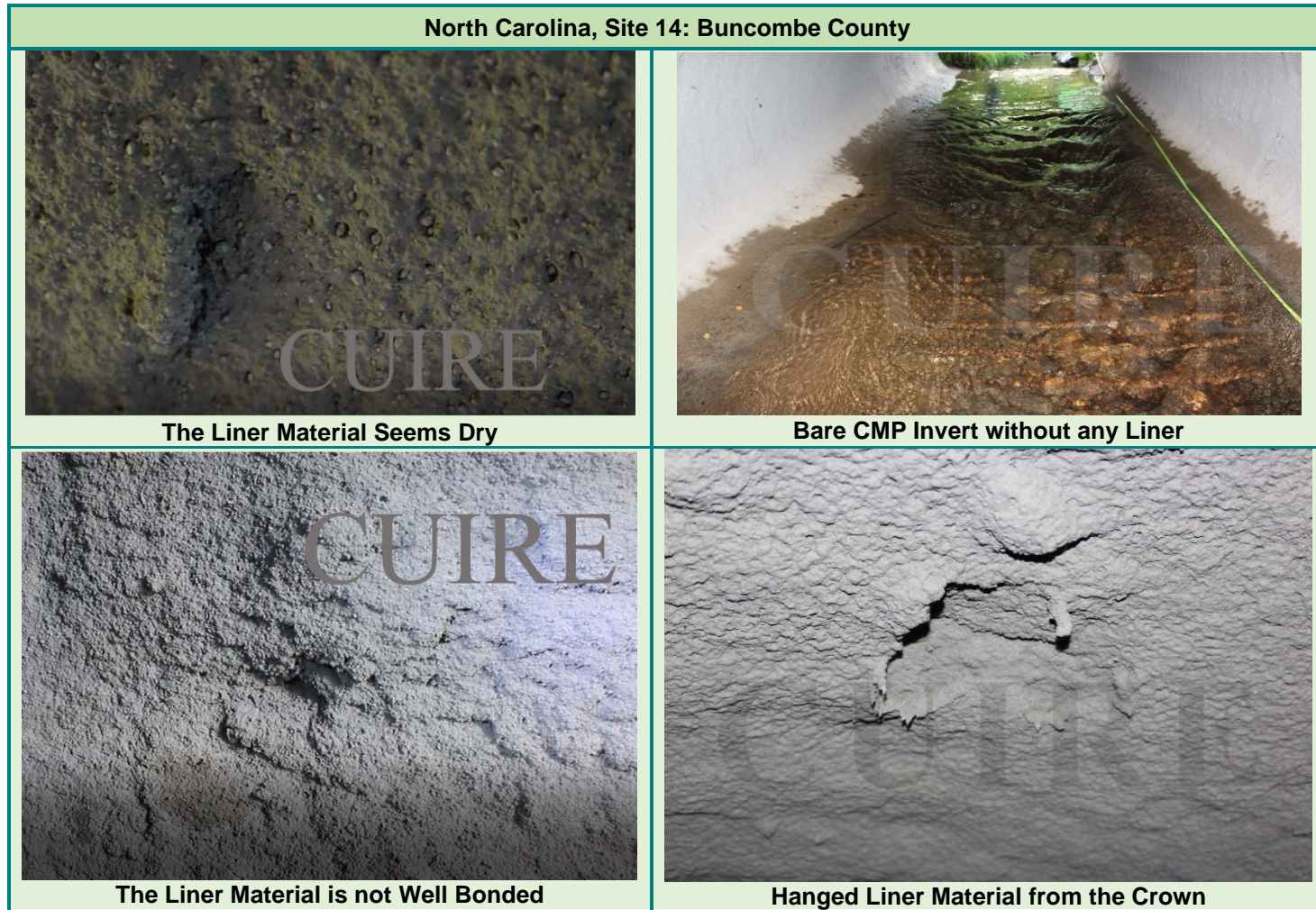


Table A- 15 NCDOT, site 15, SAPL inspection information and photos.







North Carolina, Site 15: Buncombe County		
 <p><b>Heavy Material Rolling Down on SAPL Surface</b></p>	 <p><b>Patched Concrete on SAPL Surface</b></p>	 <p><b>Patched Concrete on SAPL Surface</b></p>
 <p><b>Delamination</b></p>	 <p><b>A Lift over SAPL Material</b></p>	 <p><b>Separated Layer of SAPL Material</b></p>

Table A- 16 MnDOT, site 16, SAPL inspection information and photos.

Minnesota, Site 16: Ramsey County



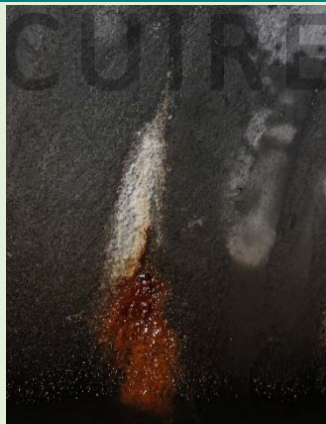
Multiple Cracks



Circumferential Crack through the Invert  
Iron Oxidation, Efflorescence



Inconsistent SAPL Thickness On RCP



Ron Oxidation  
Efflorescence



Heavy and Rough Material at the Crown



Inconsistent SAPL Thickness both Sides of  
RCP Joint

Table A- 17 MnDOT, Site 17, SAPL inspection information and photos.



Table A- 18 MnDOT, site 18, SAPL inspection information and photos.

Minnesota, Site 18: Warren County		
 <p>A close-up photograph of a grey, granular SAPL surface. A person's hand wearing a pink nitrile glove is touching the surface, highlighting an irregular, uneven texture.</p> <p><b>SAPL Irregularity</b></p>	 <p>A photograph of a grey SAPL surface showing a vertical white, crystalline deposit (efflorescence) running down the center. A blue plastic tool is visible in the bottom right corner.</p> <p><b>Efflorescence</b></p>	 <p>A vertical photograph of a grey SAPL surface with a prominent vertical streak of orange-brown rust (iron oxidation) running down the center.</p> <p><b>Iron Oxidation on SAPL Surface</b></p>
 <p>A photograph of a grey SAPL surface showing concentric circular ripples or tracks, indicating irregular application or wear.</p> <p><b>SAPL Irregularity</b></p>	 <p>A photograph of a grey SAPL surface with several distinct, irregular depressions or pits, indicating surface irregularities.</p> <p><b>SAPL Irregularity</b></p>	 <p>A photograph of a grey SAPL surface with several small, dark, irregular marks scattered across it, which are identified as vermin damage.</p> <p><b>Vermin</b></p>

Table A- 19 FLDOT, site 19, SAPL inspection information and photos.






Florida, Site 19: Clay County		
 <p>Hand Patched Concrete on Circumferential Cracks</p>	 <p>Circumferential Crack at Crown</p>	 <p>Pinholes with Active Leakage Circumferential Cracks</p>
 <p>Vermin Nest on SAPL Surface</p>	 <p>Multiple Cracks below the Springline</p>	 <p>Circumferential Crack at Crown</p>



Table A- 20 FLDOT, site 20, SAPL inspection information and photos.

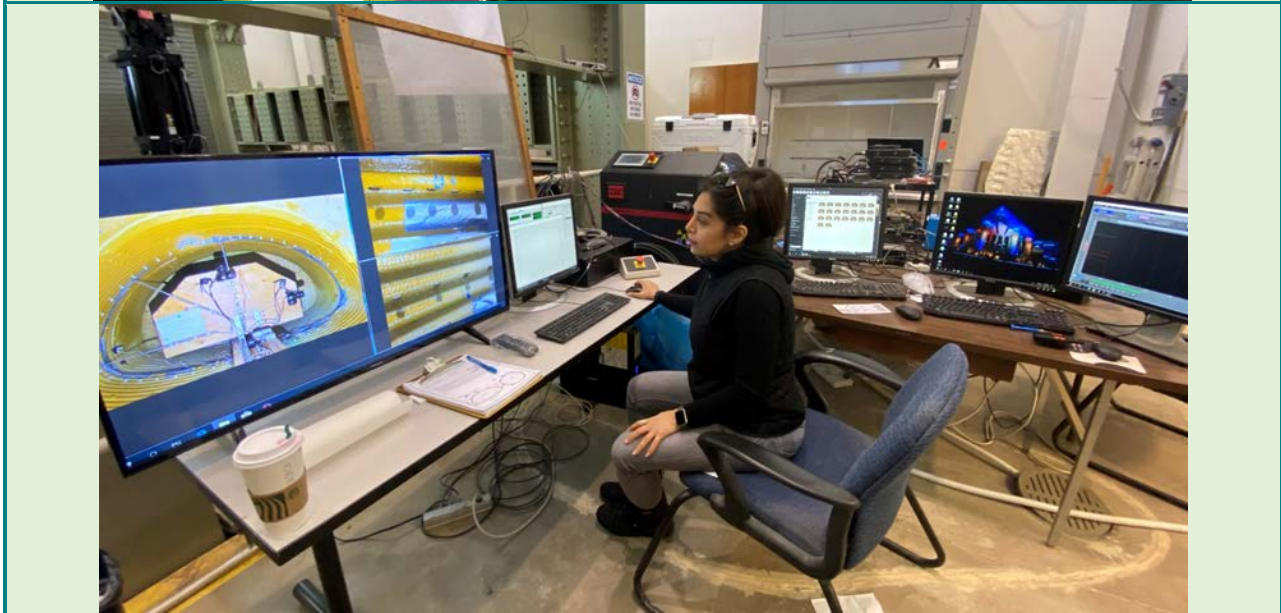
Florida, Site 20: Leon County	
 <p>A close-up photograph of a concrete surface showing a vertical streak of orange-brown rust and white crystalline deposits. A white measuring tape is visible at the bottom of the frame.</p>	 <p>A photograph showing the interior of a tunnel with a highly textured, uneven concrete surface. The word 'CUIRE' is faintly visible on the wall.</p>
 <p>A photograph of a concrete tunnel wall with several prominent, irregular cracks. The word 'CUIRE' is faintly visible on the wall.</p>	 <p>A photograph of a large, dark brown spider on a concrete surface. The word 'CUIRE' is faintly visible on the wall.</p>

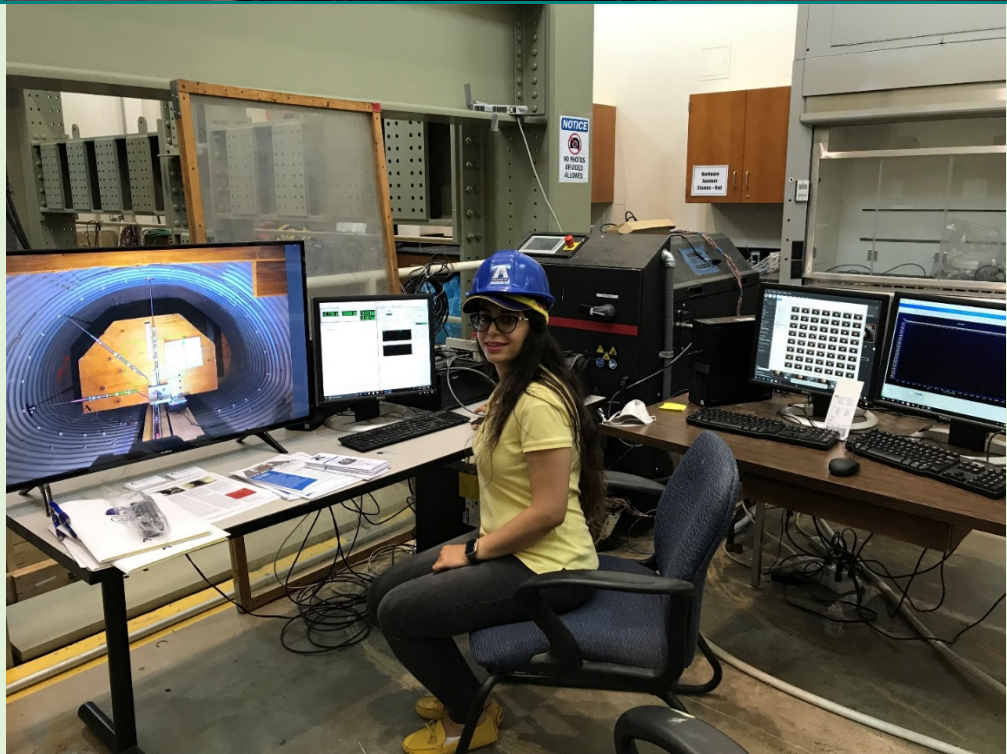
Appendix B

Photo Gallery









## Biographical Information

Zahra Kohankar Kouchesfehani is currently a post-doctoral research fellow in Civil Engineering Department at the University of Texas at Arlington (UTA). She serves as a researcher at the Center for Underground Infrastructure Research and Education (CUIRE) at UTA. Zahra hold her Master of Science in Civil Engineering with a Structural emphasis in 2011. Ms. Kohankar Kouchesfehani is an active member of ASCE, NASTT and five American Water Works Association (AWWA) Standard Committees, where



the committees develop standards, guidelines and manuals of practice for the rehabilitation of pipelines. She serves as the Chair of the Publications subcommittee of AWWA Water Main Condition Assessment Committee as well.

Zahra has 10 years of experience encompassing research, engineering, and management activities. Her expertise is trenchless technology, pipe rehabilitation, inspection and condition assessment. Zahra Kohankar Kouchesfehani is the recipient of multiple recognition awards nationally in North America, as well as the Outstanding PhD Student Award from UTA. She is the recipient of the International Society for Trenchless Technology (ISTT) No Dig Academic Research Award of the year 2019 for her excellent performance in structural evaluation of the “spray applied pipe linings (SAPLs)” trenchless renewal technique in deteriorated gravity storm sewer conveyance conduits, pipes and culverts. Ms. Kouchesfehani has published her research in several top civil engineering journals and the peer-reviewed proceedings of major conferences in the field.

